DISSERTATION

PERFORMANCE AND RELIABILITY EVALUATION OF THE SACRAMENTO DEMONSTRATION NOVEL ICPC SOLAR COLLECTORS

Submitted by

Jirachote "Pong" Daosukho

Department of Mechanical Engineering

In partial fulfillment of the requirements

For the Degree of Doctor of Philosophy

Colorado State University

Fort Collins, Colorado

Summer 2012

Doctoral Committee:

Advisor: William S. Duff
Co-Advisor: Wade O. Troxell

Patrick J. Burns
F. Jay Breidt

ABSTRACT

PERFORMANCE AND RELIABILITY EVALUATION OF THE SACRAMENTO DEMONSTRATION NOVEL ICPC SOLAR COLLECTORS

This dissertation focuses on the reliability and degradation of the novel integral compound parabolic concentrator (ICPC) evacuated solar collector over a 13 year period. The study investigates failure modes of the collectors and analyzes the effects of those failures on performance.

An instantaneous efficiency model was used to calculate performance and efficiencies from the measurements. An animated graphical ray tracing simulation tool was developed to investigate the optical performance of the ICPC for the vertical and horizontal absorber fin orientations. The animated graphical ray tracing allows the user to visualize the propagation of rays through the ICPC optics. The ray tracing analysis also showed that the horizontal fin ICPC's performance was more robust to degradation of the reflective surface. Thermal losses were also a part of the performance calculations. The two main degradation mechanisms are reflectivity degradation due to air leakage and fluid leakage into the vacuum enclosure and loss of vacuum due to leaks through cracks. Reflectivity degradation causes a reduction of optical performance and the loss of vacuum causes a reduction in thermal performance.

ACKNOWLEDGEMENTS

I wish to express my sincere appreciation to Prof. William S. Duff who is my advisor, professor, dissertation committee chairman, and a great friend during years of thoughtful, patient guidance and support. His friendship and selfless role modeling have contributed to my professional development.

In order to complete my dissertation, many thanks are also due to the faculty of the Mechanical Engineering Department. In particular, Dr. Azer Yalin and his staff who provided instructions, suggestions and help in the experiment with the laser equipment. Also, thanks to our colleagues, Jim Bergquam and Joe Brezner who answered technical questions about the ICPC array and provided onsite help in Sacramento.

Finally, and most importantly, I do acknowledge my father, Mr. Suchoti Daosukho, my mother, Mrs. Samerjai Daosukho, my aunts who gave me the opportunity to study in U.S. and my sister for her support and encouragement in completing this degree.

TABLE OF CONTENTS

LIST OF TABLES

LIST OF FIGURES

NOMENCLATURE

A	Area m^2
A_c	Effective area of a collector tube in m^2
F_R	Factor to account for the difference between the fluid and absorber Collector loss coefficient in W/m^2-^oC
G	Instantaneous total irradiance in W/m^2
G_b	Instantaneous beam radiation
G_d	Instantaneous diffuse radiation
G_H	Measured instantaneous radiation
G_T	Instantaneous total radiation on a tilted surface
G_{Tb}	Instantaneous beam radiation on tilted surface
G_{Td}	Instantaneous diffuse radiation on a tilted surface
h	Heat transfer coefficient
$h_{conv,g-a}$	Convection loss coefficient from the glass cover to the environment
$h_{conv,tube\text{-}g}$	Convection loss coefficient the heat transport tube and the absorber fin to the glass cover
$h_{rad,t\text{-}g}$	Radiation loss coefficient from the heat transport tube and absorber fin to the glass cover
$h_{rad,g-s}$	Radiation loss coefficient from the glass cover to sky
h_{wind}	Wind heat transfer coefficient
I	Total solar radiation
IAM(α, β)	Incidence angle modifier
k	Thermal conductivity

n	Refractive index
Nu	Nusselt number
$q_{loss,rad(tube-glass)}$	Radiation heat loss from the heat transport tube and the absorber fin to the glass cover, W
$\dot{Q}$	Energy rate from of the collector tube, W
$\dot{Q}_{Tube-Glass}$	Overall heat loss rate from the heat transport tube to the glass cover, W
$\dot{Q}_{Glass-Ambient}$	Overall heat loss rate from the glass cover to ambient, W
$r_{//}$	Parallel component of unpolarized radiation
$r_{\perp}$	Perpendicular component of unpolarized radiation
Ra	Rayleigh number
R_b	Rratio of beam radiation on a tilted surface
R_{total}	Total thermal resistance
R_{conv}	Convection resistance
R_{cond}	Conduction resistance
R_{rad}	Radiation resistance
ΔT	Temperature difference between the fluid and ambient in K
T_a	Ambient temperature, K
T_b	Atmospheric transmittance for beam radiation
T_d	Atmospheric transmittance for diffuse radiation
T_{fluid}	Fluid Temperature, K
T_{glass}	Cover glass temperature, K
T_{sky}	Sky temperature, K

GREEK SYMBOLS

φ	Latitude
δ	Declination
β	Slope
γ	Surface azimuth angle
γ_s	Solar azimuth angle
ω	Hour angle
θ	Angle of incidence
θ_z	Zenith angle
τ	Total transmittance
τ_r	Reflective loss, transmittance
τ_a	Absorption loss, transmittance
$(\tau\alpha)_n$	Effective transmittance/absorptance product for the glass tube and absorber
ρ_{eff}	Effective reflectance of the integral reflector

CHAPTER 1

INTRODUCTION

1.1 Introduction

This dissertation focuses on the reliability and degradation of the novel integral compound parabolic concentrator (ICPC) evacuated solar collector over a 13 year period. The study investigates failure modes of the collectors and analyzes the effects of those failures on performance. Data was collected and analyzed at ten minute intervals. An instantaneous efficiency model was used to calculate performance and efficiencies from the measurements. An animated graphical ray tracing simulation tool was developed to investigate the optical performance of the ICPC for the vertical and horizontal absorber fin orientations. A laser device was designed and fabricated and used to measure the loss of reflectivity of the internal mirrored surfaces of the ICPC. Thermal losses were also a part of the performance calculations. Each collector was examined and categorized into levels of glass cover temperature. The temperature levels were then incorporated into the thermal loss model. Then, the predicted efficiency was compared with the measured efficiency.

1.2 Background

Flat plate solar collectors are popular for ~~as~~ low cost solar energy collection. Their low efficiency and low operating temperature limitations restrict their practical uses to heating domestic hot water and warming swimming pools. However, compound parabolic concentrators (CPC) can provide higher efficiency and better performance at higher temperatures and comparable costs. Thus, their application can be broadened to air conditioning and industrial uses as well.

An integral compound parabolic concentrator, ICPC, integrates the geometry of the CPC reflector into an evacuated tube collector. Research on integral compound parabolic concentrator (ICPC) evacuated solar collectors has been going on for more than thirty years (Garrison, 1979) and (Snail et al., 1984). Recently researchers at the University of Chicago and Colorado State University developed a new ICPC design for Solar Enterprises International (SEI). The new ICPC design allows a relatively simple manufacturing approach and solves many of the operational problems of previous ICPC designs. This design and the fabrication approaches are described in Duff et al., (1997) and Winston et al., (1997).

In 1998, two new technologies were demonstrated for the first time in a commercial in Sacramento, California: The new ICPC solar collector and the solar operation of a double effect (2E) chiller. Double effect absorption chillers require substantially higher operating temperatures (around 150C) than single effect (1E) chillers (around 75C). However, 2E chillers produce nearly twice as much cooling as 1E chillers for the same energy input. The new ICPC collector operates as efficiently at these higher temperatures as do more conventional collectors at lower temperatures. This new

collector makes it possible to produce cooling with a 2E chiller using a collector field that is about half the size of that required for a 1E chiller with the same cooling output. In 1998 and 1999, while operating in the range of 120 to 160C, daily collection efficiencies of nearly 50 percent and instantaneous collection efficiencies of about 60 percent were measured. Daily chiller COPs of about 1.1 were also achieved.

The novel integral compound parabolic concentrator evacuated solar collector (ICPC) array has been in continuous operation since 1998. Failure rates in the originally installed ICPC evacuated tubes that were produced during the initial production run were less than 4 percent. Subsequently, somewhat higher degradation and failure rates have been experienced.

1.3 ICPC Initial Sacramento Demonstration Performance

Prior to the start of the 1998 Sacramento demonstration, two modules of seven tubes each were tested at Sandia National Laboratory's two-axis tracking (AZTRAK) platform. See Winston et al (5). These tests showed losses from the new ICPC collector operating at 2E chiller temperatures on a 35C summer day of only 120w/m^2 of collector aperture. (A good single glazed flat plate collector with a selective absorber has higher losses when operating at 1E chiller temperatures under the same conditions. Moreover, such a collector would produce very little energy at 2E chiller temperatures.) Thus, with nearly as much energy produced at 2E chiller temperatures as at 1E chiller temperatures, this new collector operated a 2E chiller with a collector field that is somewhat more than half the size of what would be required for a 1E chiller with the same cooling output.

1.4 Objectives

This dissertation research will include a review of collection system performance and reliability over the thirteen years of operation, animations of rays striking at various angles, and the incidence angle evaluation. Results in this dissertation are:

- The modeling and analysis for off-normal incident rays for both the vertical and horizontal fin orientations,
- The modeling of partial blocking from adjacent collectors,
- The reflectance measurement for ~~of~~ selected levels of reflector degradation,
- The tube-by-tube reflectance degradation and thermal loss map of the entire 336 tube array,
- A comparison between the ray tracing results and the experimental results for both the vertical and horizontal absorber fins,
- An analysis of the effects of the two fin orientations and two failure modes on performance,
- A matching of the physical performance model to the simulated ray tracing model,
- An optical and thermal performance model of the evacuated ICPC tube and manifold,
- A reliability and degradation analysis of the evacuated ICPC tube and array,

1.5 Organization of Dissertation

The next chapter describes the ICPC physical geometries and array layout. Chapter 3 describes the ray tracing model used to assess optical performance. The ray tracing animation will also be presented. This chapter also shows how to approach and ~~to~~ estimate the impacts of diffused~~d~~ radiation on performance. A detailed Matlab code explanation concludes this chapter. In chapter 4, results from a Sandia experiment with the ICPC modules is used to validate the Matlab model. The parameter values used in Sacramento installation analysis are also verified. Chapter 5 shows how to incorporate thermal loss into the performance analysis. Chapter 6 investigates how the optical performance varies under the influence~~s~~ of parameter values for factors for both fin orientations. This chapter concludes with the measurement of and categorization and mapping of effects of reflector degradation. Chapter 7 includes comparing estimated and measured efficiency and energy gain in for the Sacramento demonstration in 1999 and 2007. In Chapter 8, the conclusions and recommendations are presented.

CHAPTER 2

ICPC PHYSICAL GEOMETRY AND ARRAY LAYOUT

2.1 Introduction

This chapter will cover the physical geometry and material properties of the novel ICPC.

2.2 Geometry of ICPC design

An integral compound parabolic concentrating collector, or ICPC, integrates the geometry of the CPC into an evacuated tube collector, eliminating the need of an additional structure. As shown in Figure 2.1, the ICPC uses an absorber fin bonded to a heat transport pipe. The heat transport pipe is housed in the evacuated glass cylinder. The bottom half of the circumference of the glass cylinder is coated with a reflective material. A thin wedge-shaped absorber fin is attached to the heat transport pipe. The ICPC simplifies automated manufacturing and reduces material costs. An "ice-cream cone" shaped absorber configuration provides more effective concentration compared to the usual flat horizontal fin absorber evacuated tube configuration, which loses heat from both sides of the fin (Winston et al., 1999).

Each end of the glass cylinder has a glass end cap bonded to it. Both glass end caps have the same glass-to-metal seal and a copper alloy adapter cap assembly rather than glass tabulation (different from figure 2.1). The heat transport tube exits the glass cylinder through this adapter cap and is brazed to it. Water or thermal oil can serve as the heat transfer medium which flows through the coaxial heat transport pipes (Figure 2.1).

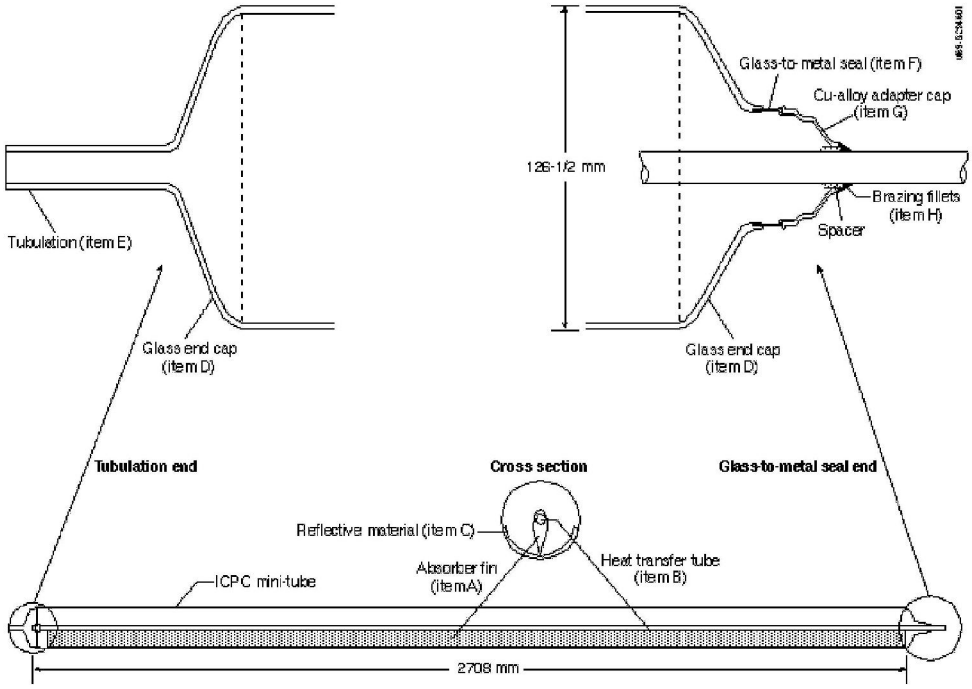

Figure 2.1: Novel ICPC Design

The ICPC length is 2.708 meters long, and the outer diameter of the tube is 126.5 millimeters. The thickness of the glass cover is 2 millimeters. The absorber fin length is 2.654 meters, and the fin has a thickness of 0.4 millimeters. The fin width before it wraps around the heat transported tube is 142 millimeters.

2.2.1 Absorber orientation

The new ICPC evacuated tubes were fabricated with two absorber orientations, one with a vertical absorber fin and one with a horizontal fin. A cross-section of the collector tube illustrating the two orientations is shown in Figure 2.2.

The vertical fin configuration has a symmetric configuration, but has the disadvantage that much of the light must be reflected onto the absorber. An alternative asymmetric horizontal fin configuration has the same effective geometric concentration and the same thermal loss characteristics but a slightly higher expected optical efficiency with a lower average number of reflections at normal incidence. For the horizontal fin, at normal incidence, for half the aperture area the sun's radiation falls directly on the top absorber surface without reflection. ICPC tubes with this horizontal orientation fin maintain the optical, thermal, and manufacturability advantages of the vertical fin orientation. However, it was believed that the lower average number of reflections might lead to better overall performance, so approximately half of the tubes were produced in each orientation, and modules of each configuration were tested at Sandia (Winston et al., 1999).

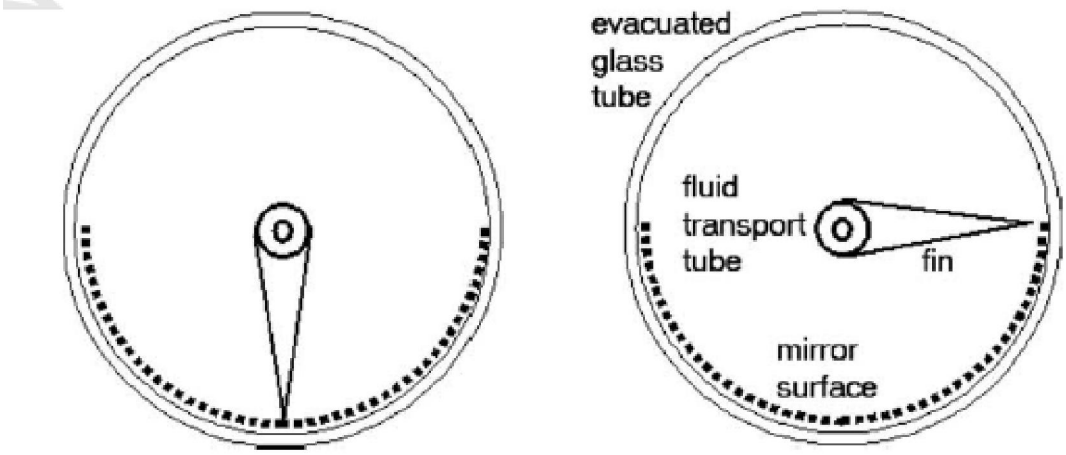

Figure 2.2: Novel ICPC design showing vertical and horizontal fin orientations

2.2.2 Effective aperture area

The effective aperture area of ICPC used in measuring efficiency is taken as the aperture plane that is a cross-section of the collector and the length of the fin. The effective aperture area can be calculated as tube length multiplied by the ICPC diameter plus 5 mm gaps on both sides, or 2.708 m x .140 m = .37912 m^2. So, the area is larger than the cross-section of the tube. In the ray tracing program, the discrete uniform rays are cast over an area greater than this aperture. All rays that hit this aperture area are counted and totaled to provide the basis for efficiency calculations. The yellow shaded plane in figure 2.3 depicts the aperture area positioned in the array plane.

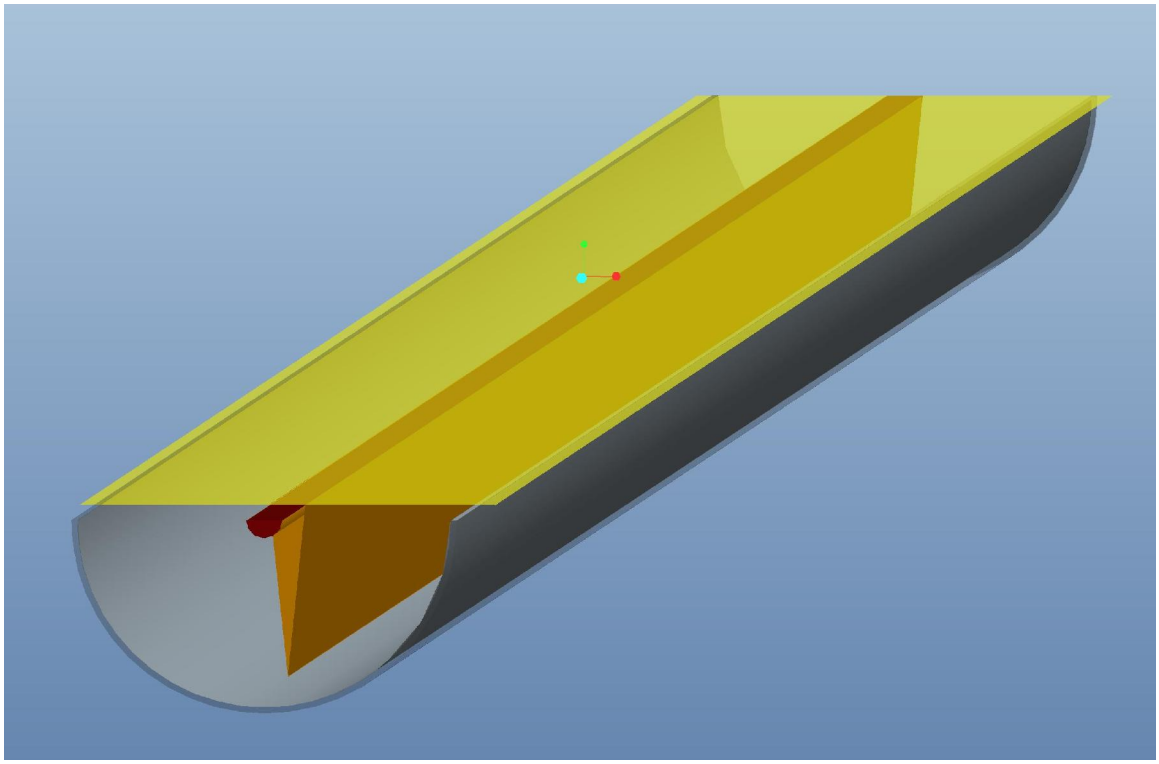

Figure 2.3: Cross-section of the novel ICPC showing the effective aperture area

2.2.3 Heat transport tube design

There are two separated sections in the heat transport tubes in the ICPC evacuated glass tube and the manifold. The heat transport tube in the ICPC consists of an outer tube attached to the absorber fin and an inner feeder tube, (See figure 2.4.). The outer tube and the feeder tube are attached to the manifold at one end so fluid travels down the feeder tube, turns around at the closed end and returns to the annulus between the two tubes creating a coaxial flow. The absorber tube diameter is 12 millimeters and the feeder tube has a diameter of 8 millimeters. The manifold also has the same coaxial arrangement as the heat transport tubes. The inner tube feeds water from a storage supply tank to the collector and the water returns to the storage through the space between the outer and inner tube. The outer tube has a diameter of 50.8 millimeters, and the inner tube diameter is 31.75 millimeters.

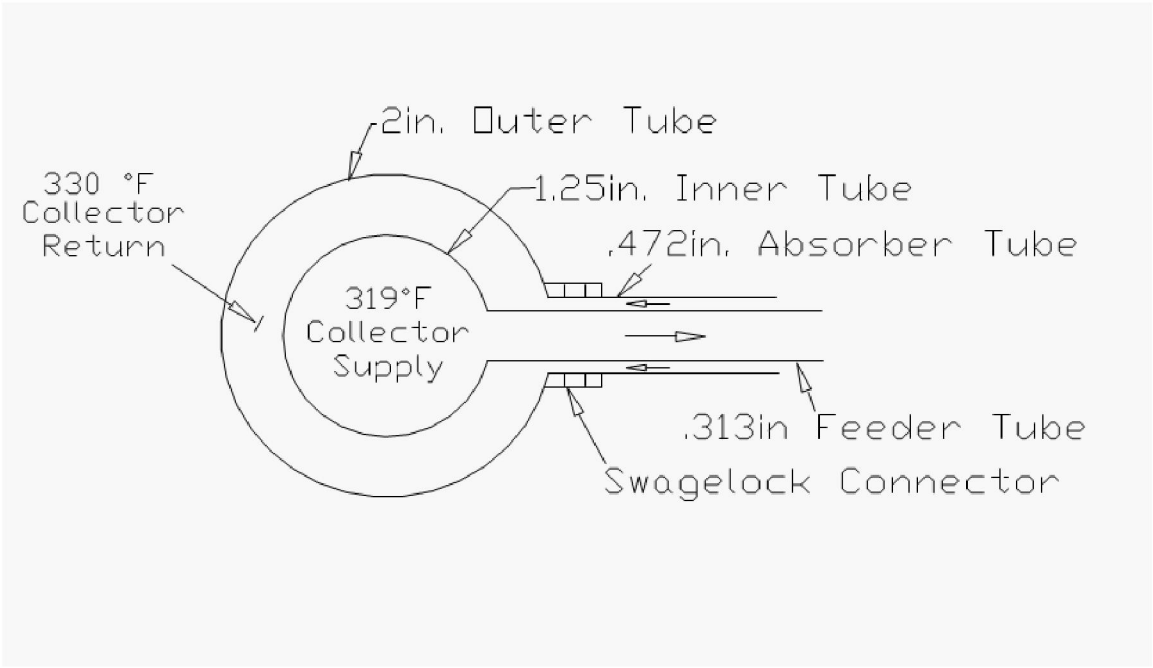

Figure 2.4: Heat transport pipe design

2.3 ICPC Array Geometry and Layout

The ICPC array is divided into three banks. Each bank is a sub-array of 112 parallel plumbed ICPC tubes. The tubes attach to the structural support at both the heat transport (upper) and the vacuum pump lower ends. Each collector lies parallel with the other tubes. The length of each manifold is 15.242 meters. The space between the ICPC tubes is 10 millimeters. The flow pattern through the 112 evacuated tubes in each bank is parallel and the three banks are plumbed in parallel. The north bank consists of all horizontal fin tubes, the middle bank consists of all vertical fin evacuated tubes, and the south bank includes an even mixture of the two types (Duff et al., 1999). All arrays are facing 10 degrees east to the south (a surface azimuth of -10 degrees). Figure 2.5 depicts

the array arrangement on the rooftop. All arrays tilt 17 degrees to the horizontal (a slope of 17 degrees).

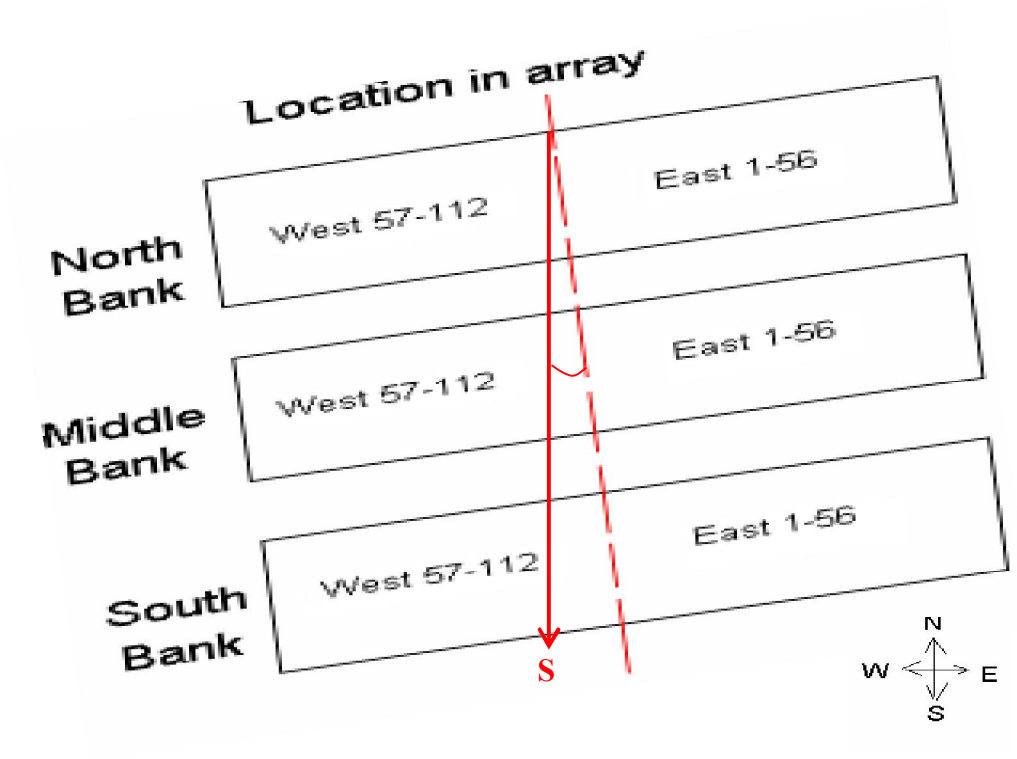

Figure 2.5: Novel ICPC arrays layout

2.4 Location of the ICPC Demonstration

The ICPC demonstration is located on the rooftop of an industrial/commercial building in Sacramento, California. The site is at latitude of North 35.55 degrees and longitude of West 121.386 degrees as shown in Figure 2.6. The ICPC array provides a heated water-antifreeze mix to a storage tank for powering a double-effect absorption chiller.

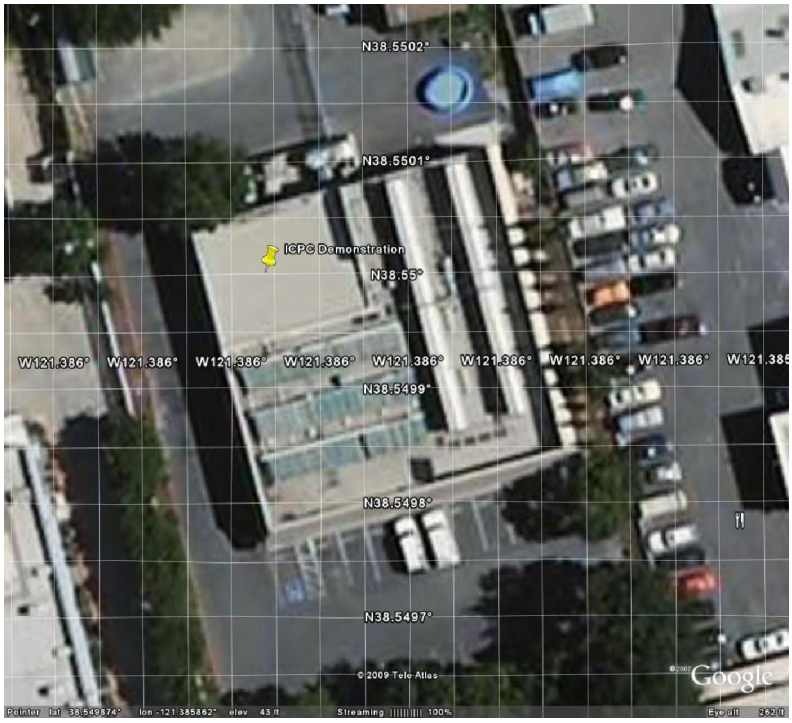

Figure 2.6: ICPC demonstration in Sacramento (lat. N38.55, long. W121.386)

2.5 Material Properties

The glass envelope of an ICPC tube is made of soda lime glass. The glass has a reflective index (n) of 1.526, and the extinction coefficient for glass material is approximately 4 m^{-1}. The absorber is copper coated with a TiN_xO_x selective surface. The absorber has an absorptance of 0.947 and a very low IR emittance (εTiN_xO_x) of 0.036. See figure 2.7. The reflector is silver coated on the bottom half of the glass cylinder. The reflectance of this surface has been measured from a sample removed from ICPC array. This undegraded surface has a reflectance of 0.9348, but when the silver reflector degrades, the reflectance will be reduced.

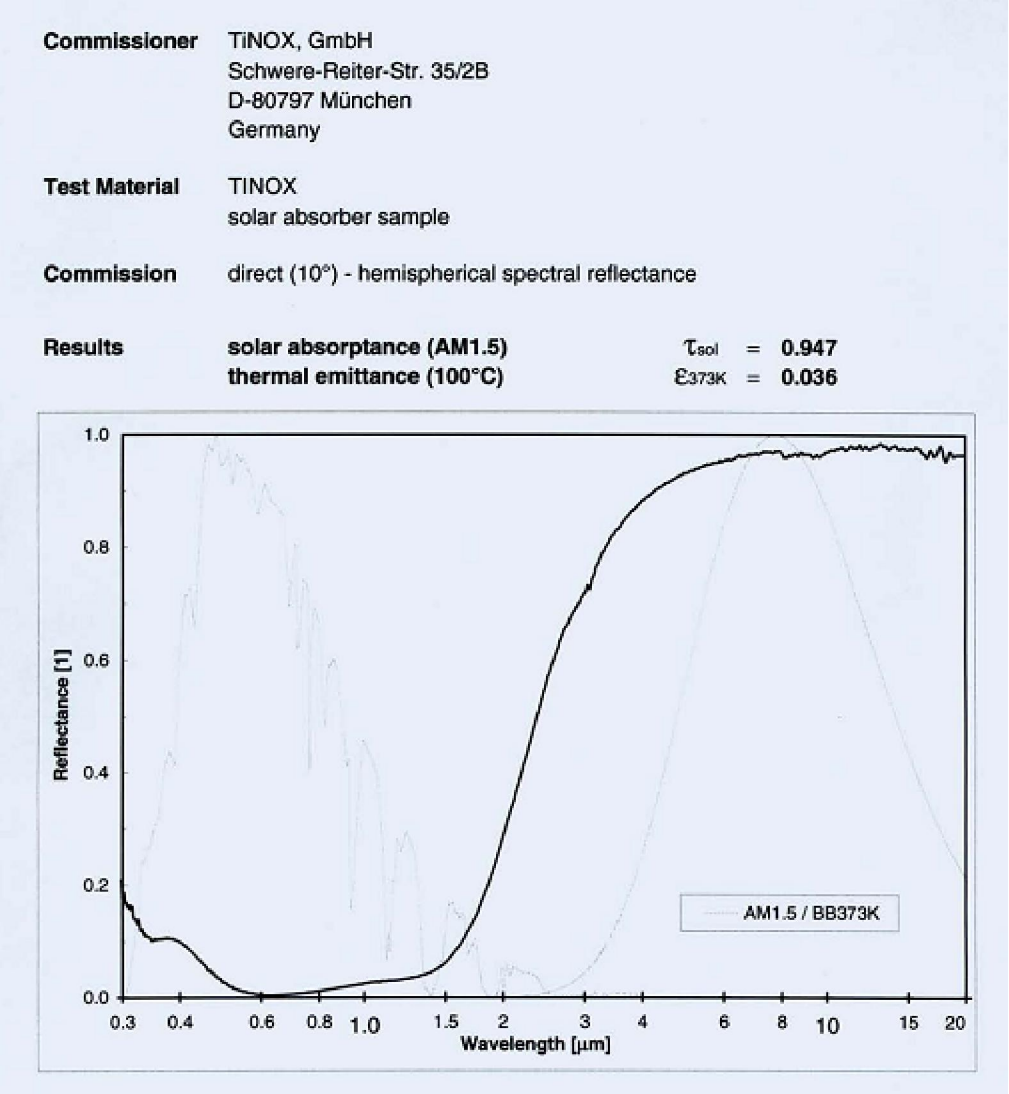

Figure 2.7: Solar absorptance and thermal emittance of selective surface (Supplied by the TiNOX corporation.)

2.6 Summary

This chapter has presented the ICPC physical geometry and the material properties. The methodology and equations involved in the ICPC performance measuring will be presented in the next chapter.

CHAPTER 3

GRAPHICAL RAY TRACING

THEORY AND MATLAB IMPLEMENTATION

3.1 Introduction

The focus of this dissertation is a reliability and degradation analysis of a novel ICPC that has been in operation for 13 years. An animated graphical ray tracing simulation tool has been created as the primary means to investigate the impact of various degradation changes on the optical performance of the ICPC. Factors incorporated in the ray tracing analysis are the transmittance of the glass tube, the reflectivity of the reflective surface, the gap between the reflective surface and the absorber fin, the interference of adjacent tubes, and the absorptance of the absorber fin.

3.1.1 Beam components of total radiation

Beam radiation is traced from the position of the sun during daylight hours. The ray tracing analysis will trace each single ray as it comes from the direction of the sun, all rays will reach the collector plane as parallel rays. Each ray is recorded as its intensity is attenuated to after hitting an absorber fin. An optical efficiency measure of the beam component is calculated in the ray tracing simulation by summing the reduced intensity

collected rays and dividing by the number of full intensity rays that would have passed through the effective aperture area of the ICPC tube array.

3.1.2 Diffuse components of total radiation

ICPCs collect a substantial amount of solar energy during overcast or cloudy days. Thus, an additional simulation analysis was designed to capture diffuse radiation coming from all directions in the hemisphere surrounding the collector. All reduced intensity diffuse rays that are absorbed by the ICPC are recorded. As was the case for beam radiation, the optical efficiency of the diffuse component is estimated in the ray tracing simulation by repeating the above calculation with changing beam to diffuse.

3.2 Direction of beam radiation and projected planes calculation

Discrete uniform rays striking the collector from 7 a.m. to 5 p.m. solar time are simulated. The rays hitting the absorber plate, the heat transfer tube, the reflector and the absorber are recorded. Since the angle of incidence is time and location dependent, the beam radiation will be traced from the actual sun position at the time of experiment. Figure 3.1 shows sun paths on a horizontal surface for each season. In winter the sun rises from the southeast and sets in the southwest. In summer, the sun rises from the northeast and sets in the northwest. The figure shows a shorter daytime in winter and a longer daytime in summer.

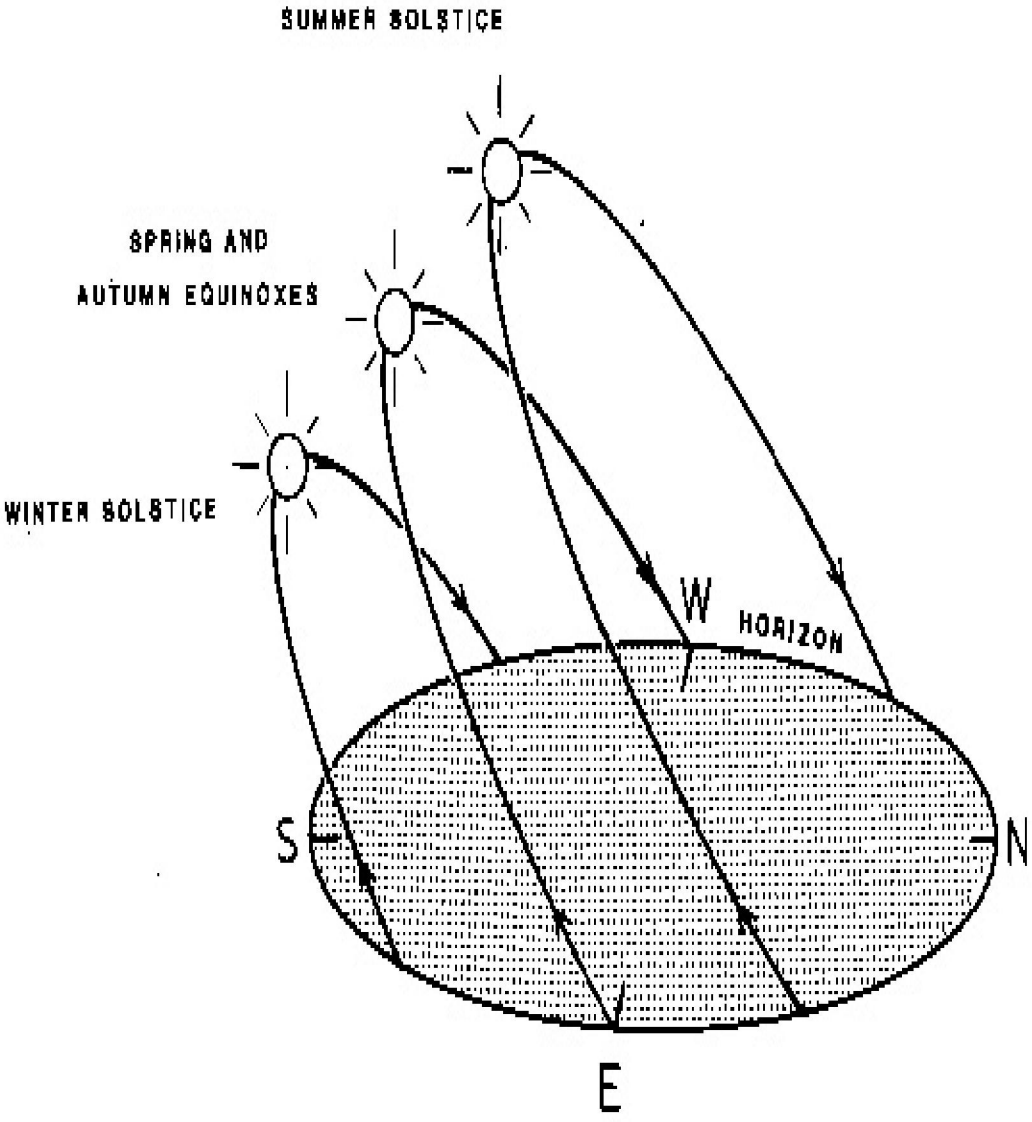

Figure 3.1: Sun solstice

A ray tracing simulation is designed to estimate the optical efficiency of the ICPC tube. The angle of incident (θ) and solar azimuth angle (γ_s) are obtained by using the geometric relationships between the array's position relative to the earth and the sun's orientation at different times of the day and year. Figure 4.2 illustrates the angles associated with these calculations.

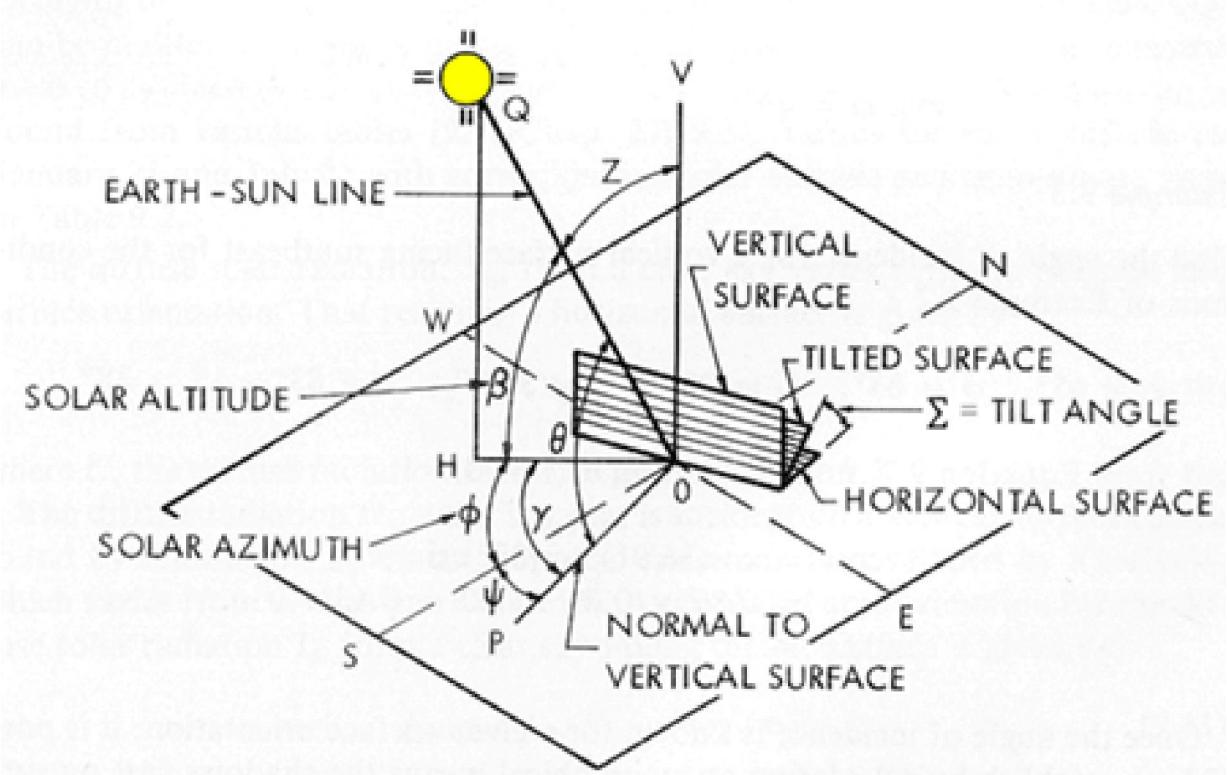

Figure 3.2: Visualization of the varying solar angles

These angles and the relationships between them, developed in Duffie and Beckman (1980), are shown below. The declination, δ, can be found from equation 3.1. Figure 3.3 shows the difference between summer solstice and winter solstice on the declination.

$$\delta = 23.45 \sin\left(360 \frac{284 + n}{365}\right) \tag{3.1}$$

Here *n* is the day of the year. Figure 3.3 shows the solar declination angle in the northern hemisphere. The relationship between the angle of incidence, θ, and the other angles is shown in equation 3.2.

$$\cos\theta = \sin\delta\sin\phi\cos\beta - \sin\delta\cos\phi\sin\beta\cos\gamma + \cos\delta\cos\phi\cos\beta\cos\omega$$
$$+ \cos\delta\sin\phi\sin\beta\cos\gamma\cos\omega + \cos\delta\sin\beta\sin\gamma\sin\omega \qquad (3.2)$$

The solar azimuth angle, γ_s, is the angular displacement from south of the projection beam radiation on the horizon. The solar azimuth angle is approximated by the following formula. See equation 3.3.

$$\cos\gamma_s = \frac{\cos\omega\cos\delta\sin\phi - \sin\delta\cos\phi}{\cos\theta} \qquad (3.3)$$

The solar azimuth angle is taken as the positive value of sine $\cos^{-1}$.

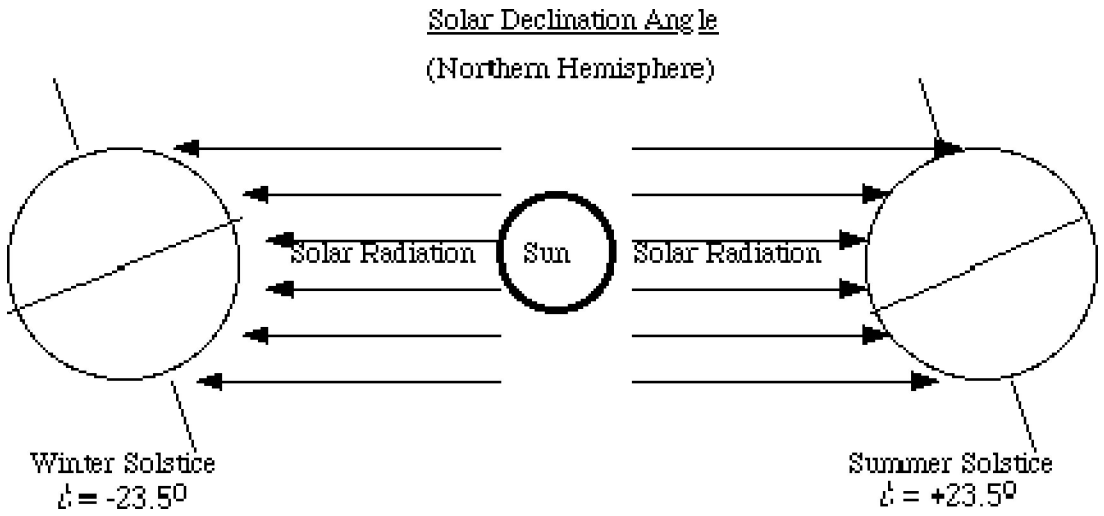

Figure 3.3: Solar declination angle

To make angle calculations consistent, we can interpret the solar azimuth angle as the angle east of south when the hour angle, ω, is negative (in the morning) and the angle west of the south when the hour angle is positive (in the evening). The projected sun radiation is presented in terms of both the angle of incidence and the solar azimuth angle. The collector plane is used as a reference in the ray tracing simulation. As shown in Figure 3.4, the sun radiation is projected to the longitudinal (side view) and the transverse (front view) planes of the ICPC arrays

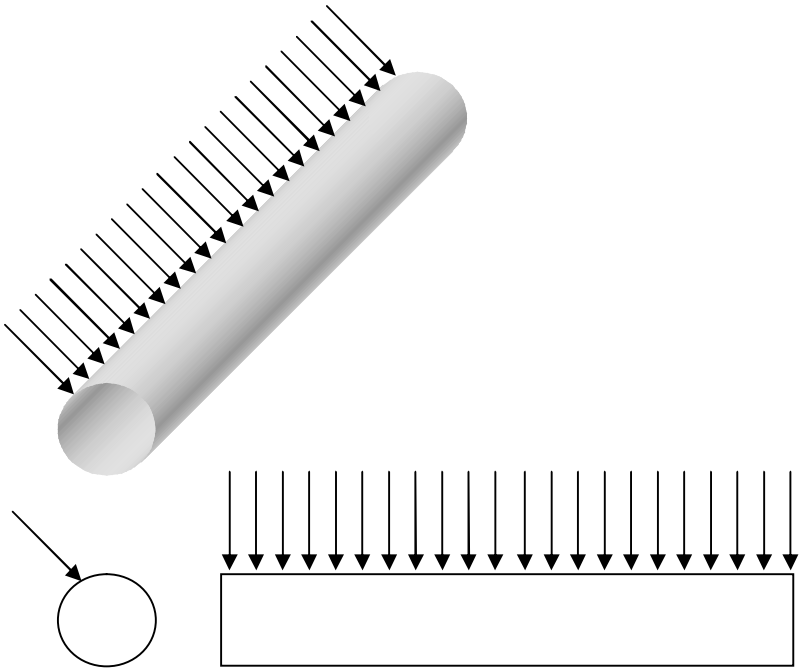

Figure 3.4: Projections of sun radiation to longitudinal (side view) and transverse (front view) planes

3.2.1 Projected plane of the ICPC

The simulated rays are transformed relative to the array plane. Then, a ray is projected onto two views, the longitudinal (side) view and the transverse (front) view. Figure 3.5 shows two rays that have the same angle in a transverse view but different angles in a longitudinal view. The figure shows three projected views and an isometric view, which depicts the path of the two rays that hit the reflector and are reflected by the reflector.

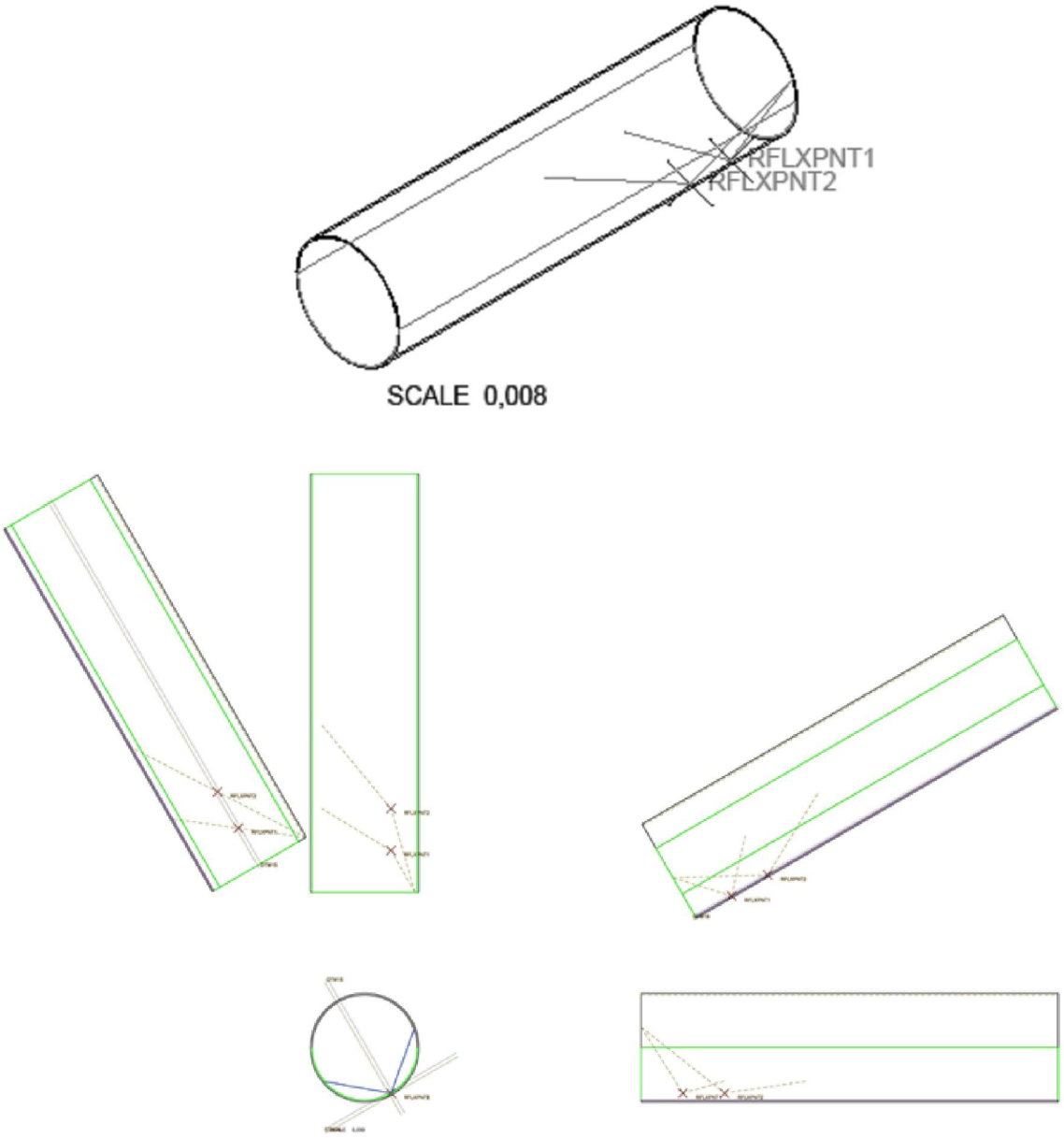

Figure 3.5: Projected ray elements on multiple views

3.3 Ray-tracing procedure

The projected solar radiation is analyzed in terms of both the longitudinal and transverse incident angles to the tube. The reference axis is adjusted to be the same plane

as the collector plane. As shown in Figure 3.4, ray tracing projects the sun's ray into longitudinal (side view) and transverse (front view) planes of the ICPC arrays.

A ray striking the collector at a given angle and in a given location is monitored as to how it responds at various surfaces and orientations of the collector. A color coding is used to depict how simulated rays respond at various surfaces. This is shown in Table 3-1.

Table 3-1: Color codes to illustrate ray action

Color	Code
Pink	Ray enters outer glass tube
Red	Hitting the heat transported tube
Blue	Ray missing the collector aperture
Yellow	Ray hitting the reflective surface
Brown	Ray hitting the absorber fin
Green	Ray reflected out

The ray tracing simulation evaluates each single ray from the transverse view and then the simulation projects the ray as a uniformly distributed set of rays in the longitudinal view. The angle of incidence of the ray is calculated using equation 3.2, and then is projected to the transverse and longitudinal views on the collector plane. First, a single ray is traced on the transverse view at 7 am. The angle of incidence at the

transverse view can be translated using the geometric translation via ~~technique on~~ equation 3.4 below.

$$\theta_{transverse} = \tan^{-1}\left(\frac{\cos\theta}{(\sin\theta)(\sin(-\phi_{collector}))}\right), \text{ when } \phi_{collector} < 0$$

$$= \tan^{-1}\left(\frac{\cos\theta}{(\sin\theta)(\sin(-\phi_{collector}))}\right), \text{ when } \phi_{collector} > 0 \qquad (3.4)$$

The ray tracing procedure is set up to trace individual rays and their intensities until one hits the absorber plate or is reflected out. The ray tracing procedure follows these steps:

- First, each ray is assigned as a line function $ax + by + c = 0$ on the x-y coordinate (transverse plane) with slope of $\theta_{transverse}$ degrees as $a = \tan(\theta_{transverse})$, $b = -1$ and $c = -y_{\text{int}ersect} \times \sqrt{a^2 + b^2}$.
- Then, we check for the rays that pass through the adjacent tube and miss to the side of the target collector (Blue) as $|c| > (r_{collector} \times |a|)$. Figure 3.6 depicts the traced rays that do not enter the tube. These rays are ruled out and not included in the calculation.

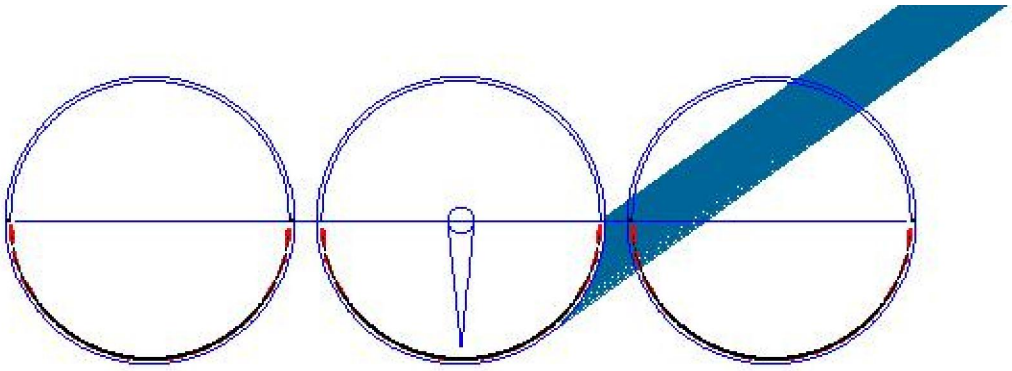

Figure 3.6: Rays missing the effective area of the collector (Blue)

- Then, we determine whether each ray passes through the adjacent collectors or not by checking the condition below:

  $r_{outerglass}^2 \times \left(a^2 + b^2\right) - c^2 - 2ac \times (2r_{outerglass} + 10) - (a^2 \times (2r_{outerglass} + 10)^2) < 0$
  $, when \quad \theta_{transverse} < 90°$

  and

  $r_{outerglass}^2 \times \left(a^2 + b^2\right) - c^2 - 2ac \times (-2r_{outerglass} - 10) - (a^2 \times (-2r_{outerglass} - 10)^2) < 0$
  $, when \quad \theta_{transverse} > 90°$. These conditions are proved geometrically as the straight line crossing the circles on both sides on the x-y coordinate.

- Each ray cast will begin with the intensity factor of 1.

- If the ray passes through the nearby collector glass cover before hitting the aperture/target collector, the blocking effect will be calculated. The blocking effect is determined by finding the transmittance as a percentage of the intensity of the ray going through before hitting the target collector. Transmittance through the reflection and absorption loss is, $\tau \cong \tau_a \tau_r$ where $\tau_r = \frac{1}{2}\left(\frac{1 - r_{//}}{1 - r_{//}} + \frac{1 - r_{\perp}}{1 - r_{\perp}}\right)$.

Also, $\tau_a = \frac{I_\tau}{I_o} = e^{-Kx}$, explained in equation A.3 to A.6, will be used to find the blocking effect as a function of angle of incidence. This blocking effect will be applied as the reduction multiplier to the ray's intensity factor. The direction of the ray is also changed as it refracts through the glass cover from the blocking tube, $\frac{n_1}{n_2} = \frac{\sin\theta_1}{\sin\theta_2}$ as in equation A.2 by Snell's law. See Figure 3.7 and Figure 3.8. Then, new *a, b, c* values are assigned to a new line corresponding to a new projected angle. Next, the y-position of the ray at the entry point is recorded.

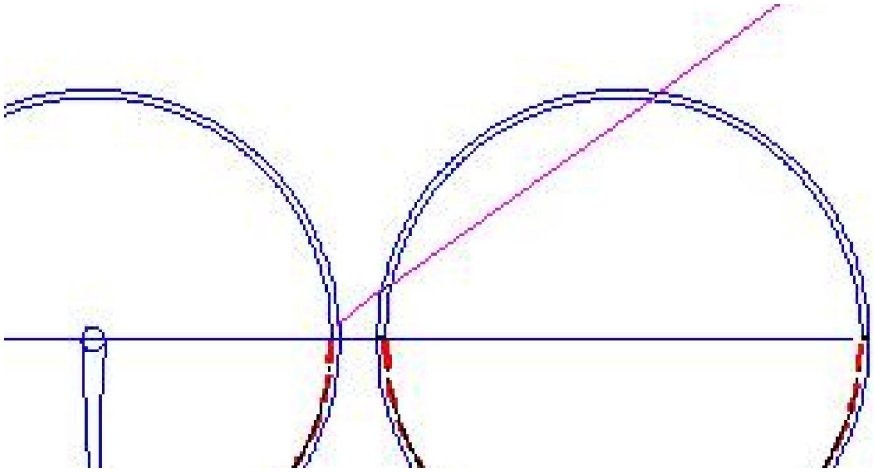

Figure 3.7: Ray passes and is refracted through the adjacent tube

- It is then determined whether each ray individually hits the reflective surface, or directly to the absorber fin by solving a basic geometric function for a straight line intersecting each circle (the reflective surface and heat transport tube). If $r_{reflect}^2 \times \left(\left(a^2 + b^2\right) - c^2\right) > 0$ then the ray hit the reflective surface. If $r_{heattrans}^2 \times \left(\left(a^2 + b^2\right) - c^2\right) > 0$ then the ray hit the top part of the fin. If

$-l_{fin} \leq \frac{-c}{b} \leq 0$ then the ray hit the absorber fin (vertical) and $0 \leq \frac{-c}{a} \leq l_{fin}$ for the horizontal fin. A fin position is set on the y-axis from 0 to minus the fin length for the vertical fin arrangement, and for the horizontal fin arrangement, the fin position is set to the x-axis from 0 to fin length on the transverse view.

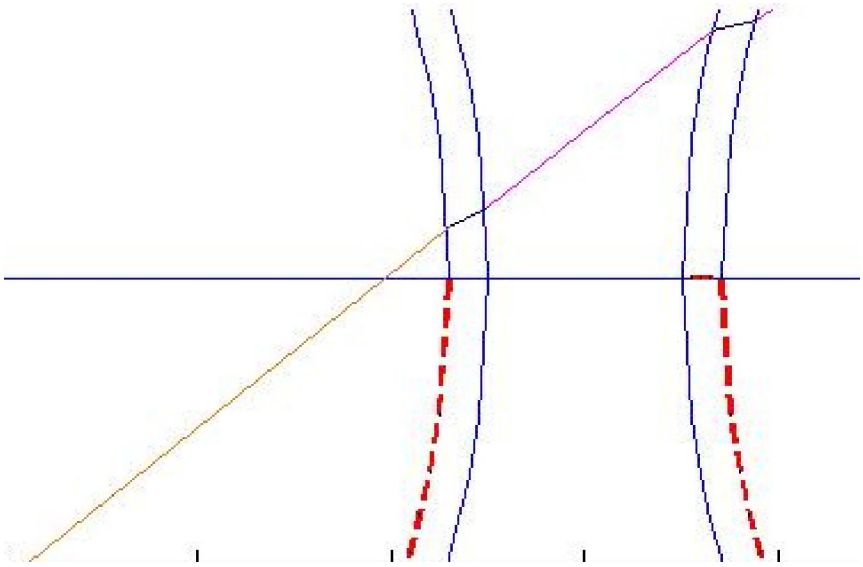

Figure 3.8: Refracted ray through the glass cover

- Rays hit an absorber fin directly in the same direction as the rays cross the absorber fin in the transverse view. If the ray hits an absorber fin, the absorber absorptance of 0.947 (Ronal D., M.S., 1997) is directly applied to the ray's intensity as a percentage of energy absorbed. See Figure 3.9. The y-axis position at the impact point is also recorded into an array.

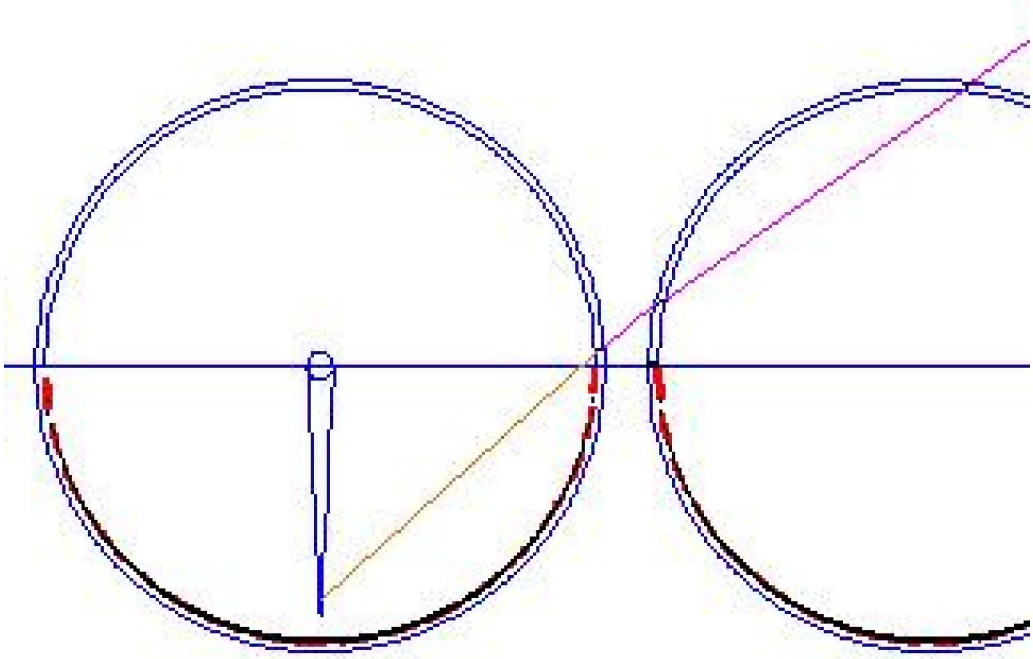

Figure 3.9: Ray hitting the absorber

- If the ray hits the reflective surface, Figure 3.10, the reflected ray will reflect as a specular reflection whose angle of reflection equals ~~to~~ the angle of incidence. Each reflection will reduce the intensity by multiplying the reflectance index by the intensity factor. (The reflectance index can will be reduced over time due to degradation~~s~~ of the collector.) A higher number of reflections will result in a lower intensity value for the ray. The y position of each reflection is also recorded into an array since this is used for tracing the ray in a longitudinal view.

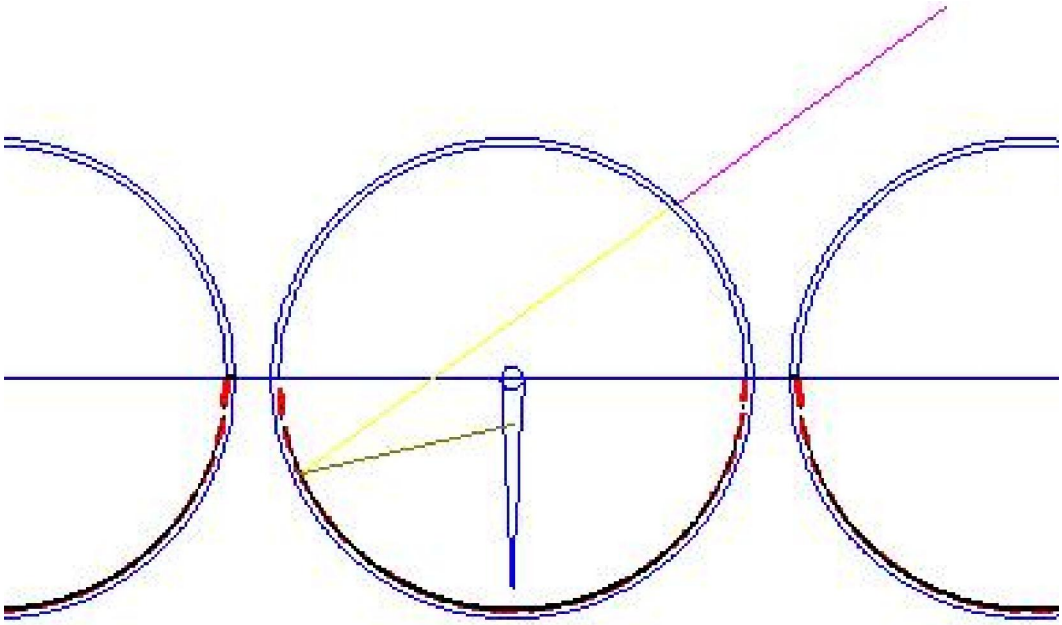

Figure 3.10: Reflected ray hitting the reflector

- The tracing sequence at the transverse plane will stop when the traced ray hits either the absorber fin, or the ray misses both targets.
- If the ray is reflected out without hitting the absorber fin, it is considered as a lost ray (Green). This ends the tracing procedure of the ray except for the projected ray trace at the longitudinal view. See Figure 3.11.
- After the tracing of each ray is done on the transverse plane, the uniformly distributed array of rays is plotted on the longitudinal view. It will be determined where each ray enters the tube from the transverse plane. The pink color code will mark the ray from the outside glass cover to the entrance point.

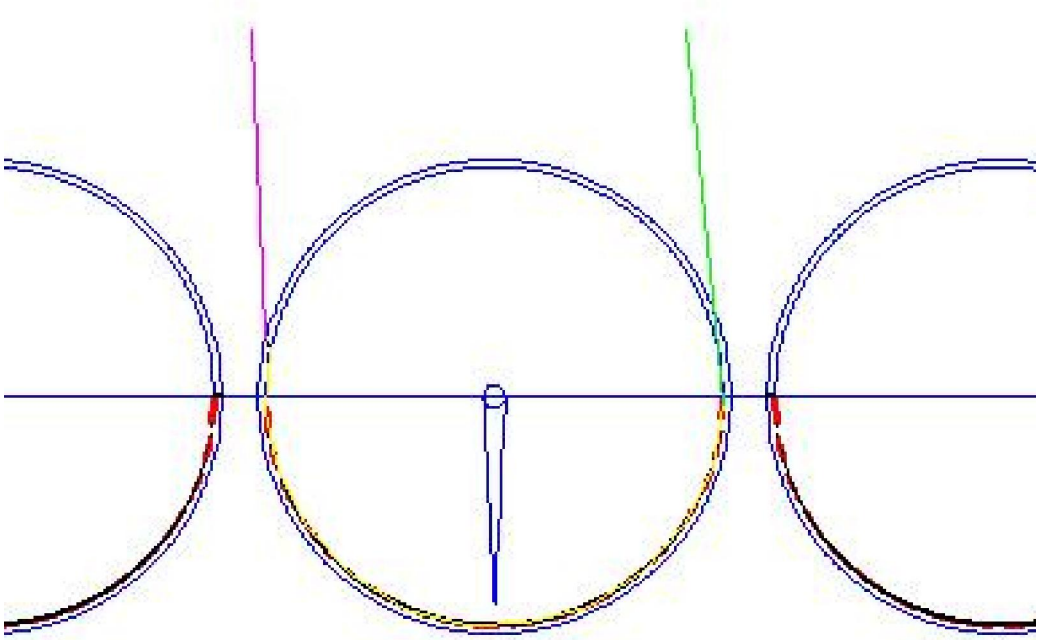

Figure 3.11: Ray missing the absorber

- In the longitudinal view, the ray direction is projected in two-dimensional coordinate. Rays enter the tube in parallel with an angle of $\theta_{longitudinal}$, shown below.

$$\theta_{longitudinal} = \tan^{-1}\left(\frac{\cos\theta}{(\sin\theta)(\cos(-\phi_{collector}))}\right), \text{ when } \phi_{collector} < 0$$

$$= \tan^{-1}\left(\frac{\cos\theta}{(\sin\theta)(\cos(\phi_{collector}))}\right), \text{ when } \phi_{collector} > 0$$

  A ray will enter the tube at the first y position in the array that is calculated before by deriving the position on the transverse view.

- The ICPC is located from -20 to 2728 mm. on the x-axis. The glass cover is from 0 to 2708 mm. on the x-axis. After pink rays enter the tube at the longitudinal view, it is determined whether the ray hits or misses the reflector. The reflector on longitudinal view is divided into 10 sections. Each section of the reflector has a

unique reflectivity value. The ray intensity is reduced depending on which section of the reflector the ray hits. Blue rays also represent the rays that miss the reflector or absorber. See Figure 3.12.

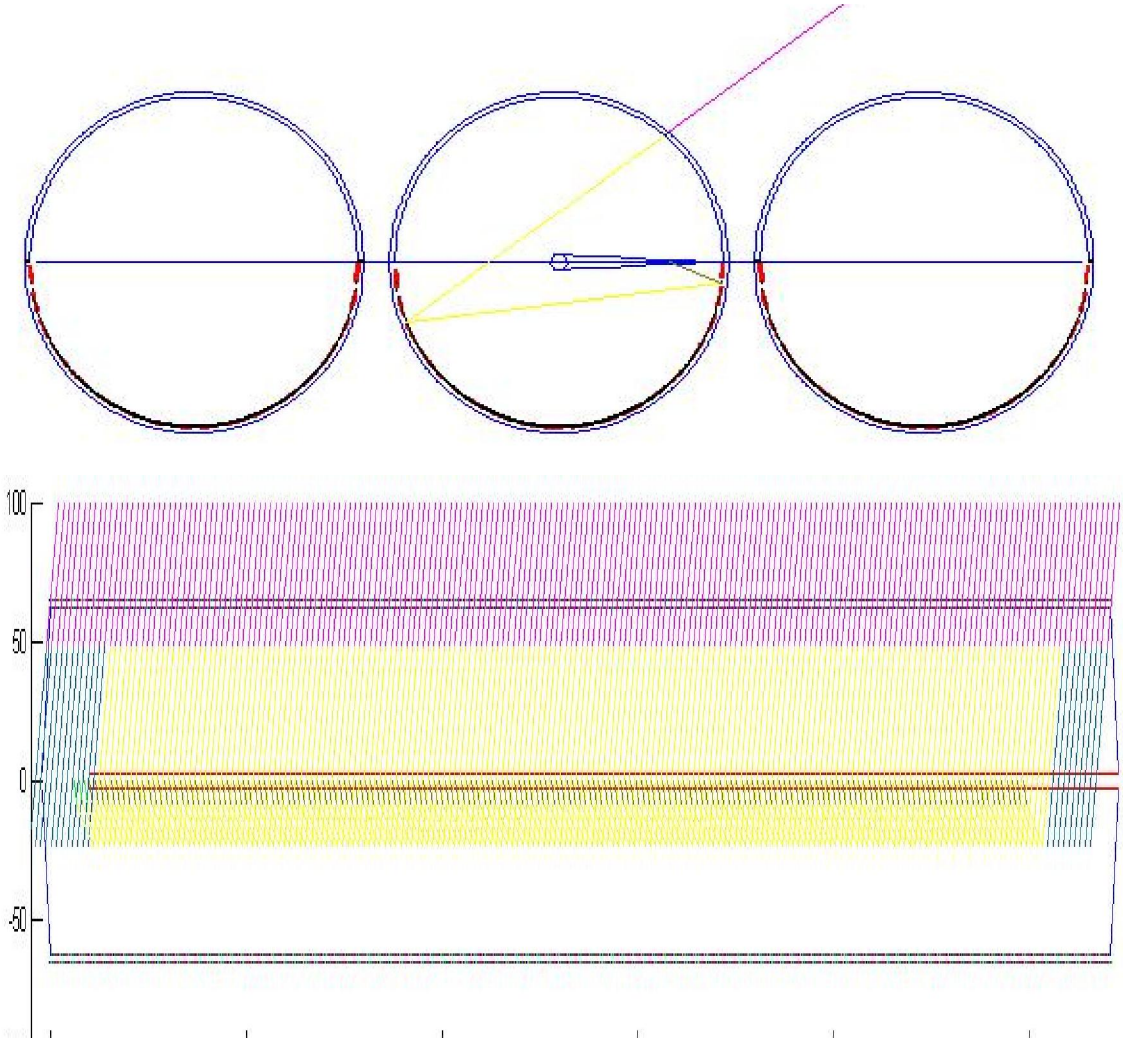

Figure 3.12: Pink rays representing the array of rays entering the collector on both transverse and longitudinal views

- As the rays hit the reflector, it is determined how many times they hit the reflector before they hit the absorber or are reflected out. The reflection angle in a longitudinal view is calculated by using the predetermined y-position from the

transverse view and applying it to the longitudinal view based on the fact that both the incident ray and the reflected ray have the same x displacement in the longitudinal view. So, the reflected angle $\theta_{refl,long}$ can be calculated by $\theta_{refl,long} = \tan^{-1}\left(\frac{\Delta y_{position}}{\Delta x_{intercept}}\right)$ where $\Delta y_{position}$ is a distance between two reflected points on y-axis, and $\Delta x_{intercept}$ is a distance horizontal between two reflected points along x-axis on the longitudinal view. Each reflection will be coded with a yellow line. See Figure 3.13.

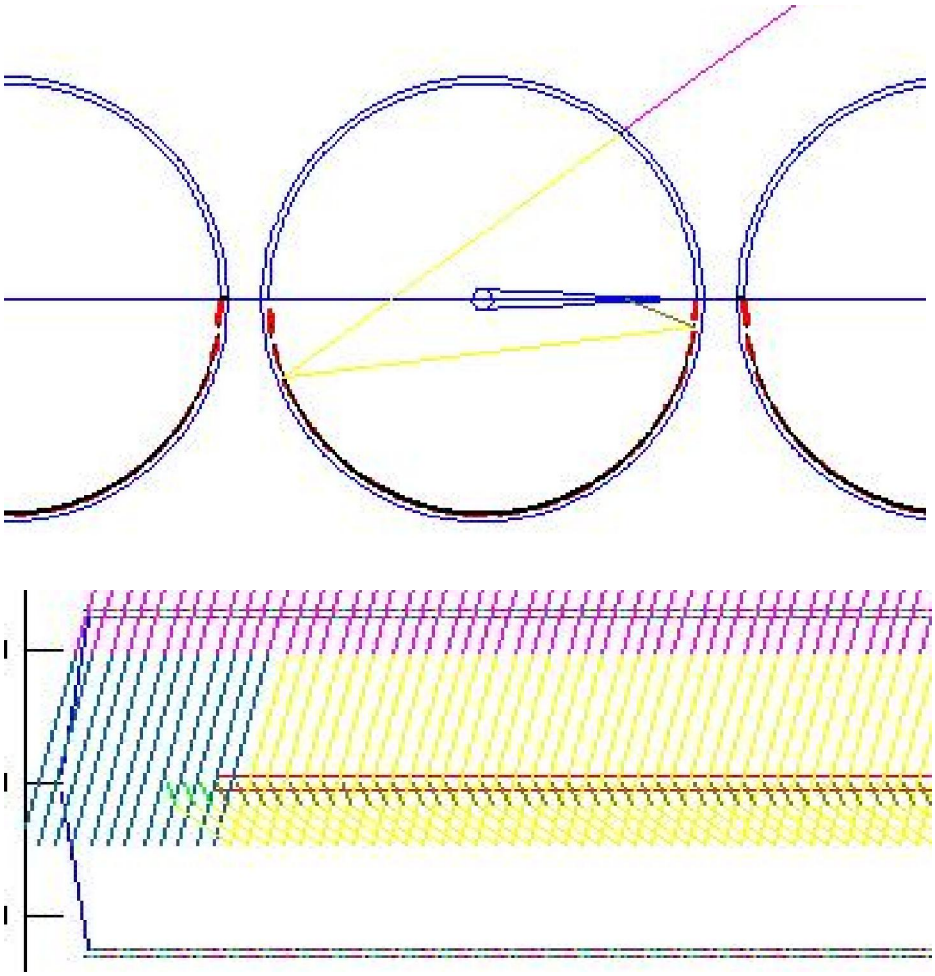

Figure 3.13: Projected ray on both transverse and longitudinal views with multiple reflections

- Next, it is determined whether the reflection of each ray in the array hits the absorber (brown ray) or is reflected out (green ray). See Figure 4.14. The absorber position on the longitudinal view is located along the length of the fin, starting at 100 millimeters from the vacuum pump out end. The ray will reflect out if it hits outside of this fin length (100, 2538.5) interval. The angle of reflection before the ray hits the absorber can be determined by $\theta_{refl,long} = \tan^{-1}\left(\frac{\Delta y_{position}}{\Delta x_{\text{int}ercept}}\right)$, and then the ray will stop at the y position where the ray hits an absorber (predetermined from the transverse view).
- Then, the rays hitting the absorber are counted and applied to the overall efficiency as a proportion of rays hitting the absorber to the total rays hitting the aperture area. See Figure 3.14.

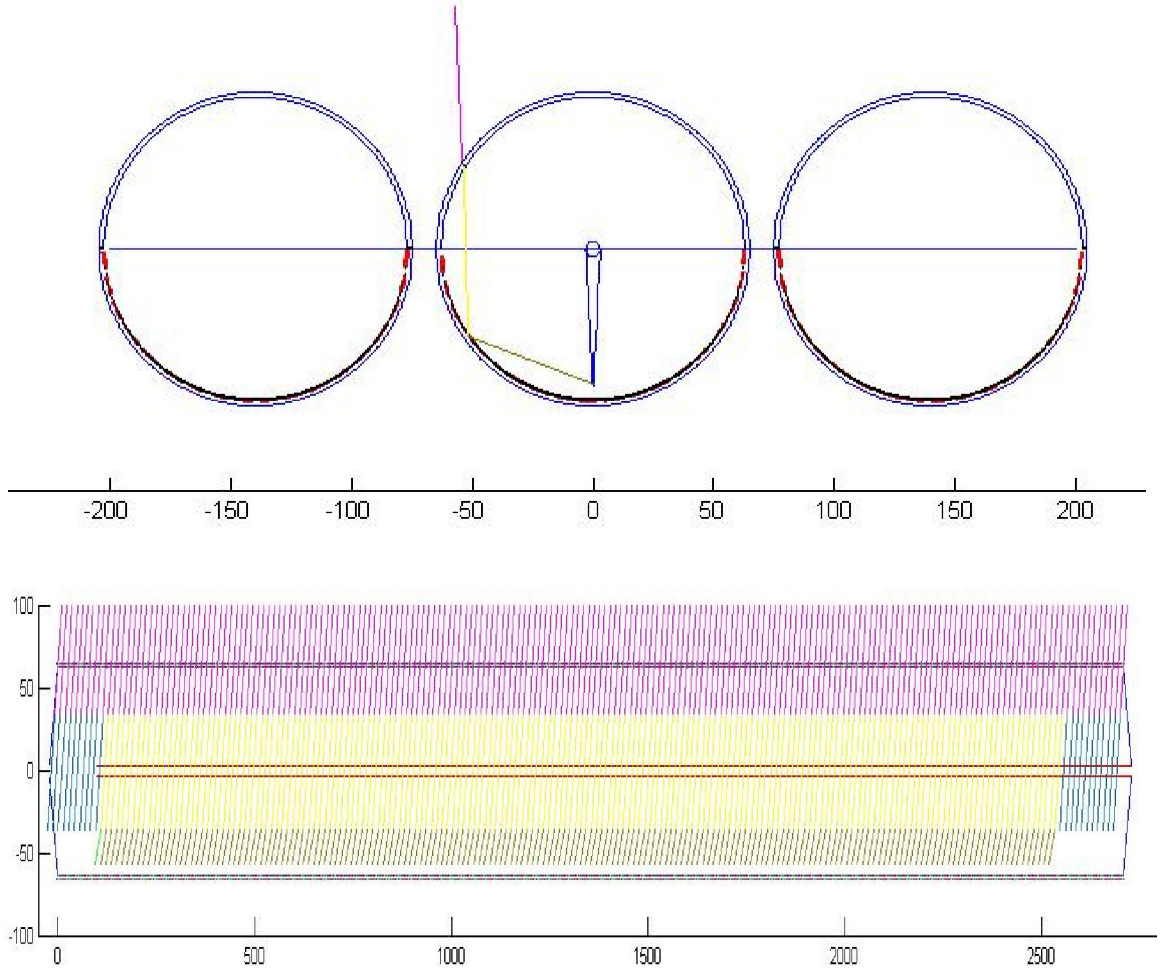

Figure 3.14: Projected beam radiation on transverse (front view) and longitudinal (side view) planes at solar noon

3.4 Diffuse ray-tracing simulation

Diffuse ray-tracing simulation is designed to capture diffuse elements by casting rays from the hemisphere to each point with the assumption that diffuse rays will come from all available directions of the hemisphere normal to the collector plane. These points are uniformly distributed along the effective area, and at each investigated point, rays will be cast uniformly from the hemisphere to the point (Fig.3.15). In the same manner as the

beam ray-tracing, each ray is traced as it loses its intensity from transmittance and reflectance before hitting an absorber fin or being reflected.

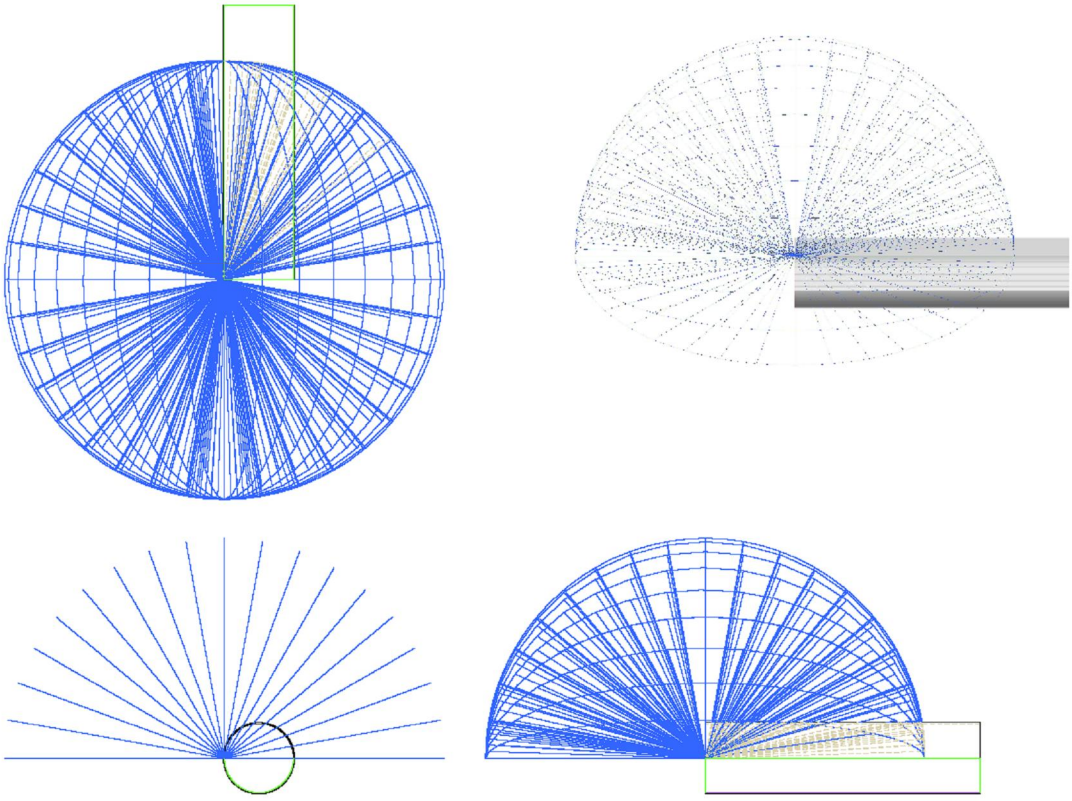

Figure 3.15: Projected diffuse ray elements on multiple views

3.5 Beam/diffuse radiation contribution to overall optical performance estimation

In the diffuse ray tracing simulation, the isotropic diffuse model introduced by Liu and Jordan (1960) has been used in order to find beam and diffuse radiation contributions. Anisotropic models are also widely used in simulation programs such as EnergyPlus, DOE-2.1e, ESP-r, and TRNSYS-TUD. The 1990 Perez model is used as the main estimation technique in most of these codes.

3.5.1 Liu and Jordan approach used in the diffuse ray tracing simulation

Finding the Beam/diffuse radiation contribution to overall optical performance is important in the ray-tracing simulation in order to determine to what degree each type of radiation influences optical efficiency.

First, the total clear sky radiation is calculated by finding atmospheric transmittance of beam and diffuse radiation. The atmospheric transmittance for beam radiation (T_b) can be estimated by using a method presented by Hottel(1976) which is given as

$$\mathrm{T}_b = a_0 + a_1 e^{-k/\cos\theta_z} \tag{3.5}$$

The constants a_0, a_1 and k for the standard atmosphere with 23 km visibility are estimated from a_0^*, a_1^* and k^*, given for altitudes less than 2.5 km, by

$$\begin{aligned} a_0^* &= 0.4237 - 0.00821(6 - A)^2 \\ a_1^* &= 0.5055 + 0.00595(6.5 - A)^2 \\ k^* &= 0.2711 + 0.01858(2.5 - A)^2 \end{aligned} \tag{3.6}$$

where A is altitude of the observer in kilometers.

Correction factors are applied to a_0^*, a_1^* and k^* to adjust to different climate types. The correction factors $r_0 \equiv a_0 / a_0^*$, $r_1 \equiv a_1 / a_1^*$, $r_k \equiv k / k^*$ are given in table 3-2 below.

Table3-2: Correction factors for climate types

Climate Type	$r_0 \equiv a_0 / a_0^*$	$r_1 \equiv a_1 / a_1^*$	$r_k \equiv k / k^*$
Tropical	0.95	0.98	1.02
Mid-Latitude Summer	0.97	0.99	1.02
Subarctic Summer	0.99	0.99	1.01
Mid-Latitude Winter	1.03	1.01	1.00

Liu and Jordan (1960) developed the following empirical relationship between the atmospheric transmission coefficient for beam and diffuse radiation for a clear sky day:

$$T_d = 0.2710 - 0.2939 T_b \tag{3.7}$$

Later, clear sky horizontal beam radiation can be described as

$$G_{cb} = G_o T_b \qquad (\mathrm{W/m^2}) \tag{3.8}$$

And also, the clear sky horizontal diffuse radiation is

$$G_{cd} = G_o T_d \qquad (\mathrm{W/m^2}) \tag{3.9}$$

where extraterrestrial radiation is

$$G_o = G_{sc}\left(1 + 0.033\cos\left(\frac{360n}{365}\right)\right)\cos\theta_z \qquad (\mathrm{W/m^2}) \tag{3.10}$$

Total clear sky radiation (G_c) can be expressed as the summation between beam (G_{cb}) and diffuse radiation (G_{cd}).

$$G_c = G_{cb} + G_{cd} \qquad (\mathrm{W/m^2}) \tag{3.11}$$

Fig. 3.16 illustrates beam and diffuse components of clear sky radiation. The estimated diffuse radiation is close to constant with small dips at the beginning and the end of the day.

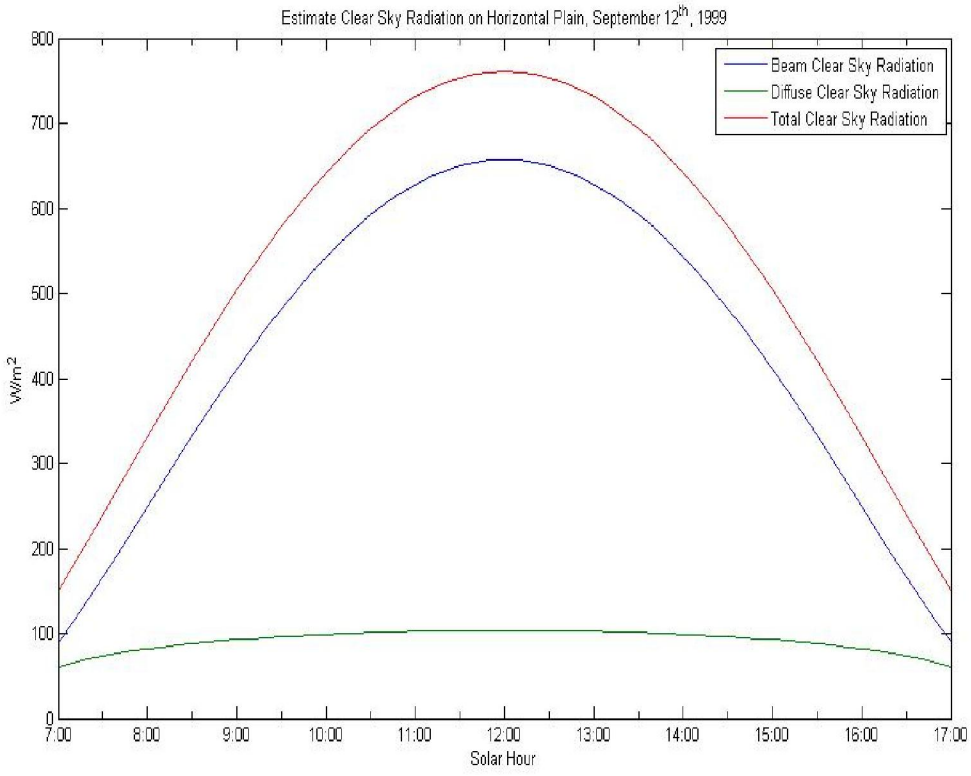

Figure 3.16: Estimated clear sky radiation on horizontal, Sept. 12th 1999

By comparing measured and estimated clear sky radiation, total clear sky radiation is used to find beam and diffuse components of clear and cloudy day radiation. Stauter and Klien (1979) developed a correlation between the proportion of diffuse radiation and measured radiation I_d/I (G_d/G_H) to the proportion of measured radiation and clear sky radiation I/I_c (G_H/G_c), on hourly radiation (instantaneous radiation). The equation, below, representing this correlation is

$$\frac{G_d}{G_H} = \begin{cases} 1.00 - 0.1\dfrac{G_H}{G_c} & ,0 \le \dfrac{G_H}{G_c} < 0.48 \\ 1.11 + 0.0396\left(\dfrac{G_H}{G_c}\right) - 0.789\left(\dfrac{G_H}{G_c}\right)^2 & ,0.48 \le \dfrac{G_H}{G_c} < 1.10 \\ 0.20 & ,1.10 \le \dfrac{G_H}{G_c} \end{cases} \quad (3.12)$$

where G_H is measured instantaneous radiation.

Beam and diffuse components of total radiation on a tilted surface are estimated by using the equation from Liu and Jordan (1963). They proposed that the radiation on a tilted surface consists of three components: beam radiation, diffuse solar radiation, and solar radiation diffusely reflected from the ground with diffuse ground reflectance (ρ). The value of ρ is set at 0.2 when there is no snow and 0.7 when there is a fresh snow cover. So, total solar radiation on a tilted surface can be written as

$$I_T = [I_b R_b] + \left[I_d \left(\frac{1+\cos\beta}{2} \right) \right] + \left[(I_b + I_d)\rho \left(\frac{1-\cos\beta}{2} \right) \right] \quad (3.13)$$

where the ratio of beam radiation on a tilted surface, R_b, is

$$R_b = \frac{\cos\theta}{\cos\theta_z} \tag{3.14}$$

Diffuse solar radiation and solar radiation diffusely reflected from the ground can be added together as I_{Td}. So, we rewrite the ratio between instantaneous beam radiation on tilted surface, G_{Tb} and instantaneous total radiation on a tilted surface, G_T as

$$\frac{G_{Tb}}{G_T} = \frac{[G_b R_b]}{G_T} \tag{3.15}$$

and the ratio between instantaneous diffuse radiation on a tilted surface G_{Td} and instantaneous total radiation on a tilted surface, G_T,

$$\frac{G_{Td}}{G_T} = \frac{\left[G_d\left(\frac{1+\cos\beta}{2}\right)\right] + \left[(G_b + G_d)\rho\left(\frac{1-\cos\beta}{2}\right)\right]}{G_T} \tag{3.16}$$

The percent of contribution of overall radiation of beam and diffuse elements are plotted to show beam and diffuse contribution characteristics during a particular day. Figure 3.17 reveals an equal contribution between beam and diffuse radiation in early morning. When the sky began to clear during the rest of the day, a higher beam contribution than diffuse contribution (September 2nd 1999) is shown. The higher percentage of diffuse radiation than beam radiation was in the earlier part of the day (September 12th 1999). Then, the

sky cleared up as the beam contribution went higher than the diffuse contribution in the later afternoon (Figure 3.18).

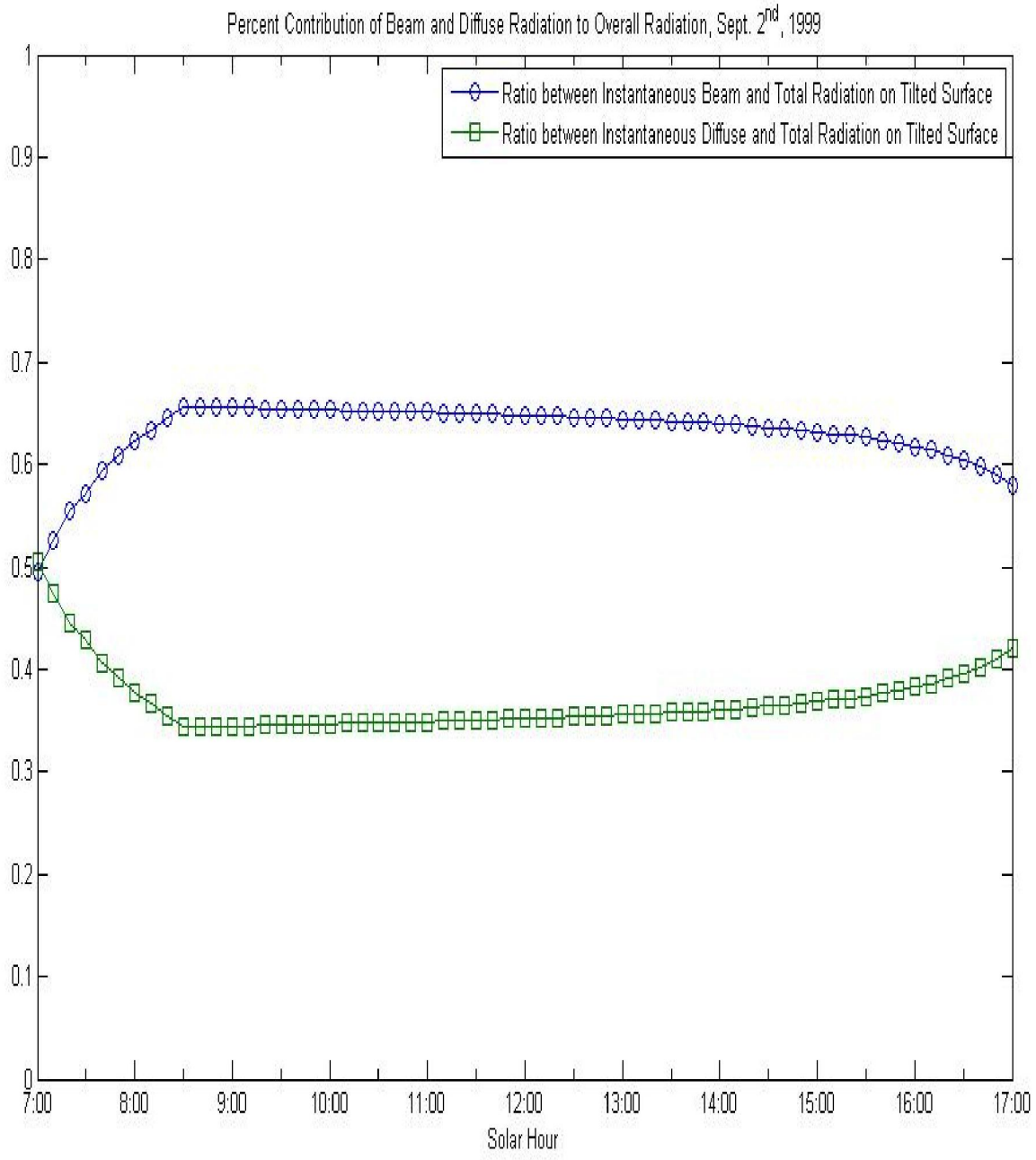

Figure 3.17: Estimated percent contribution of beam and diffuse radiation to overall radiation, Sacramento California September 2nd 1999

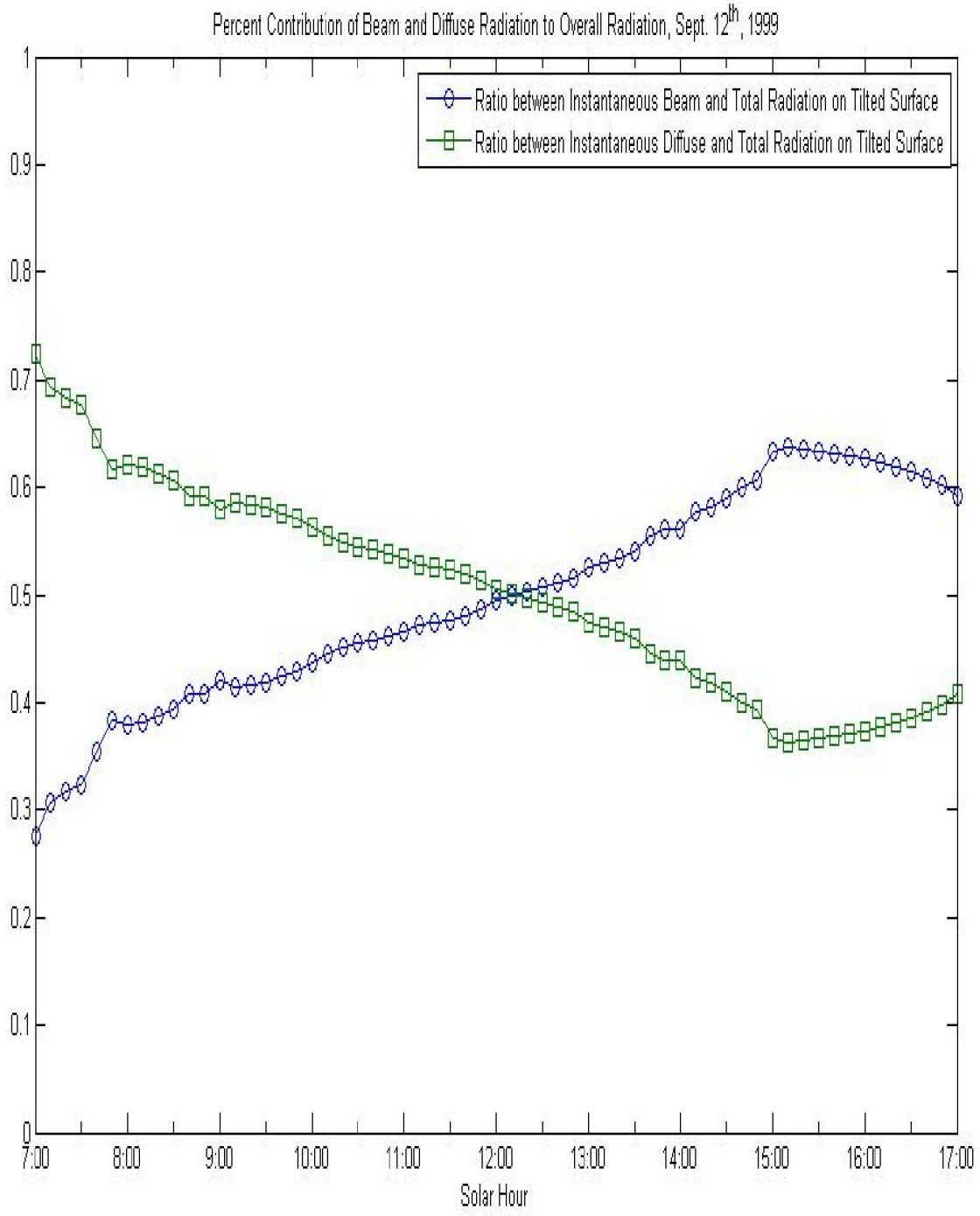

Figure 3.18: Estimated percent contribution of beam and diffuse radiation to overall radiation, Sacramento California September 12th 1999

A high diffuse or cloudy condition in the morning and a higher beam contribution toward the end of the day as the weather improved in visibility effect both fin arrangements as shown in Figure 3.19. The percent contributions of beam and diffuse radiation are directly applied to the instantaneous optical efficiency model. Figure 3.19 depicts beam and diffuse contributions to optical efficiency on both horizontal and vertical fin arrangements.

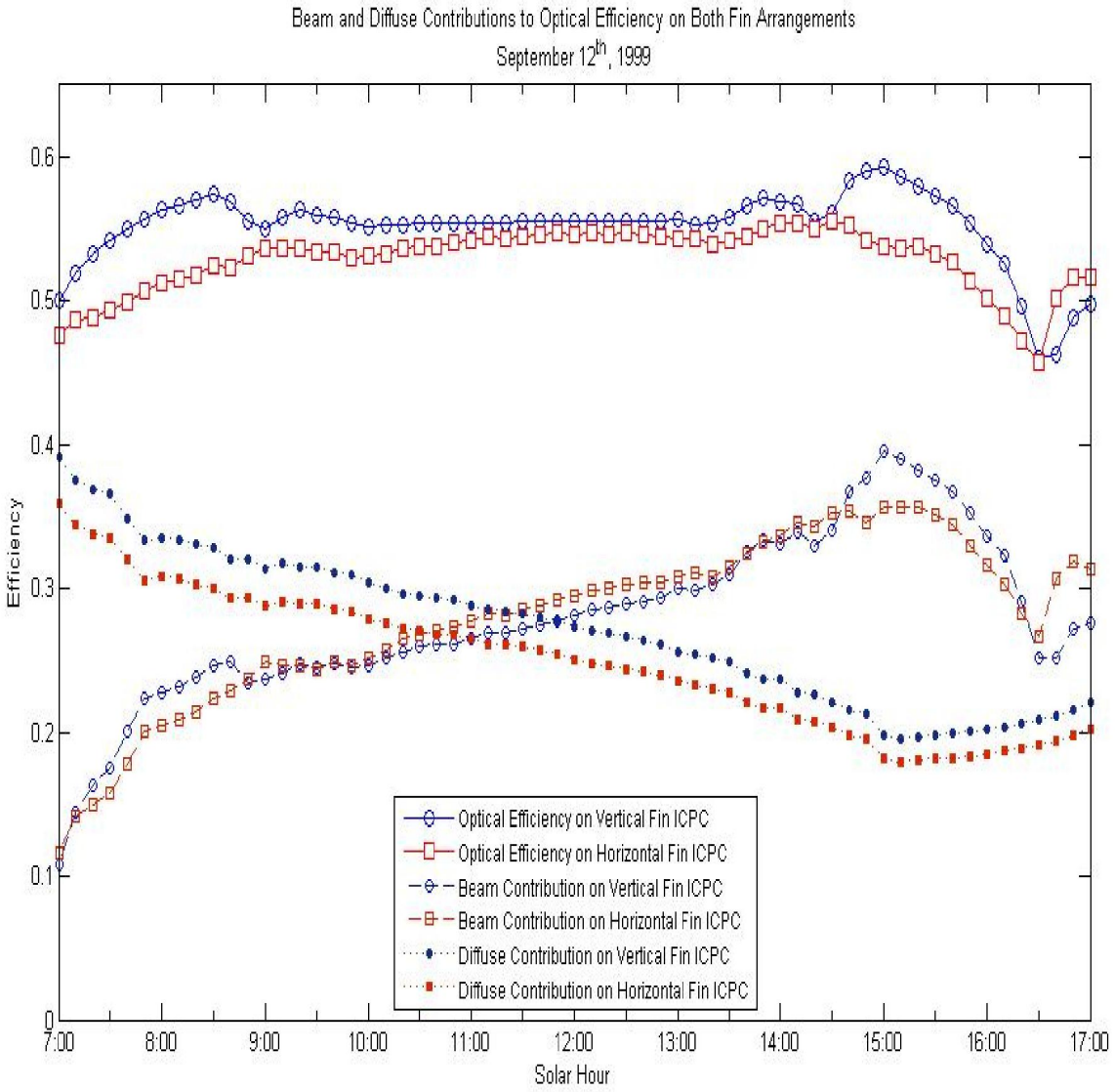

Figure 3.19: Beam and diffuse contributions to optical efficiency on both fin arrangements

3.5.2 Other approaches for finding beam and diffuse radiation

In the isotropic modeling approach, the intensity of sky diffuse radiation is assumed to be uniform over the sky hemisphere. Among the various isotropic models are those presented by Hottel and Woertz, 1942 as cited by [Duffie and Beckman, 1991], [Liu and Jordan, 1960] and [Badescu, 2002]. In the ray tracing model in this research, the Liu and Jordan (1963) equation, which assumes isotropic diffuse radiation over the hemisphere viewed by the collector, is used.

In the isotropic case, to provide a more detailed estimation of the effects of diffuse radiation, sky and ground diffuse radiation could have been separated when they were traced over the hemisphere viewed by the collector.

In further attempts to predict insolation on tilted surfaces, anisotropic models have been studied. An empirical validation of seven models widely used in building energy simulation codes is determined, Loutzenhiser et.al. (2007). The seven models are Hottel and Woertz (1942), Klucher (1979), Hay and Davies (1980), Reindl et al.(1990a), Reindl et al., (1990b), Muneer (1997), Perez et al. (1987), and Perez et al. (1990). In the anisotropic models, the diffuse component is composed of an isotropic diffuse component, $I_{T,d,iso}$ (uniform irradiance from the sky hemisphere), a circumsolar diffuse component, $I_{T,d,cs}$ (resulting from the forward scattering of solar radiation and concentrated in an area close to the sun), a horizon brightening component, $I_{T,d,hb}$ (concentrated in a band near the horizon and most pronounced in clear skies), and a reflected component that quantifies the radiation reflected from the ground to the tilted

surface, $I_{T,d,g}$. A complete version total solar irradiance containing all diffuse components is given in equation 3.17.

$$I_T = I_{T,b} + I_{T,d,iso} + I_{T,d,cs} + I_{T,d,hb} + I_{T,d,g} \tag{3.17}$$

Klucher (1979) stated that the isotopic model provides a good prediction for overcast skies but underestimates irradiance under clear and partly overcast conditions, when there is increased intensity near the horizon and in the circumsolar region of the sky. Using a model developed by Temps and Coulson (1977) and incorporating conditions of cloudy skies and clear skies, Klucher developed the following model:

$$I_T = I_{h,b}R_b + I_{h,d}\left(\frac{1+\cos\beta}{2}\right)\left[1 + F'\sin^3\left(\frac{\beta}{2}\right)\right] \times \left[1 + F'\cos^2\theta\sin^3\theta_z\right] + I_h\rho\left(\frac{1-\cos\beta}{2}\right) \tag{3.18}$$

where F' is a clearness index a modulating function given by

$$F' = 1 - \left(\frac{I_{h,d}}{I_h}\right)^2 \tag{3.19}$$

The clearness index F' is included with the two modifying factors in the sky diffuse component $I_{h,d}$. The first of the modifying expressions is a horizon brightening factor and the second modifies the effect of circumsolar radiation. Under overcast skies,

the clearness index F' becomes zero and the model reduces to the isotropic model. When F' approaches 1, the Klucher model becomes, for clear sky conditions, the model of Temps and Coulson.

The Perez model provides a more detailed analysis of the isotropic diffuse, circumsolar and horizon brightening radiation by using empirically derived coefficients (Perez et al., 1990). He also compared his model to other models. This model is based on three basic elements:

- a geometrical representation of the sky dome incorporating variable circumsolar and horizon atmosphere brightening,
- a parametric description of the insolation conditions, based on available radiative quantities,
- an experimentally-derived law governing the variations of circumsolar and horizon brightening with the insolation conditions.

In the Perez model the total irradiance on a tilted surface is

$$I_T = I_{h,b}R_b + I_{h,d}\left[(1-F_1)\left(\frac{1+\cos\beta}{2}\right) + F_1\frac{a}{b} + F_2\sin\beta\right] + I_h\rho\left(\frac{1-\cos\beta}{2}\right) \quad (3.20)$$

where F_1 and F_2 are respectively circumsolar and horizon brightness coefficients, while a and b takes the incidence angle of the sun on the collector slope into account. The terms a and b are computed using equation 3.21 and 3.22 below.

$$a = \max(0, \cos\theta) \tag{3.21}$$

$$b = \max(\cos 85°, \cos\theta_z) \tag{3.22}$$

F_1 and F_2 depend on the sky condition parameters clearness ε and brightness Δ via equations 3.23 and 3.24.

$$F_1 = \max\left[0, \left(f_{11} + f_{12}\Delta + \frac{\pi\theta_z}{180} f_{13}\right)\right] \tag{3.23}$$

$$F_2 = f_{21} + f_{22}\Delta + \frac{\pi\theta_z}{180} f_{23} \tag{3.24}$$

where

$$\varepsilon = \frac{\frac{I_{h,d} + I_n}{I_{h,d}} + 5.535 \cdot 10^{-6}\theta_z^3}{1 + 5.535 \cdot 10^{-6}\theta_z^3} \tag{3.25}$$

$$\Delta = m\frac{I_{h,d}}{I_{on}} \tag{3.26}$$

Then, by a statistical analysis of empirical data for specific locations, coefficients f_{11}, f_{12}, f_{13}, f_{21}, f_{22}, and f_{23}, are determined. See Perez (1987).

However, for simplicity, in this work the isotropic diffuse model will be used for both ground reflected and sky diffuse radiation. Should agreement between experimental and modeled data indicate poor agreement, elevating this model to greater fidelity will be explored.

3.6 Summary

This chapter presented step-by-step details of the ray tracing method and provided the equations involved in finding and projecting the beam and diffuse radiation among the relevant surfaces. The results of the ray tracing procedure are stated in the form of optical efficiency. The results of the detailed analysis of the graphical ray tracing are presented. Other possible approaches to determining the diffuse contribution are also presented.

The next chapter will incorporate thermal loss into the modeling and also show how thermal loss may be estimated from a color-coded thermal mapping table. Comparisons of estimated and measured efficiency will be presented later in that chapter. Energy graphs for both estimated and measured performance will also be shown.

CHAPTER 4

EXPERIMENTAL VALIDATION OF THE RAY TRACING APPROACH AND MODEL VERIFICATION

4.1 Introduction

Before the novel ICPC was installed at the Sacramento demonstration, seven ICPC modules of each absorber fin orientation were tested on the Sandia National Laboratory's two-axis tracking (AZTRAK) platform (Winston et al, 1997). This platform allows a non-tracking solar collector to be positioned at any angle between zero and 90 degrees in any orientation. Early instantaneous efficiency estimation models were formulated using regression analysis from these experiments. See appendix A.1. As described in section 3.3, a ray tracing model has been designed to investigate the optical performance of both the horizontal and vertical fin versions of this collector. In this Chapter this model is validated against the Sandia National Laboratory results.

4.2 Initial experimental results

Two fourteen tube modules were tested on Sandia National Laboratory's two-axis tracking (AZTRAK) platform located at the National Solar Thermal Test Facility, Albuquerque, NM. See figure 4.1.

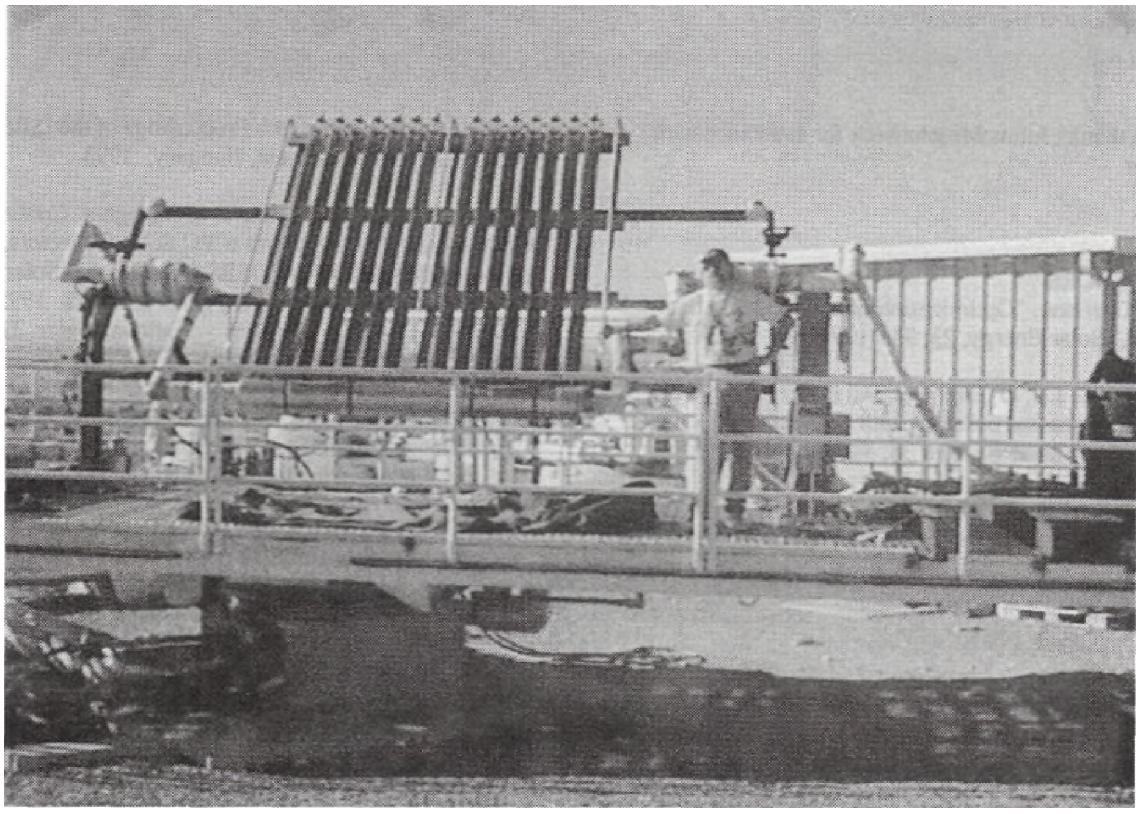

Figure 4.1: The AZTRAK rotating platform at the National Solar Thermal Test Facility (NSTTF) located at Sandia National Laboratories in Albuquerque, NM

A solar elevation tracker is attached to the rotating platform allowing the ICPC array to be positioned in any direction at any angle between -90 degrees and 90 degrees. "The prototype test module for each type of collector is a close-packed array, with 150 mm center to center spacing, and all tubes connected in parallel to a common supply and return manifold. A water filled loop was used in the AZTRAK system to determine the

optical efficiency and angular responses. A silicone-based oil filled loop was used to measured thermal efficiency and heat losses at temperatures approaching 200 °C" (Winston et al., 1999). By adjusting the tracking of the platform to the desired incident angle of the sun's rays, performance of the novel ICPC solar collector at various specified angles in the transverse and longitudinal evacuated tube directions were experimentally determined. To track the full sky coverage optical performance of the novel ICPC solar collector, the experimental incident angles were set between 0 degrees to 70 degrees and 0 degrees to -70 degrees in both transverse and longitudinal orientations.

Three measured incident angle responses were recorded at each incident angle. The error bars are believed to represent instrumentation errors. "Ten positions on each side (positive incidence and negative incidence) for the transverse orientation were tested to find the thermal responses at each angle. A regression function was established to fit the measured points along each side" (Winston et al., 1999). See figure 4.2 and figure 4.3. However, only the data from the operation of the array are used to validate the ray tracing model.

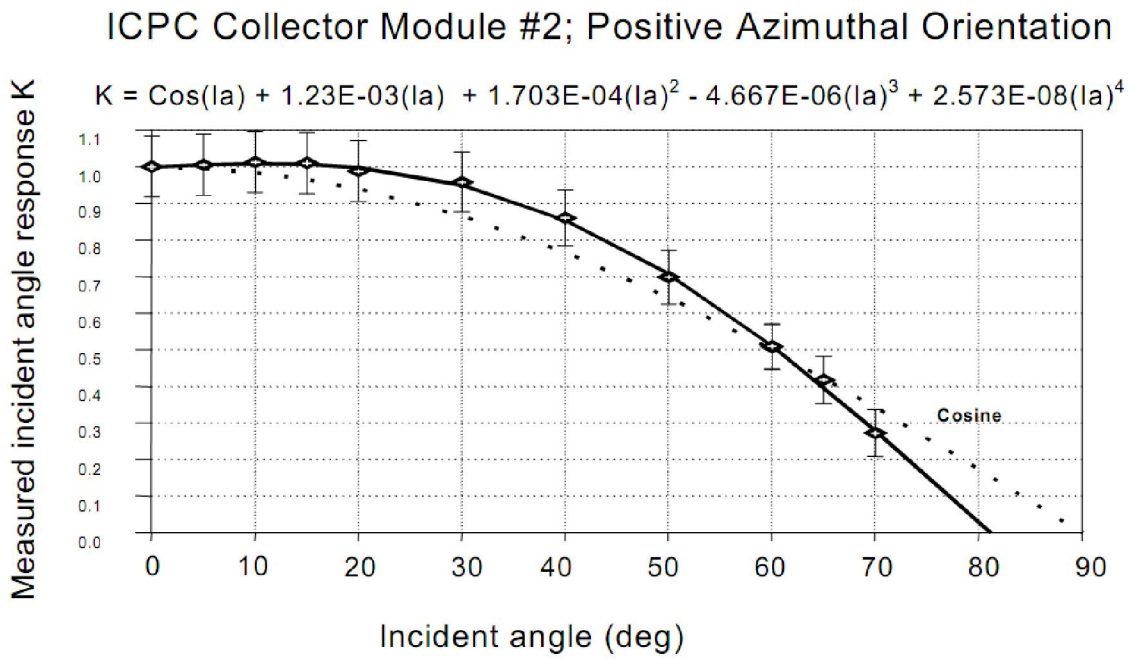

Figure 4.2: Measured Incidence Angle Modifier multiplied by cosine θ for the horizontal fin orientation for positive angles of incidence on transverse plane

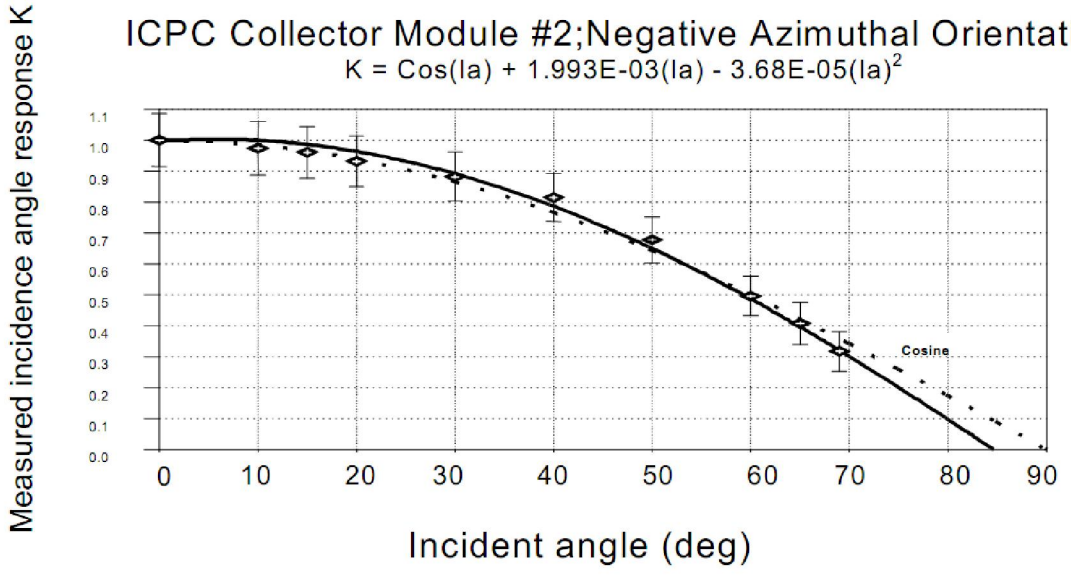

Figure 4.3: Measured Incidence Angle Modifier multiplied by cosine θ for the horizontal fin orientation for negative angles of incidence on transverse plane

4.3 Experimental validation and ray tracing model verification

To validate the ray-tracing model, the ray-tracing model will be made to recreate the Sandia experiment on the ICPC modules in 1998. The characteristics of the ICPC module are being studied as some properties of the ICPC are not reported in Winston 1998. Thus, the matching of the experimental and the ray-tracing data will be used to provide best fit estimates of the ICPC component properties. In order to verify the ray-tracing model, multiple ray tracing runs are performed while varying the values of these characteristics within reasonable ranges. Since there are data available only for the horizontal fin arrangement ICPC, the comparisons will be strictly only for the transverse plane of the ICPC. The range of each factor is selected to form a face-centered central composite design experiment (See table 4.1.):

(1) Extinction coefficient (K) of the glass-cover from 4 to13 m^{-1}

(2) Reflectivity of the reflective surface from 0.84 to 0.97

(3) Gap between the reflective surface and the absorber fin from 1.5 to 8 mm

(4) Interference of adjacent tubes (pitch), center to center spacing between tubes from 135 to 160 mm

(5) Absorptance of the absorber fin from 0.90 to 0.98

(6) Effective aperture width in the transverse view, from 120 to 125 mm.

The effective aperture width in the transverse view represents a reference area that is used in the efficiency calculation. The effective aperture area is defined and described in 2.2.2.

The optical efficiency of each run is then plotted and compared with the experimental data. The sum of squares differences between the efficiencies from experimental data and from ray-tracing process is calculated. Then, the least squares design is identified and verified for the ray-tracing analysis.

Table 4-1: Face-centered central composite design for ray tracing verification

Run Order	Pitch	Gap	Absorptance	Reflectivity	Effective aperture width	K	Y=SSD
1	135	1.5	0.90	0.84	120	4	0.134216
2	160	1.5	0.90	0.84	120	4	0.082936
3	135	8.0	0.90	0.84	120	4	0.397895
4	160	8.0	0.90	0.84	120	4	0.323996
5	135	1.5	0.98	0.84	120	4	0.032234
6	160	1.5	0.98	0.84	120	4	0.01451
7	135	8.0	0.98	0.84	120	4	0.164703
8	160	8.0	0.98	0.84	120	4	0.115172
9	135	1.5	0.90	0.97	120	4	0.038977
10	160	1.5	0.90	0.97	120	4	0.019541
11	135	8.0	0.90	0.97	120	4	0.175164
12	160	8.0	0.90	0.97	120	4	0.126404
13	135	1.5	0.98	0.97	120	4	0.086113
14	160	1.5	0.98	0.97	120	4	0.10941
15	135	8.0	0.98	0.97	120	4	0.037392
16	160	8.0	0.98	0.97	120	4	0.020363
17	135	1.5	0.90	0.84	125	4	0.222874
18	160	1.5	0.90	0.84	125	4	0.158634
19	135	8.0	0.90	0.84	125	4	0.537383
20	160	8.0	0.90	0.84	125	4	0.454323
21	135	1.5	0.98	0.84	125	4	0.064984
22	160	1.5	0.98	0.84	125	4	0.030186
23	135	8.0	0.98	0.84	125	4	0.264925
24	160	8.0	0.98	0.84	125	4	0.203035
25	135	1.5	0.90	0.97	125	4	0.068882
26	160	1.5	0.90	0.97	125	4	0.032719
27	135	8.0	0.90	0.97	125	4	0.277925
28	160	8.0	0.90	0.97	125	4	0.217009
29	135	1.5	0.98	0.97	125	4	0.042532
30	160	1.5	0.98	0.97	125	4	0.044161
31	135	8.0	0.98	0.97	125	4	0.088611
32	160	8.0	0.98	0.97	125	4	0.055567
33	135	1.5	0.90	0.84	120	13	0.191131
34	160	1.5	0.90	0.84	120	13	0.123083

Run Order	Pitch	Gap	Absorptance	Reflectivity	Effective aperture width	K	Y=SSD
35	135	8.0	0.90	0.84	120	13	0.48404
36	160	8.0	0.90	0.84	120	13	0.392796
37	135	1.5	0.98	0.84	120	13	0.054749
38	160	1.5	0.98	0.84	120	13	0.020905
39	135	8.0	0.98	0.84	120	13	0.226566
40	160	8.0	0.98	0.84	120	13	0.159917
41	135	1.5	0.90	0.97	120	13	0.060914
42	160	1.5	0.90	0.97	120	13	0.025019
43	135	8.0	0.90	0.97	120	13	0.238449
44	160	8.0	0.90	0.97	120	13	0.172524
45	135	1.5	0.98	0.97	120	13	0.063332
46	160	1.5	0.98	0.97	120	13	0.071058
47	135	8.0	0.98	0.97	120	13	0.068965
48	160	8.0	0.98	0.97	120	13	0.035215
49	135	1.5	0.9	0.84	125	13	0.293089
50	160	1.5	0.9	0.84	125	13	0.211927
51	135	8.0	0.9	0.84	125	13	0.632688
52	160	8.0	0.9	0.84	125	13	0.532292
53	135	1.5	0.98	0.84	125	13	0.105053
54	160	1.5	0.98	0.84	125	13	0.053809
55	135	8	0.98	0.84	125	13	0.339246
56	160	8	0.98	0.84	125	13	0.260116
57	135	1.5	0.9	0.97	125	13	0.108362
58	160	1.5	0.9	0.97	125	13	0.0555
59	135	8	0.9	0.97	125	13	0.353404
60	160	8	0.9	0.97	125	13	0.275254
61	135	1.5	0.98	0.97	125	13	0.042488
62	160	1.5	0.98	0.97	125	13	0.02811
63	135	8	0.98	0.97	125	13	0.136367
64	160	8	0.98	0.97	125	13	0.086381
65	135	4.75	0.94	0.905	122.5	8.5	0.123454
66	160	4.75	0.94	0.905	122.5	8.5	0.073519
67	147.5	1.5	0.94	0.905	122.5	8.5	0.035245
68	147.5	8	0.94	0.905	122.5	8.5	0.204329
69	147.5	4.75	0.9	0.905	122.5	8.5	0.178883
70	147.5	4.75	0.98	0.905	122.5	8.5	0.037715
71	147.5	4.75	0.94	0.84	122.5	8.5	0.174227
72	147.5	4.75	0.94	0.97	122.5	8.5	0.039306
73	147.5	4.75	0.94	0.905	120	8.5	0.064007
74	147.5	4.75	0.94	0.905	125	8.5	0.131493
75	147.5	4.75	0.94	0.905	122.5	4	0.073238
76	147.5	4.75	0.94	0.905	122.5	13	0.114184
77	147.5	4.75	0.94	0.905	122.5	8.5	0.092525

4.4 Results

A total of 77 runs of ray-tracing analysis has been performed individually and analyzed. Figure 4.4 depicts an example comparison plot (Run #6) of ray tracing data, experimental data, and the Sandia experiment regression function. The sum of squares differences for each of the runs are presented in the SSD column in table 4-1. Contour plots between the two factors and the response are then generated. See figure 4.5.

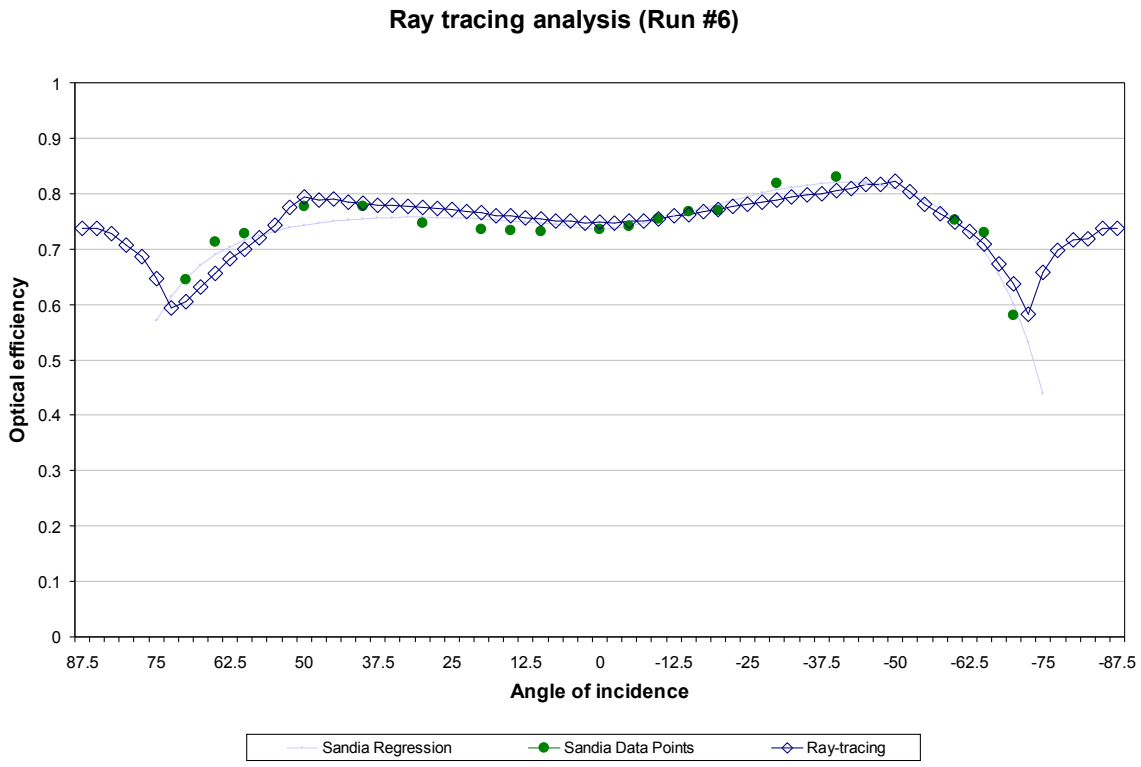

Figure 4.4: Optical efficiency plots for the ray tracing analysis (Run #6)

Table 4.2 shows some of the good fits within the face-center composite design runs.

Table 4-2: Other good fits in the ray tracing verification

Run Order	Pitch	Gap	Absorptance	Reflectivity	Effective aperture width	K	Y=SSD
5	135	1.5	0.98	0.84	120	4	0.032234
6	160	1.5	0.98	0.84	120	4	0.01451
9	135	1.5	0.90	0.97	120	4	0.038977
10	160	1.5	0.90	0.97	120	4	0.019541

Run Order	Pitch	Gap	Absorptance	Reflectivity	Effective aperture width	K	Y=SSD
15	135	8.0	0.98	0.97	120	4	0.037392
16	160	8.0	0.98	0.97	120	4	0.020363
22	160	1.5	0.98	0.84	125	4	0.030186
26	160	1.5	0.90	0.97	125	4	0.032719
29	135	1.5	0.98	0.97	125	4	0.042532
30	160	1.5	0.98	0.97	125	4	0.044161
38	160	1.5	0.98	0.84	120	13	0.020905
42	160	1.5	0.90	0.97	120	13	0.025019
48	160	8.0	0.98	0.97	120	13	0.035215
61	135	1.5	0.98	0.97	125	13	0.042488
62	160	1.5	0.98	0.97	125	13	0.02811
67	147.5	1.5	0.94	0.905	122.5	8.5	0.035245
70	147.5	4.75	0.98	0.905	122.5	8.5	0.037715
72	147.5	4.75	0.94	0.97	122.5	8.5	0.039306

By minimizing the SSD, the following parameter value settings are found:

(1) Extinction coefficient (K) of the glass-cover of 4 m^{-1}

(2) Reflectivity of the reflective surface of 0.9270

(3) Gap between the reflective surface and the absorber fin of 4 mm

(4) Interference of adjacent tubes (pitch), center to center spacing between tubes of 154 mm

(5) Absorptance of the absorber fin of 0.98

(6) Effective aperture width, in the transverse view, of 122 mm

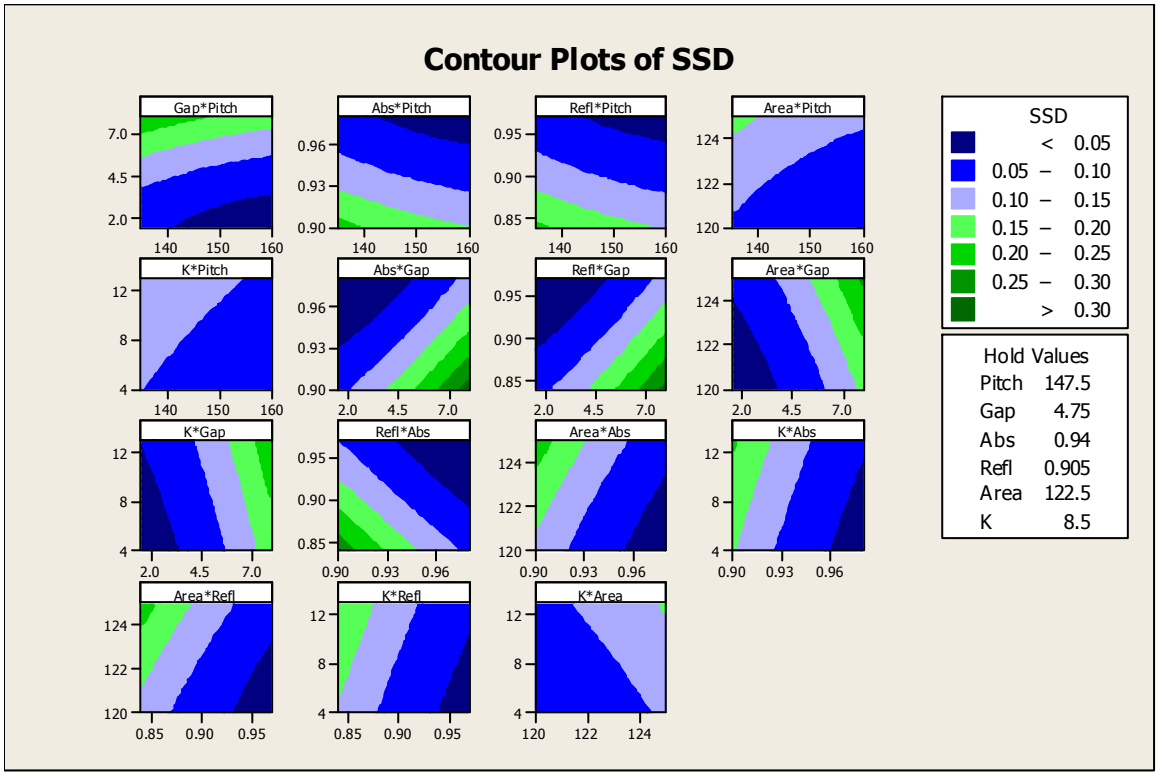

Figure 4.5: Contour plots of sum of square differences

Figure 4.6 shows the minimizing plots of the SSDs with the global minimum of 0.0176. Then, the ray tracing confirmation run of the minimizing design is analyzed. The result of ray-tracing analysis is plotted with the experimental data. See figure 4.7.

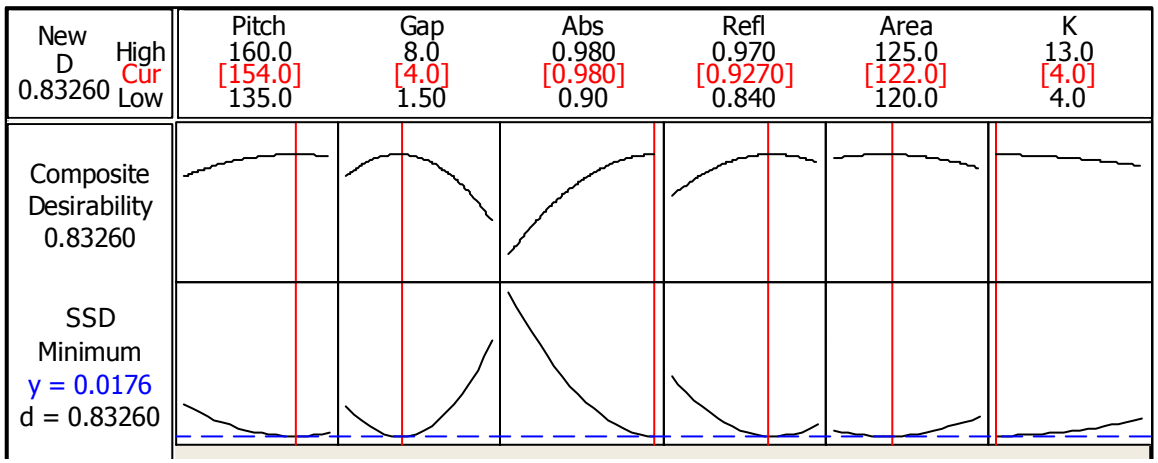

Figure 4.6: Minimizing the SSDs

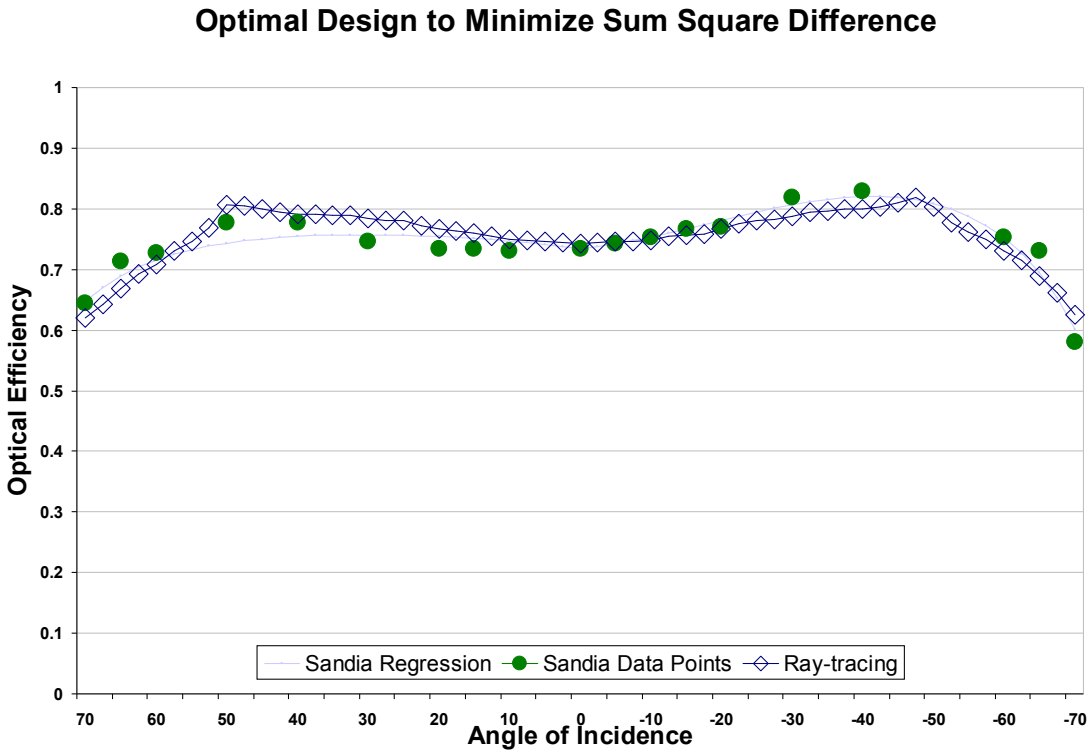

Figure 4.7: Optical efficiency plots of ray tracing analysis of the minimizing design

Table 4-3: Minimizing parameter values

Pitch	Gap	Absorptance	Reflectivity	Effective aperture	K	Y=SSD
154	4.0	0.98	0.927	122	4	0.01387

Individual ray intensities are plotted at each angle to validate the optical efficiency plot. At zero degrees incident angle, the first half of the rays strikes the fin directly. Ray intensities are attenuated by the transmittance-absorptance of the glass cover and the absorptance of the selective surface of absorber fin. As seen on figure 4.8, the ray intensities near the edge of the glass cover have lower intensities due to the extreme incident angle as they are reduced by the transmittance-absorptance of the glass cover. Later, half of rays show lower intensity due to hitting the reflector. Some rays also

escape through the gap between fin and the reflector, showing zero intensity. Multiple hits are also shown as a further reduction of intensity factor. Figure 4.9 shows a comparison between 30 degrees and -30 degrees angle of incidence. The 30 degrees angle of incidence shows more multiple reflector hits than the -30 degrees angle of incidence due to mostly single reflection hits. This will result in a slightly lower optical efficiency.

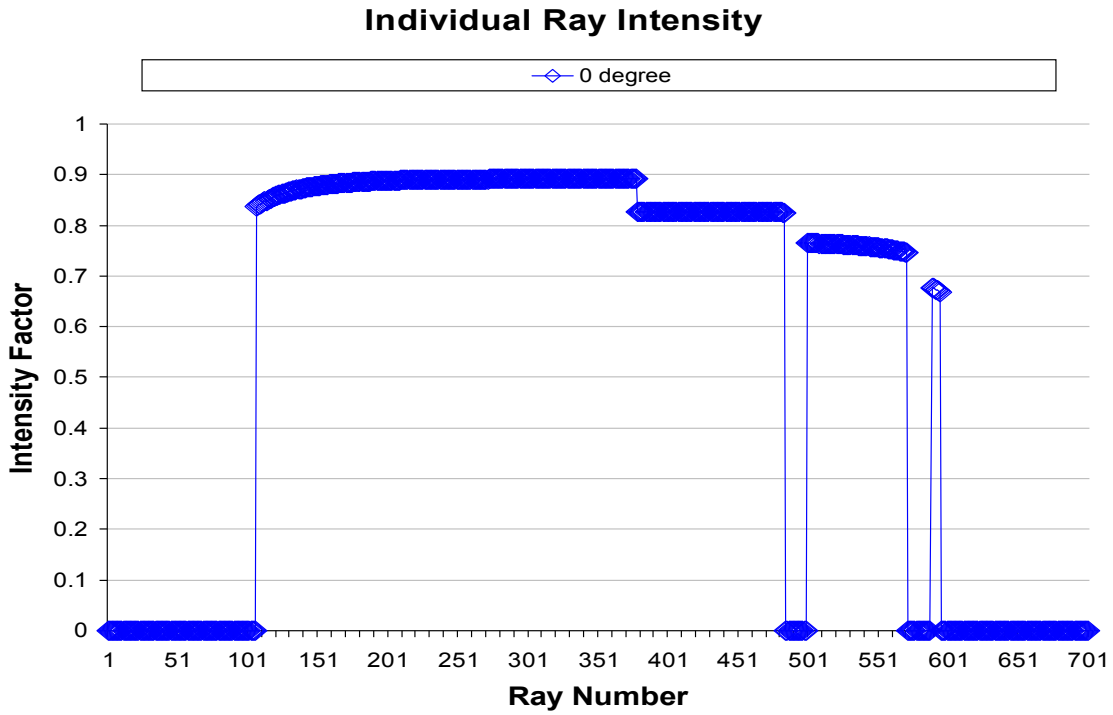

Figure 4.8: Intensity factor plots of ray striking analysis at 0 degrees angle of incidence

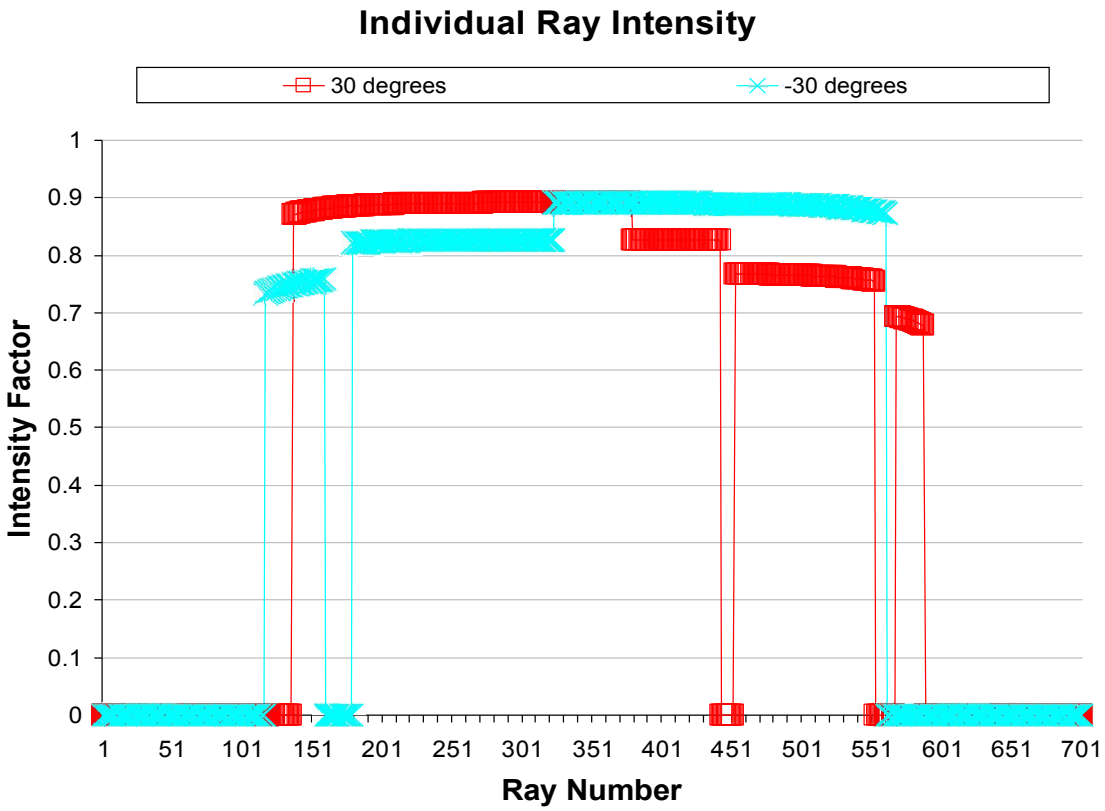

Figure 4.9: Comparing intensity factor plots of ray striking analysis between 30 degrees and -30 degree angle of incidence

Figure 4.10 and 4.12 show how the rays are blocked by the adjacent tube. The blocked rays are attenuated by passing through the glass cover of the adjacent tube. Figure 4.11 and 4.13 also show greater reduction of the ray intensity as the ray becomes closer to being tangent to the glass cover circumference, eventually going to a zero transmittance due to complete reflection off the glass cover. At a 60 degree angle of incidence there are more multiple reflector hits than at -60 degrees resulting in a lower optical efficiency at 60 degrees angle of incidence than for -60 degrees.

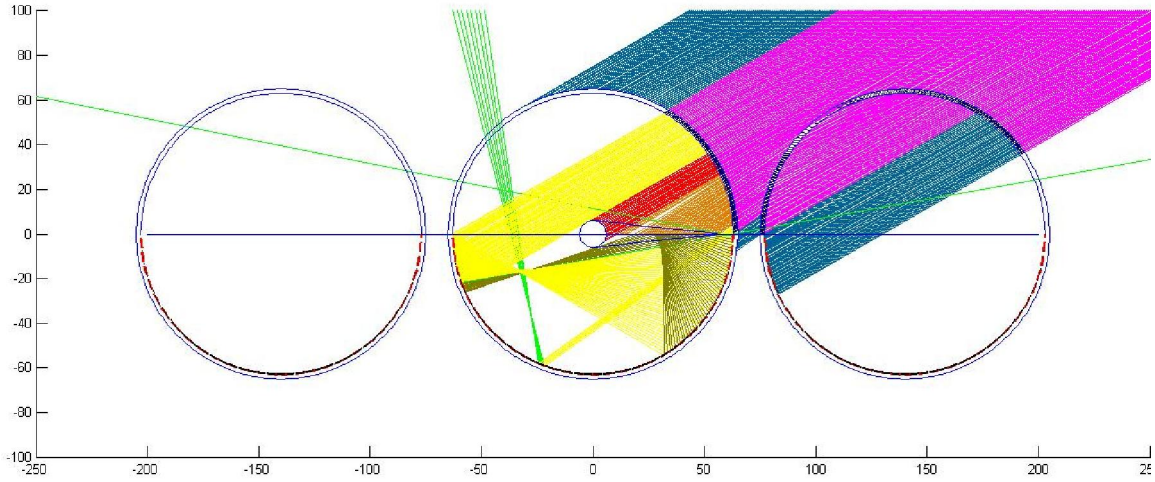

Figure 4.10: Ray tracing analysis at 60 degrees angle of incidence

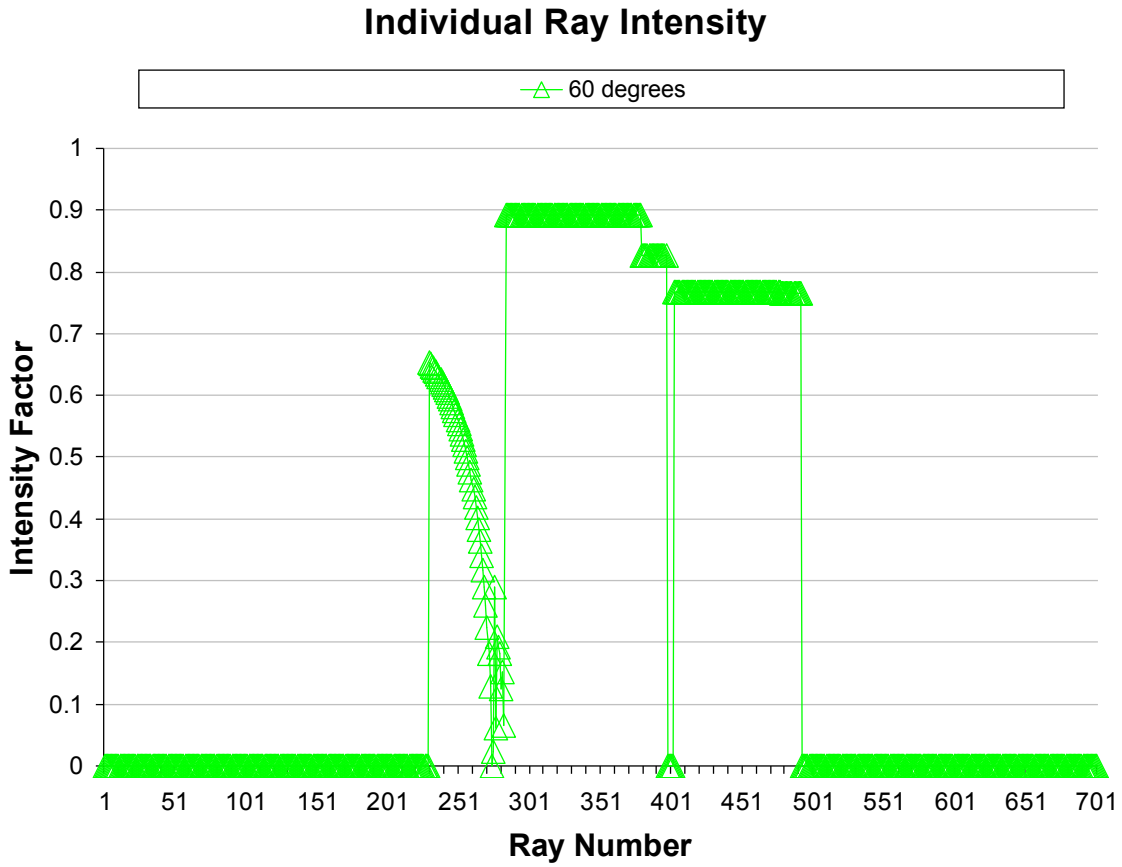

Figure 4.11: Intensity factor plots of ray striking analysis at 60 degrees angle of incidence

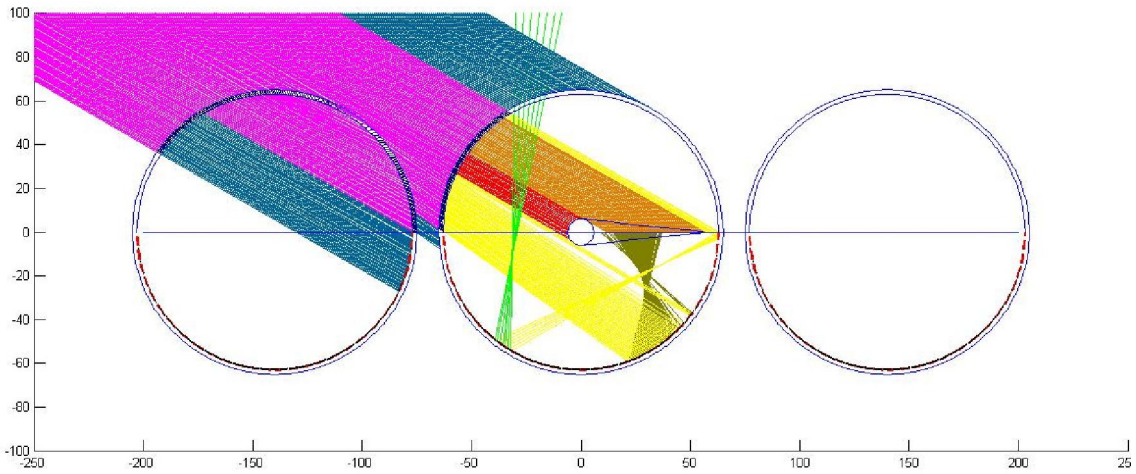

Figure 4.12: Ray tracing analysis at -60 degrees angle of incidence

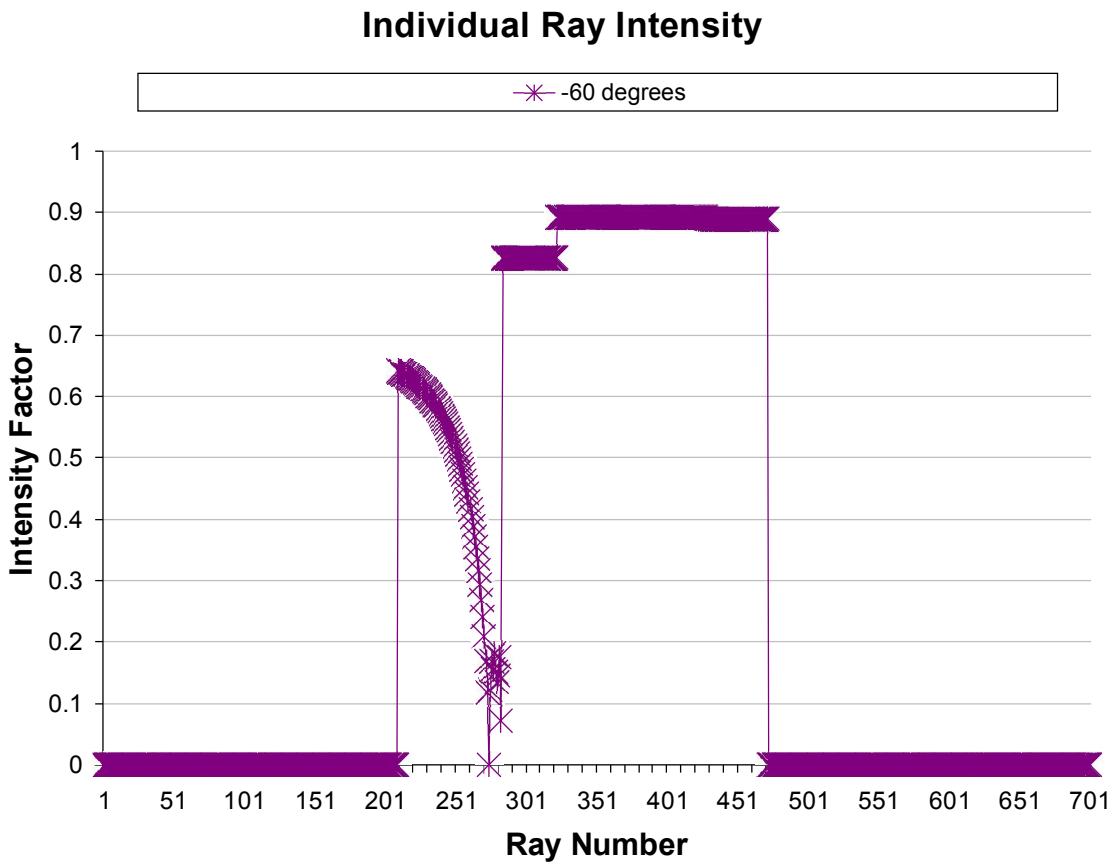

Figure 4.13: Intensity factor plots of ray striking analysis at -60 degrees angle of incidence

4.5 Sacramento installation parameters

At the Sacramento installation, the pitch (the distance between tubes) is closer than 154 mm, the value obtained in this chapter. From direct measurement, the gap between tubes is 10 mm, or a pitch of 140 mm. The aperture area width in the transverse view of 140 mm is used in the instantaneous efficiency calculation for the measured data calculations for the Sacramento installation. The values used for the array in the Sacramento installation analysis are shown in table 4-4. The difference in the aperture area width between Sandia and Sacramento experiments is quite large. The aperture width used in the Sandia experiment was found to be 122 mm and the Sacramento aperture area width used was 140 mm in both the ray tracing and computations with the measured data. If the ray trace data is normalized by the difference in the aperture widths, or 1+(140-122)/122, the Sacramento ray-tracing results match the ray tracing results and measurements for the Sandia experiment. These optical efficiencies are shown in Figure 4.14.

Table 4-4: Sacramento installation parameter values

Pitch	Gap	Absorptance	Reflectivity	Effective aperture	K	Y=SSD (Norm)	Y=SSD
140	6.0	0.947	0.9348	140	4	0.0266	0.3053

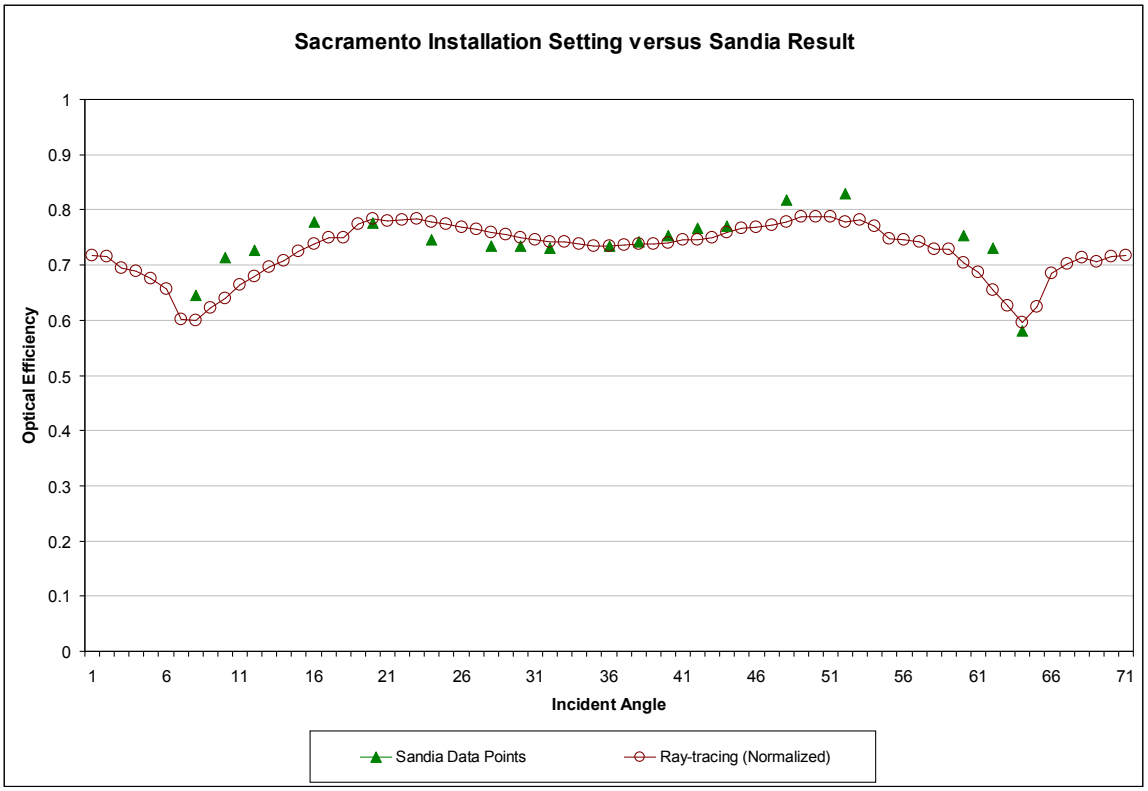

Figure 4.14: Optical efficiency plots of ray tracing analysis of the Sacramento installation setting

4.6 Summary

By matching ray tracing results with the experimental data, we have obtained a validation of the ray tracing model. Tables 4-1 and 4-3 show the SSD minimizing settings values and the sum of square differences between the data and the ray tracing analysis. These results provide a validation for parameter values for the ICPC characteristics which can then be applied in the Sacramento installation analysis.

CHAPTER 5

THERMAL LOSS ANALYSIS

5.1 Introduction

In the instantaneous efficiency model (appendix A) the thermal loss component consists of two main categories of losses. The first category is the thermal loss within the ICPC itself, and the second is the heat loss through the manifold. A good evacuated tube will retain its vacuum, so heat loss within the ICPC will consist nearly exclusively of radiation loss from the absorber fin to the environment. A crack in the glass cover will cause the tube to lose its vacuum. In this case, since air leaks into a collector, thermal energy is now also lost by convection. The second category of thermal loss is from the manifold. The heat loss from a manifold can increase over time as the insulation exposed to the environment degrades.

5.2 Thermal loss within the ICPC

At the same time as when the degradation of the reflector was mapped, the temperature of the glass evacuated tube cover was estimated. Three levels of glass cover temperature were identified and coded into a collector array map. Those temperature

levels were then used to estimate the degree of vacuum loss due to convection in a leaking tube.

The concept of an overall thermal loss coefficient for an integral compound parabolic concentrator evacuated solar collector (ICPC) is developed mathematically. The thermal network for the ICPC is mapped for both good evacuated tubes and tubes with vacuum loss tubes, considering that natural convection and radiation are occurring simultaneously. We categorize the levels of vacuum loss into three types: a good evacuated tube, partial vacuum loss, and total vacuum loss.

5.2.1 Good evacuated tube

A good evacuated tube maintains its vacuum, so there is no convection loss from the absorber fin to any medium inside the ICPC tube. The thermal network can be described by Figure 5.1, so the collector loss coefficient can be found by recalling equation A.8.

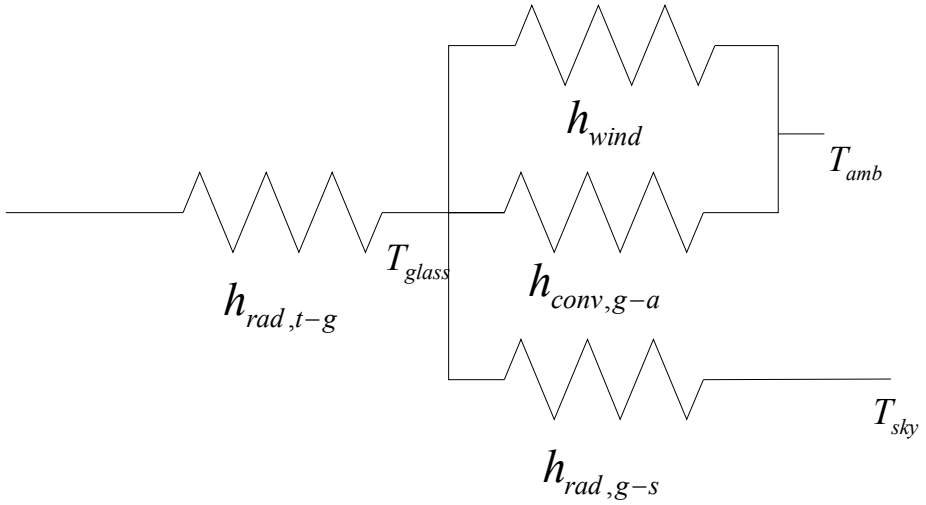

.

Figure 5.1: Thermal network for a good evacuated ICPC tube

The first part is considered heat transfer from the heat transport tube to the glass cover. Radiation heat loss is the only element in this process. The radiation loss coefficient from the heat transport tube and absorber fin to the glass cover, $h_{rad,t\text{-}g}$ is found by equation, A.16 or $h_{rad,t-g} = \frac{\sigma A_{tube+fin}(T_{tube}+T_{glass})(T_{tube}^2+T_{glass}^2)}{\frac{1}{\varepsilon_{tube+fin}}+\frac{1-\varepsilon_{glass}}{\varepsilon_{glass}}\left(\frac{A_{tube+fin}}{A_{glass}}\right)}$. The estimated effective area of heat transport tube and absorber fin is expressed in equation A.14 as $A_{tube+fin} = A_{tube} + \eta_{fin} A_{fin}$ where η_{fin} is the fin efficiency. In the ICPC case, fin efficiency is the factor which accounts for the difference between the fluid and absorber temperatures, and is approximately 1.0. The emissivity of the tube and absorber fin is 0.04 from the infrared emittance property of the selective TiN_xO_x, surface and the glass cover emissivity is 0.9. So, radiation heat loss from the heat transport tube and the absorber fin to the glass cover can be calculated by equation A.15 or $q_{loss,rad(tube-glass)} = h_{rad,t-g}(T_{tube} - T_{glass})$, which is the overall heat loss rate from the heat transport tube to the glass cover $\dot{Q}_{Tube-Glass}$

The second part of the heat loss is from the glass cover to the environment. This part consists of three heat loss elements: radiation loss, convection loss, and convection heat loss by the wind. The radiation loss coefficient from the glass cover to sky is found by using equation A.11 or $h_{rad,g-s} = \varepsilon_{glass}\sigma A_{glass}(T_{glass}+T_{sky})(T_{glass}^2+T_{sky}^2)$. From the sky blackbody property, we can estimate the sky temperature from the ambient temperature by equation A.12 or $T_{sky} = 0.0552 T_a^{1.5}$, Swinbank (1963), from Duffie and Beckman, page 122.

The convection loss coefficient from the glass cover to the environment is determined by equation A.17 or $h_{conv,g-a} = \frac{k}{D}\text{Nu}$. The Nusselt number (Nu) depends on the Rayleigh number (Ra) via equation A.18 or $\text{Nu} = \left\{0.6 + \frac{0.387\text{Ra}^{1/6}}{\left(1+\left(0.559/\text{Pr}\right)^{9/16}\right)^{8/27}}\right\}^2$. The Rayleigh number can also be found using equation A.19 or $\text{Ra} = \frac{g\beta\left(T_{glass} - T_{sky}\right)D^3}{v^2}\text{Pr}$. Lastly, the wind heat transfer coefficient, h_{wind} has been determined by A.27 or $h_{wind} = MAX(h_{wind,free}, h_{wind,forced})$. Nusselt number (Nu) for $h_{wind,free}$ is described in A.24 and A.25. The past wind speed data is obtained from the data collected by the National Climatic Center and $h_{wind,forced}$ can be calculated using A.26. The heat loss rate from the glass cover to the environment can be written as in equation 5.1. (Note that there is a convection loss in the opposite direction since the glass cover temperature will be lower than the ambient temperature.)

$$\dot{Q}_{Glass-Ambient} = (h_{conv,g-a} + h_{wind})(T_{glass} - T_{amb}) + (h_{rad,g-s})(T_{glass} - T_{sky}) \qquad (5.1)$$

Thermal equilibrium is established as the steady state operation is reached. The two heat transfer rates are equal as shown in equation 5.2.

$$\dot{Q}_{Tube-Glass} = \dot{Q}_{Glass-Ambient} \qquad (5.2)$$

From the equilibrium condition, we can solve for the glass cover temperature by the Generalized Reduced Gradient (GRG2) Algorithm in Microsoft Excel Solver.

Here the constraints and the optimum cell are functions of the adjustable cells. The first derivative of a function measures its rate of change as the input is varied. The function consists of several partial derivatives measuring its rate of change with respect to each of the changing input values. At the same time, the partial derivatives form the gradient of the function. By changing surface temperature cell values, we find the optimum cell which minimize the differences between $\dot{Q}_{Tube-Glass}$ and $\dot{Q}_{Glass-Ambient}$.

Then, the resultant U_L is directly applied to the instantaneous efficiency model in equation 5.3.

$$\text{Instantaneous Efficiency} = \rho_{eff}(IAM)(\tau\alpha)_n - \frac{U_L \Delta T - Manifold\_Losses}{G} \qquad (5.3)$$

5.2.2 Partial vacuum loss

Over time, the collectors may lose their vacuum by the leaking of air or heat transfer fluid molecules into the glass enclosure. Before completely losing their vacuum, some tubes exhibit partial leakage. These tubes are indentified by higher glass cover temperatures than perfectly evacuated tubes. We assume the glass cover temperature at this stage of leakage to be equal to the ambient temperature. The thermal network in the case of partial vacuum loss is depicted in Figure 5.2, where the collector loss coefficient can be found by recalling equation A.7

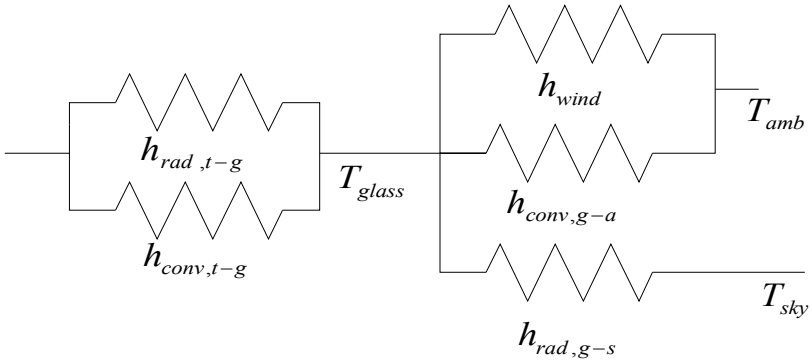

Figure 5.2: Thermal network for a partial leaking ICPC tube

In tubes with partial leaks, $h_{conv,tube\text{-}g}$ is added to the thermal loss coefficient from the heat transport tube and the absorber fin to the glass cover. This convection loss happens when air or heat transfer fluid leaks into the vacuum tube. $h_{conv,tube\text{-}g}$ can be calculated by equation A.20 or $h_{conv,tube-g} = \frac{k}{\delta}\text{Nu}$. The Nusselt number (Nu) incorporates the Rayleigh number (Ra) as in equation A.21 or $\text{Nu} = 0.11\text{Ra}^{0.29}$. The Rayleigh number can also be found using equation A.22 or $\text{Ra} = \frac{g\beta\left(T_{tube} - T_{glass}\right)\delta^3}{v^2}\text{Pr}$. Since the glass cover temperature equals to ambient temperature, as in our assumption, the collector loss coefficient U_L is obtained from the loss coefficients directly and then applied to the instantaneous efficiency equation 5.3.

5.2.3 Total vacuum loss

For total vacuum loss, cracks in the glass expand over time and air fully leaks into the glass enclosure, causing the ICPC to completely lose its vacuum. The thermal network for full vacuum loss is the same as for the partial leak case, as shown in Figure 5.2, and the collector loss coefficient also can be found by recalling equation A.7. The

heat loss rate from the heat transfer tube to the glass cover can be written as in equation 5.4, and the heat loss rate equation from the glass cover to the environment is the same as in perfect vacuums, equation 5.1

$$\dot{Q}_{Tube-Glass} = (h_{rad,t-g} + h_{conv,t-g})(T_{tube} - T_{glass}) \tag{5.4}$$

Thermal equilibrium is established as steady state operation and is reached through equation 5.2. We also solve this glass cover temperature by the Generalized Reduced Gradient (GRG2) Algorithm in Microsoft Excel Solver by changing surface temperature cell values to minimize the differences between $\dot{Q}_{Tube-Glass}$ and $\dot{Q}_{Glass-Ambient}$. Then, the U_L is directly applied to the instantaneous efficiency model (equation 5.3).

5.3 Thermal losses from the manifold

There are two significant sources for losses in the manifold. The first is from the larger heat transport tube that runs perpendicular to the heat transport end of ICPC tube. This area of the manifold has ~~a~~ fiberglass insulation covering the tube. The fiberglass insulation is one inch thick. The thermal resistance network consists of four resistances~~,~~ and the total thermal resistance (R_1) can be found by summing them (equation 5.5). The four resistances are: the convection resistance from the hot heat transport fluid to the heat transport tube, $R_{conv,w\text{-}t}$, the conduction resistance of the heat transport tube, $R_{cond,tube}$~~,~~ , the conduction resistance of the insulation, $R_{cond,insu}$ and the convection resistance from the insulation to the environment, $R_{conv,insu\text{-}env}$.

$$R_1 = R_{conv,w\text{-}t} + R_{cond,tube} + R_{cond,insu} + R_{conv,insu\text{-}env} \quad (5.5)$$

The convection resistance from the heated fluid to the heat transport tube, $R_{conv,w\text{-}t}$, is calculated by using equation A.30. Using an h_i of 70 W/m^2 and the contact area of 2.4322 m^2, $R_{conv,w\text{-}t}$ is 0.005873587 K/W. The conduction resistance of the heat transport tube, $R_{cond,tube}$, is the resistance of the copper tube from the inner surface to the outer surface. Equation A.31 is used to find this conduction resistance. The k_1 of the copper tube is 52 W/m^2.K and the resultant resistance, $R_{cond,tube}$ has a value of 8.009 * 10^{-7} K/W. The conduction resistance of the insulation $R_{cond,insu}$ is calculated by using k_2 of 0.038 K/W (fiberglass) and a thickness of 1 inch; Therefore, $R_{cond,insu}$ has a value of 0.11273 K/W. The last resistance is the convection resistance from the insulation to the environment, $R_{conv,insu\text{-}env}$. Also using equation A.30, the convection resistance from the insulation to the ambient is 0.006282 K/W, using h_o of 20 W/m^2. So, the total thermal resistance is 0.124885 K/W, which is the combination of all resistances.

The second significant source for losses is the connection from the main heat transport tube to each ICPC. These connections have small air gaps that are exposed to the environment with little or no insulation. The calculation of R_2 is shown in equation 5.6.

$$R_2 = R_{conv,w\text{-}t} + R_{cond,tube} + R_{conv,insu\text{-}env} \quad (5.6)$$

Smaller tubes are used at the connecting point, and each tube has a diameter of 0.011989 meters and a length of 0.12 meter. Adding up all of the connecting points in the manifolds, the total thermal resistance of the connecting points is 0.112914 K/W. This is comparable to the thermal resistance of 0.124885 K/W in the manifold itself.

The total steady-state rate of heat loss from the fluid can then be calculated from a known ΔT, and the two thermal resistances (R_1, R_2). This is shown in equation 5.7.

$$\dot{Q} = (T_{fluid} - T_{ambient})\left(\frac{1}{R_1} + \frac{1}{R_2}\right) \tag{5.7}$$

5.4 Levels of vacuum loss within the ICPC

The overall thermal losses for an integral compound parabolic concentrator evacuated solar collector (ICPC) with different levels of vacuum loss can also be developed via a thermal network. The thermal network for the ICPC is made up of both good evacuated tubes and those with vacuum losses. To this end, we categorize the levels of vacuum loss into three types: a good evacuated tube, partial vacuum loss, and total vacuum loss.

5.4.1 Color mapped cover glass temperature

In 2007 all ICPC tubes were individually characterized in ten sections by their level of thermal loss and mapped into a color coded chart. See the "Temp" column in Figure 5.3. The mapping was done simultaneously with the reflectivity degradation map (Figure 5.3). The three levels of glass cover temperatures represent the three levels of

thermal loss. Light blue in the "Temp" column represents a perfectly evacuated tube with a cold cover temperature when the system is operating. Partial vacuum loss is marked by a yellow color. The glass cover temperature of a tube with partial vacuum loss feels warm to the touch. We assume the temperature of glass cover at this level to be equal to the ambient temperature. In tubes with total loss of vacuum, the glass cover feels hot to the touch. At the complete loss of vacuum stage, we mark the map with a red color. While investigating glass cover temperature, we also recorded physical failures of individual ICPC tubes, such as fluid leaks and cracks.

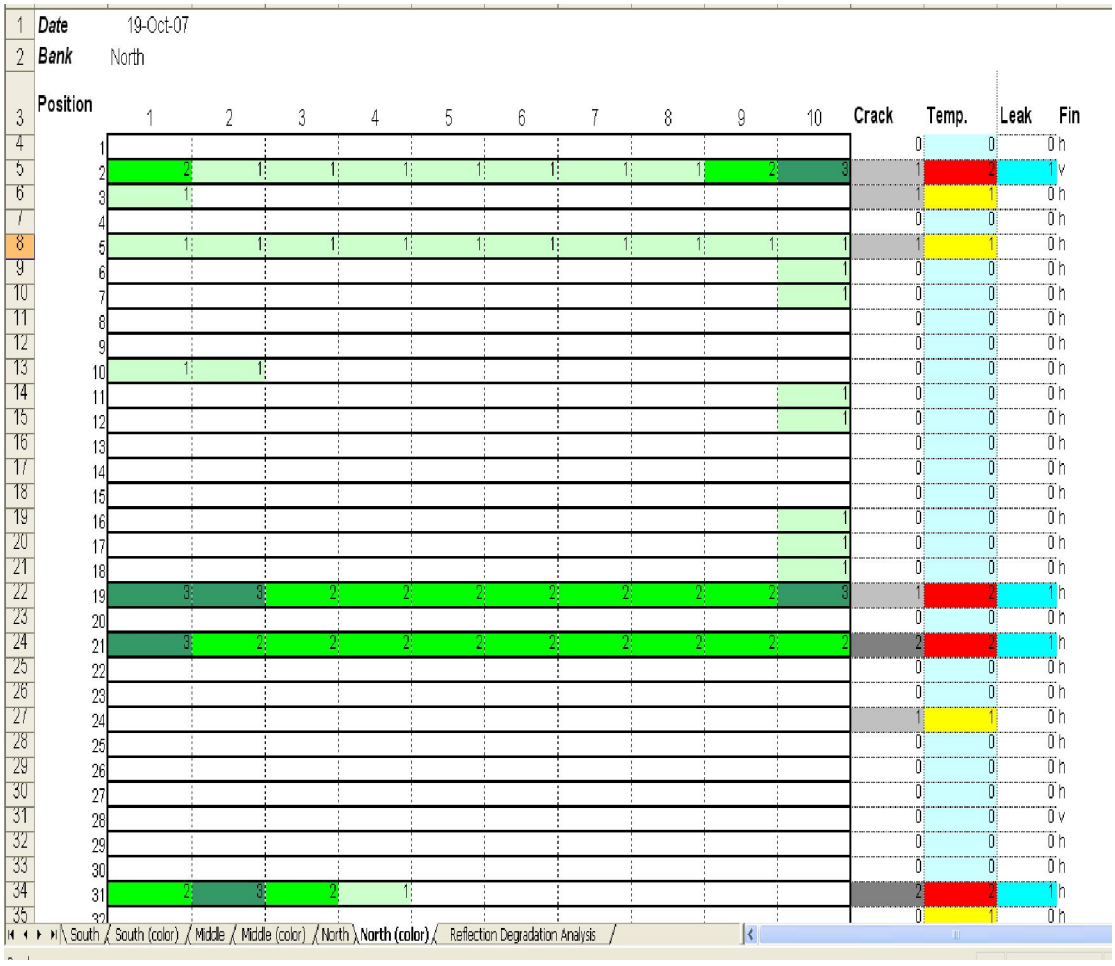

Figure 5.3: Map of tube degradation

5.5 Summary

In this chapter, the heat loss from both the ICPC and manifold is described. Performance degraded by the loss of vacuum in the tube is also described. Later an analysis of the performance consequences of reflector degradation and loss of vacuum is integrated into the reliability study and related to the measured data in Figures 5.3. The next chapter will report the detailed ray-tracing analysis, including the effects on performance of each ICPC component. Also, the method of measuring the degrading reflectors and the on-site mapping of each individual ICPC are presented.

CHAPTER 6

THE IMPACT OF VARIOUS FACTORS ON PERFORMANCE, FAILURE MECHANISMS AND MEASUREMENTS

6.1 Introduction

A primary focus of this dissertation is on a reliability and degradation analysis of the novel ICPC that has been in operation for 13 years. An animated graphical ray tracing simulation tool has been designed to determine the nature and degree of degradation effects on the collector optical performance.

The impact of changes in the various factors on the performance of the ICPC is investigated. Those factors incorporated in the ray tracing analysis are the transmittance of the glass tube, the reflectivity of the reflective surface, the gap between the reflective surface and the absorber fin, the interference of adjacent tubes, and the absorptance of the absorber fin. Varying the various factor values will show how those factors effect ~~to~~ the ICPC optical performance.

Lastly in this chapter, the two main factors of degradation are categorized. Each tube of 336 at the Sacramento's site has been individually investigated. The four stages of degradation of the silver reflector and the three stages of air leakage into the evacuated space have been identified.

6.2 Investigation of optical performance on both fin arrangements

Characteristics of optical efficiency are studied by adjusting important factors such as reflectivity of the compound parabolic concentrator, the distance between the absorber fin's tip and the glass cover, transmittance of the glass cover, and partial blocking of the rays by the adjacent tubes. Each characteristic is added into the ray-tracing analysis one by one to see its effect on the overall optical efficiency. Both fin arrangements are first investigated with no loss, and then the 0.9348 reflectivity of the reflector is added, and its effect is investigated. Next, the 6 millimeter gap between the absorber fin and the glass cover and then the loss of intensity of the rays from partial blocking from adjacent tubes are individually added in order. The optical efficiency graphs are plotted to compare each loss characteristic in both fin arrangements.

In the vertical fin case (Figure 6.1) adding a reflectivity of 0.9348 of the reflector reduces its efficiency at the same rate in both morning and afternoon. A greater drop in performance occurs at around 90 degrees incidence angle (around noon) (See Figure 6.2). This is a result of more rays reflecting from the reflector when the angle of incidence is closer to 90 degrees than when the angle is lesser or higher such as is the case in the morning and in the evening. Adding a 6 millimeter gap between the absorber fin and the glass cover results in a huge drop in performance around the middle part of the day. This happens when the ray passes through the gap and reflects out (green rays) of the collector in the middle part of the day, while there is no such gap loss in early morning and late afternoon (Figure 6.3).

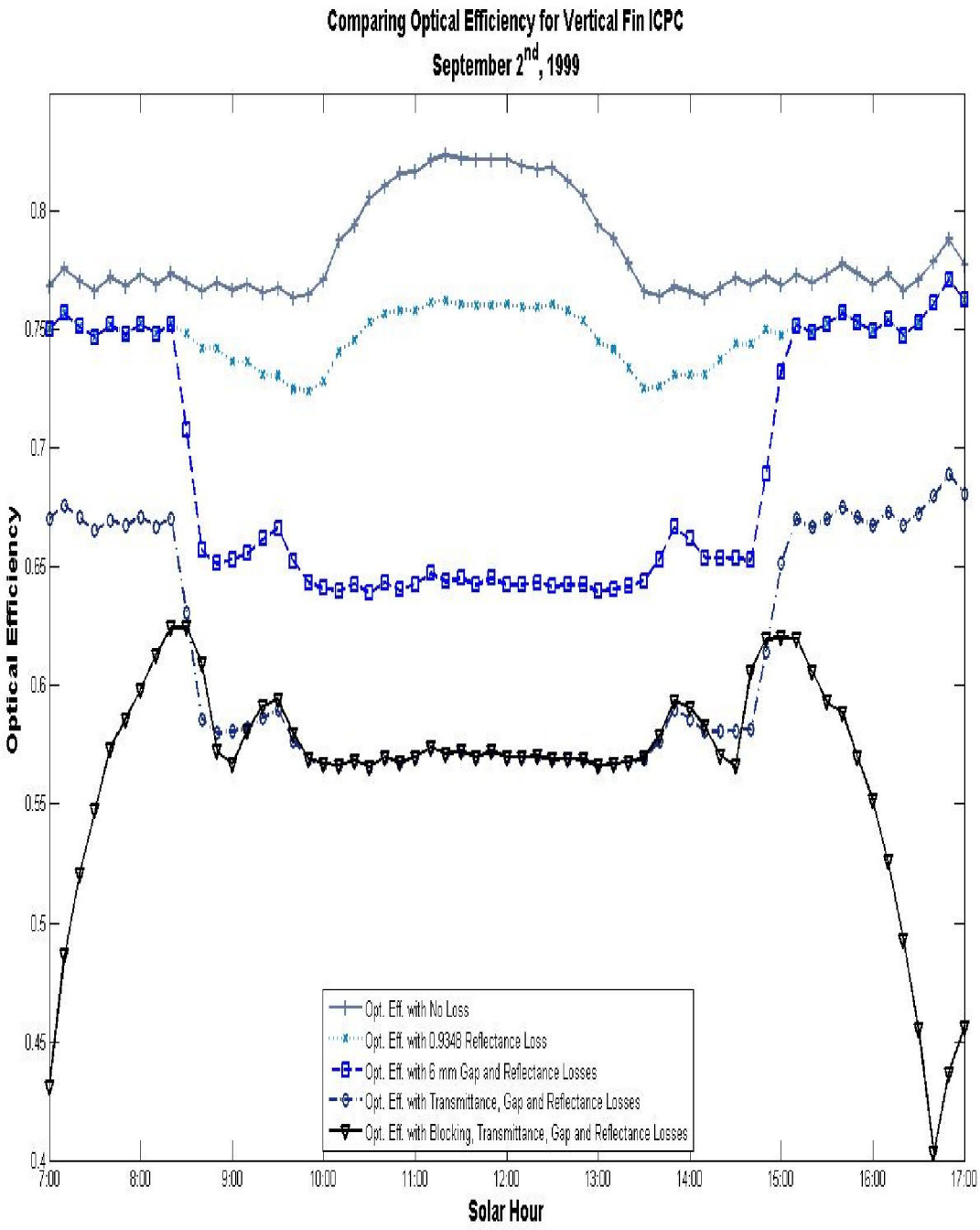

Figure 6.1: Comparing optical efficiency for vertical fin ICPC, September 2nd 1999 [beam radiation]

Next, transmittance from the glass cover with a reflective index of 1.526 is added. Transmittance is labeled as the product of absorptance and reflectance properties. It

causes a uniform drop of performance across the day. Finally, the effect of partial blocking from the adjacent tubes is added. Both extremely small and large incidence angles show a heavy drop in performance (Figure 6.3).

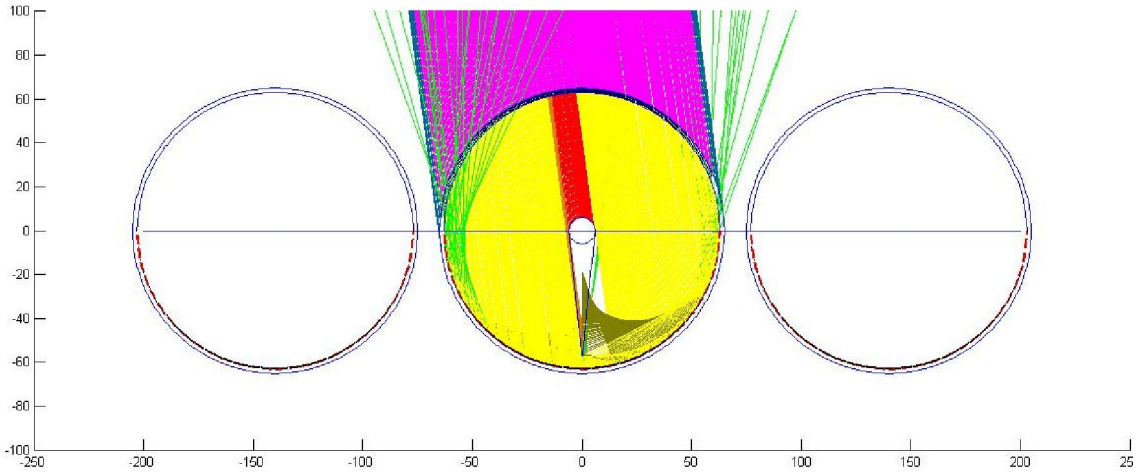

Figure 6.2: Gap loss when the angle of incidence is close to 90 degrees

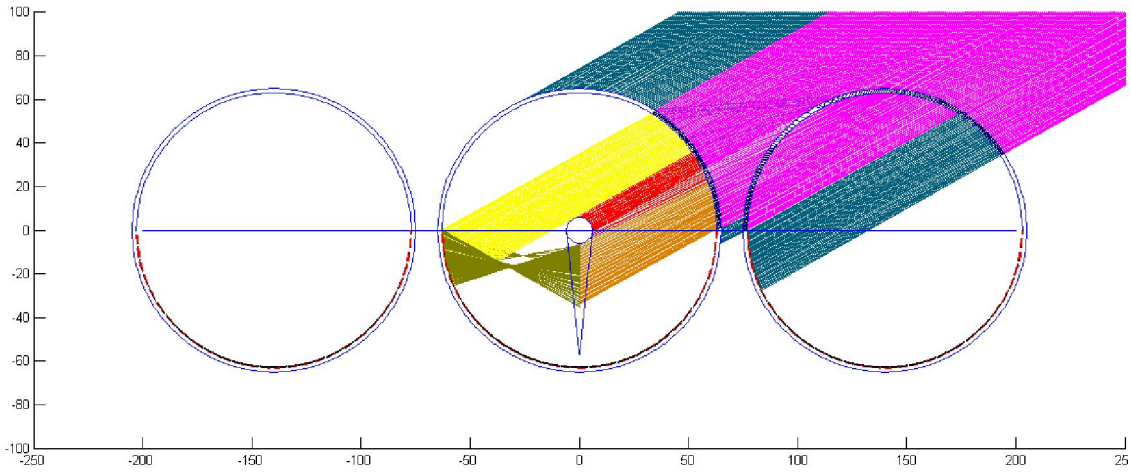

Figure 6.3: No gap loss in the lower angle of incidence and blocking of the rays from adjacent collectors

In the horizontal fin case (Figure 6.4) incorporating a reflectivity of 0.935 produces a greater drop in performance in the morning than in the afternoon. The greater drop in performance in the morning is due to rays experiencing multiple reflections

before hitting the absorber (Figure 6.5). The lesser drop in performance in the evening is a result of rays only having single reflections in the afternoon (Figure 6.6).

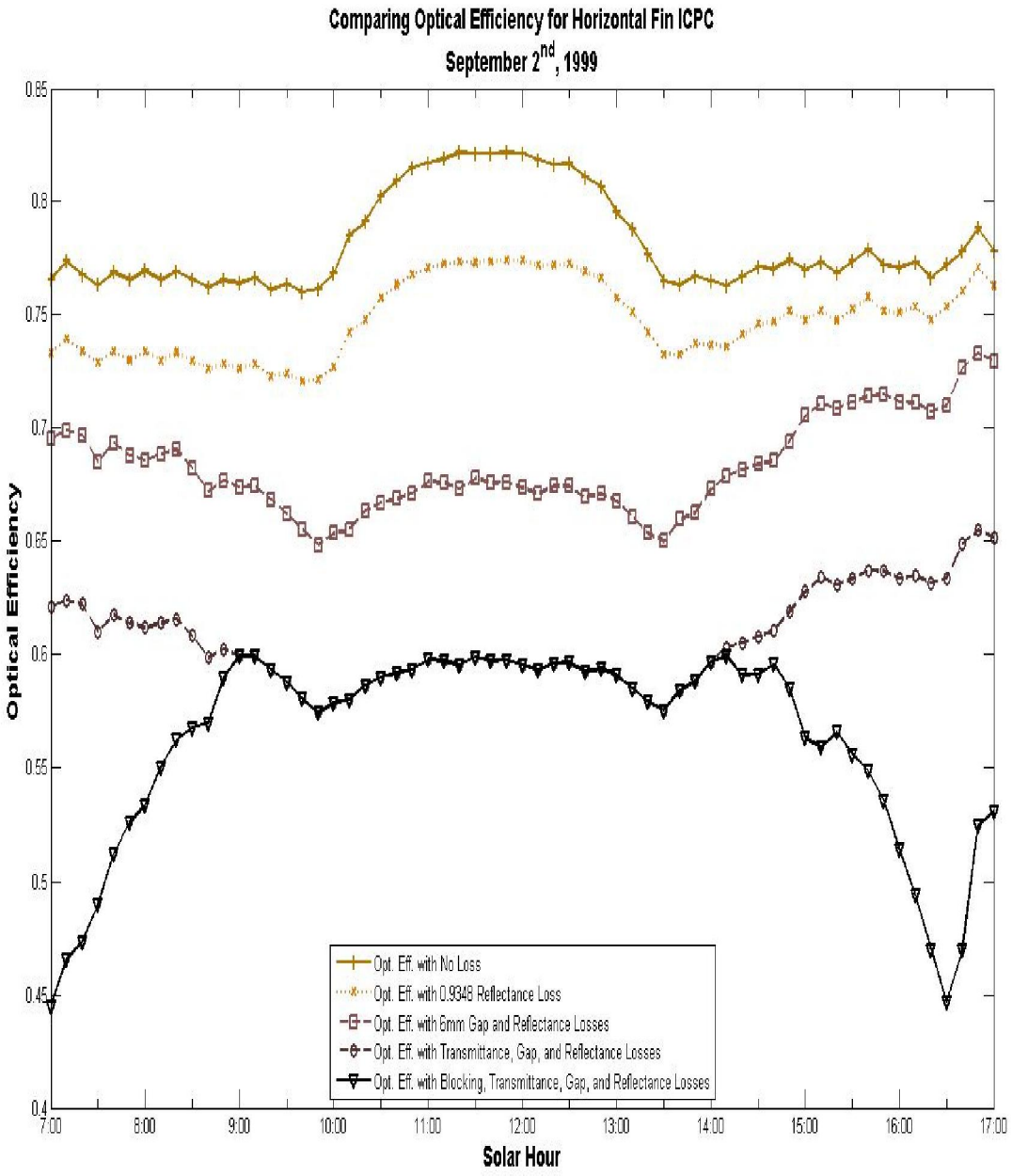

Figure 6.4: Comparing optical efficiency for horizontal fin ICPC, September 2nd 1999 [beam radiation]

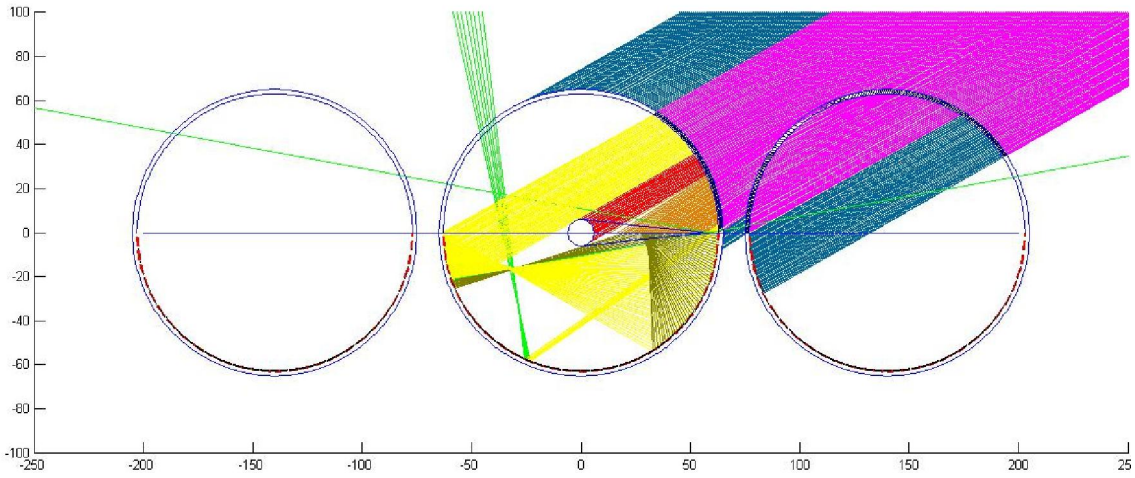

Figure 6.5: Ray-tracing analysis showing multiple reflections in the morning for horizontal fin ICPC, September 2nd 1999

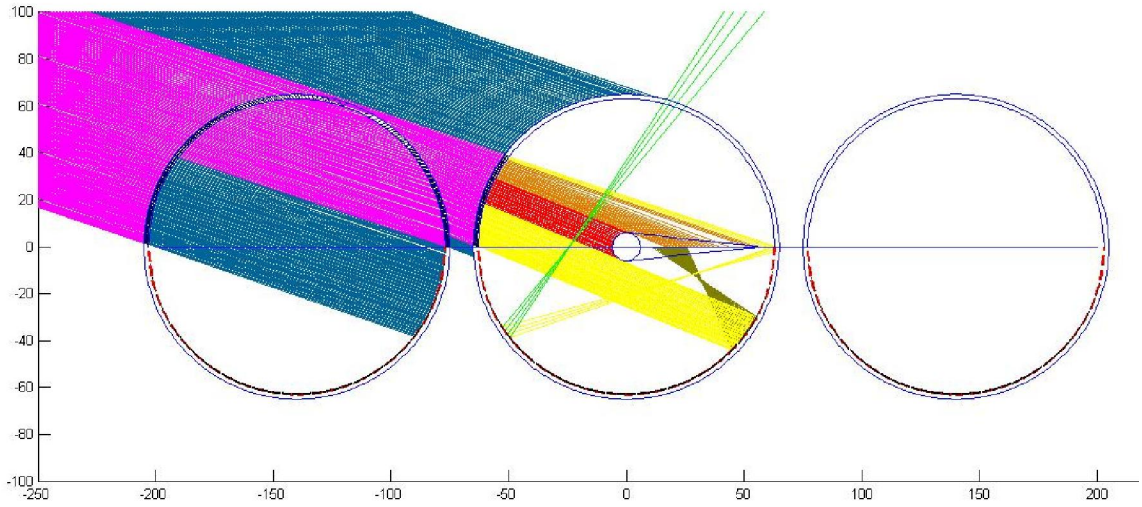

Figure 6.6: Ray-tracing analysis showing single reflection in the morning for horizontal fin ICPC, September 2nd 1999

Adding a 6 millimeter gap between the absorber fin and the glass cover on the horizontal fin arrangement yields a drop in performance in all angles with a greater drop

when the angle of incidence is close to 90 degrees at noon. Figure 6.5 and 6.6 also show the ray escaping through the gap and out of the collector (green rays).

Next, transmittance from the glass cover with a reflective index of 1.526 is then added to the analysis of this horizontal absorber fin. Transmittance is estimated as the product of its absorptance and reflectance properties. It produces a uniform drop in performance throughout the day, similar to the vertical fin configuration. Last, the effect of partial blocking from the adjacent tubes is added. As in the vertical fin arrangement, both very small and large incident angle produce a substantial drop in performance due to the blocking from adjacent tubes (Figure 6.5 and 6.6).

6.2.1 Effects of the gap between the absorber fin and the glass cover

As illustrated earlier, the gap between the absorber fin and the glass cover plays an important role in the optical performance of the ICPC. When there are different gaps for both vertical and horizontal fin arrangements, different decreases in optical performance are observed for the two absorber fin arrangements.

First, the vertical fin arrangement with no gap between the absorber fin and the glass cover ICPC is investigated as a base case. Then gaps of 3, 6, 9, and 12 mm are addressed. Figure 6.7 shows that the vertical fin performance decreases for all gaps between 8:30 and 15:00 solar time.

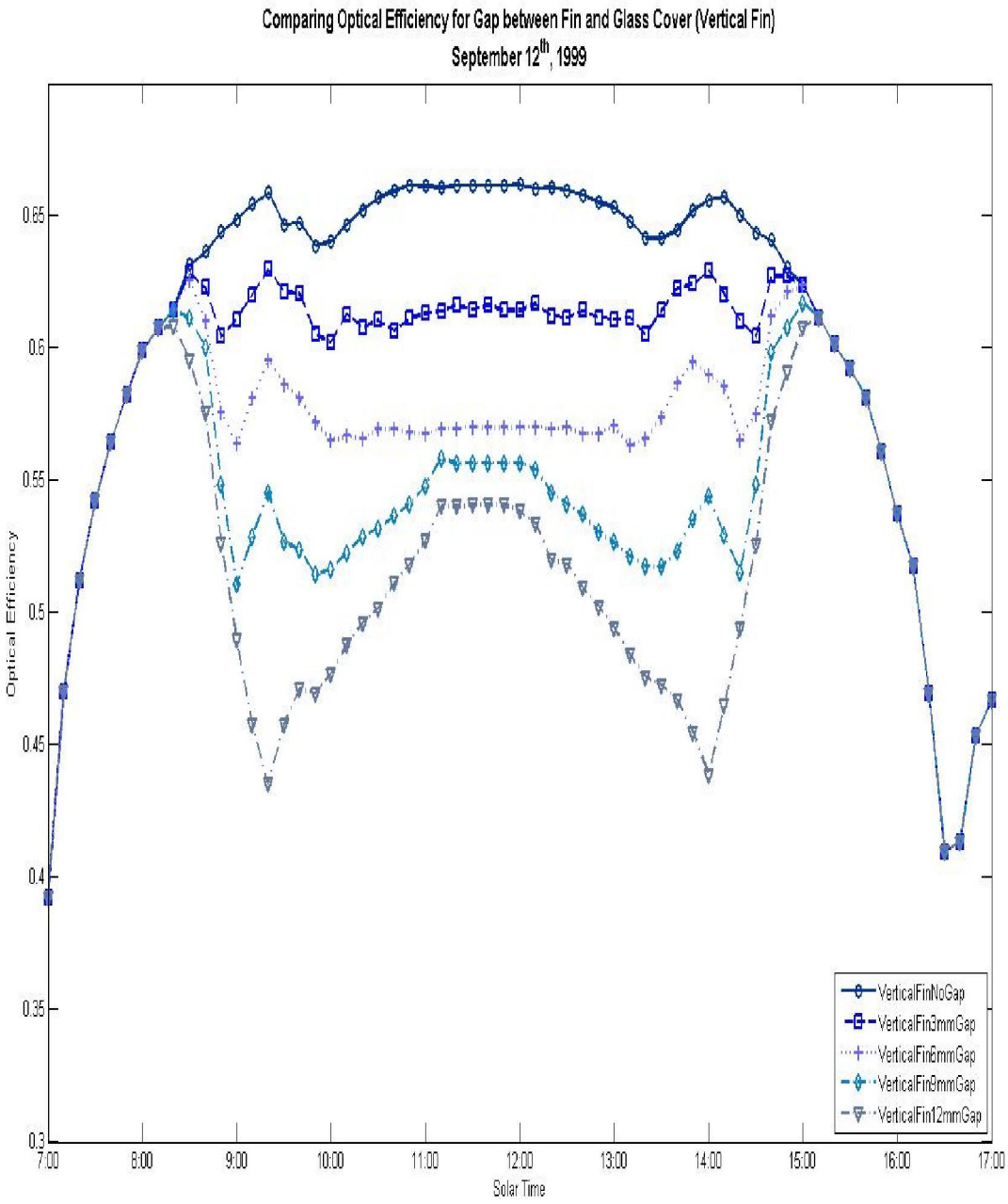

Figure 6.7: Comparing optical efficiency for different gaps for vertical fin ICPC, September 12th 1999 [beam radiation]

In the early morning and late afternoon, all rays hit the absorber fin toward its middle. In the later morning or early afternoon, the decrease in the incident angle causes the rays to hit the absorber fin farther toward the tip, so the performance falls off as some

rays slip through the gap and reflect out of the glass tube. The significant drop in performance from 8:30 to 15:00 is amplified when the gap increases from zero to 6 mm. There is also some recovery in performance around middle of the day for gaps of 9 and 12 millimeters.

The effect of the gap between the absorber fin and the glass cover in the horizontal fin arrangement shows a close to uniform performance drop across most of the day (Figure 6.8).

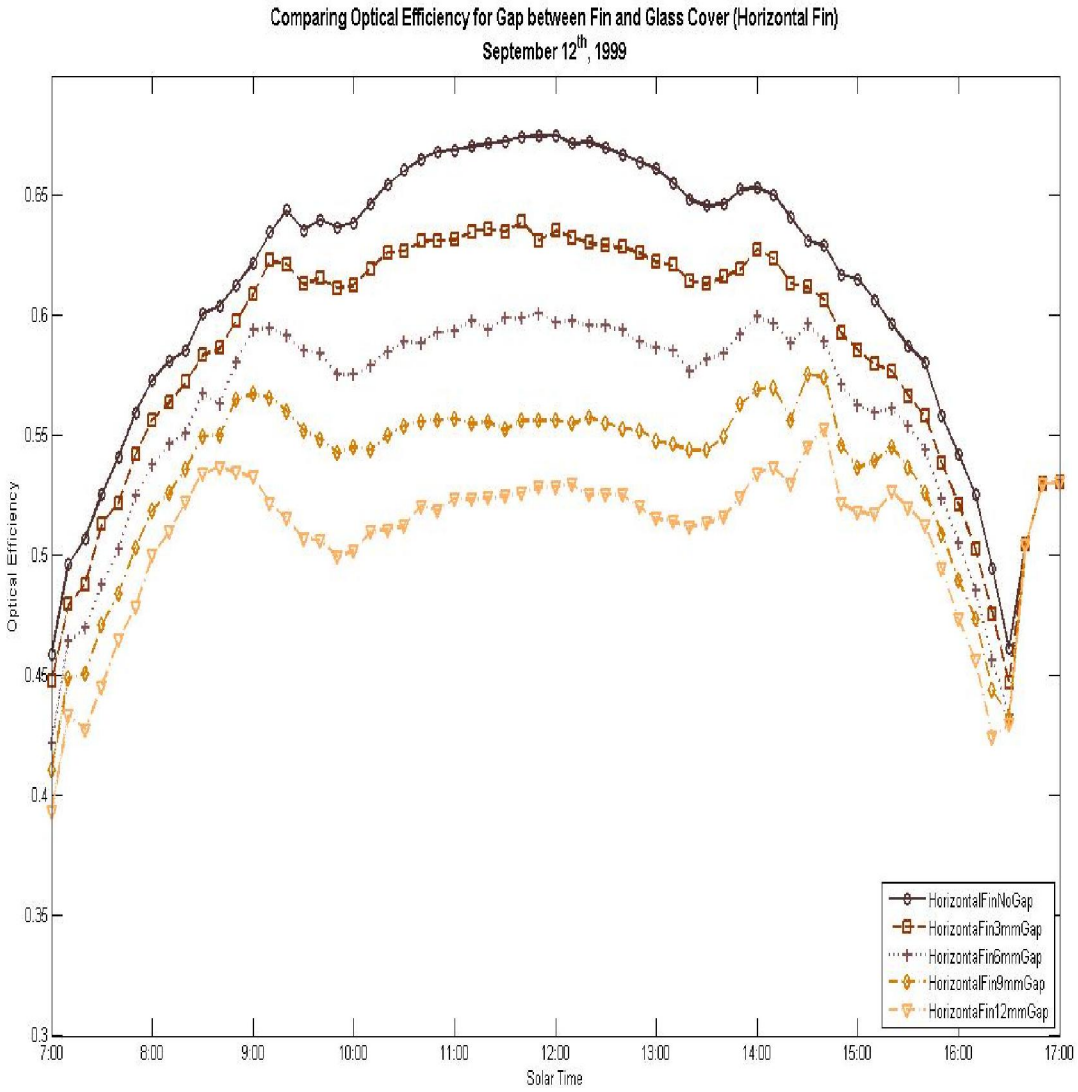

Figure 6.8: Comparing optical efficiency for different gaps for horizontal fin ICPC, September 12th 1999 [beam radiation]

The larger gap causes a greater drop in performance in the time interval from 7:00 to 16:30. In the very late afternoon, the angle of incidence is extremely small, so all traced rays hit the absorber fin without reflecting out of the collector (Figure 6.9).

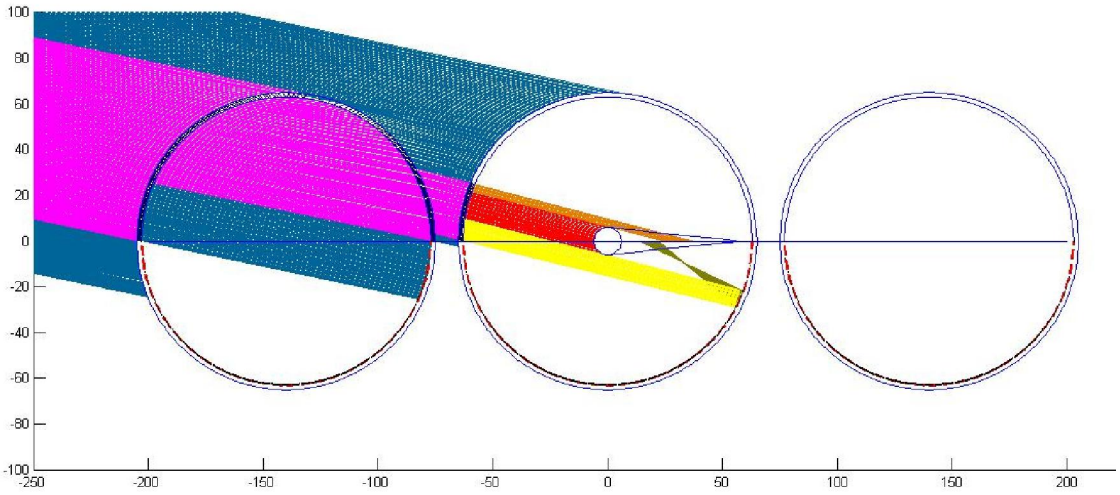

Figure 6.9: Ray-tracing analysis showing extreme angle of incidence in late afternoon for horizontal fin ICPC, September 12th 1999

6.3 Reflectivity measurement

The device shown in Figure 6.10, consisting of a laser and detector mounted on a support structure, was used to measure the reflectance of mirror surface samples taken from the ICPC array in 2007. Using this device, a map of reflector performance that is keyed to the appearance of the reflective surface for the tubes in the ICPC array has been generated. Four levels of reflectance degradation are identified for the Sacramento site by the appearance of the reflective surface. At level 1, (Fig. 6.11), the reflector still performs well and only a minor change in the reflector appearance is observed. At level 2, (Fig. 6.12), there is some whitening of the reflector. At level 3, (Fig. 6.13), there is a

substantial amount of degradation of the reflector. At level 4, (Fig. 6.14), most of reflector is gone and you can easily see through it.

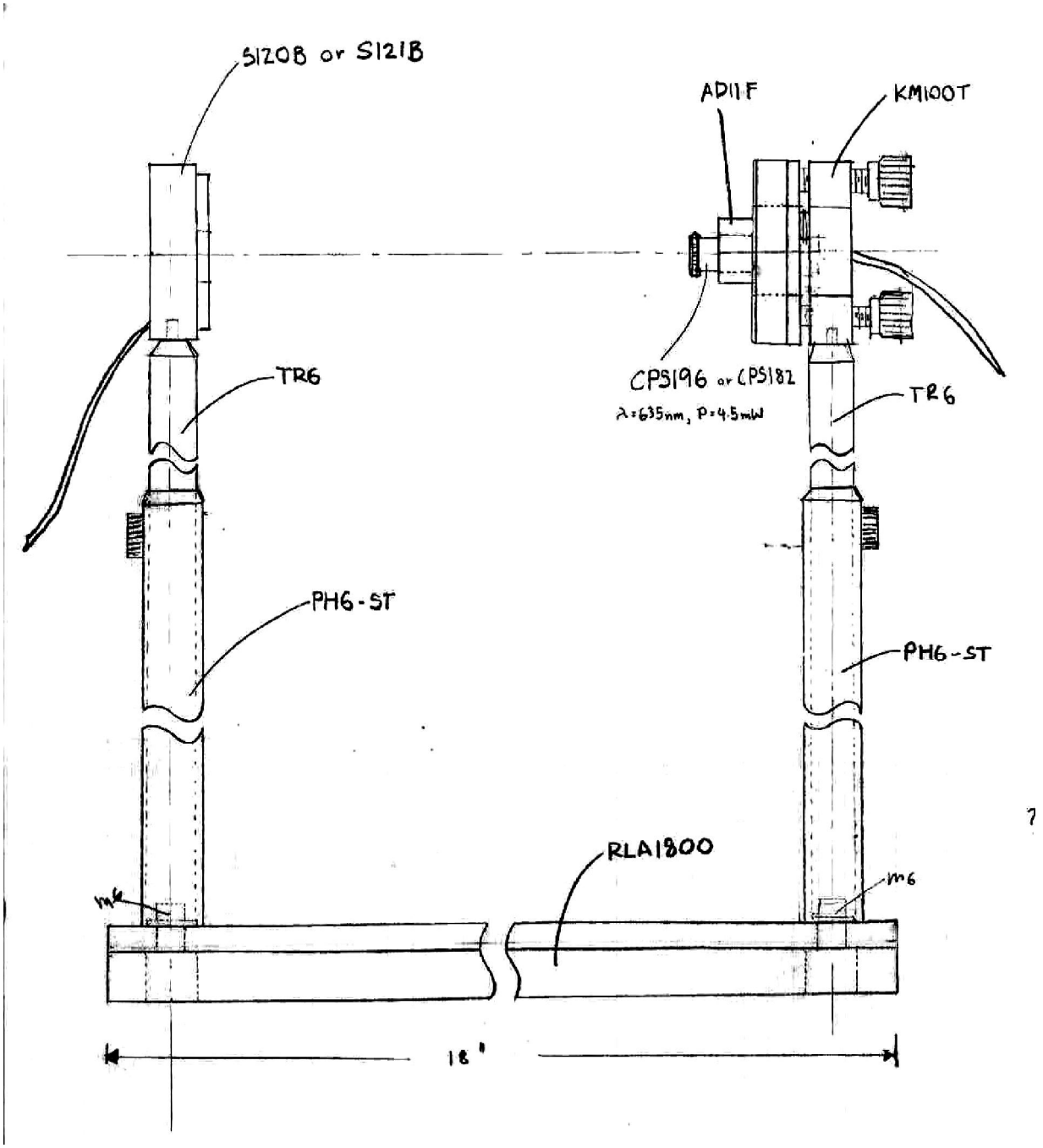

Figure 6.10: Laser and sensor assembly

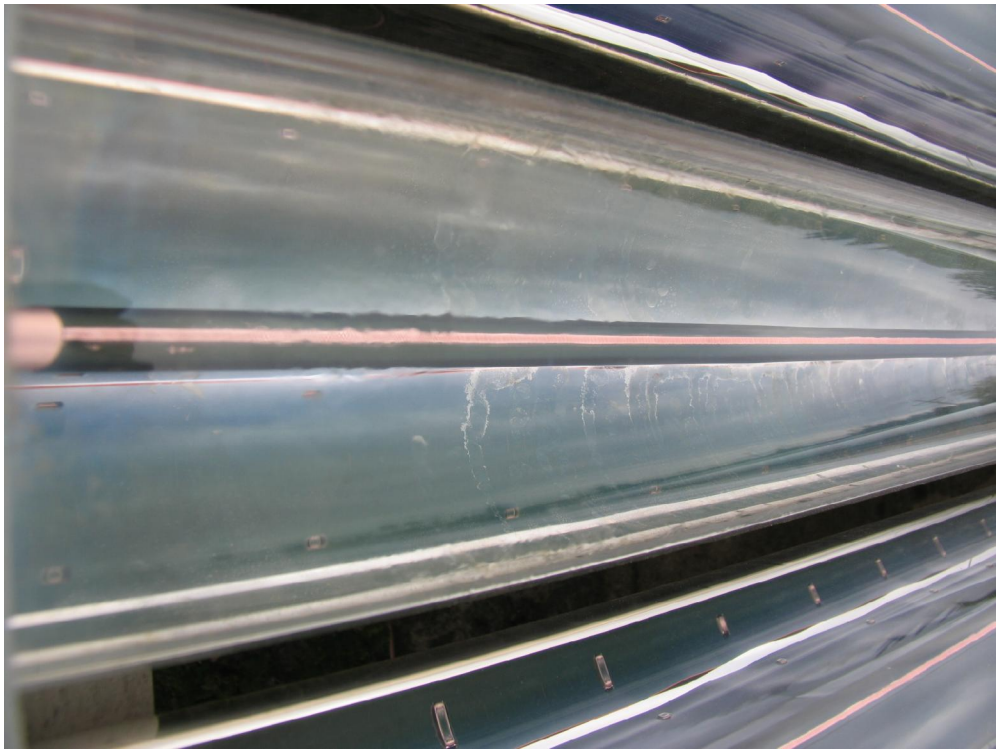

Figure 6.11: First level of reflectivity degradation

Figure 6.12: Second level of reflectivity degradation

Figure 6.13: Third level of reflectivity degradation

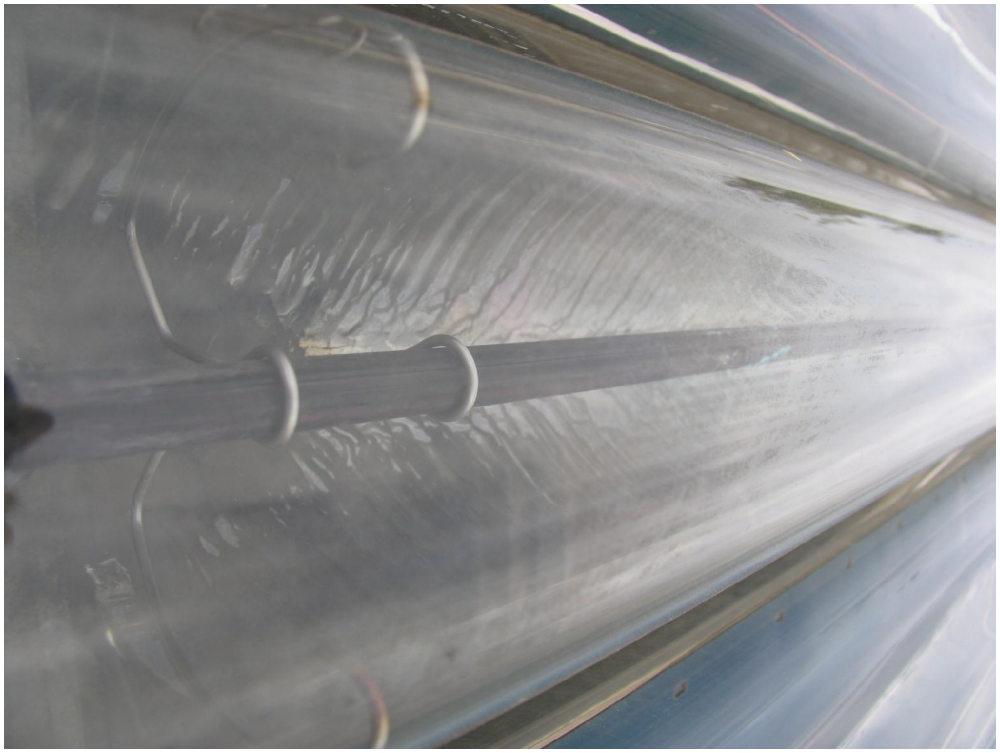

Figure 6.14: Fourth level of reflectivity degradation

At the site, all 336 tubes were categorized, one-by-one, by the above reflectivity appearance levels, existence of glass cracks, surface temperature, water leakage, and fin orientation. Each tube was divided into ten sections along its length. Degradation levels were identified and marked for each of the ten sections. Fig. 6.15 shows a color mapping of tube degradation information for a portion of the array.

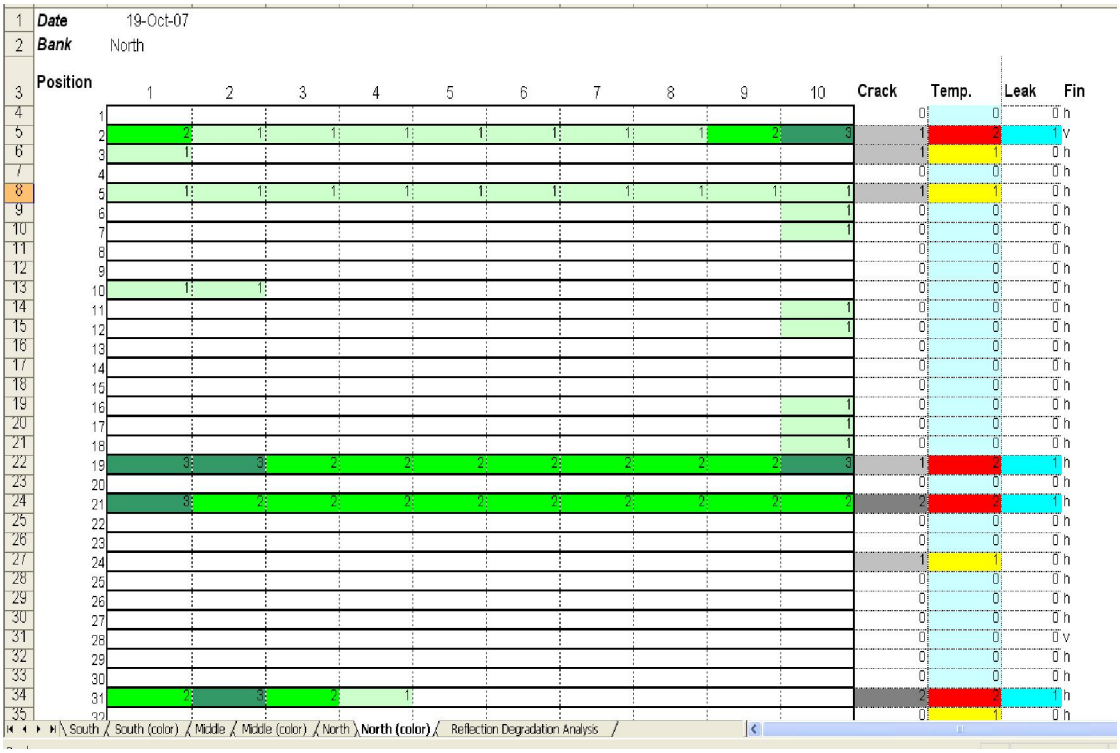

Figure 6.15: Sample map of tube degradation

Reflector samples representative of the four different degradation levels were taken from the Sacramento site to the laser laboratory at Colorado State University (Figure 6.16). The samples for the four levels of degradation and good reflector samples were measured for their reflectivity by the laser detection device.

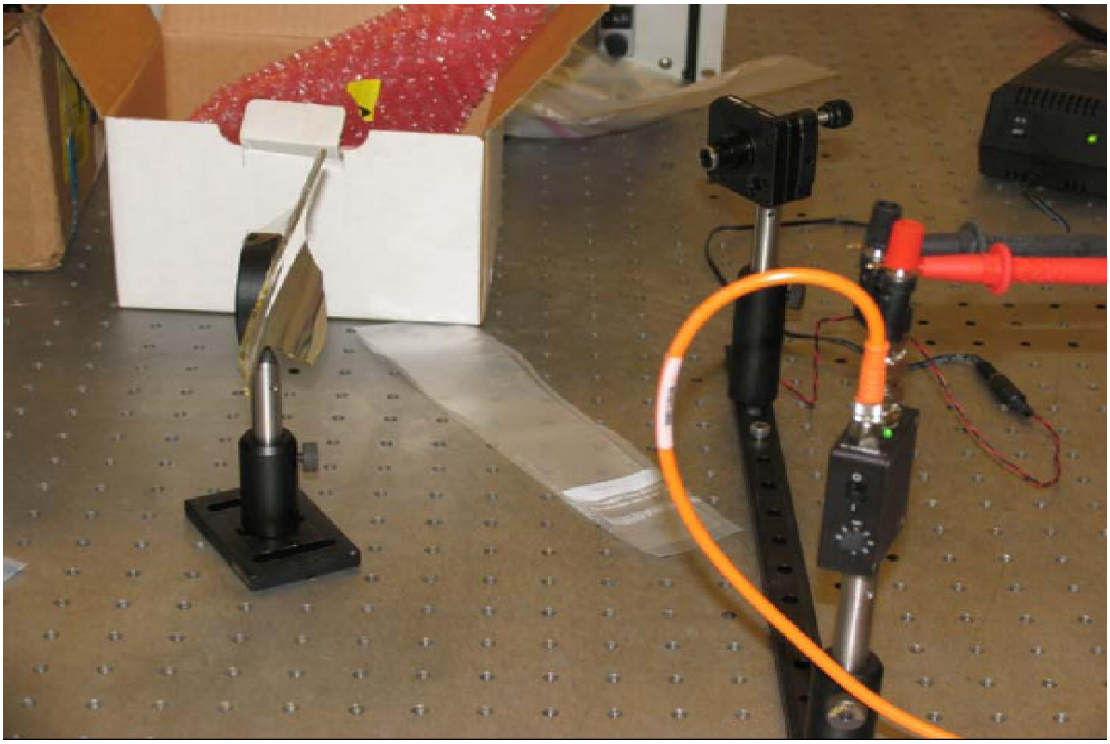

Figure 6.16: Sample map of tube degradation

Using this device, a map of reflector performance for the ICPC array is being generated. The reflectivity results are shown in Table 6-1 for each level of degradation.

6.4 Analysis of the on-site mapping of two fin orientations on performance

Reflectivity degradation plays an important role in the performance of the evacuated tube. As reflectivity degrades, the performance of tubes with the two fin orientation falls off in different ways. The ray tracing simulation is performed to find how those degradations affect the optical performances. By applying each level of reflectivity to an entire length of the ICPC, the ray tracing simulation depicts the characteristic of reflectivity degradation for both absorber fin arrangements. For the vertical fin, performance drops rapidly for angle of incidence close to 90 degrees (Figure

6.17). This behavior is as expected since the vertical absorber fin collects the energy mostly from the reflected ray. So, the higher the degradation, the higher the performance rate drops near solar noon.

Table 6-1: Measurement of reflectivity

Degradation Level	Percent Reflectivity
Good	93.48
1st	79.66
2nd	38.46
3rd	22.93
4th	1.24

The horizontal arrangement is more robust to the reflector degradation than the vertical arrangement, In this case the performance drops at about the same ratio as the reflector degradation rate (Figure 6.18). The horizontal absorber fin performs better than the vertical absorber fin when the reflector degrades since the horizontal fin absorbs some of the radiation directly.

Next, the degradation map from the actual site in Sacramento is included in the three dimensional ray tracing simulation. The simulation allows us to set different reflectivity values for each section of the tube in the longitudinal view. Figure 6.19 and 6.20 shows the optical efficiency when the measured reflector degradation characteristics of each ICPC tube are incorporated into the ray tracing.

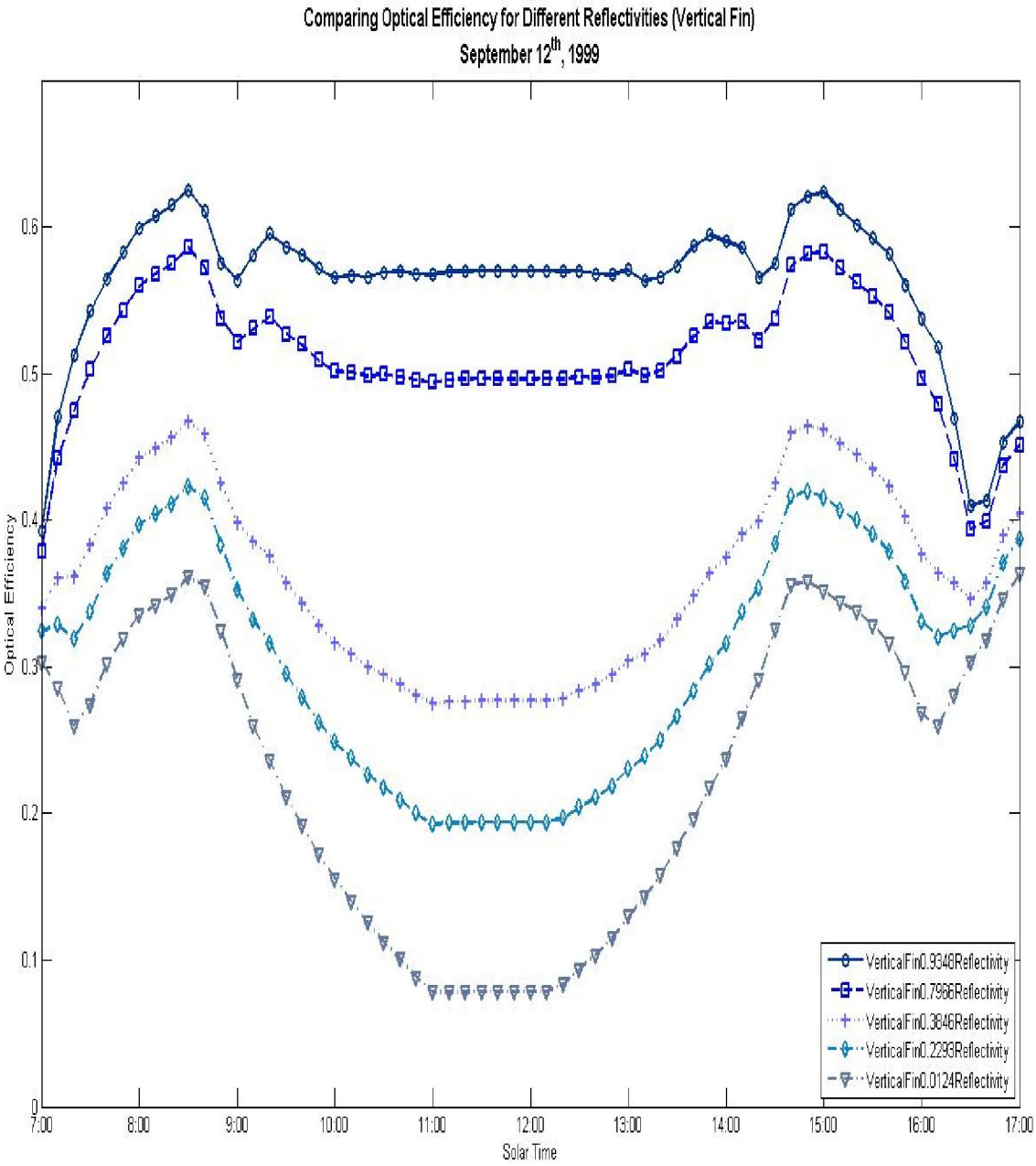

Figure 6.17: Comparing optical efficiency for different reflectivities for vertical fin ICPC, September 12th 1999 [beam radiation]

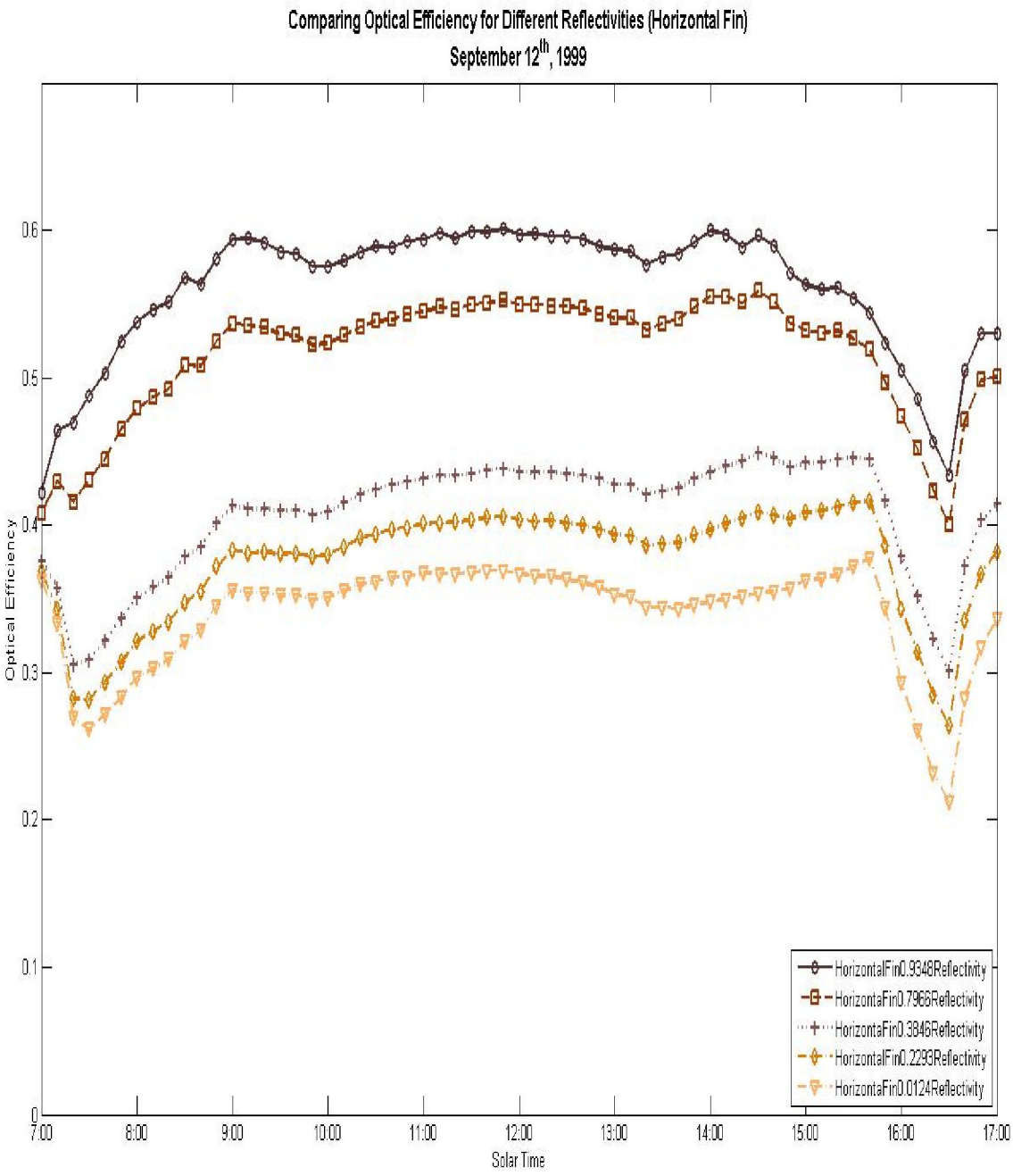

Figure 6.18: Comparing optical efficiency for different reflectivities for horizontal Fin ICPC, September 12th 1999 [beam radiation]

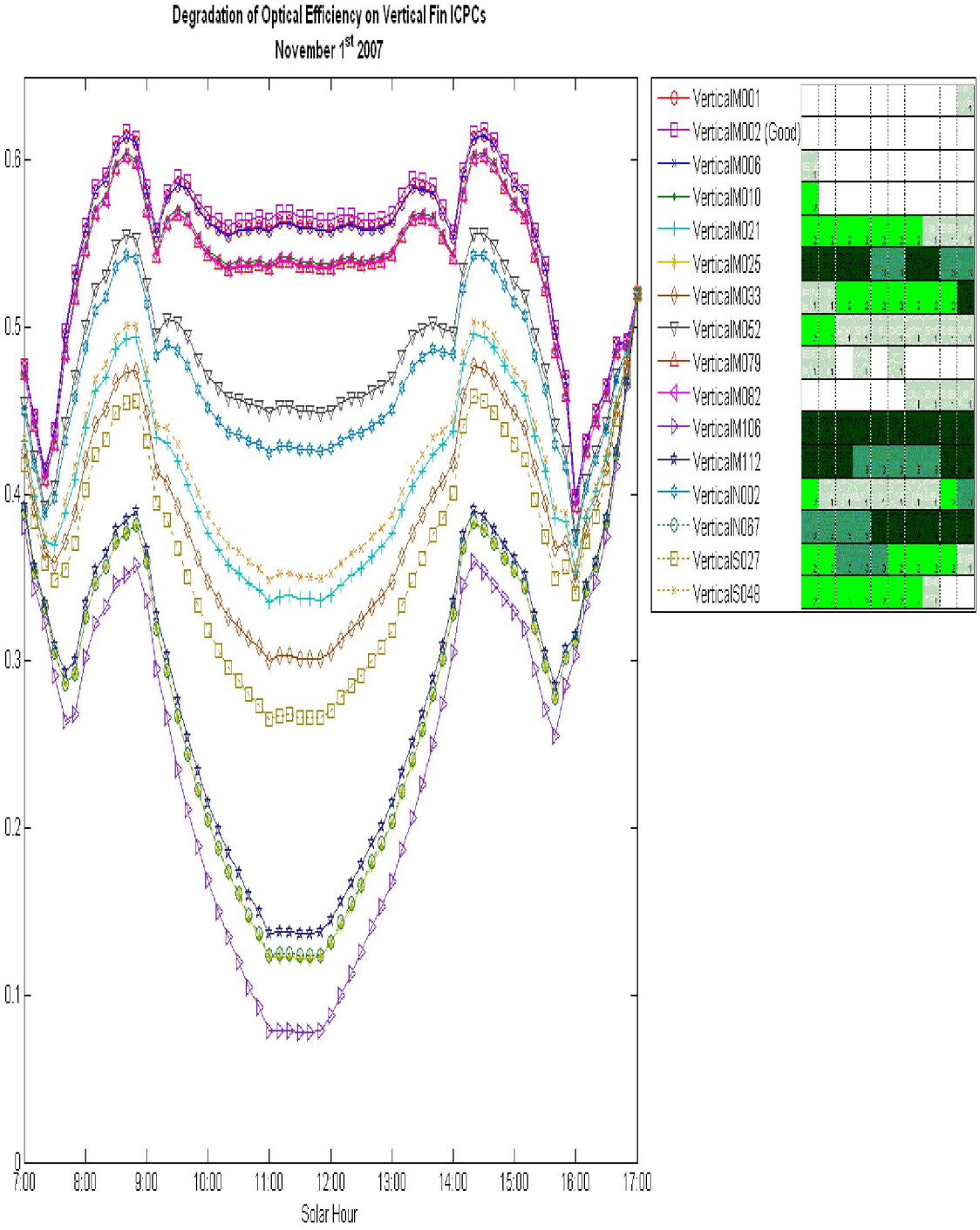

Figure 6.19: Matching optical efficiency with degradation map from middle bank (vertical fin) [beam radiation]

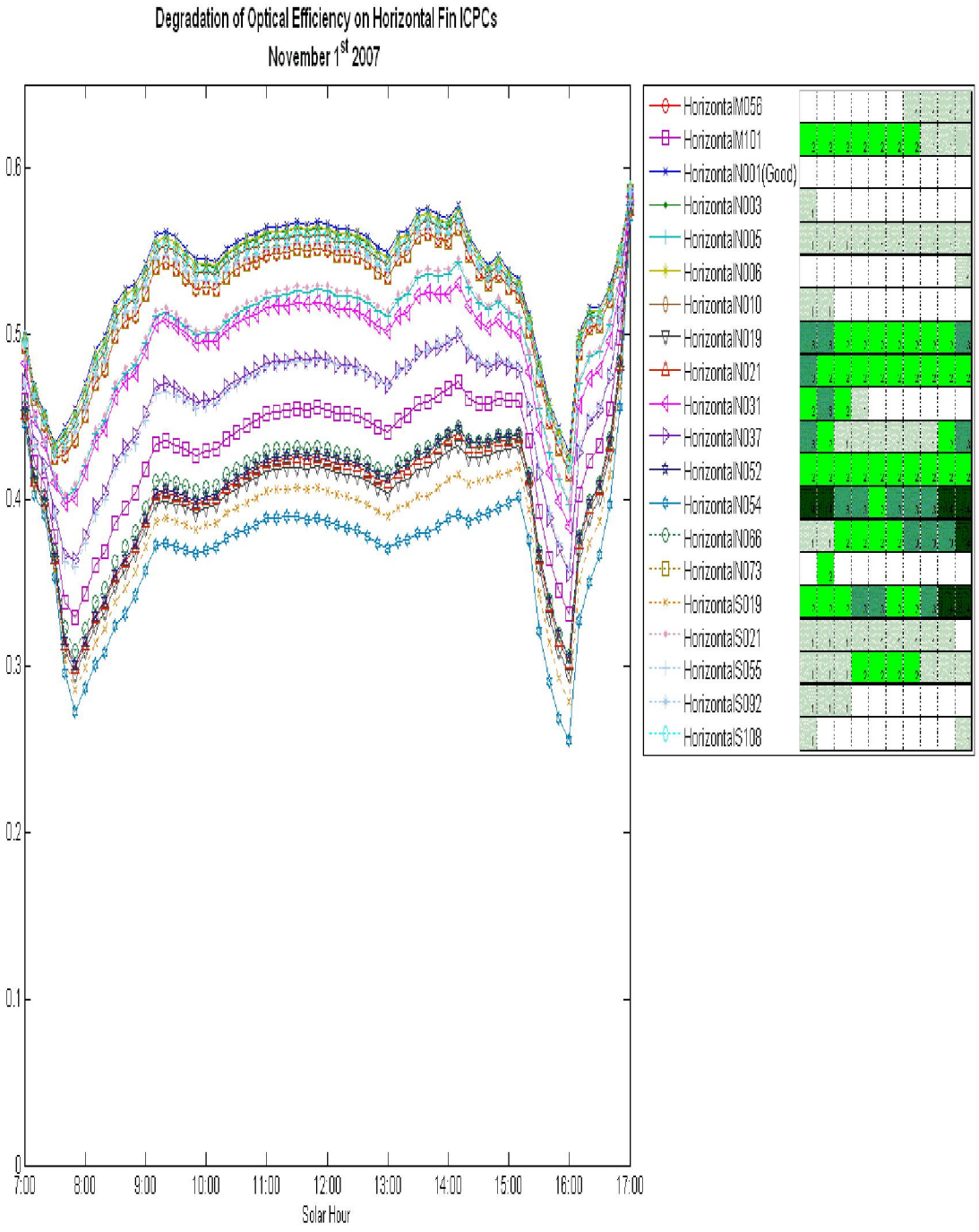

Figure 6.20: Matching optical efficiency with degradation map from north bank (horizontal fin) [beam radiation]

6.5 Summary

This chapter has shown the results of detailed analysis using the graphical ray-tracing tool that was developed. The next chapter will incorporate thermal loss into the ray tracing efficiency model analysis, using estimated thermal losses via the color mapping table. Comparisons of estimated and measured efficiency will be presented later in the chapter, and energy graphs for both estimated and measured will be shown.

CHAPTER 7

COMPARISON OF RAY TRACING ANALYSIS WITH THE SACRAMENTO DEMONSTRATION PROJECT RESULTS

7.1 Introduction

This chapter will present comparisons between predicted and measured performance for the Sacramento Demonstration project. In order to best match the ray-tracing analysis to the measured results, all parameter values such as reflector reflectivity, absorptance of the selective coating, the extinction coefficient, the gap between absorber fin and the glass cover and the pitch between the collector tubes will be incorporated. The predicted overall array performance is made up of a predicted optical efficiency from ray tracing analysis and predicted thermal losses from the evacuated tubes and manifolds, as calculated in chapter 5. There are two time frames of interest: 1999 and 2007. In 1999, early September data were since all tubes were inspected and in a good condition and all instrumentations were carefully monitored and calibrated. See appendix B.1. In 2007, degradation was investigated and mapped in detail on site. See sections 5.4 and 6.3. Overall efficiency of the ICPC was found by using ray tracing analysis and thermal loss analysis based on a one by one investigation of every one of the 336 tubes.

7.2 Comparing estimated and measured efficiencies

7.2.1 1999 comparisons

The initial comparisons in September 1999 were made when all the tubes were without any degradation and all instruments were newly calibrated and closely monitored. Each individual bank was investigated and measured. See Duff et al, 2000. Since all tubes held a complete vacuum, there was no convection loss from the heat transport tube to the glass cover and to the environment.

On September 2, 3, and 4, each of the three banks were run individually. The north bank was tested alone on September 2nd. The measured instantaneous efficiencies are shown by a blue line in Figure 7.1. The ray tracing analysis of the North bank horizontal finned ICPC was performed with the insolation data for that day. Then, heat loss~~es~~ estimates for the ICPCs (Figure 7.1, magenta line) and manifold were calculated and added to obtain the overall efficiency (Figure 7.1, brown line). Comparing overall calculated efficiency (Figure 7.1, brown line) with the measured efficiency (Figure 7.1, blue line) shows a very good match during 8:30 to 16:30 solar time. The same analysis is presented on a thermal energy plot (Figure 7.2).

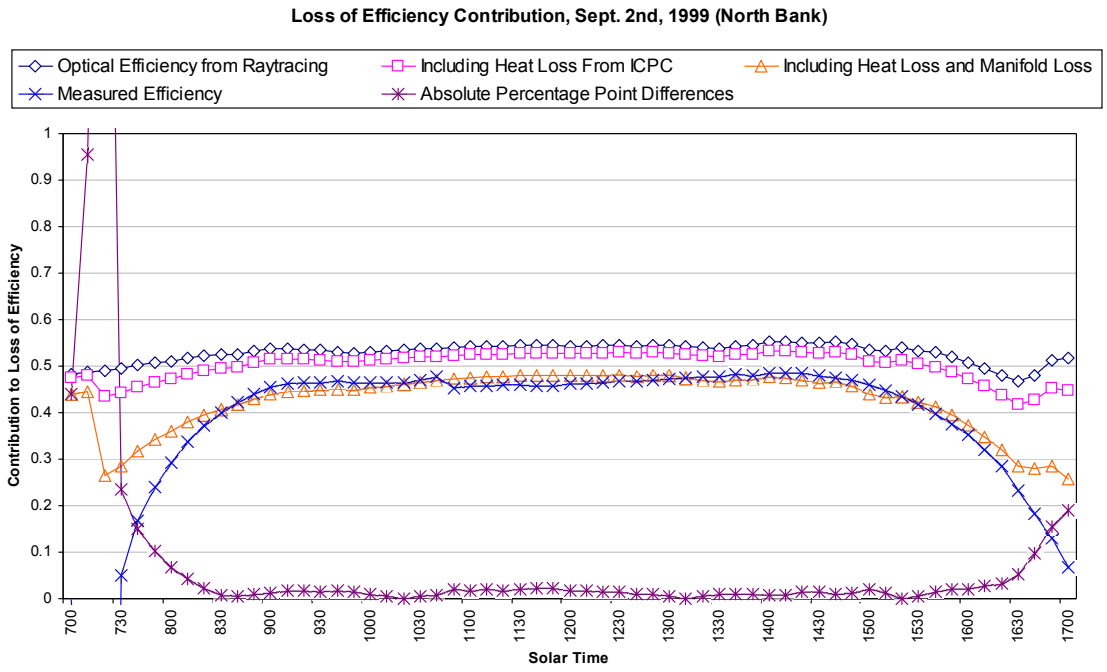

Figure 7.1: Comparison between predicted instantaneous efficiency and measured instantaneous efficiency, Sept. 2nd, 1999

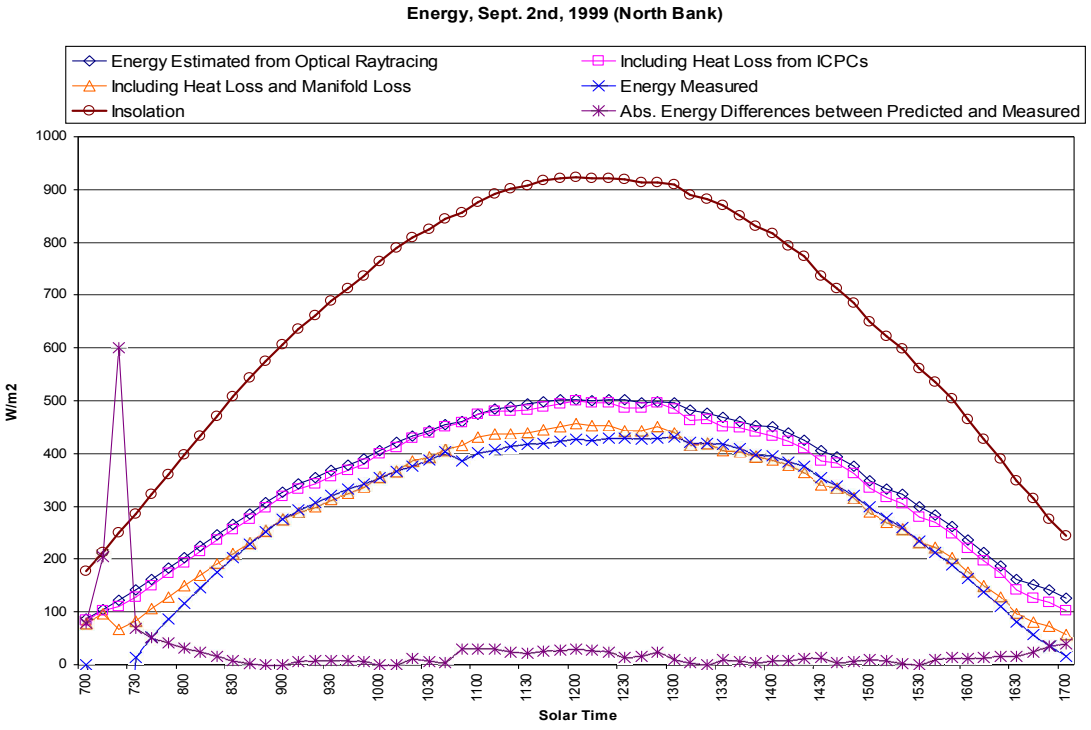

Figure 7.2: Comparison between estimated instantaneous energy and measured instantaneous energy, Sept. 2nd, 1999

On September 3rd, the middle bank was operated alone. The ray tracing analysis of the vertical finned ICPCs in the middle bank was used to find the array optical efficiency. Figure 7.3 shows the same steps of combining the optical efficiencies (dark blue) and thermal efficiencies to reach the overall efficiency (brown). Comparing overall efficiency (Figure 7.3, brown line) with the measured efficiency (Figure 7.3, blue line), the predicted efficiency (brown) shows a close match, a bit flatter in the middle part of the day, with the measured efficiency displaying a slightly concave appearance in the middle part of the day. The thermal energy plot (Figure 7.4) also shows the same, though not as discernible, behavior.

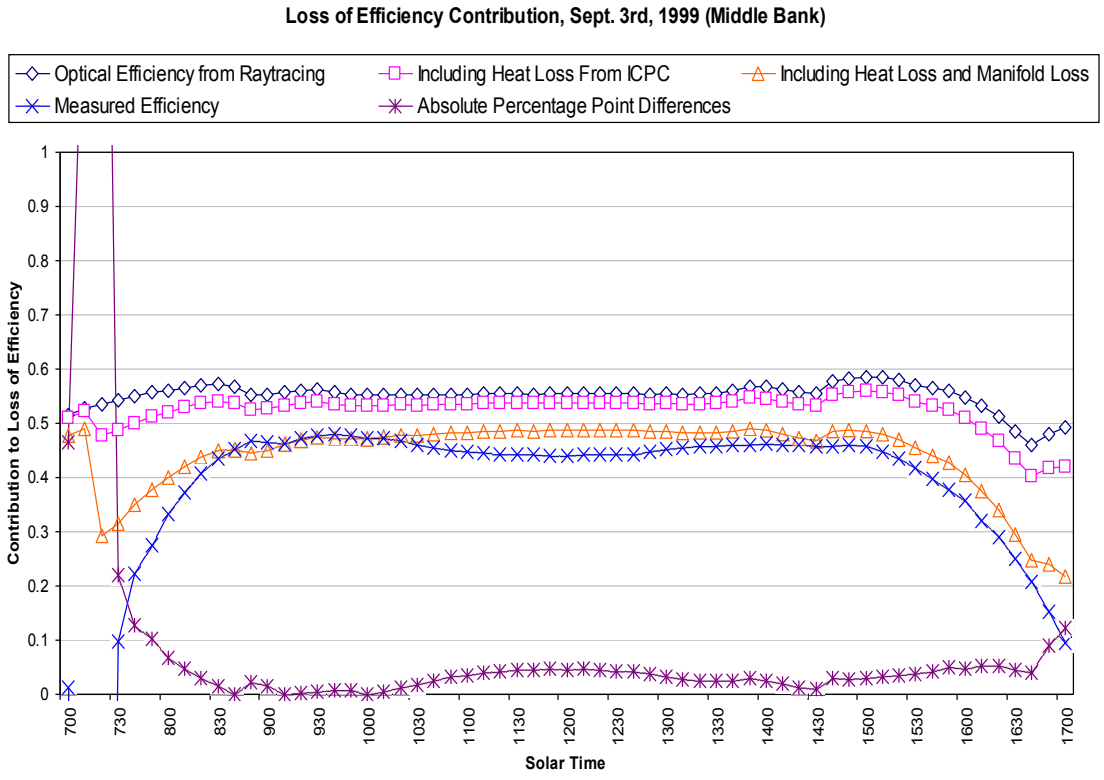

Figure 7.3: Comparison between predicted instantaneous efficiency and measured instantaneous efficiency, Sept. 3rd, 1999

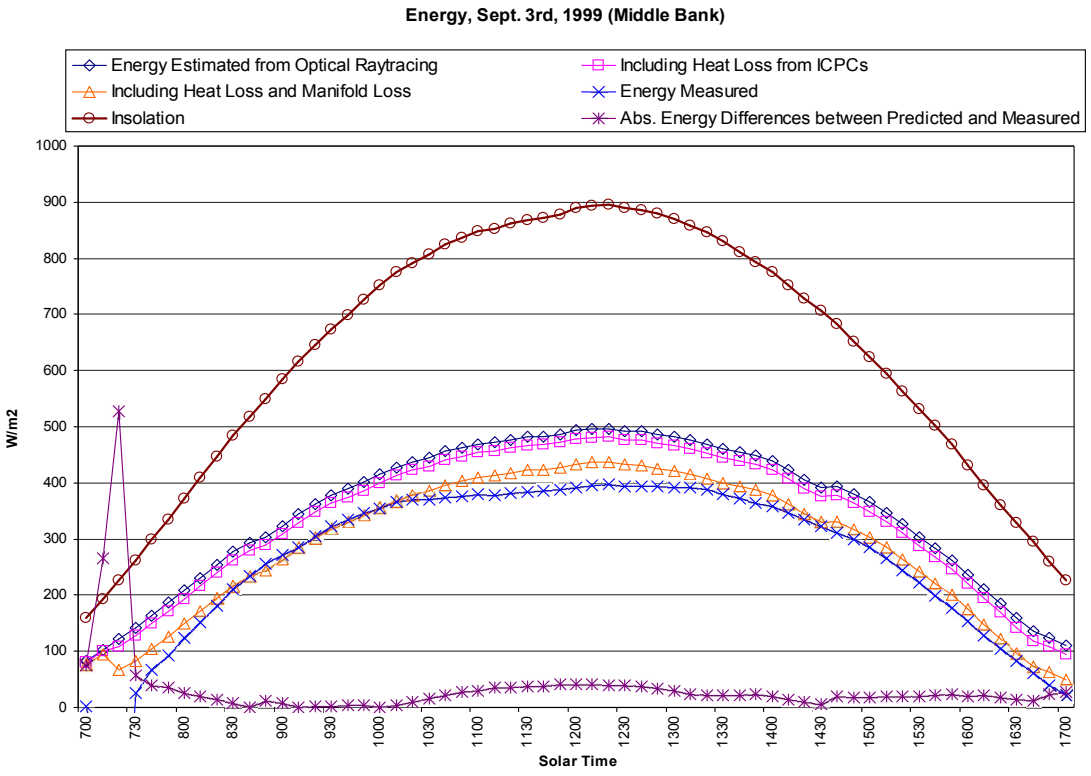

Figure 7.4: Comparison between estimated instantaneous energy and measured instantaneous energy, Sept. 3rd, 1999

On September 4th, only south bank was operated. The South bank consists of half vertical finned ICPCs and ~~a~~ half ~~of~~ horizontal finned ICPCs. The ray tracing analyses were performed for a half and half mixture of both fin (Figure 7.5, dark blue). By including all the thermal losses, the overall efficiency (brown) can be compared to the measured efficiency (blue) in Figure 7.5. The match is again close. There is a slightly higher percentage point differences (purple) in the middle of the day as compared to differences from 9:00 to 10:30 and 13:30 to 16:00. The energy plot (Figure 7.6) also shows the same information, though the differences are again less discernible in this plot.

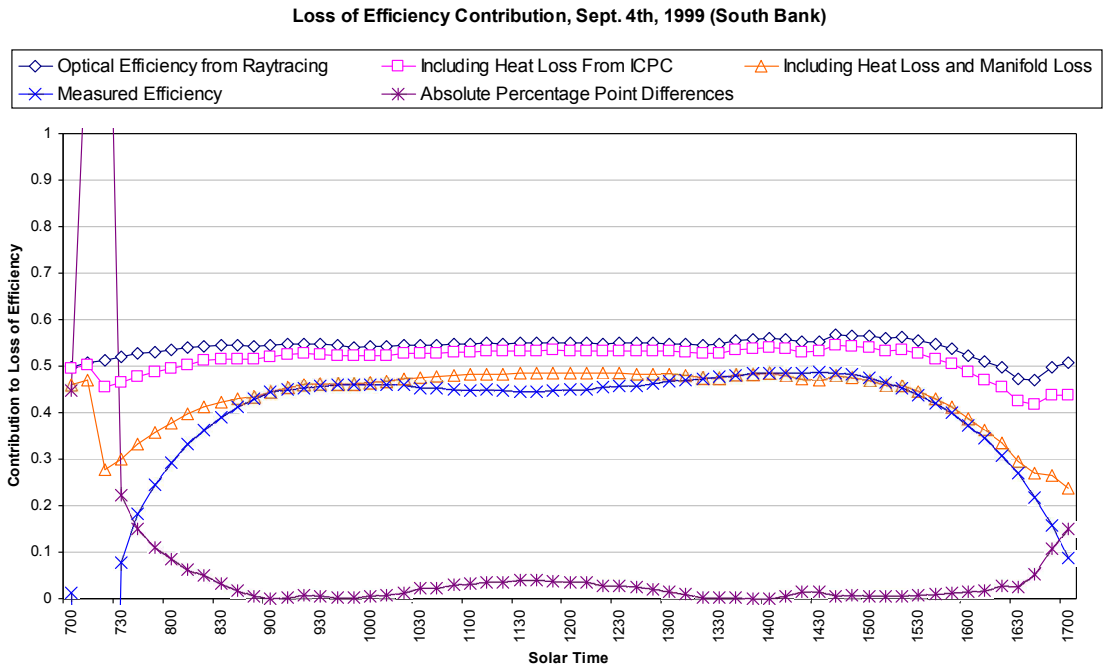

Figure 7.5: Comparison between predicted instantaneous efficiency and measured instantaneous efficiency, Sept. 4th, 1999

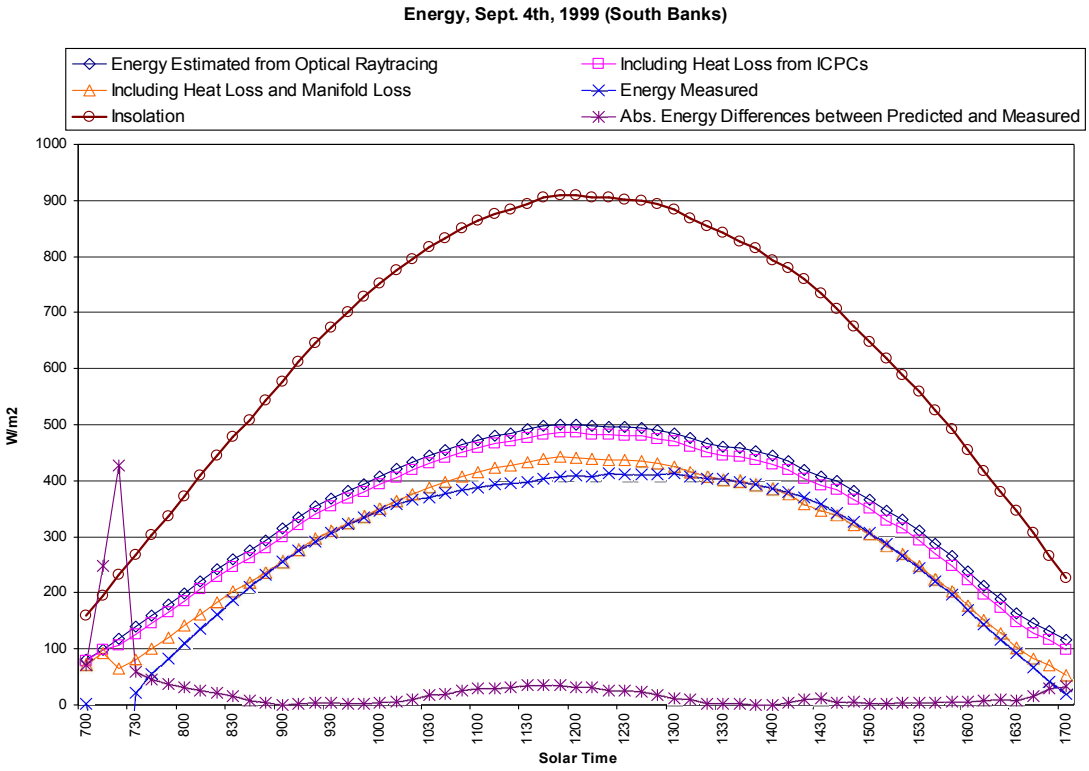

Figure 7.6: Comparison between estimated instantaneous energy and measured instantaneous energy, Sept. 4th, 1999

All banks are operated on September 8th, a day that was chosen to analyze because the sky was particularly clear. The ray tracing analyses were performed for both fin arrangements. By comparing the predicted overall efficiency to the measured efficiency, the absolute percentage point differences (Figure 7.7, purple line) between the two shows a less than 10 percent differences. The greatest differences are again in the middle of the day. The average difference from 9:00 to 15:00 is 0.052. Figure 7.8 shows the thermal energy plots on this day.

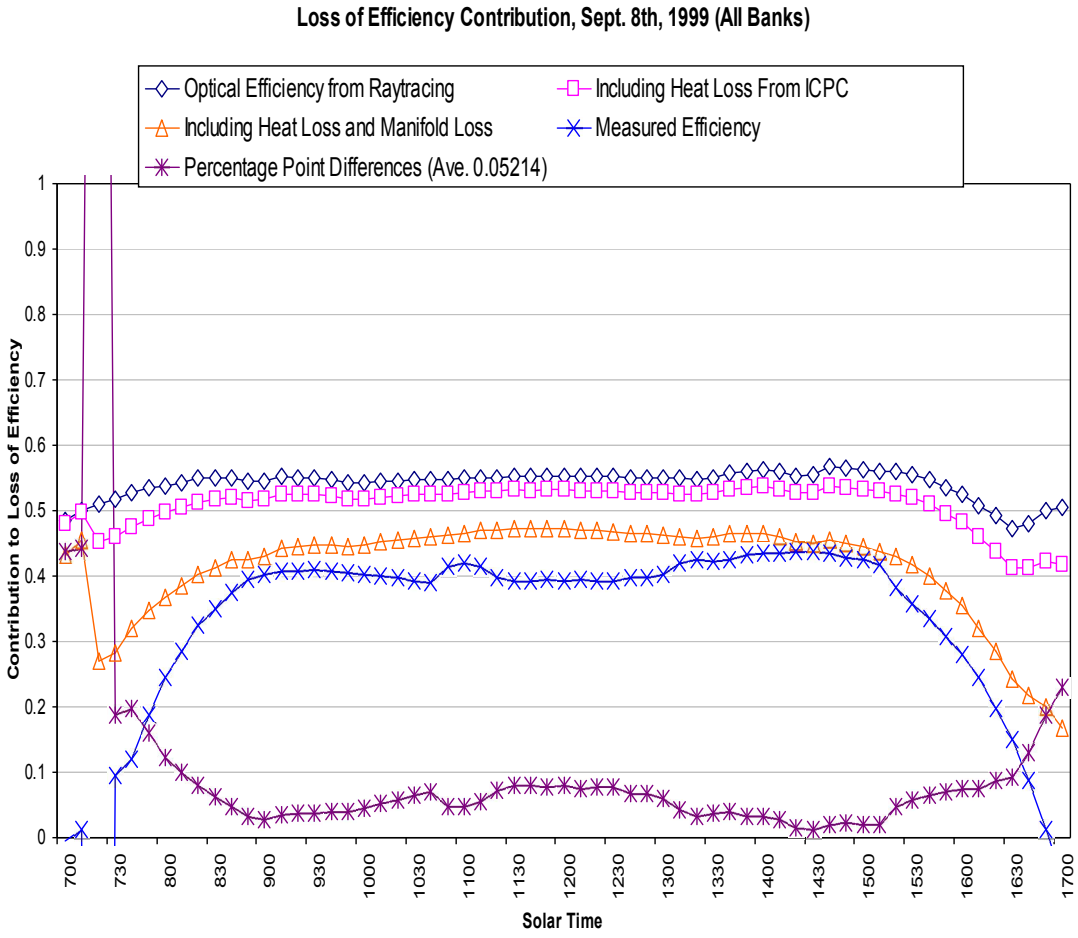

Figure 7.7: Comparison between predicted instantaneous efficiency and measured instantaneous efficiency, Sept. 8th, 1999

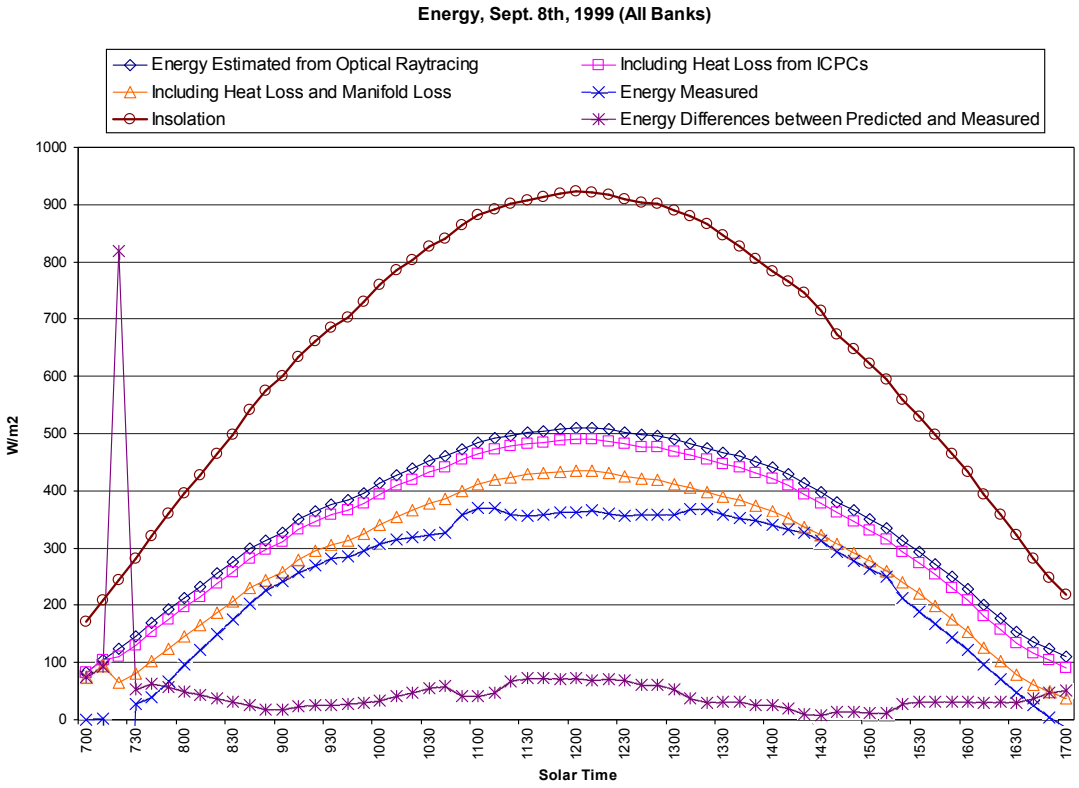

Figure 7.8: Comparison between estimated instantaneous energy and measured instantaneous energy, Sept. 8th, 1999

In all the Figures, a magenta line shows that there is a lesser heat loss from the ICPC tube than from the manifold (the brown line). Collectively, the charts show how the estimated ICPC thermal loss and manifold loss augment the estimated energy from the ray tracing analysis. From the mapped cover temperature, three ICPC heat loss levels are estimated. Overall heat loss is estimated by matching ICPC heat loss tube-by-tube to their positions in the array and then adding estimated manifold. In all the figures the quantities are plotted against solar time.

7.2.2 2007 comparisons

In October 2007, all the tubes were inspected and mapped for reflector degradation and cover temperatures (Chapter 5 and 6). November 1st and November 2nd were chosen due to clear sky and reliable data collecting as compared to other days. The ray tracing analysis is performed for all the tubes in the array. The predicted optical efficiency for each tube as mapped was plugged into the ray tracing routine and then the thermal losses are added to each tube. The predicted overall efficiency was found by averaging all the tube efficiencies.

On both November 1st and November 2nd, the measured efficiency showed a late system start. When comparing measured efficiency (blue) and predicted efficiency (brown) (Figure 7.9, 7.11), a good match occurs later in the days and there is about 10 percent difference prior to that. The average differences from 9:00 to 15:00 are 0.052~~14~~ on November 1st and 0.049 on November 2nd. Figures 7.10 and 7.12 also depict the same behavior.

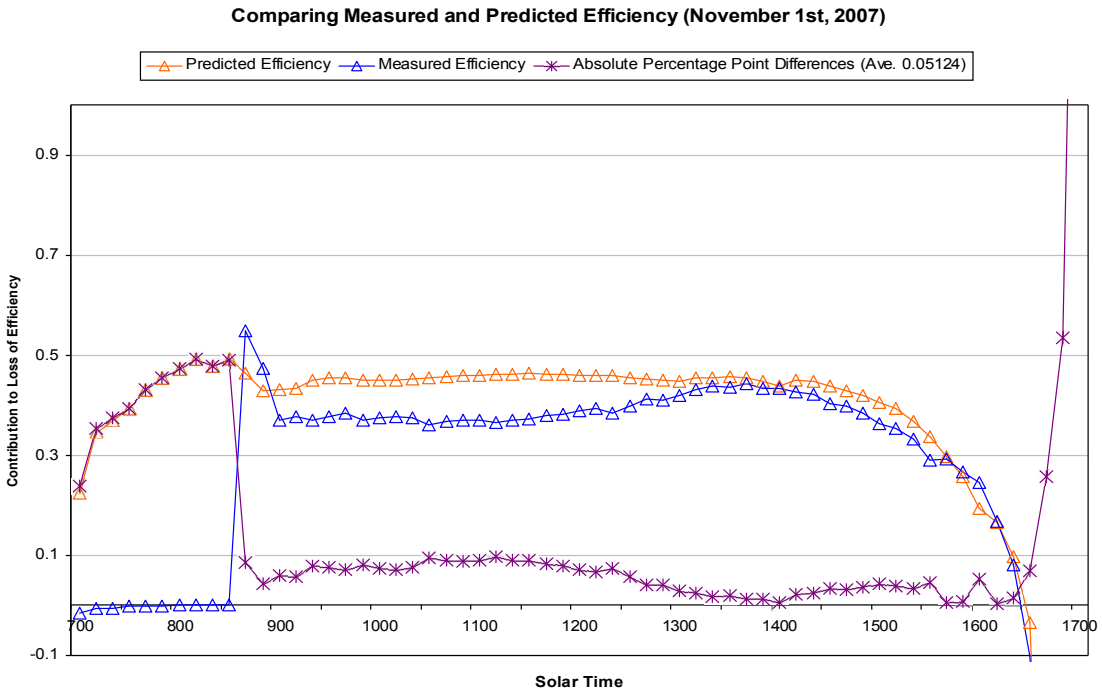

Figure 7.9: Comparison between predicted instantaneous efficiency and measured instantaneous efficiency, Nov. 1st, 2007

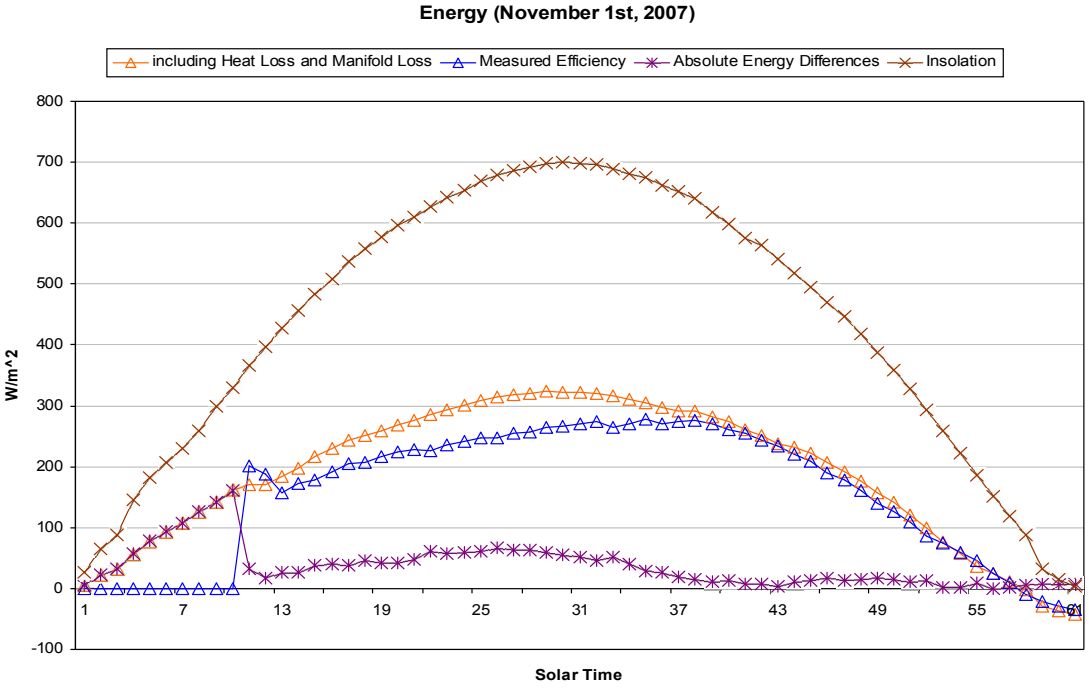

Figure 7.10: Comparison between estimated instantaneous energy and measured instantaneous energy, Nov. 1st, 2007

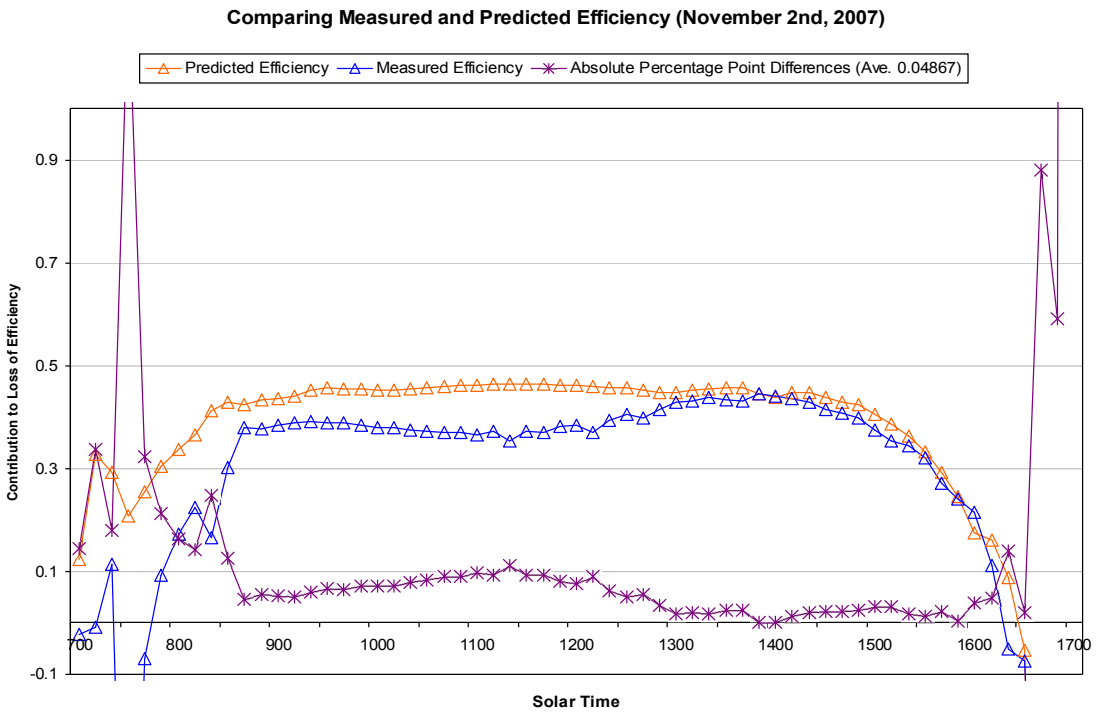

Figure 7.11: Comparison between predicted instantaneous efficiency and measured instantaneous efficiency, Nov. 2nd, 2007

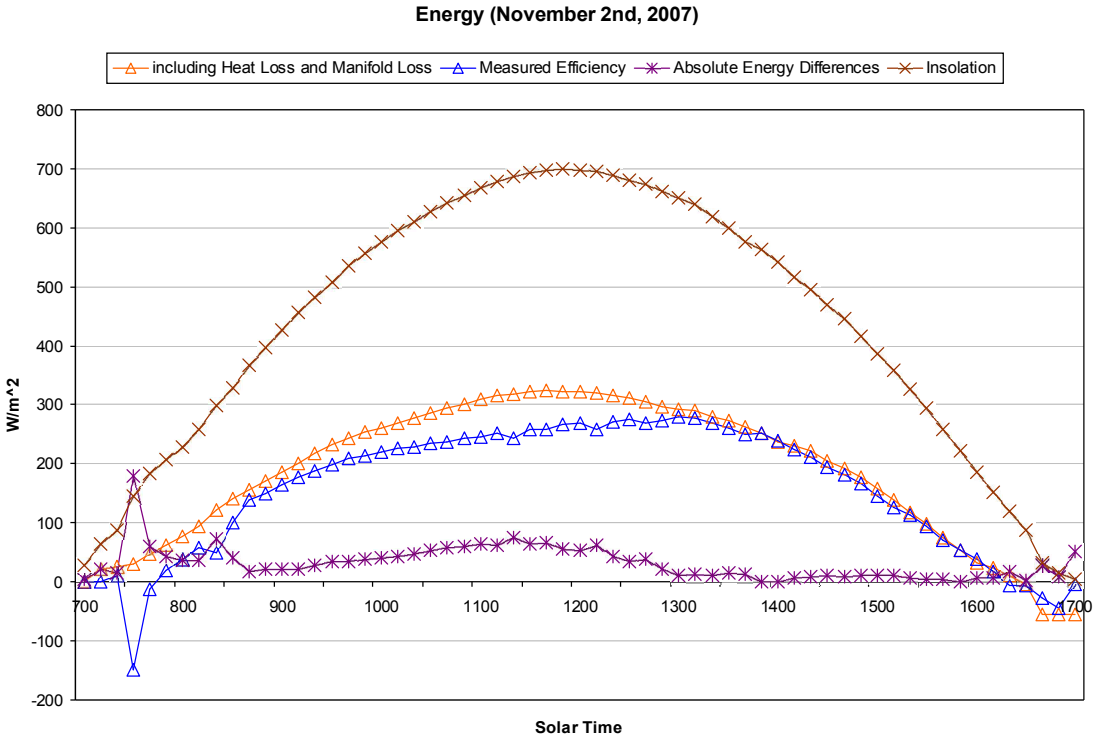

Figure 7.12: Comparison between estimated instantaneous energy and measured instantaneous energy, Nov. 2nd, 2007

7.3 Comparing an all good tube scenario performance in 2007 against predicted performance

The expected efficiency using all good tubes is plotted against the 2007 calculated efficiency with degradation in order to derive a good estimate of the decrease in array performance due to the two major sources of degradation, loss of vacuum due to cracks and leakage of fluid into the vacuum enclosure. See Figure 7.13 and 7.14. These figures show that there is about a 5 percent differences. Since the 1998/99 and 2007 measured versus predicted differences are nearly the same, degradation in performance could reasonably be assumed to be wholly attributable to these two sources.

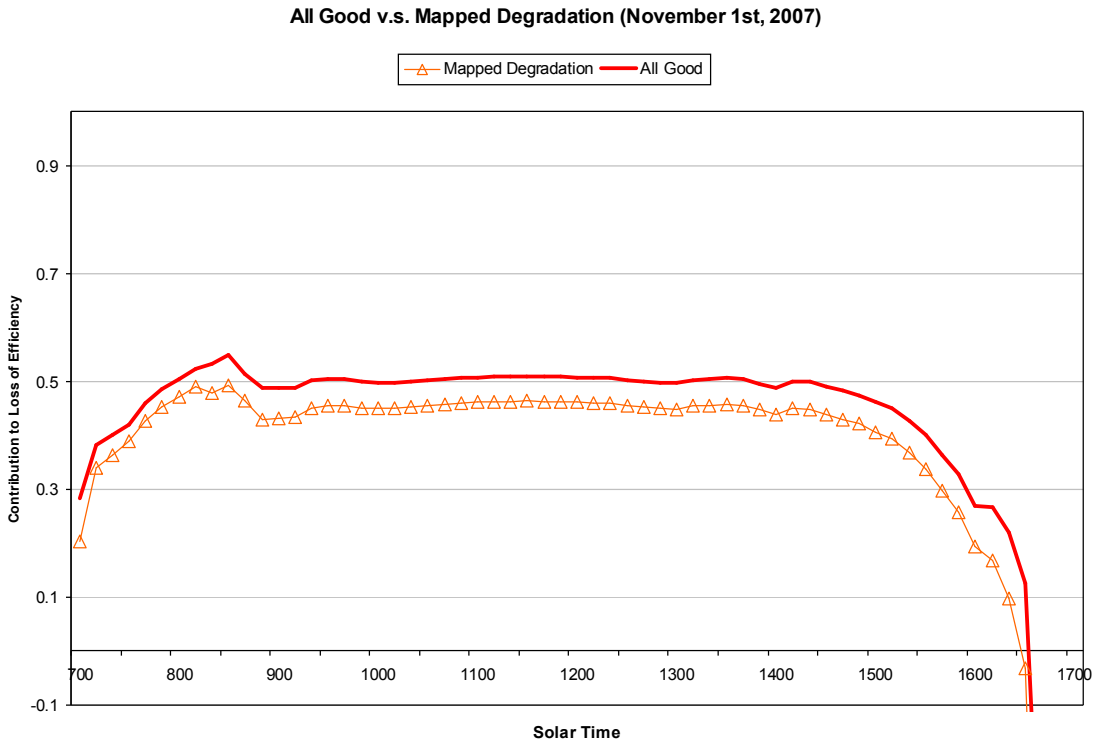

Figure 7.13: Comparison between all good tube and mapped degradation efficiency, Nov. 1st, 2007

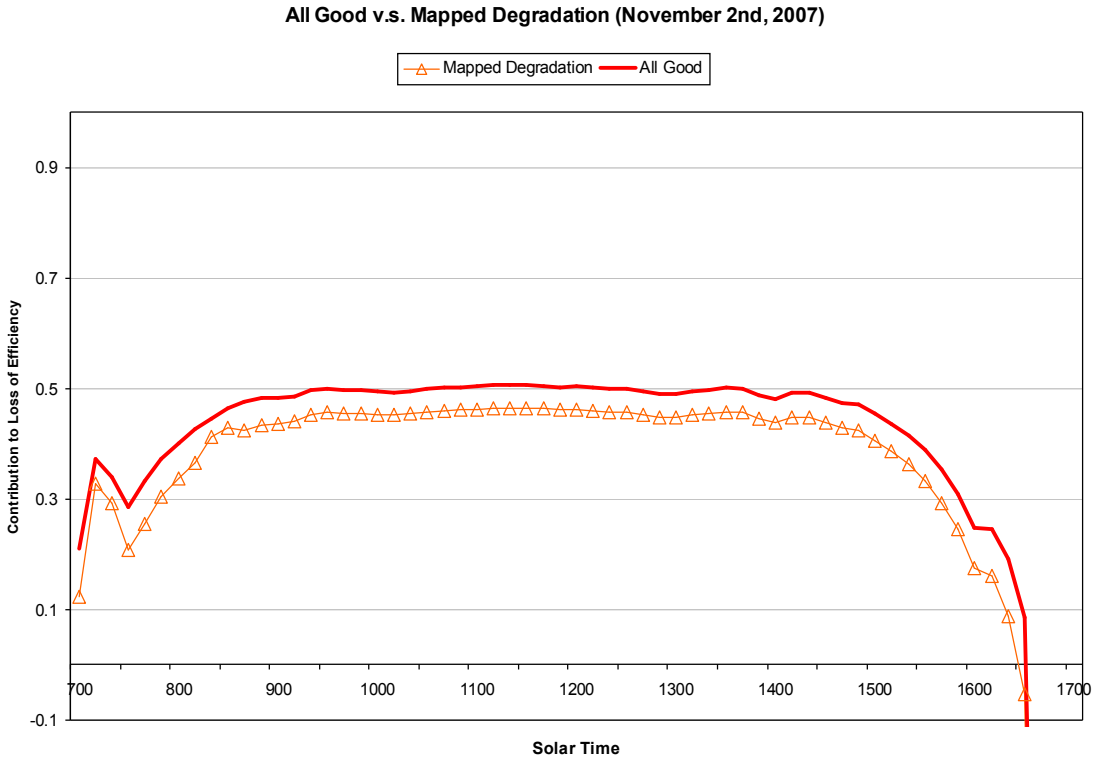

Figure 7.14: Comparison between all good tube and mapped degradation efficiency, Nov. 2nd, 2007

7.4 Summary

Heat loss from both the ICPC tubes and the manifold plays an important role in overall performance. Overall performance is also degraded by the loss of vacuum in the tube and leakage of fluid into the vacuum enclosure. An analysis of the performance consequences of reflector degradation due to fluid leakage and loss of vacuum has been compared with measured data. The predicted efficiency matches well with the measured efficiency, especially during at the beginning and the end of the day. The average differences in efficiencies are quite close for the time interval from 9:00 to 15:00 in both

1999 and 2007. Thus the predicted extent of the decrease in efficiency from an all good tube situation and the 2007 level of degradation appear to substantiate the dominating importance of the two identified degradation mechanisms. The next chapter will address conclusions and recommendations.

CHAPTER 8

CONCLUSIONS AND RECOMMENDATIONS

8.1 Conclusions

The ray tracing analysis provides an understanding of the optical performance and detailed optical efficiencies of the novel ICPC at various incident angles. The detailed ray tracing shows how each ray's intensity is attenuated. The animated graphical ray tracing allows the user to visualize the propagation of rays through the ICPC optics. Using the ray tracing analysis the optical efficiencies during daytime operating hours for both vertical and horizontal fin orientations of the ICPC have been investigated. It was found that a horizontal fin ICPC has a slightly better optical performance than a vertical fin ICPC. The ray tracing analysis also showed that the horizontal fin ICPC's performance was more robust to degradation of the reflective surface. The ray tracing analysis also provides a two-dimensional incident angle modifier formulation that is superior to earlier IAM characterizations.

The degradation and failure mechanisms for 13 years of operation of the ICPC mounted on a commercial building in Sacramento, California are investigated. The two main degradation mechanisms are reflectivity degradation due to air leakage and fluid leakage into the vacuum enclosure and loss of vacuum due to leaks through cracks. Reflectivity degradation causes a reduction of optical performance and the loss of

vacuum causes a reduction in thermal performance. Under substantial degradation of the reflector, the horizontal fin ICPC retains better optical performance than the vertical fin ICPC. Air leaking into the evacuated space of ICPC causes convection heat loss from the heat transport tube to the glass cover. This leads to a lower overall efficiency. All of the 336 evacuated tubes' reflectivities and glass cover temperatures were mapped. Ray tracing analysis and heat loss analysis were performed for each tube and the resultant degraded array efficiency was predicted. In comparing predicted array efficiency and measured array efficiency, the two efficiencies show close agreement, especially near the end of the day in 2007. It was also found that the average differences between measured and predicted efficiencies maintain the same levels, of about 5% in the time interval 9:00 to 15:00 from 1999 to 2007.

8.2 Recommendations

This dissertation focuses on the performance and the reliability study of the novel ICPC. The graphical ray tracing approach can provide a basic understanding of optical performance of evacuated tubes and reflectors. The heat loss analysis can provide a basic understanding on how the vacuum loss affects overall efficiency. This approach can be applied to a broader range of applications. Standardized analysis of array performance and reliability of all solar collectors could be of further interest. Also, by using the ray tracing technique, ICPC parameters could be modified to identify the optimum design of an ICPC.

BIBLIOGRAPHY

1. A.M. El-Nashar, The effect of dust accumulation on the performance of evacuated tube collectors. *Solar Energy*, *Volume 53*, *Issue 1, 1994, Pages 105–115*

2. Alvarez, J.J. Flores, J.O. Aguilar, O. Gómez-Daza, C.A. Estrada, M.T.S. Nair, P.K. Nair, Spectrally selective laminated glazing consisting of solar control and heat mirror coated glass: preparation, characterization and modeling of heat transfer, *Solar Energy, Volume 78, 2005, Pages 113–124*

3. Adel A. Hegazy, Effect of dust accumulation on solar transmittance through glass covers of plate-type collectors, *Renewable Energy, Volume 22, Issue 4, April 2001, Pages 525-540*

4. Andreas Schüler, Jürgen Geng, Peter Oelhafen, Stefan Brunold, Paul Gantenbein and Ueli Frei, Application of titanium containing amorphous hydrogenated carbon films (a-C:H/Ti) as optical selective solar absorber coatings, *Solar Energy Materials and Solar Cells, Volume 60, Issue 3, 31 January 2000, Pages 295-307*

5. B. Carlsson, (1987), Mathematical Models for Service Life Prediction., *IEA Task X Report*, Research on Materials for Solar Heating and Cooling Systems; report available from the Swedish National Testing flat- and Research Institute, P.O. Box 857, S-50115 Boras, Sweden.

6. B. Carlsson (1988), Survey of service life prediction methods for materials in solar heating and cooling, A Technical Report of Task X: Solar Energy Materials Research and Development of the International Energy Agency, Solar Heating and Cooling Programme, Swedish Council for Building Research Document D16, ISBN 91-540-5063-4

7. B. Carlsson, Frei U, Köhl M, Möller K.(1994), Accelerated life testing of solar energy materials. Report of Task X Solar Materials Research and Development. International Energy Agency Solar Heating and Cooling Programme, report available from the Swedish National Testing flat- and Research Institute, P.O. Box 857, S-50115 Boras, Sweden.

8. B. Carlsson, K. Möller, M. Köhl, U. Frei and S. Brunold, Qualification test procedure for solar absorber surface durability. *Solar Energy Mater., Solar Cells 61, 2000, Pages 255–275*

9. B. Carlsson, K. Möller, U. Frei, S. Brunold and M. Köhl, Comparison between predicted and actually observed in-service degradation of a nickel pigmented anodized aluminium absorber coating for solar DHW systems. *Solar Energy Mater. Solar Cells* 61, *2000, Pages 223–238*

10. B. Vitt, Characterization of a solar selective black cobalt coating, *Solar Energy Materials, Volume 13, Issue 5, June 1986, Pages 323-350*

11. B. Feuermann and A. Zemel, Dust-induced degradation of pyranometer sensitivity. *Solar Energy, Volume 50, Issue 6, 1993, Pages 483–486*

12. C. Goossens, Z.Y. Offer and A. Zangvil, Wind tunnel experiments and field investigations of eolian dust deposition on photovoltaic solar collectors. *Solar Energy*, *Volume 50* , *Issue 1, 1993, Pages 75–84*

13. Close, The performance of solar water heaters with natural circulation, *Solar Energy, Volume 6, Issue 1, January-March 1962, Pages 33-40*

14. Duff, William S., "Solar Cooling and other Thermal Uses of Improved ICPC Solar Collectors," In Search of the Sun: Proceedings of the International Solar Energy Society Congress, Harare, Zimbabwe, September 1995.

15. Duff, William S., "The ICPC: Design and Development", presentation at the Enrico Fermi Institute Symposium: Roland Winston Celebration, University of Chicago, May 2003.

16. Duff, William S., "Long-Term Performance and Reliability Evaluation of the Solarhaus Freiburg Evacuated Collectors", invited presentation at the 25th Anniversary Celebration of the Solarhaus Freiburg, Freiburg, Germany, June, 2004.

17. Duff, William S. and Arun Menon, "Computation of Incidence Angle Modifiers for Asymmetric Solar Collectors," Bright Star for the Blue Planet: Proceedings of the American Solar Energy Society Conference, Cocoa Beach, Florida, June 1992.

18. Duff, William S. and Arun Menon, "The Increased Availability of Collectable Radiation for Cylindrical Absorber Geometry Evacuated Tubular Collectors," Solar Energy Forum: Proceedings of the American Solar Energy Society Conference, Washington D.C., April 1993.

19. Duff, William S. and Arun Menon, "Modeling and Validation of Integral Collector Storage Evacuated Collectors," Solar Energy Forum: Proceedings of the American Solar Energy Society Conference, Washington D.C., April 1993.

20. Duff, William S. and Arun Menon, "Increased Availability of Collectable Radiation for Tubular Collectors with Cylindrical Absorbers," Harmony with Nature: Proceedings of the International Solar Energy Society Congress, Budapest, Hungary, August 1993.

21. Duff, William, D. Hodgson, and L. Hamasaki, "Experimental Evaluation of Selective Surfaces in Evacuated Collectors", Proceedings of the 1998 American Solar Energy Society Conference -- Renewable Energy for the Americas, Albuquerque NM, June, 1998.

22. Duff, William and D Hodgson, "Calorimetric Evaluation of Selective Surfaces in a Vacuum", Proceedings of the American Solar Energy Society Conference -- SOLAR 99, Portland Maine, June 1999.

23. Duff, William and D Hodgson, "Experimental Evaluation of Selective Surfaces in a High Vacuum", Proceedings of the1999 International Solar Energy World Congress: Solar is Renewable, Jerusalem, Israel, July 1999.

24. Duff, William and D Hodgson, "Testing of a Flat Plate Collector with Selective and Non-selective Absorbers that are Otherwise Identical", Proceedings of the 1999 International Solar Energy World Congress B Solar is Renewable, Jerusalem, Israel, July 1999.

25. Duff, William and D Hodgson, "Experimental Evaluation of Selective Surfaces in Different Configurations", Proceedings of the American Solar Energy Society Conference -- SOLAR 2000, Madison Wisconsin, June 2000.

26. Duff, William S. and David Hodgson, "Development of a Density Driven Solar Water Pasteurization System", International Solar Energy Society 2005 Congress, Orlando, Florida, August 2005.

27. Duff, William, Jirachote Daosukho, Roland Winston, Joseph O'Gallagher, Tom Henkel and Jim Bergquam, "Performance and Reliability Evaluation of the Sacramento Demonstration Novel ICPC Solar Collectors", International Solar Energy Society 2005 Congress, Orlando, Florida, August 2005.

28. Duff, William S. and Jirachote Daosukho, "Reliability and Degradation Study of the Sacramento Demonstration Novel ICPC Solar Collectors", American Solar Energy Society 2006 Congress, Denver, Colorado, July 2006.

29. Duff, William S. and Jirachote Daosukho, "Recent Progress in the Reliability and Degradation Study of the Sacramento Demonstration Novel ICPC Solar Collectors",

American Solar Energy Society 2007 Conference, Cleveland, Ohio, July 2007.

30. Duff, William S. and Jirachote Daosukho, “A Performance and Reliability Study of a Novel ICPC Solar Collector Installation”, International Solar Energy Society 2007 Solar World Congress, Beijing. China, September 2007.

31. Duff, William S. and Jirachote Daosukho, “New Optical Modeling and Material Degradation Results in the Long Term Study of a Novel ICPC Solar Collector Installation”, International Solar Energy Society and American Solar Energy Society 2008 Congress, San Diego, California, May 2008.

32. Duff, William S. and Jirachote Daosukho, "Ten Year Study of a Novel ICPC Solar Collector Installation: Optical Modeling and Material Degradation", International Solar Energy Society 2008 EuroSun Conference, Lisbon, Portugal, October 2008.

33. Duff, William S. and Jirachote Daosukho, “Eleven Year Evaluation of a Novel ICPC Solar Collector Installation: The Role of Failure Modes in Changing Optical and Thermal Performance”, International Solar Energy Society and American Solar Energy Society 2009 Congress, Buffalo, New York, May 2009.

34. Duff, William S. and Jirachote Daosukho, “Twelve Year Evaluation of a Novel ICPC Solar Collector Installation: The Role of Failure Modes in Changing Optical and Thermal Performance”, American Solar Energy Society 2010 Congress, Phoenix, Arizona, May 2010.

35. Duff, William S. and Jirachote Daosukho, “Three Dimensional Ray Tracing and Reliability Analyses of a Novel ICPC Collector after Twelve Years of Operation ", 2010 Solar World Congress and 2010 EuroSun Conference, Graz, Switzerland, September 2010.

36. Duff, William S. and Jirachote Daosukho, “Evaluation of a Novel ICPC Solar Collector Installation: Degradation Analysis and Comparison between Measured and Predicted Performance”, American Solar Energy Society 2011 Congress, Raleigh, North Carolina, May 2011.

37. Duff, William S. and Jirachote Daosukho, “Evaluation of a Novel ICPC Solar Collector Installation: Degradation Analysis Including Diffuse and Beam Analysis and Comparison between Measured and Predicted Performance", 2011 Solar World Congress, Kassel, Germany, September 2011.

38. Duff, William, Jirachote Daosukho, Klaus Vanoli, Roland Winston, Joseph O’Gallagher, Tom Henkel and Jim Bergquam, “Comparisons of the Performance of Three Different Types of Evacuated Tubular Solar Collectors”, American Solar Energy Society 2006 Congress, Denver, Colorado, July 2006.

39. Duff, William S. and Klaus Vanoli, “Long Term Performance and Reliability of Two Evacuated Collectors”, International Solar Energy Society 2005 Congress, Orlando,

Florida, August 2005.

40. Duff, William, R. Duquette, R. Winston, and J. O'Gallagher, "Development, Fabrication, and Testing of a New Design for the Integral Compound Parabolic Evacuated Solar Collector," Proceedings of the 1997 American Solar Energy Society Conference -- Solar Energy Forum, Washington, DC, April, 1997

41. Duff, William S., Roland Winston, and Joseph O'Gallagher, "A Solar Cooling Commercial Building Demonstration: Cost and Performance Studies," Golden Opportunities for Solar Prosperity: Proceedings of the American Solar Energy Society Conference, San Jose California, June 1994.

42. Duff, William S., Roland Winston, and Joseph O'Gallagher, "Cooling of Commercial Buildings with ICPC Solar Collectors," 1995 ASME International Solar Energy Conference, Maui, Hawaii, April 1995.

43. Duff, William S., R. Winston, J. O'Gallagher, T. Henkel, R. Christiansen and J. Bergquam, "Demonstration of A New ICPC Design With a Double-Effect Absorption Chiller in an Office Building in Sacramento California", American Solar Energy Society Conference, Portland, Maine, June 1999

44. Duff, William S., R. Winston, J. O'Gallagher, T. Henkel, and J. Bergquam, "Update on the New High Performance ICPC Sacramento Cooling Demonstration", American Solar Energy Society Conference, Madison Wisconsin, June 2000.

45. Duff, William S., R. Winston, J. O'Gallagher, T. Henkel, R. Christensen and J. Bergquam, "Operating Experience with the New ICPC Solar Collector and Double-Effect Absorption Chiller", International Solar Energy Society Forum 2000, Mexico City, September 2000

46. Duff, W. S., Winston, R., O'Gallagher, J., Henkel, T. and Bergquam, J., "Performance of a New ICPC Collector and Double Effect Chiller", 2000 American Solar Energy Society Conference, Washington, DC, April 2000

47. Duff, William, Roland Winston, Joseph O'Gallagher, Tom Henkel and Jim Bergquam, "Performance of a New ICPC Collector and Double Effect Chiller", Proceedings of the American Solar Energy Society, Washington DC, April 2001.

48. Duff, W. S., Winston, R., O'Gallagher, J., Henkel T. and Bergquam, J., "Performance of the Sacramento Demonstration ICPC Collector and Double-Effect Chiller in 2000 and 2001", 2001 International Solar Energy Society Congress, Adelaide, Australia, December 2001

49. Duff, W. S., Winston, R., O'Gallagher, J., Henkel T. and Bergquam, J., "ICPC Collector/Double-Effect Chiller Sacramento project Update", 2001American Solar Energy Society Conference, Reno, Nevada, June 2001

50. Duff, William S., Winston, R., O'Gallagher, J., Henkel, T. and Bergquam, J., "Performance of the Sacramento Demonstration ICPC Collector and Double Effect Chiller in 2000 and 2001", *Solar Energy vol. 76, pages 175-180, January 2004*

51. Duff, William, Roland Winston, Joseph O'Gallagher, Tom Henkel and Jim Bergquam, "Novel ICPC Solar Collector/Double Effect Absorption Chiller Demonstration Project", Proceedings of the 2003 American Society of Mechanical Engineers International Solar Energy Conference, Mauna Kea, Hawaii Island, Hawaii, March 2003.

52. Duff, W. S., Winston, R., O'Gallagher, J., Henkel T. and Bergquam, J., "Novel ICPC Solar Collector/Double-Effect Chiller Demonstration Project", 2003 American Society of Mechanical Engineers' International Solar Energy Conference, Kohala Coast HI, March 2003

53. Duff, W. S., Winston, R., O'Gallagher, J., Henkel T. and Bergquam, J., "Five Year Novel ICPC Solar Collector Performance", 2003 American Solar Energy Society Solar Energy Conference, Austin TX, June 2003

54. Duff, William S. and Klaus Vanoli, "Long-Term Performance and Reliability Evaluation of Three Evacuated Collectors", International Solar Energy Society 2004 - EuroSun Conference, Freiburg Germany, June 2004.

55. Duff, William, Roland Winston, Joseph O'Gallagher, Tom Henkel and Jim Bergquam, "Six Year Evaluation of the Novel ICPC Sacramento Demonstration", American Solar Energy Society Conference 2004 - A Solar Harvest: Growing Opportunities, Portland Oregon, July 2004

56. Duffie J. A. and Beckman W. A. (1991). In *Solar engineering of thermal processes*, 2nd ed., pp. 303–312, Wiley-Inter- science, New York.

57. Garrison, J. D., Optimization of Fixed Solar Thermal Collectors, *Solar Energy, v23, 1979*

58. Garg, P., Effect of dirt on transparent covers in flat-plate solar energy collectors. *Solar Energy Volume 15, Issue 4*, *1974, pages 299–302*

59. Henklel, E. Thomas, William S. Duff, Roland Winston, Joseph J. O'Gallagher, Richard Christiansen and James Bergquam, "Solar-Powered Double Effect Absorption Cooling for Commercial HVAC Systems", 22nd World Energy Engineering Congress (WEEC), October, 1999 in Atlanta.

60. Jürgen Schnieders, Comparison of the energy yield predictions of stationary and dynamic solar collector models' and the models accuracy in the description of a vacuum tube collector, *Solar Energy, Volume 61, Issue 3, September 1997, Pages 179-190*

61. Klucher, T.M., 1979. Evaluation of models to predict insolation on tilted surfaces. Solar Energy 23 (2), 111–114.

62. Knappmiller, K. and William S. Duff, "Computing Incidence Angle Modifiers for Advanced Solar Collectors," Solar Energy for the 21st Century: Proceedings of the International Solar Energy Society Congress, Denver, Colorado, August 1991.

63. Liu, B.Y.H., Jordan, R.C., 1960. The interrelationship and characteristic distribution of direct, diffuse and total solar radiation. Solar Energy 4, 1–19.

64. Loutzenhiser, P.G., Manz, H., Felsmann, C., Strachan, P.A., Frank, T., Maxwell, G.M., 2007. Empirical validation of models to compute solar irradiance on inclined surfaces for building energy simulation. Solar Energy 81, 254–267.

65. M. Bosanac and J. E. Nielsen, *In situ* check of collector array performance, *Solar Energy, Volume 59, Issues 4-6, April-June 1997, Pages 135-142*

66. M. Koehl, Durability of solar energy materials, *Renewable Energy, Volume 24, Issues 3-4, November 2001, Pages 597-607*

67. M. Köhl, M. Heck, S. Brunold, U. Frei, B. Carlsson and K. Möller, Advanced procedure for the assessment of the lifetime of solar absorber coatings, *Solar Energy Materials and Solar Cells, Volume 84, Issues 1-4, October 2004, Pages 275-289*

68. M.S. El-Shobokshy and F.M. Hussein, Effect of dust with different physical properties on the performance of photovoltaic cells. *Solar Energy, Volumn 51, Issue 6, 1993, Pages 505–511*

69. M. Souliotis and Y. Tripanagnostopoulos, Experimental study of CPC type ICS solar systems, *Solar Energy, Volume 76, Issue 4, April 2004, Pages 389-408*

70. Michael W. Edenburn, Performance analysis of a cylindrical parabolic focusing collector and comparison with experimental results, *Solar Energy, Volume 18, Issue 5, 1976, Pages 437-444*

71. O'Gallagher, Joseph J., Roland Winston, Dave Cooke, and William Duff, "The New Integrated CPC," Bright Star for the Blue Planet: Proceedings of the American Solar Energy Society Conference, Cocoa Beach, Florida, June 1992.

72. O'Gallagher, Joseph J., Roland Winston, Robert Holman, and William S. Duff, "Towards a Low Cost Integrated CPC," Solar Energy Forum: Proceedings of the ASME Solar Energy Conference, Washington D.C., April 1993

73. Ole Holck , Svend Svendsen, Stefan Brunold, Ueli Frei, Michael Köhl, Markus Heck, Henk Oversloot, Solar collector design with respect to moisture problems, *Solar Energy, Volume 75, 2003, 269–276*

74. Paul Wencil Brown, Kevin G. Galuk and Walter J. Rossiter, Jr , Characterization of potential thermal degradation products from the reactions of aqueous ethylene glycol and propylene glycol solutions with copper metal, *Solar Energy Materials, Volume 16, Issue 4, October 1987, Pages 309-313*

75. Per Nostell, Arne Roos, Björn Karlsson, Ageing of solar booster reflector materials, *Solar Energy Materials and Solar Cells, v54, p235–246, 1998*

76. Perez, R., Stewart, R., Arbogast, C., Seals, R., Scott, J., 1986. An anisotropic hourly diffuse radiation model for sloping surfaces: Description, performanace validation, site dependency evaluation. *Solar Energy 36 (6), 481–497.*

77. Perez, R., Seals, R., Ineichen, P., Stewart, R., Menicucci, D., 1987. A new simplified version of the Perez diffuse irradiance model for tilted surfaces. *Solar Energy 39 (3), 221–232.*

78. Perez, R., Ineichen, P., Seals, R., Michalsky, J., Stewart, R., 1990. Modeling daylight availability and irradiance components from direct and global irradiance. *Solar Energy 44 (5), 271–289*

79. Peter J. Lunde, Prediction of the monthly and annual performance of solar heating systems, *Solar Energy, Volume 20, Issue 3, 1978, Pages 283-287*

80. R. Winston and H. Hinterberger, Principles of cylindrical concentrators for solar energy, *Solar Energy, Volume 17, Issue 4, 1975 Pages 255-258*

81. Reindl, D.T., Beckmann, W.A., Duffie, J.A., 1990b. Evaluation of hourly tilted surface radiation models. Solar Energy 45 (1), 9–17.

82. S. A. Biryukov, Degradation of optical properties of solar collectors due to the ambient dust deposition as a function of particle size, *Journal of Aerosol Science, Volume 27, Supplement 1, September 1996, Pages S37-S38*

83. S. Brunold, U. Frei, B. Carlsson, K. Moller and M. Kohl, Accelerated life testing of solar absorber coatings: testing procedure and results, *Solar Energy, Volume 68, No. 4, pp. 313–323, 2000*

84. S. Brunold, U. Frei, B. Carlsson, K. Möller and M. Köhl, Round robin on accelerated life testing of solar absorber surface durability. *Solar Energy Mater. Solar Cells 61, 2000, pp. 239–253*

85. Schüler, C. Roecker, J. Boudaden, P. Oelhafen, J.-L. Scartezzini, Potential of quarterwave interference stacks for colored thermal solar collectors, *Solar Energy, Volume 79, 2005, Pages 122-130*

86. S. K. Das and A. Chakraverty , Performance of a solar collector with different glazing materials and their degradation under the condition prevailing in a solar collector, *Energy Conversion and Management, Volume 31, Issue 3, 1991, Pages 233-242*

87. S. Malato Rodríguez, J. Blanco Gálvez, M. I. Maldonado Rubio, P. Fernández Ibáñez, D. Alarcón Padilla, M. Collares Pereira, J. Farinha Mendes and J. Correia de Oliveira, Engineering of solar photocatalytic collectors, *Solar Energy, Volume 77, Issue 5, November 2004, Pages 513-524*

88. S. N. Patel, O. T. Inal, A. J. Singh and A. Scherer, Optimization and thermal degradation study of black nickel solar collector coatings, *Solar Energy Materials, Volume 11, Issues 5-6, January-February 1985, Pages 381-399*

89. S. P. Chow, G. L. Harding and R. E. Collins, Degradation of all-glass evacuated solar collector tubes, *Solar Energy Materials, Volume 12, Issue 1, March-April 1985, Pages 1-41*

90. Snail, J. J., O'Gallagher and R. Winston, A Stationary Evacuated Collector with Integrated Concentrator, *Solar Energy, v33, 1983*

91. Suehrcke and P. G. McCormick, A performance prediction method for solar energy systems
Solar Energy, Volume 48, Issue 3, 1992, Pages 169-175

92. Symons and R. Gani, Thermal performance predictions and sensitivity analysis for high temperature flat-plate solar collectors, *Solar Energy, Volume 24, Issue 4, 1980, Pages 407-410*

93. T. Hollands, A. Karagiozis and A. P. BrungerG. Brouwer, Effect of selective surface degradation on the performance of solar water heating systems, *Solar Energy Materials and Solar Cells, Volume 25, Issues 1-2, January 1992, Pages 125-141*

94. Tesfamichael T. and Wackelgard E. (1999) Angular solar absorptance and incident angle modifier of selective absorbers for solar thermal collectors *Solar Energy* Vol. 68, No. 4, pp. 335–341, 2000

95. Winston, R, J. J. O'Gallagher, William S. Duff and Alberto Cavallaro, The Integrated Compound Parabolic Concentrator: From Development to Demonstration, Proceedings of the ASES/ASME Solar Energy Forum, Washington D. C., April, 1997.

96. Winston, R. W., Joseph J. O'Gallagher, William Duff, and Alberto Cavallaro, "Nonimaging Evacuated Concentrating Collectors: from Development to

Demonstration," Proceedings of the International Solar Energy Society World Congress, Taejon, Korea, August, 1997.

97. Winston, R. W., Joseph J. O'Gallagher, David Jenkins, and William S. Duff, Developments in the Integrated CPC, Proceedings of the 1996 American Solar Energy Society Conference, Ashville NC, April 1996.

98. Winston, R, O'Gallagher, J., Mahoney, A. R., Dudley, V. E. and Hoffman, R., "Initial Performance Measurements from a Low Concentration Version of an Integrated Compound Parabolic Concentrator (ICPC)", Proceedings of the 1998 ASES Annual Conference, Albuquerque NM, June, 1998

99. Winston, Roland, W. Duff, J. O'Gallagher, T. Henkel, R. Christiansen and J. Bergquam, "Demonstration of A New Type of ICPC in a Double-Effect Absorption Cooling System", International Solar Energy Society Congress, Jerusalem, Israel, July 1999

100. Wolfgang Spirkl, Julius Muschaweck, Peter Kronthaler, Wolfgang Schölkopf and Justus Spehr,In situ characterization of solar flat plate collectors under intermittent operation, *Solar Energy, Volume 61, Issue 3, September 1997, Pages 147-152*

101. X. A. Wang and L. G. Wu, Analysis and performance of flat-plate solar collector arrays
Solar Energy, Volume 45, Issue 2, 1990, Pages 71-78

102. Y. Tripanagnostopoulos, P. Yianoulis, S. Papaeflhimiou. M. Souliotis and Th. Nousia, Cost Effective Asymmetric CPC Solar Collectors, *Renewable Energy, Volume 16, 1999, Pages 628-631*

APPENDIX A

SOME THEORETICAL CONSIDERATIONS

A.1 Instantaneous collector efficiency model

The performance of solar collectors can be characterized in terms of an instantaneous steady-state value, referenced to normal solar incidence. See Duffie and Beckman (1990). For our purposes, to calculate whole day performance, small time increments were used. The study will include how the collector performance (individual bankand array) reacts for changes in solar incidence angle using the angles corresponding to the real time10 minute increment insolation data. Measured collector thermal performance was used as a benchmark against which the degradation of collectors was compared. It must be noted that there is some built-in uncertainty associated with the measured values of thermal performance.

A simple instantaneous collector performance model can be derived from the energy rate. See equation A.1. We will use a more accurate expression with a squared ΔT term later in this document.

$$\dot{Q} = \rho_{eff}(IAM)(\tau\alpha)_n A_c G - F_R A_c U_L \Delta T \qquad \text{(A.1)}$$

The performance equation can be divided into two components: the first term ($\rho_{eff}(IAM)(\tau\alpha)_n A_c G$) referring the optics and the second term referring to the thermal losses ($F_R A_c U_L \Delta T$).

A.1.1 Optical efficiency calculation

The optical term in the instantaneous model depends heavily on the incidence angle of the radiation. The effective reflectance of the integral reflector (ρ_{eff}) and the effective transmittance/absorptance product for the glass tube ($(\tau\alpha)_n$) are adjusted for each incident angle.

The effective reflectance of the integral reflector calculation is included in the ray tracing analysis. In the ray tracing the effective reflectance value of the integral reflector is tagged to each past ray (this will be explained in more detail in the next chapter). As each ray passes through the glass cover, the ray will be refracted and redirected to a different angle. The refraction angle of unpolarized radiation can be described by Snell's law as a proportion of the reflective indices represented by the following formula.

$$\frac{n_1}{n_2} = \frac{\sin\theta_2}{\sin\theta_1} \tag{A.2}$$

The effective transmittance/absorptance product for the glass tube is also incorporated into the ray tracing analysis. Ray tracing includes the analysis of solar transmittance/absorptance and solar refraction of the cover material (glass). Solar transmittance/absorptance of the glass cover is made up of two types of losses. The

first, τ_r, is the reflective loss at the two surfaces. The reflectance loss of initially unpolarized radiation is the average of the reflectance of the two parallel and perpendicular reflective components. See equation A.3.

$$\tau_r = \frac{1}{2}\left(\frac{1-r_{//}}{1+r_{//}} + \frac{1-r_{\perp}}{1+r_{\perp}}\right) \tag{A.3}$$

The terms $\frac{1-r_{\perp}}{1+r_{\perp}}$ and $\frac{1-r_{//}}{1+r_{//}}$ are derived from the infinite sum of reflection shown in Figure A1.

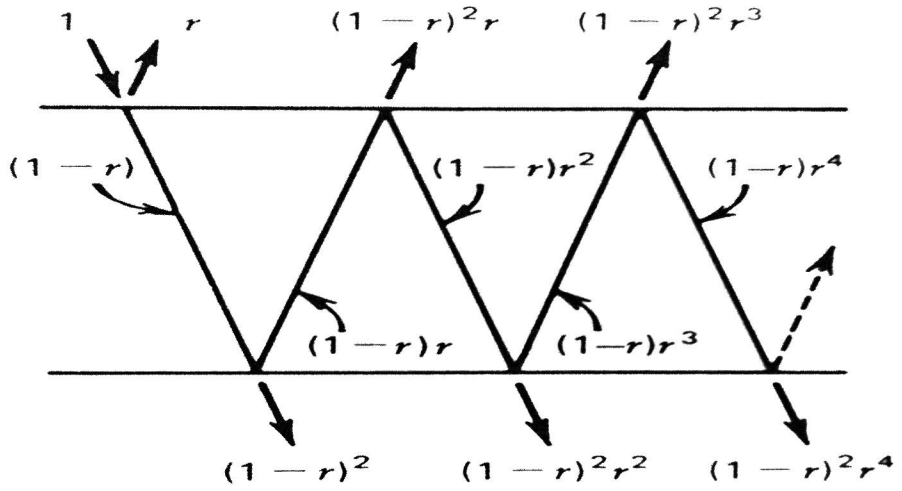

Figure A1: Transmission through one nonabsorbing cover

The transmission of radiation through the cover as there are two interfaces to cause a reflection loss. Figure shows the series of reflections and refraction of a perpendicular

component through one cover. By summing up the transmitted terms, the transmittance for the perpendicular component of polarization is

$$\begin{aligned}\tau_{\perp} &= (1-r_{\perp})^2 \sum_{n=0}^{\infty} r_{\perp}^{2n} \\ &= \frac{(1-r_{\perp})^2}{(1-r_{\perp}^2)} \\ &= \frac{(1-r_{\perp})}{(1+r_{\perp})}\end{aligned} \tag{A.4}$$

Using assumption of a flat plate, the estimation will be a good approximation for the curved surface for the incident angles close to normal to the surface. As incident angles increase, the approximation will overstate the effects of multiple reflections due to increasing influence of the curvature of the cover glass.

The second, τ_a, considers the absorption loss in the glass medium. The absorption of radiation is expressed by Bouguer's law which assumes that the absorbed radiation is proportional to local intensity in the medium and the distance the radiation travels in the medium. See equation A.5.

$$\tau_a = \frac{I_{\tau}}{I_o} = e^{-Kx} \tag{A.5}$$

The value K is the proportional constant called the extinction coefficient, which is assumed to be constant over the solar spectrum. The extinction coefficient for the glass

material for n = 1.526 is approximately 13 m^{-1} and "x" is the distance which the radiation travels in the medium.

The equation for the total transmittance is simplified by using the product of the two types of transmittance. See equation A.6.

$$\tau \cong \tau_a \tau_r \tag{A.6}$$

Considering the circular geometry of the ICPC for a given nominal incidence angle, the local incident angle will vary around the circular surface of the tube.

Reflection of unpolarized radiation on passing from medium 1 to medium 2 is expressed by the average of the parallel and perpendicular components which can be described by the following formula. See equation A.7.

$$r = \frac{I_r}{I_i} = \frac{1}{2}\left(r_{\perp} + r_{//}\right) \tag{A.7}$$

Where

$$r_{//} = \frac{\tan^2(\theta_2 - \theta_1)}{\tan^2(\theta_2 + \theta_1)}$$

$$r_{\perp} = \frac{\sin^2(\theta_2 - \theta_1)}{\sin^2(\theta_2 + \theta_1)}$$

A.1.2 Thermal losses for the ICPC

Thermal loss is derived from an energy balance equation. The collector loss coefficient, U_L, consists of four types of losses: radiation loss, h_{rad}, natural convection

loss, h_{conv}, conduction loss, h_{cond}, and forced (wind) convection loss h_{wind}. U_L is found by the following equation.

$$U_L = \left(\frac{1}{h_{rad,t-g} + h_{conv,t-g}} + \frac{1}{h_{rad,g-a} + h_{conv,g-a} + h_{wind}} \right)^{-1} \tag{A.8}$$

If there is no convection loss from heat transport tube to glass cover, as in the case of the hard vacuum, the $h_{conv,t-g}$ term drops out. See equation A.9.

$$U_L = \left(\frac{1}{h_{rad,t-g}} + \frac{1}{h_{rad,g-a} + h_{conv,g-a} + h_{wind}} \right)^{-1} \tag{A.9}$$

There are two locations relative to the collector where radiation losses occur. The first location is where the radiation loss from a glass cover to the environment takes place. The radiation loss coefficient from glass cover to ambient, $h_{rad,g-a}$, is derived from the radiation loss from the glass cylinder equation, $q_{loss,rad(glass-ambient)}$. See equation A.10. Then, the $q_{loss,rad(glass-ambient)}$ equation can be simplified by formulary $h_{rad,g-a}$ a nearly temperature independent term, so the radiation loss coefficient can be shown. See equation A.11 and A.12.

$$q_{loss,rad(glass-ambient)} = \varepsilon_{glass} \sigma A_{glass} (T_{sky}^4 - T_{glass}^4) \tag{A.10}$$

$$q_{loss,rad(glass-ambient)} = h_{rad,g-a} (T_{glass} - T_{sky}) \tag{A.11}$$

$$h_{rad,g-a} = \varepsilon_{glass}\sigma A_{glass}(T_{glass} + T_{sky})(T_{glass}^2 + T_{sky}^2) \quad \text{(A.12)}$$

The sky is considered a blackbody, and the sky temperature can be estimated as a function of ambient temperature from equation A.13. See page 122 in Duffie and Beckman (1999).

$$T_{sky} = 0.0552T_a^{1.5} \quad \text{(A.13)}$$

The second location is where radiation loss from the heat transfer tube/absorber fin to the glass cover takes place. See equation A.14.

$$q_{loss,rad(tube-glass)} = \frac{\sigma A_{tube+fin}(T_{tube}^4 - T_{glass}^4)}{\frac{1}{\varepsilon_{tube+fin}} + \frac{1-\varepsilon_{glass}}{\varepsilon_{glass}}\left(\frac{A_{tube+fin}}{A_{glass}}\right)} \quad \text{(A.14)}$$

$$A_{tube+fin} = A_{tube} + \eta_{fin}A_{fin} \quad \text{(A.15)}$$

The effective surface of the heat transport tube and the absorber fin is $A_{tube+fin,}$ where η_{fin} is the fin efficiency shown in equation A.15. The simplified form of the $q_{loss,rad(tube-glass)}$ can be reduced. See equation A.16. So, the radiation loss coefficient, $h_{rad,t-g}$. See equation A.17.

$$q_{loss,rad(tube-glass)} = h_{rad,t-g}(T_{tube} - T_{glass}) \quad \text{(A.16)}$$

$$h_{rad,t-g} = \frac{\sigma A_{tube+fin}(T_{tube}+T_{glass})(T_{tube}^2+T_{glass}^2)}{\frac{1}{\varepsilon_{tube+fin}}+\frac{1-\varepsilon_{glass}}{\varepsilon_{glass}}\left(\frac{A_{tube+fin}}{A_{glass}}\right)} \quad \text{(A.17)}$$

The convection loss coefficient h_{conv} is also separated into two parts. There is a convection loss from the glass cover to environment and a convection loss from the heat transport tube to the glass cover. However an evacuated tube with the hard vacuum will have no convection loss from the heat transport tube to the glass cover. Since a cracked tube allows air from the environment to enter, the convection coefficient for the non-evacuated case can be calculated. The convection loss coefficient from the glass cover to environment, $h_{conv,g-a}$, is described by the relationship between the glass cover's diameter and the Nusselt number. See equation A.18. The Nusselt number (Nu) or the convection heat transfer coefficient, is also given as a Rayleigh number (Ra) as shown in equation A.19.

$$h_{conv,g-a} = \frac{k}{D}\mathrm{Nu} \quad \text{(A.18)}$$

$$\mathrm{Nu} = \left\{0.6+\frac{0.387\mathrm{Ra}^{1/6}}{\left(1+\left(0.559/\mathrm{Pr}\right)^{9/16}\right)^{8/27}}\right\}^2 \quad \text{(A.19)}$$

The Rayleigh number can be determined by equation A.20. We also need to calculate the cover glass temperature, which is not available. A successive approximation approach is

used to find the glass cover temperature by balancing the heat removing rates. This glass temperature will be applied to all required equations.

$$\mathrm{Ra} = \frac{g\beta\left(T_{glass} - T_{amb}\right)D^3}{v^2}\mathrm{Pr} \tag{A.20}$$

where

$\beta = 1/T_f$

$T_f = (T_{glass} + T_{amb})/2$

The convection loss from a heat transfer tube to a glass cover will be included in to the analysis since some tubes lose their vacuum. This considers the convection loss through the medium, air that leaks into the tube. The convection loss coefficient from the heat transport tube to the glass cover, $h_{conv,t\text{-}g}$, is derived from the relationship between the heat transport tube diameter and the Nusselt number. See equation A.21. The convection heat transfer coefficient, Nu and Rayleigh number, Ra, can be determined by equation A.22 and A.23.

$$h_{conv,tube-g} = \frac{k}{\delta}\mathrm{Nu} \tag{A.21}$$

$$\mathrm{Nu} = 0.11\mathrm{Ra}^{0.29} \tag{A.22}$$

$$\mathrm{Ra} = \frac{g\beta\left(T_{tube} - T_{glass}\right)\delta^3}{v^2}\mathrm{Pr} \tag{A.23}$$

The wind heat transfer coefficient, h_{wind}, can come into play when a significant amount of thermal energy is removed from the collector glass cover by wind. For free convection, Lloyd and Moran (1974) gave the equation for horizontal flat plate as

$$\text{Nu} = 0.76\text{Ra}^{0.25};\ 2.6 \times 10^4 < \text{Ra} < 10^7 \tag{A.24}$$

$$\text{Nu} = 0.15\text{Ra}^{0.3333};\ 10^7 < \text{Ra} < 3 \times 10^{10} \tag{A.25}$$

A forced convection conditions over building equation was expressed by Mitchell (1976) as

$$h_{wind,forced} = \frac{8.6V^{0.6}}{L^{0.4}} \tag{A.26}$$

where V is in meters per second and L is the cube root of the house volume in meters.

McAdams (1953) recommended that when free and forced convections happen simultaneously, the larger value of the two will be used in the h_{wind} calculation and can be express as

$$h_{wind} = MAX(h_{wind,free}, h_{wind,forced}) \tag{A.27}$$

A.1.3 Thermal loss efficiency on the manifold

Manifolds connect the ICPCs in parallel at their heat transport (upper) end. The manifold insulation is a fiberglass covering along the tube. Heat loss from the manifolds can be estimated by equation A.28. The steady rate of heat loss from the fluid can be described by the term ΔT and the total thermal resistance (R_{total}).

$$\dot{Q} = \frac{T_{fluid} - T_{ambient}}{R_{total}} \tag{A.28}$$

The thermal resistance network in the manifolds consists of four resistances in series, so the total thermal resistance (R_{total}) can be found by the summation of four resistances See equation A.29. The four resistances are a convection resistance from hot water to the heat transport tube, $R_{conv,w\text{-}t}$, a conduction resistance of the heat transport tube, $R_{cond,tube}$, conduction resistance of the insulation, $R_{cond,insu}$ and a convection resistance from insulation to environment, $R_{conv,insu\text{-}env}$.

$$R_{total} = R_{conv,w\text{-}t} + R_{cond,tube} + R_{cond,insu} + R_{conv,insu\text{-}env} \tag{A.29}$$

The convection resistance, $R_{conv,}$ can be found by equation A.30, which involves the heat transfer coefficient, h, and the convection area, A.

$$R_{conv} = \frac{1}{hA} \tag{A.30}$$

Conduction resistance, $R_{cond,}$ in cylinder surface can be described by equation A.31. The thermal conductivity, k, is a property of the material.

$$R_{cond} = \frac{\ln(r_{out}/r_{in})}{2\pi kL} \tag{A.31}$$

A.2 ICPC initial performance measurements

A.2.1 Sandia efficiency regression model

In 1998, before the Sacramento demonstration, Sandia National Laboratory tested two modules, each with seven individual tubes with their manifolds plumbed in series on their two-axis tracking (AZTRAK) platform. The tests were performed separately for two setups, one with the vertical absorber fined modules and one with the horizontal fined modules. An efficiency curve was found by regression analysis on the measurements. The equation for efficiency also included a squared term for ΔT as shown in equation A.32 and equation A.33

Experimentally derived efficiency for horizontal fin

$$= 0.7346\text{-}0.559\left(\frac{\Delta T}{G}\right) \text{-}0.00425\left(\frac{\Delta T}{G}\right)^2 .G, \tag{A.32}$$

and

Experimentally derived efficiency for vertical fin

$$= 0.6846\text{-}0.559\left(\frac{\Delta T}{G}\right) \text{-}0.00425\left(\frac{\Delta T}{G}\right)^2 .G \qquad \text{(A.33)}$$

A.2.2 Incidence angle modifier

The transmittance of the cover glazing of the collector changes with incident angle. The relationship between the incident angle and the transmittance can easily be calculated for materials with smooth flat surfaces and simple geometries. However, this is not the case here. The collector cover glazing is not flat and the geometry of the collector is a CPC which incorporates a reflector. Moreover, the collector is not symmetric in all dimensions. Thus, the angle-dependent response can no longer be easily calculated. The tradition approach to non-symmetry has been to approximate this non-symmetric dependence by the product of two IAMs for longitudinal (α) and transverse (β) angles, (Duffie and Beckman, page 176). See equation A.34.

$$\text{IAM}(\alpha, \beta) = \text{IAM}_{\text{long}}(\alpha) \text{ x } \text{IAM}_{\text{trans}}(\beta) \qquad \text{(A.34)}$$

This approximation was shown (Duff et al, 1999) to result in substantial errors at larger angles. However, in the Sandia experiment measurements were only taken in two directions, longitudinally and transversely. The IAM for the longitudinal angle variation for both fin orientations was treated as in a flat plat collector cover (Duffie and Beckman, page 266). See equation A.35.

$$\text{IAM}_{\text{long}}(\theta) = K_{\tau\alpha} = \frac{(\tau\alpha)}{(\tau\alpha)_n} = 1 + 1.1 \times \left(\frac{1}{\cos\theta} - 1\right) \qquad \text{(A.35)}$$

The IAM for the transverse angle is derived from the Sandia experimental results (Duff 1999). See equation A.36 and A.37.

$IAM_{trans}(\theta_{trans})$ for horizontal fin =

$$\begin{cases} 1+\{(0.001993-0.0000368\theta_{trans})\times\theta_{trans}\} & ;\theta_{trans}\geq 0 \\ 1+\left\{\dfrac{(0.00123+(0.0001703+(-0.0000002573(-\theta_{trans}))(-\theta_{trans}))(-\theta_{trans}))}{\cos\theta_{trans}}\right\} & ;\theta_{trans}<0 \end{cases} \quad \text{(A.36)}$$

$IAM_{trans}(\theta_{trans})$ for vertical fin =

$$0.995137980911+[(0.0023425031919+(0.000156907772+(-0.00000497061919+ 0.000000030539\times|\theta_{trans}|)\times|\theta_{trans}|)\times|\theta_{trans}|)\theta_{trans}|)\Big/\cos\theta_{trans}] \quad \text{(A.37)}$$

The incidence angle modifier should augment the first constant term of the efficiency model, $\rho_{eff}(\tau\alpha)_n$ as in equation A.38 and A.39.

Sandia efficiency for horizontal fin =

$$0.7346(IAM_{\tau\alpha}(\alpha, \beta))-0.559\left(\frac{\Delta T}{G}\right) -0.00425\left(\frac{\Delta T}{G}\right)^2.G \quad \text{(A.38)}$$

And

Sandia efficiency for vertical fin =

$$0.6846(IAM_{\tau\alpha}(\alpha, \beta))-0.559\left(\frac{\Delta T}{G}\right) -0.00425\left(\frac{\Delta T}{G}\right)^2.G \quad \text{(A.39)}$$

A.2.3 Instantaneous efficiency calculation

The instantaneous efficiency is calculated as

$$\text{Instantaneous efficiency} = \frac{\dot{Q}/A_c}{G} = \frac{\rho_{eff}(IAM)(\tau\alpha)_n A_c G - F_R A_c U_L \Delta T}{A_c} \Big/ G$$

$$= \rho_{eff}(IAM)(\tau\alpha)_n - \frac{F_R U_L \Delta T}{G}$$

, since $F_R \approx 1$,

$$\text{Instantaneous efficiency} = \rho_{eff}(IAM)(\tau\alpha)_n - \frac{U_L \Delta T}{G} \qquad \text{(A.40)}$$

A.2.4 Measured bank efficiency calculation

Bank efficiency is calculated by using direct data from the data acquisition system in the form of energy input and energy output. See equation A.41.

$$\text{Measured efficiency} = Q_u / G.A \qquad \text{(A.41)}$$

where

Q_u is actual collected energy.
A is an effective aperture area.

APPENDIX B

SELECTED SACRAMENTO DEMONSTRATION PROJECT RESULTS BASED ON THE MEASURED DATA

B.1 1999 experiments to measure the differences in performance for the different fin orientations

The 1998 results reported in (Duff et al, 1999) and (Winston et al, 1999) were insufficient to substantiate superior performance of either the horizontal or vertical absorber fin orientations.

In September 1999 a series of six daylong tests were performed on the individual banks. There were no broken or inoperative collector tubes in the north or middle banks during the tests. Two of the banks were covered for the entire day of testing, while the other bank was left uncovered. Results of the tests are given in Table 5.1. It can be seen that under virtually identical conditions the north and middle banks delivered nearly identical 48 percent collection efficiencies.

As can be seen in the table, three days of tests under virtually identical conditions were performed on the South array. These three tests can be used to calculate an estimate of the standard deviation for the percentage energy collected so that a confidence interval for the difference between the results for the north and middle banks can be established. Calculations using a t-distribution produce a 95 percent confidence interval of (-0.9%,

+1.3%) for the difference in the percentage energy collected between the north and middle banks when the incident solar energy is in the mid to high 800 MJ range.

Substantially more data was collected on the performance of the new ICPC collector array and the double effect chiller during 1999 as compared with 1998. The performance of the collectors was close to that of the 1998 performance reported earlier in (Duff et al 1999) and (Winston et al 1999).

TABLE B.1. INDIVIDUAL BANK TESTS

Date 1999	Bank	Daily Mean ΔT in C	Total Daily Incident Solar Energy in MJ	Percent Total Daily Energy Collected
09/01	north	108.3	667	41.3
09/02	north	102.8	881	48.2
09/03	middle	103.3	842	48.0
09/04	south	100.3	858	48.8
09/05	south	99.2	844	49.0
09/06	south	100.7	872	48.3

B.2 Comparing 1998 and 1999 ICPC measured results

The daily solar collection efficiencies(Duff et al 2001) (based on the total solar energy falling on the collector)of the non-tracking ICPC evacuated solar collector array in the Sacramento Demonstration closes to fifty percent at the 140C to 160C, the temperatures required by the demonstration's 2E absorption chiller. Throughout much of 1999, the collector array was not optimally controlled. Figure 8.1 shows a typical daily

operating profile during 1998 and during several days of controlled experiments in 1999. Figure 8.2 shows a typical daily operating profile throughout 1999. By comparing figure 8.1 with figure 8.2, you can see that some collectable energy has been lost because the array was not turned on early enough. As a consequence, the daily energy collection appears to be lower in 1999 than in 1998.However, if we consider the results from the period in 1999 when the controlled experiments were being run, 1999 performance is virtually identical to 1998 performance. Thus, we can reasonably conclude that the performance of the array has not changed after two years of operation.

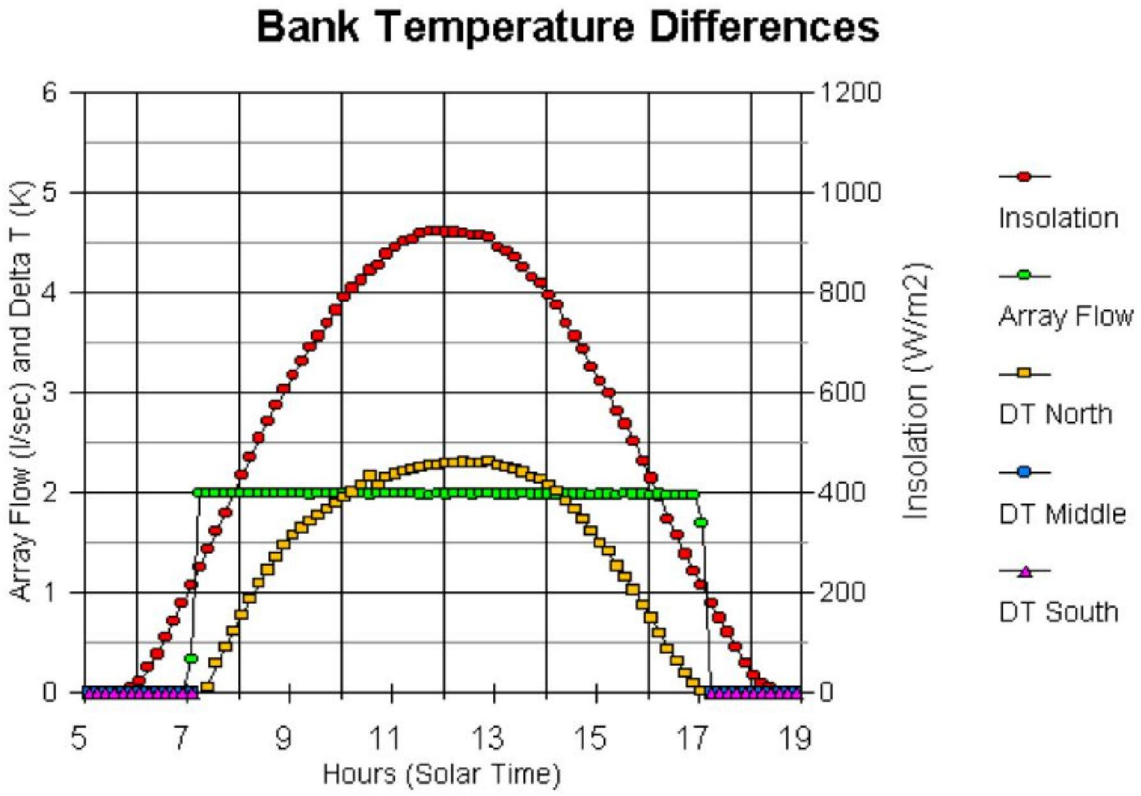

Figure 8.1: September 2, 1999 insolation, array flows and bank temperature differences

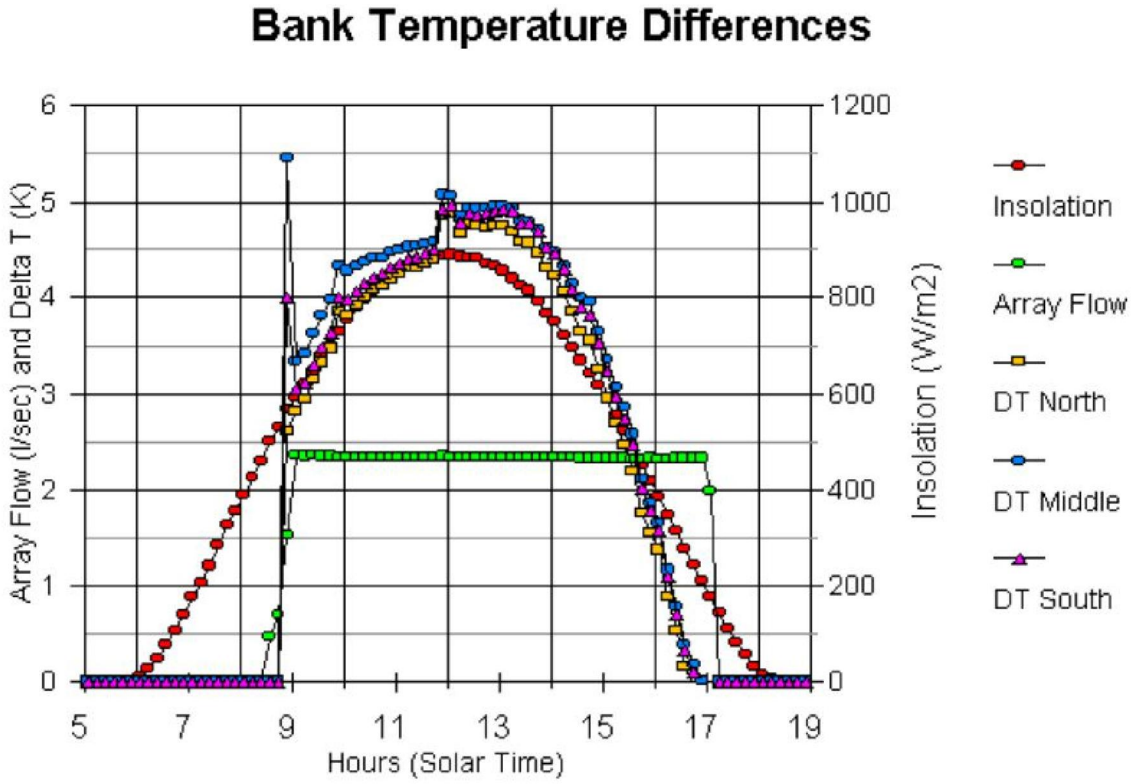

.

Figure 8.2: September 12, 1999 Insolation, Array Flows and Bank Temperature Differences

B.3 2000/2001 ICPC measured results

During 2000/2001 solar energy from the ICPC collectors and an existing set of parabolic through collectors supplied energy to a 1E chiller (Duff et al, 2002). Since a 1E chiller requires lower operating temperatures, the ICPC array was operated at around 125C. As of February 2001 there were a few tubes that were not performing at their designed level due to their having cracked or due to other types of failure. These tubes were not replaced prior to the cooling season, as was the case with a smaller number of tubes in 1999. (It was believed that most of the sources of tube failure have now been identified.) Allowing for the reduced performance of these tubes, overall performance

would be expected to be a few percent lower for 2000 and 2001. The 2000/2001 data was being analyzed and the preliminary calculations indicate that the expected level of performance was being attained.

B.4 2002 ICPC measured results

During 2002 the ICPC collectors were operated in the 75 to 100C range (Duff et al, 2003). As can be seen in figure 8.3, control of the array was again well implemented most of the time. Figure 8.4 shows these results, with daily efficiencies as high as 53.8 percent. Performance in June and July, shown in the figure as data with daily input energy above 2900 MJ, matched the 2001 performance regression line closely. Performance in Mid August through mid September, shown as data with daily input energy from 2200 to 2700 MJ, was about four percent below the 2001 results. One possible explanation would be that the decrease is due to additional failed tubes. Another explanation, more likely because of the apparent parallel shift to the energy input/output curve relationship, is that there were more performance reducing instances of the vapor locking and recovery in some of the tubes accompanying low flow rates in August and September, see figures 8.2 and 8.3. A confirmation of this as a possible explanation is that related sounds can be heard from the array. (As mentioned earlier, some additional higher flow rate experiments are planned and another evacuated tube-by-tube inspection will be made. This will further clarify possible explanations for the decrease in performance.)

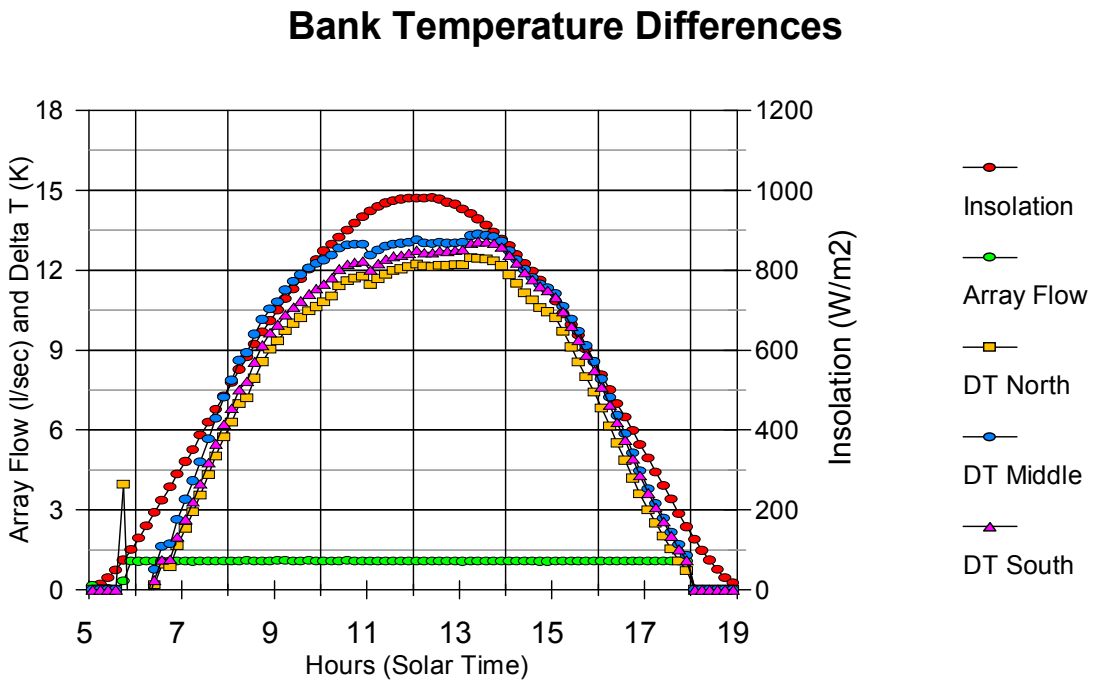

Figure 8.3: June 5, 2002 insolation, array flows and bank temperature differences

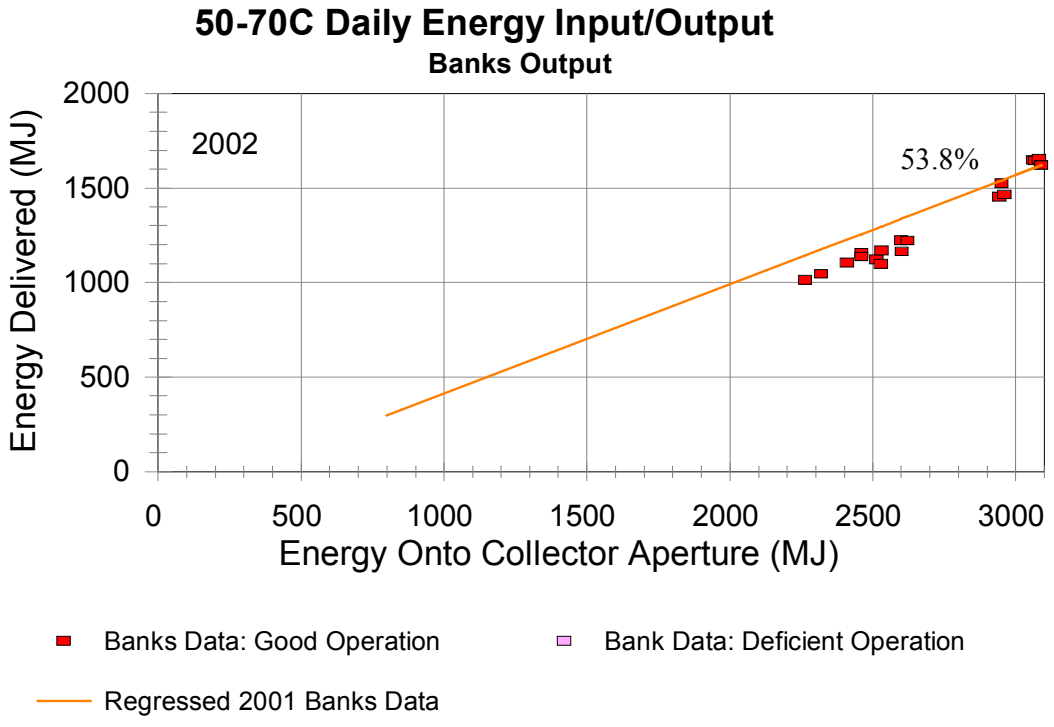

Figure 8.4: 2002 daily collection performance for operation at 50 to 70C collector to ambient temperature differences.

B.5 2003/2004 ICPC measured results

During 2003 to 2004 the ICPC collectors were operated in the lower temperature between 60 to 80C (Duff at el, 2004, 2005). During this period the array was on and off at the appropriate times. As can be seen in Fig. 8.5, daily efficiencies of 47.5 percent were attained. Fig. 8.5 also shows that these 2004 data were only a few percentage points below the 2001 results.

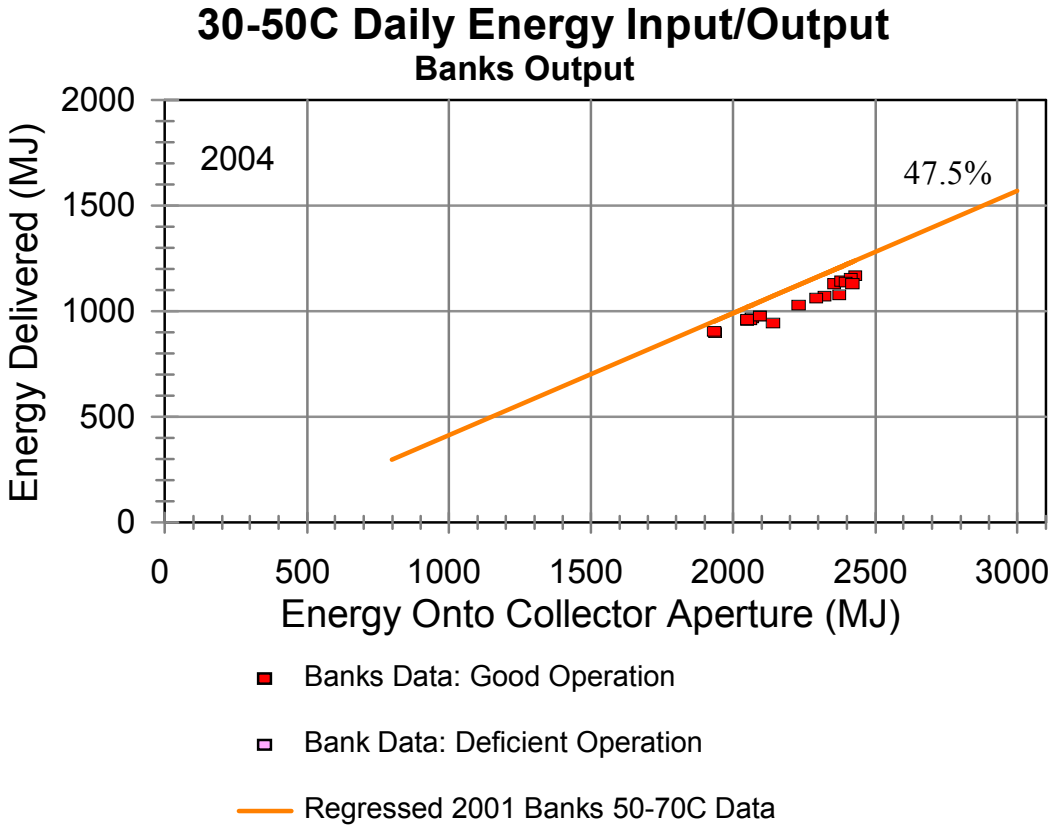

Figure 8.5: 2004 Daily collection performance for operation at 30 to 50C collector to ambient temperature differences

A count in December 2003 showed a few failed evacuated collector tubes and eight tubes that had been removed and the manifold openings plugged. (The removal of a tube results in a greater loss of contributed energy than a tube that has lost vacuum. A

tube that has lost vacuum performs like a selective concentrating non-evacuated collector and is still able to deliver a substantial fraction of the energy of its evacuated counterpart.) These factors would account for the observed decrease in performance from 2001 to 2004.

APPENDIX C

LIST OF INSTRUMENTS USED IN SACRAMENTO INSTALLATION

TABLE: C-1 Instruments

Description	***Vender***	***Remarks***
Pyranometer, Collector-plane insolation	Kipp&Zonen, LI-COR?	Collector-Plane
Pyranometer, Rotating Shadow Band	LI-COR?	
Rotating Shadow Band Motor Rotation Control	LI-COR?	
Rotating Shadow Band Motor Location Feedback	LI-COR?	
Vortex-shedding flow meter		Collector loop
Vortex-shedding flow meter		Generator loop
Turbine flow meter		Cooling tower
Turbine flow meter		Load
T&RH excitation	Humitter	
Reference Thermistor(s)excitation DAS		
Collectors (ICPC)	Solar Enterprises International	Evacuated tube ICPC solar collectors. With 1,000 W/m^2 normal to the plane of the collectors

Collector Pump	MP Pump, Inc.	1 HP centrifugal pump. Rating: 177°C (350°F), 1 MPa (150 psi). Nominal flow: 2.52 l/sec (40 gpm).
Expansion Tank	Wassels	24 NA 65, 450 liter (120 gal.), 0.85 MPa (125 psi) steel tank.
Chiller	McQuay/Sanyo	20 ton (70 kW) double-effect, absorption chiller model ME-21E
Cooling Tower	Marley	Model 4831 Aquatower, sized to reject heat at the rate of 128.6 kW (440,000 Btu/hr), with a 5.6°C (10°F) temperature drop from 35°C to 29.4°C (95°F to 85°F).
Chiller Hot Water Pump	MP Pump, Inc.	1 HP centrifugal pump. Rating: 177°C (350°F), 1 MPa (150 psi). Nominal flow: 2.27 l/sec (36 gpm)
Chilled Water Pump	STA-RITE	2 HP centrifugal pump, nominal flow: 3 l/sec (48 gpm)
Cooling Tower Pump	Dura-Glas II	1 HP centrifugal pump, nominal flow: 5.5 l/sec (88 gpm)

TABLE C-2: Material list

Description	***Used For***	***Vender***	***Part Number***
Type T thermocouple wire, twisted-shielded	Thermopile refs, tank temps.	OMEGA	TT-T-24S-TWSH
Type K thermocouple wire, twisted-shielded	Tube temps.	OMEGA	TT-K-24S-TWSH
Multiconductor feed-through	Tank temperature measurements	OMEGA	MFT-14-3
Type T sheathed thermocouples	Tank temperature measurements	OMEGA	CPSS-14U-24, CPSS-14U-36, CPSS-14U-48
Type T connectors	Tank temperature measurements	OMEGA	USTW-T-F
Type K connectors	Tank temperature measurements	OMEGA	SMPW-K-MF
Type T SLE 5-wire shield cable	Thermopiles	OMEGA	Custom-Made

22 awg 2-conductor TWSH instrument wire	Thermopiles, CT's, Pyranometer	NEWARK	36F165WM
23 awg 3-conductor shielded instrument wire	Flow meters	NEWARK	36F168WM
?? awg ?-conductor wire	Rotating Shadowband	NEWARK	
Thermally-conductive paste	Thermowells	OMEGA	OT-201-2
32-channel multiplexer	Xtra channels	Campbell	AM416
Enclosure	Multiplexer	Campbell	ENC 12/14
Reference Thermistor	Multiplexer	Campbell	CR10XTCR
Frequency-to-voltage signal conditioner	Turbine meter	OMEGA	DRN-FP-M

APPENDIX D

MATLAB PROGRAMMING

The Matlab ray-tracing program consists of a main program and eight subprograms. The main program calls RayEnter (RayEnter.m), which is the variables initialization, axis conversion, beam/diffuse calculation, subprogram activation, and efficiency calculation. There are eight subprograms such as DrawSideview.m, DrawTube.m, Exposure.m, ReflexRay.m, Refraction.m, Shading.m, SideRayEnter.m and TransmittanceP.m. These subprograms will be called from the main program or subprogram itself.

D.1 Main program (RayEnter.m)

There are three main parts in the RayEnter.m. The first part is to initialize the variables. Some important variables will be explained below.

Days: day of year from 1 to 365
TubeRadius: inner glass tube radius
OutTubeRadius: outer glass tube radius
InRadius: heat transport tube radius
Length: fin length measured vertically/horizontally from the center point
Latitude: the angular location north or south of equator, north positive, -90 to 90
Altitude: the height from sea level

SurfaceAz: Surface azimuth angle, deviation of the projection on a horizontal plane of the normal to the surface from the local meridian, with zero due south, east negative, west positive, -180 to 180

DiffusedRay: diffused radiation ratio from prior simulated diffuse radiation

GrndReflc: ground reflectance

G: insolation metric

The initialized variable part of the main program shows below.

```
%clear
%Assign initial -By=Ax+C
Days = 255;
CosLad = 0.7826;
SinLad = 0.6225;
TubeRadius = 63;
InRadius = 6;
Length = 57;
OutTubeRadius = 65;
Angle = 0;
TotalRay = 0;
DirectHit = 0;
AbsorberHit = 0;
LossRay = 0;
ReflexFactor = 1;
Reflection = 0;
NumAngle = 0;
NumFrame = 0;
NumFrame1 = 0;
Energy(:,:) = 0;
RFactor = 1;
AbsFactor = 1;
colormap('jet')
GapLossRay = 0;
ExposureRay = 0;
hr = 2*OutTubeRadius+10;
hl = -2*OutTubeRadius-10;
Slope = 17;
Latitude = 38.55;
Altitude = 0.0076; %0.0076km from sea level
SurfaceAz = -10;
TotalLossRay=0;
RayCount=0;
RayBlocked = 0;
TBeam = 0;
DiffusedRay = 0.541051;
GrndReflc = 0.2;
G0(61,1) = 0;
Gcb(61,1)= 0;
Gcd(61,1)= 0;
Gc(61,1) = 0;
GTcb(61,1)= 0;
GTcd(61,1)= 0;
```

```
GTc(61,1) = 0;
GTb(61,1)= 0;
GTd(61,1)= 0;
GT(61,1) = 0;
G=[110.74;137.67;163.44;189;221.78;255.6;280.94;307.81;336.04;363.68;394
.56;419.32;449.04;469.73;493.56;515.42;539.99;561.25;584.53;606.09;626.7
;643.27;658.61;671.98;686.13;698.86;707.43;715.66;722.7;729.31;735.62;73
8.52;738.58;737.61;735.13;730.94;728.42;720.85;711.08;701.1;693.94;680.7
7;662.12;650.86;631.22;612.03;592.14;568.24;551.85;529.07;505.46;479.3;4
52.35;425.51;398.29;372.88;341.62;312.9;283.94;254.29;225.51;];
```

The second part is to find all related angles. First, a ray will cast at 15 degrees solar hour angle or 7 am (15 degree). Solar hour. Then, the angle of incidence (*AngleIncident*), zenith angle (*ZenithAngle*) and solar azimuth angle (*SolarAz*) are calculated for further angle related calculations. The angle of incidence or *AngleIncident* can be found using equation 3.3. The zenith angle or *ZenithAngle* can be calculated by the equation 3.4 from Duffie and Beckman (1980) as the zenith angle of the sun, θ_z

$$\theta_z = \cos^{-1}(\cos\delta\cos\phi\cos\omega + \sin\delta\sin\phi) \qquad \text{(D.1)}$$

The solar azimuth, γ_s (*SolarAz*) is approximated using equation 3.3 or $\cos\gamma_s = \dfrac{\cos\omega\cos\delta\sin\phi - \sin\delta\cos\phi}{\cos\theta}$ from the previous chapter. The Matlab code for the second part is shown below.

```
for FAngle = 15:2.5:165 %HourAngle from 15 degree to 165 degree at 2.5
increment (from 7am to 5pm)
    HourAngle = FAngle - 90;
    Declination = 23.45*sind(360*(284+Days)/365);
    AngleIncident =
real(acosd((sind(Declination)*sind(Latitude)*cosd(Slope))-
(sind(Declination)*cosd(Latitude)*sind(Slope)*cosd(SurfaceAz))+(cosd(Dec
lination)*cosd(Latitude)*cosd(Slope)*cosd(HourAngle))+(cosd(Declination)
*sind(Latitude)*sind(Slope)*cosd(SurfaceAz)*cosd(HourAngle))+(cosd(Decli
nation)*sind(Slope)*sind(SurfaceAz)*sind(HourAngle))));
    ZenithAngle =
real(acosd((cosd(Declination)*cosd(Latitude)*cosd(HourAngle))+(sind(Decl
ination)*sind(Latitude))));
    SolarAz = real(acosd((sind(90-ZenithAngle)*sind(Latitude)-
sind(Declination))/(cosd(90-ZenithAngle)*cosd(Latitude))));
```

The next part is finding a clear sky diffuse/beam radiation on the equator. The atmospheric transmittance for beam radiation or *TBeam* can be found using equation 3.5 and 3.6 or $T_b = a_0 + a_1 e^{-k/\cos\theta_z}$. The atmospheric transmittance for diffuse radiation or *TDiffuse* can also be found using equation 3.7 or $T_d = 0.2710 - 0.2939 T_b$. Clear sky beam radiation (*Gcb*) and diffuse radiation (*Gcd*) the equator are described by equation 3.8 and 3.9 or $G_{cb} = G_o T_b$ and $G_{cd} = G_o T_d$. The extraterrestrial radiation (*G0*) is found by equation 3.10 or $G_o = G_{sc}\left(1 + 0.033\cos\left(\frac{360n}{365}\right)\right)\cos\theta_z$. Finally the clear sky radiation (*Gc*) on the equator equals to the combination of Clear sky beam radiation (*Gcb*) and diffuse radiation (*Gcd*) the equator. The Matlab code for this part is shown below.

```
    %Diffuse and Beam ratio (clear sky)
    NumAngle = NumAngle + 1;
    aZero = 0.4237 - 0.00821*(6 - Altitude)^2;
    aOne = 0.5055 + 0.00595*(6.5 - Altitude)^2;
    k = 0.2711 + 0.01858*(2.5 - Altitude)^2;
    TBeam = aZero + aOne*exp(-k/cosd(ZenithAngle));% Duffie and Beckman
2.8.1
    TDiffuse = 0.2710 - 0.2939*TBeam;% Duffie and Beckman 2.8.7

    G0(NumAngle,1) =
1353*(1+0.033*(cosd(360*Days/365)))*cosd(ZenithAngle);% Duffie and
Beckman
    Gcb(NumAngle,1) = G0(NumAngle,1)*TBeam;
    Gcd(NumAngle,1) = G0(NumAngle,1)*TDiffuse;
    Gc(NumAngle,1) = Gcb(NumAngle,1)+Gcd(NumAngle,1);
```

Next, the casted ray giving incoming angle as *FAngle* is projected to the collector plane to find the angle of incidence at the transverse view. Figure 3.4 also shows how each ray is projected to the transverse view. The angle of incidence at the transverse view

(*Angle*) is found by projecting the ray using basic geometric algebra into the transverse plane. Then, we use two dimension x-y coordinate as the main coordinate system at the transverse plane (equation D.2).

$$\theta_{Transverse} = \tan^{-1}\left(\frac{\cos\theta}{\sin\theta \times \sin\gamma_{Transverse}}\right) \tag{D.2}$$

The Matlab code used in this part is shown below:

```
if FAngle < 90
        SAzimuth=90-SolarAz;
    else
        SAzimuth=90+SolarAz;
    end

    PlaneAz=SAzimuth-90-SurfaceAz; %East of SurfaceAz will be negative

    if PlaneAz <0
       Angle = atand(cosd(AngleIncident)/(sind(AngleIncident)*sind(-
PlaneAz)));
    elseif PlaneAz >0
       Angle = 180-
atand(cosd(AngleIncident)/(sind(AngleIncident)*sind(PlaneAz)));
    else
       Angle = 90;
    end
```

Then, the ray is assigned as a line function, $-By = Ax+C$ on xy-plane. To simplify the function, we assign B = -1 and A = tan(*Angle*). The C value will be assigned from the first ray touching the target ICPC to the last touching ray. The C values will be calculated and assigned from $-R\times\sqrt{A^2+B^2}$ to $R\times\sqrt{A^2+B^2}$. The C value will begin at $-R\times\sqrt{A^2+B^2}$ then the C value will be increase with the increment of $\frac{2\times R\times\sqrt{A^2+B^2}}{300}$. At this increment of C, there will be about 300 rays simulated at each angle across the cross-section ICPC. After a function of the ray is assigned, the subprograms are activated. The subprograms are called in order of *DrawTube*(),

Refraction(), and *Exposure*() respectively. The function of each subprogram will be described individually later. *RayCount* is a variable to count number of simulated rays. *TotalRay* is a variable to collect number of rays passing through the effective aperture area defined on 2.2.2 (Figure 2.3). The Matlab code for this part is shown below:

```
        Ai = tand(Angle);
        Bi = -1;
        Ai1 = Ai;
        Bi1 = Bi;


    step = 2*OutTubeRadius * sqrt((Ai*Ai)+(Bi*Bi))/300;
    for Ci = -OutTubeRadius * sqrt((Ai*Ai)+(Bi*Bi)):step:OutTubeRadius *
sqrt((Ai*Ai)+(Bi*Bi))%from the first touching ray to the last touching
ray
        ynumber = 0;

        subplot(2,1,1);
        DrawTube()
        Reflection = 0;
        Ci1 = Ci;
        Refraction()
        Exposure()
        RayCount = RayCount+1;
        if -Ci/Ai <= OutTubeRadius+5 && -Ci/Ai >= -OutTubeRadius-5
            TotalRay = TotalRay + 1;
        end
    end
```

Next, the ratio of tilted beam radiation (*ClearSkyBeamFactor*) and diffuse radiation (*ClearSkyDiffuseFactor*) on the clear sky assumption is calculated. To find ratio of tilted beam radiation and diffuse radiation on the clear sky, we need to find the geometric factor, R_b (*RRb*), the clear sky beam radiation on tilted surface, $G_{Tb,ClearSky}$ (*GTcb*), and the clear sky diffuse radiation on tilted surface, $G_{Td,ClearSky}$ (*GTdb*). The geometric factor, R_b (*RRb*) or the ratio of beam radiation on the tilted surface is described in equation 3.14 or $R_b = \frac{\cos\theta}{\cos\theta_z}$. The clear sky beam radiation on tilted surface, $G_{Tb,ClearSky}$

(*GTcb*) is also calculated by multiplying the geometric factor, R_b (*RRb*), to the clear sky radiation (equation D.3).

$$G_{Tb,Clearsky} = G_{b,Clearsky} \times R_b \tag{D.3}$$

The clear sky diffuse radiation on tilted surface, $G_{Td,ClearSky}$ (*GTcd*) is also found using equation D.4.

$$G_{Td,Clearsky} = \left[G_{d,Clearsky} \left(\frac{1+\cos\beta}{2} \right) \right] + \left[\left(G_{b,Clearsky} + G_{d,Clearsky} \right) \rho \left(\frac{1-\cos\beta}{2} \right) \right] \tag{D.4}$$

Then, the total tilted clear sky radiation $G_{T,Clearsky}$ (*GTc*) can be calculated by combining the two radiations shown in equation D.5.

$$G_{T,Clearsky} = G_{Tb,Clearsky} + G_{Td,Clearsky} \tag{D.5}$$

The ratio of beam radiation (*ClearSkyBeamFactor*) and the ratio of diffused radiation (*ClearSkyDiffuseFactor*) are then solved by dividing the beam or diffuse radiation on the clear sky by total clear sky radiation described in equation 3.15 and 3.16. The Matlab code in this section is shown below:

```
 %Clear Sky Assumption%
    RRb(NumAngle,1) = cosd(AngleIncident)/cosd(ZenithAngle);
    GTcb(NumAngle,1) = Gcb(NumAngle,1)*RRb(NumAngle,1);
    GTcd(NumAngle,1) =
(Gcd(NumAngle,1)*(1+cosd(Slope))/2)+(Gc(NumAngle,1)*GrndReflc*(1+cosd(Sl
ope)/2));
    GTc(NumAngle,1) = GTcb(NumAngle,1)+GTcd(NumAngle,1);
    ClearSkyBeamFactor(NumAngle,1) = GTcb(NumAngle,1) /GTc(NumAngle,1);
    ClearSkyDiffuseFactor(NumAngle,1) =
GTcd(NumAngle,1)/GTc(NumAngle,1);
    CSBeamEff255V(NumAngle,1) =
(ClearSkyBeamFactor(NumAngle,1)*real((AbsorberHit+DirectHit) /
TotalRay));
    CSDiffEff255V(NumAngle,1) =
(ClearSkyDiffuseFactor(NumAngle,1)*DiffusedRay);
    CSOpticalEff255V(NumAngle,1) =
(ClearSkyBeamFactor(NumAngle,1)*real((AbsorberHit+DirectHit) /
TotalRay))+ (ClearSkyDiffuseFactor(NumAngle,1)*DiffusedRay);
    xxxx(NumAngle,1) =
CSBeamEff255V(NumAngle,1)+CSDiffEff255V(NumAngle,1);
```

Next part is to find the ratio of tilted beam radiation (*BeamFactor*) and diffuse radiation (*DiffuseFactor*) with the cloud/clear sky estimation. The proportion of measured radiation and clear sky radiation, G_H/G_c (*ClearSkyRatio*), on instantaneous radiation is used to indicate diffuse radiation function at a time interval. Equation 3.12 shows three ranges of G_H/G_c which are $0 \le \frac{G_H}{G_c} < 0.48$, $0.48 \le \frac{G_H}{G_c} < 1.10$, and $1.10 \le \frac{G_H}{G_c}$. Each range of G_H/G_c corresponds to a different function of diffuse radiation. At the first range of G_H/G_c where the ratio value is from 0 to 0.48, the diffuse radiation function (G_d) is

$$G_d = \left(1.00 - 0.1\frac{G_H}{G_c}\right) \times G_H \tag{D.6}$$

The second interval of G_H/G_c where the ratio value is from 0.48 to1, the diffuse radiation function (G_d) is

$$G_d = \left(1.11 + 0.0396\left(\frac{G_H}{G_c}\right) - 0.789\left(\frac{G_H}{G_c}\right)^2\right) \times G_H \tag{D.7}$$

The third range of G_H/G_c where the ratio value is more than 1.10, the diffuse radiation function (G_d) is

$$G_d = 0.2 \times G_H \tag{D.8}$$

Then, the beam radiation (G_b) is calculated by subtracting the measured instantaneous radiation (G_H) with the diffuse radiation (G_d) or

$$G_b = G_H - G_d \tag{D.9}$$

After the beam and diffuse radiations (on horizontal plane) are calculated, the beam (*GTb*) and diffuse radiations (*GTd*) on tilted surface can be found. By modifying equation

3.8 and 3.9, we can find the beam (*GTb*) and diffuse radiations (*GTd*) on tilted surface by substituting the clear sky beam radiation on tilted surface, $G_{Tb,ClearSky}$ (*GTcb*) with the beam radiation on tilted surface, G_{Tb} (*GTb*) (Equation D.10) and replacing the clear sky diffuse radiation on tilted surface, $G_{Td,ClearSky}$ (*GTdb*) with the diffuse radiation on tilted surface, G_{Td} (*GTd*) (Equation D.11).

$$G_{Tb} = G_b \times R_b \tag{D.10}$$

$$G_{Td} = \left[G_d \left(\frac{1+\cos\beta}{2} \right) \right] + \left[(G_b + G_d)\rho \left(\frac{1-\cos\beta}{2} \right) \right] \tag{D.11}$$

Also, the total radiation on tilted surface is

$$G_T = G_{Tb} + G_{Td} \tag{D.12}$$

Then, the ratio of beam radiation to total radiation on tilted surface (*BeamFactor*) and the ratio of diffuse radiation to total radiation on tilted surface (*DiffuseFactor*) can be found by equation 3.15 and 3.16 or $\frac{G_{Tb}}{G_T} = \frac{[G_b R_b]}{G_T}$ and $\frac{G_{Td}}{G_T} = \frac{\left[G_d \left(\frac{1+\cos\beta}{2} \right) \right] + \left[(G_b + G_d)\rho \left(\frac{1-\cos\beta}{2} \right) \right]}{G_T}$. Matlab code on this section is shown below.

```
%with Cloud and Clear Sky Estimation (Duffie & Beckman)
    ClearSkyRatio = G(NumAngle,1)/Gc(NumAngle,1);
    if ClearSkyRatio < 0.48
        Gd(NumAngle,1) = (1.00-0.1*ClearSkyRatio)*G(NumAngle,1);
        Diffused(NumAngle,2)=1;
    elseif ClearSkyRatio < 1.10
        Gd(NumAngle,1) = (1.11+0.0396*ClearSkyRatio-
0.789*(ClearSkyRatio^2))*G(NumAngle,1);
        Diffused(NumAngle,2)=2;
    else
        Gd(NumAngle,1) = 0.20*G(NumAngle,1);
        Diffused(NumAngle,2)=3;
```

```
    end
    Gb(NumAngle,1) = G(NumAngle,1)- Gd(NumAngle,1);
    GTb(NumAngle,1) = Gb(NumAngle,1)*RRb(NumAngle,1);
    GTd(NumAngle,1) =
(Gd(NumAngle,1)*(1+cosd(Slope))/2)+(G(NumAngle,1)*GrndReflc*(1+cosd(Slop
e)/2));
    GT(NumAngle,1) = GTb(NumAngle,1)+GTd(NumAngle,1);
    NumFrame1 = NumFrame1+1;
    BeamFactor(NumAngle,1) = GTb(NumAngle,1) /GT(NumAngle,1);
    DiffuseFactor(NumAngle,1) = GTd(NumAngle,1)/GT(NumAngle,1);
```

Lastly the total optical efficiency (*OpticalEff255V*), optical beam efficiency (*BeamEff255V*), and optical diffuse efficiency (*DiffEff255V*) are calculated. The optical beam efficiency (*BeamEff255V*) is found by multiplying the beam efficiency from ray tracing with the ratio of beam radiation to total radiation on tilted surface (*BeamFactor*). The beam efficiency from ray tracing is calculated by combining the rays that hit the absorber with reduced intensity divided by the total rays which are projected to effective aperture area from chapter 2.2.2 (Figure 2.2). So, the optical beam efficiency can be written as equation D.13.

$$BeamEff255V = BeamFactor \times \left(\frac{\sum \text{reduced intensity rays}}{\text{total rays}} \right) \qquad \text{(D.13)}$$

The optical diffuse efficiency (*DiffEff255V*) is found by multiplying the diffuse efficiency from prior diffuse simulation (*DiffusedRay*) with the ratio of diffuse radiation to total radiation on tilted surface (*DiffuseFactor*) which can be formulated as

$$DiffEff255V = DiffuseFactor \times DiffusedRay \qquad \text{(D.14)}$$

Then, the optical efficiency (*OpticalEff255V*) is the combination of beam and diffuse efficiency (equation D.15)

Optical efficiency = optical beam efficiency + optical diffuse efficiency (D.15)

The Matlab code for the last part is

```
    Frames1(NumFrame1) = getframe; %record pictures to array
    BeamEff255V(NumAngle,1) =
(BeamFactor(NumAngle,1)*real((AbsorberHit+DirectHit) / TotalRay));
    DiffEff255V(NumAngle,1) = (DiffuseFactor(NumAngle,1)*DiffusedRay);
    OpticalEff255V(NumAngle,1) =
(BeamFactor(NumAngle,1)*real((AbsorberHit+DirectHit) / TotalRay))+
(DiffuseFactor(NumAngle,1)*DiffusedRay);
    yyyy(NumAngle,1)  = BeamEff255V(NumAngle,1)+DiffEff255V(NumAngle,1);
    disp(HourAngle)
```

D.2 Subprogram

D.2.1 Subprogram *DrawTube()*

The *DrawTube()* subprogram will be called only when animation is required. The Malab processes will portray three ICPCs on the transverse view Figure D.1.

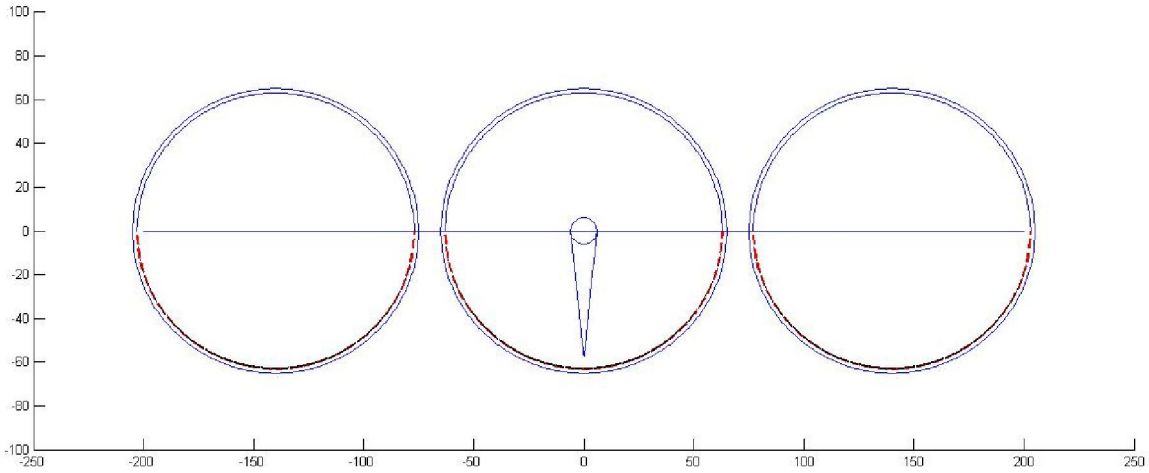

Figure D.1: Three cross-section ICPCs on the transverse view

X-Y plane is used as a reference coordinate system. The middle tube is the target tube and has a center point at (0,0). The glass cover is plotted by two circle functions ($x^2 + y^2 = r^2$), one for the outer glass and another for the inner glass. The radius of outer glass

(*OutTubeRadius*) and the radius of inner glass (*TubeRadius*) are assigned in the first part of the main program (*RayEnter()*). Then, the absorber fin and heat transporting tube are plotted. The heat transporter tube is plotted by using a circle function with radius of the outer heat transporting tube (*InRadius*) also defined in the main program. The absorber fin is defined by the length (*Length*) of the straight line from the center point (0,0) to the end of the absorber. The absorber cone is plotted by drawing straight line from the heat transporting tube radius from both sides to the end point of the fin (0,-*Length*).

Next, the adjacent tubes are created. The main purpose for plotting the adjacent tubes is to visualize the blocking effect which is reducing ray intensity by transmittance and reflectance effects. Each tube has a space between tubes of 10 millimeters. The position for both adjacent tubes will be on the same plane of the collector plane see Figure D.1. The Matlab code for this sub program is illustrated next page.

```
% Cross section of the ICPC tube

offset_x=0;
offset_y=150;
fraction_x=1;
fraction_y=.75;

set(0,'defaultFigurePosition',get(0,'Screensize').*[1 1 fraction_x
fraction_y]+[offset_x offset_y 0 0])


set(gca,'DataAspectRatio',[1 1 1],...
        'PlotBoxAspectRatio',[1 1 1])


%Draw outer glass tube
X = -OutTubeRadius:0.5:OutTubeRadius;
Y = sqrt(OutTubeRadius^2-(X.^2));
hold on
plot(X,Y)
Y = -sqrt(OutTubeRadius^2-(X.^2));
plot(X,Y)
axis([-250 250 -100 100]);
```

```
%Draw inner glass tube

X = -TubeRadius:0.5:TubeRadius;
Y = sqrt(TubeRadius^2-(X.^2));
hold on
plot(X,Y)
Y = -sqrt(TubeRadius^2-(X.^2));
plot(X,Y,'--rs','LineWidth',2,'MarkerEdgeColor','k',...
                'MarkerFaceColor','g',...
                'MarkerSize',1)

%Draw copper tube
X = -InRadius:0.5:InRadius;
Y = sqrt(InRadius^2-(X.^2));
plot(X,Y)
Y = -sqrt(InRadius^2-(X.^2));
plot(X,Y)

%Draw absorber

X = 0:0.5:InRadius;
Y = (Length/InRadius) * X - Length;
plot(X,Y)
X = -InRadius:0.05:0;
Y = -(Length/InRadius) * X - Length;
plot(X,Y)
hold on

%Draw center line
line([-200 200],[0 0])
hold on


%Draw second tube

%Draw outer glass tube
X = OutTubeRadius+10:0.5:3*OutTubeRadius+10;
Y = sqrt(OutTubeRadius^2-((X-2*OutTubeRadius-10).^2));
hold on
plot(X,Y)
Y = -sqrt(OutTubeRadius^2-((X-2*OutTubeRadius-10).^2));
plot(X,Y)


%Draw inner glass tube

X = OutTubeRadius+12:0.5:3*OutTubeRadius+8;
Y = sqrt(TubeRadius^2-((X-2*OutTubeRadius-10).^2));
hold on
plot(X,Y)
Y = -sqrt(TubeRadius^2-((X-2*OutTubeRadius-10).^2));
plot(X,Y,'--rs','LineWidth',2,'MarkerEdgeColor','k',...
                'MarkerFaceColor','g',...
```

```
                'MarkerSize',1)
hold off

%Draw third tube

%Draw outer glass tube
X = -3*OutTubeRadius-10:0.5:-OutTubeRadius-10;
Y = sqrt(OutTubeRadius^2-((X+2*OutTubeRadius+10).^2));
hold on
plot(X,Y)
Y = -sqrt(OutTubeRadius^2-((X+2*OutTubeRadius+10).^2));
plot(X,Y)


%Draw inner glass tube

X = -3*OutTubeRadius-8:0.5:-OutTubeRadius-12;
Y = sqrt(TubeRadius^2-((X+2*OutTubeRadius+10).^2));
hold on
plot(X,Y)
Y = -sqrt(TubeRadius^2-((X+2*OutTubeRadius+10).^2));
plot(X,Y,'--rs','LineWidth',2,'MarkerEdgeColor','k',...
                'MarkerFaceColor','g',...
                'MarkerSize',1)
hold off
```

D.2.2 Subprogram *Shading.m*

Shading() is a subprogram which is activated by *Refraction()*. This subprogram will be first run before determining refraction effect on the target ICPC tube. The *Shading()* has two main parts blocking from the right tube and from the left tube. Since the two parts are symmetry, we will explain only for the first part (*Angle* < 90). *Shading()*will first check whether the ray is blocked by the adjacent tube or not. By solving analytic geometry, we check the intersection point between a ray (line function $Ax+By+C=0$) and the adjacent tube outer cover (circle function $(x-h)^2+y^2=r^2$). Then, we can determine whether the ray is blocked or not using the delta value. If the delta value is less than 0, the ray will not be blocked by the adjacent tube. The function of delta can be written as

$$\text{Delta} = r^2(A^2+B^2) - (Ah+C)^2 \qquad \text{(D.16)}$$

The values of *A, B*, and *C* will stay the same if the ray is not blocked or shading. The point of origin of the ray will be assigned for both cases as

$$(a_1, b_1) = \left(\frac{-(100B + C)}{A}, 100 \right) \tag{D.17}$$

If the delta value is more than 0, the points of intersection are found by solving quadratic equation. The two points of intersection have coordinates

$$x = (B^2h\text{-AC}+B \text{ sqrt[Delta]})/(A^2+B^2), \tag{D.18}$$

$$\text{y} = (-ABh\text{-}BC\text{-}A \text{ sqrt[Delta]})/(A^2+B^2)$$

and

$$x = (B^2h\text{-}AC\text{-}B \text{ sqrt[Delta]})/(A^2+B^2), \tag{D.19}$$

$$y = (-ABh\text{-}BC+A \text{ sqrt[Delta]})/(A^2+B^2)$$

The entry point will be chosen the first intersecting point or in this case the higher value of *y*. The ray is then checked that it hits the reflector by testing the *y* value if it less than zero. If the ray hits the reflector of the adjacent tube, the ray will be totally blocked and will not be collected (*RayBlocked* = 1). Next, the line will be drawn from the point of origin or $\left(\frac{-(100B + C)}{A}, 100 \right)$ to the new entry point (x, y), blue line for the total blocked ray and yellow line for the ray getting through the glass cover. The Matlab code explained before is shown below.

```
%Check for shading
ShadingEff = 1;
RayBlocked = 0;
if Angle < 90 %Hitting right tube
```

```
    if OutTubeRadius*OutTubeRadius*(Ai*Ai+Bi*Bi)-Ci*Ci-2*Ai*Ci*hr-
Ai*Ai*hr*hr<0 %Check for No shading

        b2 = 100;
        a2 = -((Bi*100)+ Ci)/Ai;
        Ai2=Ai;
        Bi2=Bi;
        Ci2=Ci;

    else
        Ai1=Ai;
        Bi1=Bi;
        Ci1=Ci;
        Delta=OutTubeRadius*OutTubeRadius*(Ai*Ai+Bi*Bi)-Ci*Ci-
2*Ai*Ci*hr-Ai*Ai*hr*hr;
        X1=(hr*Bi*Bi-Ai*Ci+Bi*sqrt(Delta))/(Ai*Ai+Bi*Bi);
        Y1=(-Ai*Bi*hr-Bi*Ci-Ai*sqrt(Delta))/(Ai*Ai+Bi*Bi);
        X2=(hr*Bi*Bi-Ai*Ci-Bi*sqrt(Delta))/(Ai*Ai+Bi*Bi);
        Y2=(-Ai*Bi*hr-Bi*Ci+Ai*sqrt(Delta))/(Ai*Ai+Bi*Bi);
        b1 = 100;
        a1 = -((Bi*100)+ Ci)/Ai;
        if Y1 > Y2
            a2 = X1;
            b2 = Y1;
            if b2 < 0
                line([a1 a2],[b1 b2],'color',[0,0.4,0.6])
                RayBlocked = 1;
                return
            else
                line([a1 a2],[b1 b2],'color',[1,0,1])
            end
            %NumFrame1 = NumFrame1+1;
            %Frames1(NumFrame1) = getframe;

        else
            a2 = X2;
            b2 = Y2;
            if b2 < 0
                line([a1 a2],[b1 b2],'color',[0,0.4,0.6])
                RayBlocked = 1;
                return
            else
                line([a1 a2],[b1 b2],'color',[1,0,1])
            end
            %NumFrame1 = NumFrame1+1;
            %Frames1(NumFrame1) = getframe;
        end
```

Finding the refracted ray in the glass cover is next. Snell's law (equation A.2) is used to determine the refracted angle. In order to find the refracted angle, a line

perpendicular to the cover glass (outer circle) at the entry point is assigned. Then, the angle between the ray and the perpendicular line is calculated by

$$\tan\theta = \frac{m_1 - m_2}{1 + m_1 m_2} \tag{D.20}$$

After we get the impact angle, we can find the refracted angle by using equation A.2 or $\frac{n_1}{n_2} = \frac{\sin\theta_2}{\sin\theta_1}$. Since the refractive index of air is 1, the new angle can be found as

$$\theta_{Glass} = \sin^{-1}\left(\frac{\sin\theta_{Air}}{1.526}\right) \tag{D.21}$$

Since the average refractive index of glass is 1.526 (*RefracIndex*), we substitute n_2 with the refractive index for glass. Then, the new *A*, *B*, and *C* values are assigned to the line function of the refracted ray. Next, the process of finding exit point from the glass cover to inside the ICPC tube is by repeating the same step as finding the entry point. Then, the line is drawn from entry point to exit point. Then, the Estimated transmittance (*Transmittance*) is calculated by the subprogram *TransmittanceP*(). The shading effect (*ShadingEff*) will be estimated from the transmittance (*Transmittance*) as it reduces the ray intensity. The Matlab code explaining these processes is shown below.

```
%Find refracted rays
Oa = a1;
Ob = b1;
Ra1 = a2;
Rb1 = b2;

%Assign perpendicular line Ax + By + C = 0
%(draw the line from (hr,0) to (a2,b2))
B = 1;
A = -Rb1 / (Ra1-hr);
C = Rb1*hr/(Ra1-hr);
```

```
%Find angle between two lines

m1 = (Rb1-Ob)/(Ra1-Oa);
m2 = -A;


if m2 == 0
    OldAngle = atan(abs(m1));
elseif Ra1 == 0
    OldAngle = atan(abs(1/m2));
else
    OldAngle = atan(abs((m1-m2)/(1+m1*m2)));
end


%Find refracted angle

q=sin(OldAngle)/RefracIndex;
NewAngle = asin(q);

%Assign new line Ai2x + Bi2y + Ci2 = 0

if abs(m2-m1)<0.00001
    Ai2 = A;
    Bi2 = B;
    Ci2 = C;

elseif Bi1 == 0
    if m2 > 0

            Ai2 = tan(atan(m2)+NewAngle);
            Bi2 = -1;
            Ci2 = b2-Ai2*a2;

    elseif m2 < 0

            Ai2 = tan(atan(m2)-NewAngle);
            Bi2 = -1;
            Ci2 = b2-Ai2*a2;

    end

elseif m1 > 0
    if m2 > 0
        if atan(abs(m2))>atan(abs(m1))
            Ai2 = tan(atan(m2)-NewAngle);
            Bi2 = -1;
            Ci2 = b2-Ai2*a2;
        elseif atan(abs(m2))<atan(abs(m1))
            Ai2 = tan(atan(m2)+NewAngle);
            Bi2 = -1;
            Ci2 = b2-Ai2*a2;
        end
    elseif m2 < 0
```

```
                if atan(abs(m2))>atan(abs(m1))
                    Ai2 = tan(atan(m2)-NewAngle+pi());
                    Bi2 = -1;
                    Ci2 = b2-Ai2*a2;
                elseif atan(abs(m2))<atan(abs(m1))
                    Ai2 = tan(atan(m2)-NewAngle);
                    Bi2 = -1;
                    Ci2 = b2-Ai2*a2;
                end
            end

        elseif m1 < 0
            if m2 > 0
                if atan(abs(m2))>atan(abs(m1))
                    Ai2 = tan(atan(m2)+NewAngle);
                    Bi2 = -1;
                    Ci2 = b2-Ai2*a2;
                elseif atan(abs(m2))<atan(abs(m1))
                    Ai2 = tan(atan(m2)+NewAngle);
                    Bi2 = -1;
                    Ci2 = b2-Ai2*a2;
                end
            elseif m2 < 0
                if atan(abs(m2))>atan(abs(m1))
                    Ai2 = tan(atan(m2)+NewAngle);
                    Bi2 = -1;
                    Ci2 = b2-Ai2*a2;
                elseif atan(abs(m2))<atan(abs(m1))
                    Ai2 = tan(atan(m2)-NewAngle);
                    Bi2 = -1;
                    Ci2 = b2-Ai2*a2;
                end
            end
        end

        Delta=TubeRadius*TubeRadius*(Ai2*Ai2+Bi2*Bi2)-Ci2*Ci2-
2*Ai2*Ci2*hr-Ai2*Ai2*hr*hr;
        X1=(hr*Bi2*Bi2-Ai2*Ci2+Bi2*sqrt(Delta))/(Ai2*Ai2+Bi2*Bi2);
        Y1=(-Ai2*Bi2*hr-Bi2*Ci2-Ai2*sqrt(Delta))/(Ai2*Ai2+Bi2*Bi2);
        X2=(hr*Bi2*Bi2-Ai2*Ci2-Bi2*sqrt(Delta))/(Ai2*Ai2+Bi2*Bi2);
        Y2=(-Ai2*Bi2*hr-Bi2*Ci2+Ai2*sqrt(Delta))/(Ai2*Ai2+Bi2*Bi2);

        b1 = b2;
        a1 = a2;
        if Y2 < Y1
            a2 = X1;
            b2 = Y1;
            line([a1 a2],[b1 b2],'color',[0,0,0.3])
            %NumFrame1 = NumFrame1+1;
            %Frames1(NumFrame1) = getframe;

        else
            a2 = X2;
            b2 = Y2;
            line([a1 a2],[b1 b2],'color',[0,0,0.3])
            %NumFrame1 = NumFrame1+1;
```

```
    %Frames1(NumFrame1) = getframe;
end

%Calculate transmittance 'Duffie amd Beckman (5.1.8)
TransmittanceP()
ShadingEff = ShadingEff*Transmittance;
```

The same concept will be applied as the ray travels from the glass cover to the space inside the adjacent ICPC. Since the ray travels from glass cover to the space inside, the refracted angle can be calculated as

$$\theta_{Air} = \sin^{-1}\left(\sin\theta_{Glass} \times 1.526\right) \tag{D.22}$$

Then, the new ray direction is set as the new *A, B*, and *C* values are assigned to the line. We consider that there is no transmittance loss in the air inside the tube. Then, the program checks if the ray is totally blocked from hitting the reflector of the adjacent tube. If the ray is totally blocked, we will consider this a loss ray, and the dark blue color will be applied. The Matlab code for this part is shown below.

```
%Refraction from glass to air
Oa = a1;
Ob = b1;
Ra1 = a2;
Rb1 = b2;

%Assign perpendicular line Ax + By + C = 0
%(draw the line from (hr,0) to (a2,b2))
A = -Rb1 / (Ra1-hr);
C = Rb1*hr/(Ra1-hr);
B = 1;


m1a = (Rb1-Ob)/(Ra1-Oa);
m2a = -A;
```

```
if m2a == 0
    OldAngle = atan(abs(m1a));
elseif Bi1 == 0
    OldAngle = atan(abs(1/m2a));
elseif m1a == m2a
    OldAngle = 0;
else
    OldAngle = atan(abs((m1a-m2a)/(1+m1a*m2a)));
end


%Find refracted angle

q=sin(OldAngle)*RefracIndex;
NewAngle = asin(q);

%Assign new line Ai2x + Bi2y + Ci2 = 0

if abs(m2a-m1a) < 0.0001
    Ai2 = A;
    Bi2 = 1;
    Ci2 = C;

elseif Bi1 == 0
    if m2a > 0

            Ai2 = tan(atan(m2a)+NewAngle);
            Bi2 = -1;
            Ci2 = b2-Ai2*a2;

    elseif m2a < 0

            Ai2 = tan(atan(m2a)-NewAngle);
            Bi2 = -1;
            Ci2 = b2-Ai2*a2;

    end

elseif m1a > 0
    if m2a > 0
        if atan(abs(m2a))>atan(abs(m1a))
            Ai2 = tan(atan(m2a)-NewAngle);
            Bi2 = -1;
            Ci2 = b2-Ai2*a2;
        elseif atan(abs(m2a))<atan(abs(m1a))
            Ai2 = tan(atan(m2a)+NewAngle);
            Bi2 = -1;
            Ci2 = b2-Ai2*a2;
        end
    elseif m2a < 0
        if atan(abs(m2a))>atan(abs(m1a))
            Ai2 = tan(atan(m2a)-NewAngle+pi());
            Bi2 = -1;
            Ci2 = b2-Ai2*a2;
```

```
                elseif atan(abs(m2a))<atan(abs(m1a))
                    Ai2 = tan(atan(m2a)-NewAngle);
                    Bi2 = -1;
                    Ci2 = b2-Ai2*a2;
                end
            end

        elseif m1a < 0
            if m2a > 0
                if atan(abs(m2a))>atan(abs(m1a))
                    Ai2 = tan(atan(m2a)+NewAngle);
                    Bi2 = -1;
                    Ci2 = b2-Ai2*a2;
                elseif atan(abs(m2a))<atan(abs(m1a))
                    Ai2 = tan(atan(m2a)+NewAngle);
                    Bi2 = -1;
                    Ci2 = b2-Ai2*a2;
                end
            elseif m2a < 0
                if atan(abs(m2a))>atan(abs(m1a))
                    Ai2 = tan(atan(m2a)+NewAngle);
                    Bi2 = -1;
                    Ci2 = b2-Ai2*a2;
                elseif atan(abs(m2a))<atan(abs(m1a))
                    Ai2 = tan(atan(m2a)-NewAngle);
                    Bi2 = -1;
                    Ci2 = b2-Ai2*a2;
                end
            end
        end

        Delta=TubeRadius*TubeRadius*(Ai2*Ai2+Bi2*Bi2)-Ci2*Ci2-
2*Ai2*Ci2*hr-Ai2*Ai2*hr*hr;
        X1=(hr*Bi2*Bi2-Ai2*Ci2+Bi2*sqrt(Delta))/(Ai2*Ai2+Bi2*Bi2);
        Y1=(-Ai2*Bi2*hr-Bi2*Ci2-Ai2*sqrt(Delta))/(Ai2*Ai2+Bi2*Bi2);
        X2=(hr*Bi2*Bi2-Ai2*Ci2-Bi2*sqrt(Delta))/(Ai2*Ai2+Bi2*Bi2);
        Y2=(-Ai2*Bi2*hr-Bi2*Ci2+Ai2*sqrt(Delta))/(Ai2*Ai2+Bi2*Bi2);

        b1 = b2;
        a1 = a2;
        if Y2 > Y1
            a2 = X1;
            b2 = Y1;
            if b2 < 0
                line([a1 a2],[b1 b2],'color',[0,0.4,0.6])
                RayBlocked = 1;
                return
            else
                line([a1 a2],[b1 b2],'color',[1,0,1])
            end
            %NumFrame1 = NumFrame1+1;
            %Frames1(NumFrame1) = getframe;

        else
            a2 = X2;
            b2 = Y2;
```

```
    if b2 < 0
        line([a1 a2],[b1 b2],'color',[0,0.4,0.6])
        RayBlocked = 1;
        return
    else
        line([a1 a2],[b1 b2],'color',[1,0,1])
    end
    %NumFrame1 = NumFrame1+1;
    %Frames1(NumFrame1) = getframe;
end
```

Then, the same process is repeated as the ray will hit glass cover from inside out as the ray passes through the glass cover for the second time. The shading effect will be applied again as it reduces the ray intensity by the transmittance (*Transmittance*) from subprogram *TransmittanceP*(). The equation D.23 shows how the shading effect is calculated.

$$Shading\ Effect = Transmitance_{\text{enter ICPC}} \times Transmittance_{\text{exit ICPC}} \qquad (D.23)$$

After the ray passes through the glass cover the ray refracts back to the air outside and the new value of *A*, *B*, and *C* are assigned. The new assigned line will be used as the ray entering the target ICPC. The Matlab code for the second refraction is shown below.

```
%Find refracted rays 2
Oa = a1;
Ob = b1;
Ra1 = a2;
Rb1 = b2;

%Assign perpendicular line Ax + By + C = 0
%(draw the line from (hr,0) to (a2,b2))
B = 1;
A = -Rb1 / (Ra1-hr);
C = Rb1*hr/(Ra1-hr);

%Find angle between two lines

m1 = (Rb1-Ob)/(Ra1-Oa);
m2 = -A;
```

```
if m2 == 0
    OldAngle = atan(abs(m1));
elseif Ra1 == 0
    OldAngle = atan(abs(1/m2));
%elseif m1 == m2

else
    OldAngle = atan(abs((m1-m2)/(1+m1*m2)))-pi();
end


%Find refracted angle

q=sin(OldAngle)/RefracIndex;
NewAngle = asin(q);

%Assign new line Ai2x + Bi2y + Ci2 = 0

if abs(m2-m1)<0.00001
    Ai2 = A;
    Bi2 = B;
    Ci2 = C;

elseif Bi1 == 0
    if m2 > 0

            Ai2 = tan(atan(m2)+NewAngle);
            Bi2 = -1;
            Ci2 = b2-Ai2*a2;

    elseif m2 < 0

            Ai2 = tan(atan(m2)-NewAngle);
            Bi2 = -1;
            Ci2 = b2-Ai2*a2;

    end

elseif m1 > 0
    if m2 > 0
        if atan(abs(m2))>atan(abs(m1))
            Ai2 = tan(atan(m2)-NewAngle);
            Bi2 = -1;
            Ci2 = b2-Ai2*a2;
        elseif atan(abs(m2))<atan(abs(m1))
            Ai2 = tan(atan(m2)+NewAngle);
            Bi2 = -1;
            Ci2 = b2-Ai2*a2;
        end
    elseif m2 < 0
        if atan(abs(m2))>atan(abs(m1))
            Ai2 = tan(atan(m2)-NewAngle+pi());
            Bi2 = -1;
            Ci2 = b2-Ai2*a2;
```

```
            elseif atan(abs(m2))<atan(abs(m1))
                Ai2 = tan(atan(m2)-NewAngle);
                Bi2 = -1;
                Ci2 = b2-Ai2*a2;
            end
        end

    elseif m1 < 0
        if m2 > 0
            if atan(abs(m2))>atan(abs(m1))
                Ai2 = tan(atan(m2)+NewAngle);
                Bi2 = -1;
                Ci2 = b2-Ai2*a2;
            elseif atan(abs(m2))<atan(abs(m1))
                Ai2 = tan(atan(m2)+NewAngle);
                Bi2 = -1;
                Ci2 = b2-Ai2*a2;
            end
        elseif m2 < 0
            if atan(abs(m2))>atan(abs(m1))
                Ai2 = tan(atan(m2)+NewAngle);
                Bi2 = -1;
                Ci2 = b2-Ai2*a2;
            elseif atan(abs(m2))<atan(abs(m1))
                Ai2 = tan(atan(m2)-NewAngle);
                Bi2 = -1;
                Ci2 = b2-Ai2*a2;
            end
        end
    end

    Delta=OutTubeRadius*OutTubeRadius*(Ai2*Ai2+Bi2*Bi2)-Ci2*Ci2-
2*Ai2*Ci2*hr-Ai2*Ai2*hr*hr;
    X1=(hr*Bi2*Bi2-Ai2*Ci2+Bi2*sqrt(Delta))/(Ai2*Ai2+Bi2*Bi2);
    Y1=(-Ai2*Bi2*hr-Bi2*Ci2-Ai2*sqrt(Delta))/(Ai2*Ai2+Bi2*Bi2);
    X2=(hr*Bi2*Bi2-Ai2*Ci2-Bi2*sqrt(Delta))/(Ai2*Ai2+Bi2*Bi2);
    Y2=(-Ai2*Bi2*hr-Bi2*Ci2+Ai2*sqrt(Delta))/(Ai2*Ai2+Bi2*Bi2);

    b1 = b2;
    a1 = a2;
    %if Ai2 < 0
        a2 = X1;
        b2 = Y1;
        line([a1 a2],[b1 b2],'color',[0,0,0.3])
        %NumFrame1 = NumFrame1+1;
        %Frames1(NumFrame1) = getframe;


    %Calculate transmittance 'Duffie amd Beckman (5.1.8)
    TransmittanceP()
    ShadingEff = ShadingEff*Transmittance;


    %Refraction from glass to air
    Oa = a1;
```

```
Ob = b1;
Ra1 = a2;
Rb1 = b2;

%Assign perpendicular line Ax + By + C = 0
%(draw the line from (hr,0) to (a2,b2))
A = -Rb1 / (Ra1-hr);
C = Rb1*hr/(Ra1-hr);
B = 1;

m1a = (Rb1-Ob)/(Ra1-Oa);
m2a = -A;


if m2a == 0
    OldAngle = atan(abs(m1a));
elseif Bi1 == 0
    OldAngle = atan(abs(1/m2a));
elseif m1a == m2a
    OldAngle = 0;
else
    OldAngle = atan(abs((m1a-m2a)/(1+m1a*m2a)));
end


%Find refracted angle

q=sin(OldAngle)*RefracIndex;
NewAngle = asin(q);

%Assign new line Ai2x + Bi2y + Ci2 = 0

if abs(m2a-m1a) < 0.0001
    Ai2 = A;
    Bi2 = 1;
    Ci2 = C;

elseif Bi1 == 0
    if m2a > 0

            Ai2 = tan(atan(m2a)+NewAngle);
            Bi2 = -1;
            Ci2 = b2-Ai2*a2;

    elseif m2a < 0

            Ai2 = tan(atan(m2a)-NewAngle);
            Bi2 = -1;
            Ci2 = b2-Ai2*a2;

    end

elseif m1a > 0
    if m2a > 0
```

```
            if atan(abs(m2a))>atan(abs(m1a))
                Ai2 = tan(atan(m2a)-NewAngle);
                Bi2 = -1;
                Ci2 = b2-Ai2*a2;
            elseif atan(abs(m2a))<atan(abs(m1a))
                Ai2 = tan(atan(m2a)+NewAngle);
                Bi2 = -1;
                Ci2 = b2-Ai2*a2;
            end
        elseif m2a < 0
            if atan(abs(m2a))>atan(abs(m1a))
                Ai2 = tan(atan(m2a)+NewAngle+pi());
                Bi2 = -1;
                Ci2 = b2-Ai2*a2;
            elseif atan(abs(m2a))<atan(abs(m1a))
                Ai2 = tan(atan(m2a)+NewAngle);
                Bi2 = -1;
                Ci2 = b2-Ai2*a2;
            end
        end

    elseif m1a < 0
        if m2a > 0
            if atan(abs(m2a))>atan(abs(m1a))
                Ai2 = tan(atan(m2a)+NewAngle);
                Bi2 = -1;
                Ci2 = b2-Ai2*a2;
            elseif atan(abs(m2a))<atan(abs(m1a))
                Ai2 = tan(atan(m2a)+NewAngle);
                Bi2 = -1;
                Ci2 = b2-Ai2*a2;
            end
        elseif m2a < 0
            if atan(abs(m2a))>atan(abs(m1a))
                Ai2 = tan(atan(m2a)+NewAngle);
                Bi2 = -1;
                Ci2 = b2-Ai2*a2;
            elseif atan(abs(m2a))<atan(abs(m1a))
                Ai2 = tan(atan(m2a)-NewAngle);
                Bi2 = -1;
                Ci2 = b2-Ai2*a2;
            end
        end
    end
end
```

D.2.3 Subprogram (*TransmittanceP.m*)

TransmittanceP() will be activated within subprogram *Shading*() and *Refraction*(). The subprogram TransmittanceP() will estimate the total transmittance by

multiplying transmittance of reflectance, τ_r, with transmittance of absorbance, τ_a, (equation A.6). The transmittance of reflectance (τ_r) can be found using equation A.3 or $\tau_r = \frac{1}{2}\left(\frac{1-r_{//}}{1-r_{//}} + \frac{1-r_{\perp}}{1-r_{\perp}}\right)$. The parallel component (*ParaRad*) of the reflection is described in equation A.6 as $r_{//} = \frac{\tan^2(\theta_2 - \theta_1)}{\tan^2(\theta_2 + \theta_1)}$ and the perpendicular component (*PerpRad*) of the reflectance is $r_{\perp} = \frac{\sin^2(\theta_2 - \theta_1)}{\sin^2(\theta_2 + \theta_1)}$. The transmittance of absorbance (*TransmittanceA*) is also described in equation A.4 or $\tau_a = \frac{I_\tau}{I_o} = e^{-Kx}$. Since the extinction coefficient of the glass cover is approximately 4 to13 m^{-1}, the transmittance of absorbance (*TransmittanceA*) will be described as $\tau_a = e^{-13x}$ where x is the distance where the ray travels through the glass cover. Then, the transmittance (*Transmittance*) can be estimated multiplying the two kinds of transmittances or $\tau \cong \tau_a \tau_r$. The Matlab code is also shown below.

```
if OldAngle == 0
    RadZero = (RefracIndex-1)/(RefracIndex+1);
    TransmittanceR = (1-RadZero)/(1+RadZero);

else
    PerpRad = (sin(NewAngle-OldAngle)^2)/(sin(NewAngle+OldAngle)^2);
    ParaRad = (tan(NewAngle-OldAngle)^2)/(tan(NewAngle+OldAngle)^2);
    TransmittanceR = abs(0.5*(((1-ParaRad)/(1+ParaRad))+((1-
PerpRad)/(1+PerpRad))));

end
distance = sqrt(((a2-a1)^2)+((b2-b1)^2))*0.001;
TransmittanceA = exp(-13*distance);
Transmittance = real(TransmittanceA*TransmittanceR);
```

D.2.4 Subprogram (*Refraction.m*)

The subprogram *Refraction()* is activated in the main program. First, *Refraction()* activates another subprogram *Shading()* which is explained before. The subprogram *Refraction*() acts like *Shading*() when the ray passes through the cover glass of the target tube.

After run the *Shading*() subprogram, *Refraction*() will check whether the ray is totally blocked from the adjacent tube. If the ray is blocked we will count that ray as a loss ray (*TotalLossRay*). Then the ray will be checked that whether it is blocked by lower half or just miss the reflector of the target tube by checking if $|C| \geq r_{tube} \times |A|$. If the ray is blocked, we will include this to the loss ray and assign blue color to the ray and stop simulating. The ray that isn't blocked will be refracted while traveling through the glass cover. The refracted direction will be determined by Snell's law (equation A.2) and the loss of the ray's intensity will be determined by the subprogram *TransmittanceP*() described on 3.2.4. The ray will be plotted with the dark blue for refracted ray in the glass cover (Figure 3.8). Lastly, the direction of the refracted ray from glass cover to the space inside the tube is updated (new *A*, *B*, and *C* values). The *Exposure*() subprogram will be activated next in the main program (*RayEnter*()). Matlab code for *Refraction.m* is shown below.

```
RefracIndex = 1.526;
Shading()
```

```
if RayBlocked == 1
    LossRay=1;
    TotalLossRay=TotalLossRay+1;
    return
end
if abs(Ci2) > TubeRadius * abs(Ai2) %Check for the loss ray
    LossRay=1;
    TotalLossRay=TotalLossRay+1;
    Ai1=Ai2;
    Bi1=Bi2;
    Ci1=Ci2;
    Delta=OutTubeRadius*OutTubeRadius*(Ai1*Ai1+Bi1*Bi1)-Ci1*Ci1;
    X1=(-Ai1*Ci1+Bi1*sqrt(Delta))/(Ai1*Ai1+Bi1*Bi1);
    Y1=(-Bi1*Ci1-Ai1*sqrt(Delta))/(Ai1*Ai1+Bi1*Bi1);
    X2=(-Ai1*Ci1-Bi1*sqrt(Delta))/(Ai1*Ai1+Bi1*Bi1);
    Y2=(-Bi1*Ci1+Ai1*sqrt(Delta))/(Ai1*Ai1+Bi1*Bi1);
    b1 = b2;
    a1 = a2;

    if Delta <= 0
        b2 = 100;
        a2 = -((Bi2*100)+ Ci2)/Ai2;

    elseif Y1 > Y2
        a2 = X1;
        b2 = Y1;


    else
        a2 = X2;
        b2 = Y2;

    end
    line([a1 a2],[b1 b2],'color',[0,0.4,0.6])
    %NumFrame1 = NumFrame1+1;
    %Frames1(NumFrame1) = getframe;
else

    LossRay=0;
    Ai1=Ai2;
    Bi1=Bi2;
    Ci1=Ci2;
    Delta=OutTubeRadius*OutTubeRadius*(Ai1*Ai1+Bi1*Bi1)-Ci1*Ci1;
    Xi1=(-Ai1*Ci1+Bi1*sqrt(Delta))/(Ai1*Ai1+Bi1*Bi1);
    Yi1=(-Bi1*Ci1-Ai1*sqrt(Delta))/(Ai1*Ai1+Bi1*Bi1);
    Xi2=(-Ai1*Ci1-Bi1*sqrt(Delta))/(Ai1*Ai1+Bi1*Bi1);
    Yi2=(-Bi1*Ci1+Ai1*sqrt(Delta))/(Ai1*Ai1+Bi1*Bi1);
    b1 = b2;
    a1 = a2;


    if Yi1 > Yi2
        a2 = Xi1;
        b2 = Yi1;
        line([a1 a2],[b1 b2],'color',[1,0,1])
```

```
        %NumFrame1 = NumFrame1+1;
        %Frames1(NumFrame1) = getframe;

    else
        a2 = Xi2;
        b2 = Yi2;
        line([a1 a2],[b1 b2],'color',[1,0,1])
        %NumFrame1 = NumFrame1+1;
        %Frames1(NumFrame1) = getframe;
    end


%Find refracted rays
        Oa = a1;
        Ob = b1;
        Ra1 = a2;
        Rb1 = b2;

        %Assign perpendicular line Ax + By + C = 0
        %(draw the line from (0,0) to (a2,b2))
        B = 1;
        A = -Rb1 / Ra1;
        C = 0;

        %Find angle between two lines
        if Angle == 90
            m2 = -A;
            m1 =100000000000;
        else
            m1 = (Rb1-Ob)/(Ra1-Oa);
            m2 = -A;
        end

        if m2 == 0
            OldAngle = atan(abs(m1));
        elseif Ra1 == 0
            OldAngle = atan(abs(1/m2));
        %elseif m1 == m2

        else
            OldAngle = atan(abs((m1-m2)/(1+m1*m2)));
        end


        %Find refracted angle

        q=sin(OldAngle)/RefracIndex;
        NewAngle = asin(q);

        %Assign new line Ai2x + Bi2y + Ci2 = 0

        if abs(m2-m1)<0.00001
            Ai2 = A;
            Bi2 = B;
```

```
    Ci2 = C;

elseif Bi1 == 0
    if m2 > 0

            Ai2 = tan(atan(m2)+NewAngle);
            Bi2 = -1;
            Ci2 = b2-Ai2*a2;

    elseif m2 < 0

            Ai2 = tan(atan(m2)-NewAngle);
            Bi2 = -1;
            Ci2 = b2-Ai2*a2;

    end

elseif m1 > 0
    if m2 > 0
        if atan(abs(m2))>atan(abs(m1))
            Ai2 = tan(atan(m2)-NewAngle);
            Bi2 = -1;
            Ci2 = b2-Ai2*a2;
        elseif atan(abs(m2))<atan(abs(m1))
            Ai2 = tan(atan(m2)+NewAngle);
            Bi2 = -1;
            Ci2 = b2-Ai2*a2;
        end
    elseif m2 < 0
        if atan(abs(m2))>atan(abs(m1))
            Ai2 = tan(atan(m2)-NewAngle+pi());
            Bi2 = -1;
            Ci2 = b2-Ai2*a2;
        elseif atan(abs(m2))<atan(abs(m1))
            Ai2 = tan(atan(m2)-NewAngle);
            Bi2 = -1;
            Ci2 = b2-Ai2*a2;
        end
    end

elseif m1 < 0
    if m2 > 0
        if atan(abs(m2))>atan(abs(m1))
            Ai2 = tan(atan(m2)+NewAngle);
            Bi2 = -1;
            Ci2 = b2-Ai2*a2;
        elseif atan(abs(m2))<atan(abs(m1))
            Ai2 = tan(atan(m2)+NewAngle);
            Bi2 = -1;
            Ci2 = b2-Ai2*a2;
        end
    elseif m2 < 0
        if atan(abs(m2))>atan(abs(m1))
            Ai2 = tan(atan(m2)+NewAngle);
            Bi2 = -1;
```

```
                Ci2 = b2-Ai2*a2;
            elseif atan(abs(m2))<atan(abs(m1))
                Ai2 = tan(atan(m2)-NewAngle);
                Bi2 = -1;
                Ci2 = b2-Ai2*a2;
            end
        end
    end


    Delta=TubeRadius*TubeRadius*(Ai2*Ai2+Bi2*Bi2)-Ci2*Ci2;
    X1=(-Ai2*Ci2+Bi2*sqrt(Delta))/(Ai2*Ai2+Bi2*Bi2);
    Y1=(-Bi2*Ci2-Ai2*sqrt(Delta))/(Ai2*Ai2+Bi2*Bi2);
    X2=(-Ai2*Ci2-Bi2*sqrt(Delta))/(Ai2*Ai2+Bi2*Bi2);
    Y2=(-Bi2*Ci2+Ai2*sqrt(Delta))/(Ai2*Ai2+Bi2*Bi2);
    b1 = b2;
    a1 = a2;
    if Y2 < Y1
        a2 = X1;
        b2 = Y1;
        line([a1 a2],[b1 b2],'color',[0,0,0.3])
        %NumFrame1 = NumFrame1+1;
        %Frames1(NumFrame1) = getframe;

    else
        a2 = X2;
        b2 = Y2;
        line([a1 a2],[b1 b2],'color',[0,0,0.3])
        %NumFrame1 = NumFrame1+1;
        %Frames1(NumFrame1) = getframe;
    end
    TransmittanceP()


%Refraction from glass to air
Oa = a1;
Ob = b1;
Ra1 = a2;
Rb1 = b2;

%Assign perpendicular line Ax + By + C = 0
%(draw the line from (0,0) to (a2,b2))
B = 1;
A = -Rb1 / Ra1;
C = 0;

%Find angle between two lines

    m1a = (Rb1-Ob)/(Ra1-Oa);
    m2a = -A;


if m2a == 0
    OldAngle = atan(abs(m1a));
elseif Bi1 == 0
```

```
    OldAngle = atan(abs(1/m2a));
elseif m1a == m2a
    OldAngle = 0;
else
    OldAngle = atan(abs((m1a-m2a)/(1+m1a*m2a)));
end


%Find refracted angle

q=sin(OldAngle)*RefracIndex;
NewAngle = asin(q);

%Assign new line Ai2x + Bi2y + Ci2 = 0

if abs(m2a-m1a) < 0.0001
    Ai2 = A;
    Bi2 = 1;
    Ci2 = C;

elseif Bi1 == 0
    if m2a > 0

            Ai2 = tan(atan(m2a)+NewAngle);
            Bi2 = -1;
            Ci2 = b2-Ai2*a2;

    elseif m2a < 0

            Ai2 = tan(atan(m2a)-NewAngle);
            Bi2 = -1;
            Ci2 = b2-Ai2*a2;

    end

elseif m1a > 0
    if m2a > 0
        if atan(abs(m2a))>atan(abs(m1a))
            Ai2 = tan(atan(m2a)-NewAngle);
            Bi2 = -1;
            Ci2 = b2-Ai2*a2;
        elseif atan(abs(m2a))<atan(abs(m1a))
            Ai2 = tan(atan(m2a)+NewAngle);
            Bi2 = -1;
            Ci2 = b2-Ai2*a2;
        end
    elseif m2a < 0
        if atan(abs(m2a))>atan(abs(m1a))
            Ai2 = tan(atan(m2a)-NewAngle+pi());
            Bi2 = -1;
            Ci2 = b2-Ai2*a2;
        elseif atan(abs(m2a))<atan(abs(m1a))
            Ai2 = tan(atan(m2a)-NewAngle);
            Bi2 = -1;
```

```
                Ci2 = b2-Ai2*a2;
            end
        end

    elseif m1a < 0
        if m2a > 0
            if atan(abs(m2a))>atan(abs(m1a))
                Ai2 = tan(atan(m2a)+NewAngle);
                Bi2 = -1;
                Ci2 = b2-Ai2*a2;
            elseif atan(abs(m2a))<atan(abs(m1a))
                Ai2 = tan(atan(m2a)+NewAngle);
                Bi2 = -1;
                Ci2 = b2-Ai2*a2;
            end
        elseif m2a < 0
            if atan(abs(m2a))>atan(abs(m1a))
                Ai2 = tan(atan(m2a)+NewAngle);
                Bi2 = -1;
                Ci2 = b2-Ai2*a2;
            elseif atan(abs(m2a))<atan(abs(m1a))
                Ai2 = tan(atan(m2a)-NewAngle);
                Bi2 = -1;
                Ci2 = b2-Ai2*a2;
            end
        end
    end
end
```

D.2.5 Subprogram (*Exposure.m*)

The *Exposure*() subprogram is run next in the main program. First, the subprogram will test whether the ray hits the heat transport tube directly (wrapped with the absorber material) or not. The Delta value is tested if the value is more than 0; the Delta function described in equation D.24 is used.

$$\text{Delta} = r^2_{\text{HeatTrans}}(A^2+B^2) - (C)^2 \tag{D.24}$$

If the ray hits the heat transport tube, the hitting point is calculated by equation D.25 and D.26. The points of intersection between the line (simulated ray) and the circle (heat transport tube) are found by solving quadratic equation. The two points of intersection have coordinates

$$x = (\text{-AC}+B\ \text{sqrt[Delta]})/(A^2+B^2), \tag{D.25}$$

$$\text{y} = (\text{-}BC\text{-}A\ \text{sqrt[Delta]})/(A^2+B^2)$$

and

$$x = (-AC-B \text{ sqrt[Delta]})/(A^2+B^2), \qquad (D.26)$$

$$y = (-BC+A \text{ sqrt[Delta]})/(A^2+B^2)$$

The first point that the ray hits will be the point with the higher y value. The if, elseif logic in Matlab is used to decide which point is the hitting point by testing the higher value of y. Then, the y position (*YPlotValue*) is recorded for future use in the sub-program *SideRayEnter*(). Next, the red color will be assigned to the ray. Then, the sub-program *SideRayEnter*() is activated. *SideRayEnter*() will return the value of variable *EndLossPercent* which is accounted for the array of rays at the same angle from the side view. The reduced intensity ray is then recorded as the array of rays at the same angle along the longitudinal view. Figure 3.14 shows how the array of rays on the longitudinal view portrays as one ray at the transverse view. The Matlab explaining these processes is shown below.

```
% Jirachote Daosukho
% Cross section of the ICPC tube
% Check exposure point.
hold on
ynumber=0;
DHit = 0;
AbHit = 0;
ReHit = 0;
if LossRay==1 %Check for the loss ray

elseif InRadius * InRadius * ((Ai2*Ai2)+(Bi2*Bi2))-(Ci2*Ci2)> 0
%Checking for direct hitting
    ExposureRay = ExposureRay + 1;
    A=Ai2;
    B=Bi2;
    C=Ci2;
    DeltaS = InRadius*InRadius*(A*A+B*B)-C*C;
    X1=(-A*C+B*sqrt(DeltaS))/(A*A+B*B);
    Y1=(-B*C-A*sqrt(DeltaS))/(A*A+B*B);
    X2=(-A*C-B*sqrt(DeltaS))/(A*A+B*B);
    Y2=(-B*C+A*sqrt(DeltaS))/(A*A+B*B);
    b1 = b2;
```

```
    a1 = a2;
    ynumber = ynumber+1;
    YPlotValue(:,ynumber) = b1;
    if Y1 > Y2
        a2 = X1;
        b2 = Y1;
        line([a1 a2],[b1 b2],'color','r')
        %NumFrame1 = NumFrame1+1;
        %Frames1(NumFrame1) = getframe;
    elseif Y2 > Y1
        a2 = X2;
        b2 = Y2;
        line([a1 a2],[b1 b2],'color','r')
        %NumFrame1 = NumFrame1+1;
        %Frames1(NumFrame1) = getframe;
    end
    ynumber = ynumber+1;
    YPlotValue(:,ynumber) = b2;
    DHit = 1;
    AbHit = 0;
    ReHit = 0;
    SideRayEnter()
    DirectHit = DirectHit + Transmittance * ShadingEff * (1-
EndLossPercent);
```

The second part checks if the ray hit the absorber fin by finding if the ray (line) intersects the absorber. For vertical fin absorber, we simplified the absorber by substitute the fin by a straight line on the y-axis from 0 to – fin length. So checking for absorber hit is simply by checking the ray y-axis intersection, and the y position (*YPlotValue*) is recorded. Then the brown line is drawn as the ray hits the absorber. Next, the subprogram *SideRayEnter*() is activated and returns the *EndLossPercent* value. Then the reduced ray intensity is recorded to *AbsorberHit*. A 94.7% absorber fin efficiency is also applied to the ray intensity as the ray loss 5.3% of its intensity through heat absorbing process. The Matlab explaining these processes is shown below.

```
elseif Bi2 < 0 && -Ci2/Bi2 >= -Length && -Ci2/Bi2 <0 %Check for hitting
an absorber plate
```

```
    A=Ai2;
    B=Bi2;
    C=Ci2;
    b1 = b2;
    a1 = a2;
    b2 = -C/B;
    a2 = 0;
    ynumber = ynumber+1;
    YPlotValue(:,ynumber) = b1;
    ExposureRay = ExposureRay + 1;
    line([a1 a2],[b1 b2],'color',[0.9,0.5,0])
    %NumFrame1 = NumFrame1+1;
    %Frames1(NumFrame1) = getframe;
    %end
    ynumber = ynumber+1;
    YPlotValue(:,ynumber) = b2;
    DHit = 0;
    AbHit = 1;
    ReHit = 0;
    SideRayEnter()
    AbsorberHit = AbsorberHit + 0.947 * Transmittance * ShadingEff * (1-
EndLossPercent);
```

Last, the ray that misses the absorber or the heat transport tube is checked that if it hit the reflector inside the ICPC. The Delta value is tested again if the value is more than 0 as the ray hits the reflector. The Delta function where r is a reflector radius described in equation D.27 is used.

$$\text{Delta} = r^2_{\text{Reflector}}(A^2+B^2) - (C)^2 \tag{D.27}$$

The hitting point is calculated by equation D.28 and D.29 where the points of intersection between the line (simulated ray) and the circle (reflector) are found by solving quadratic equation. The two points of intersection have coordinates

$$x = (\text{-AC}+B\ \text{sqrt[Delta]})/(A^2+B^2), \tag{D.28}$$

$$\text{y} = (\text{-}BC\text{-}A\ \text{sqrt[Delta]})/(A^2+B^2)$$

and

$$x = (-AC-B\ \text{sqrt[Delta]})/(A^2+B^2), \qquad \text{(D.29)}$$

$$y = (-BC+A\ \text{sqrt[Delta]})/(A^2+B^2)$$

Then, the lower point between two intersected points is a reflecting point. Yellow color is then assigned to the ray. Next, the y position (*YPlotValue*) is recorded. Last, the subprogram ReflexRay() is activated. The Matlab processes are shown below.

```
elseif TubeRadius*TubeRadius*(Ai2*Ai2+Bi2*Bi2)-(Ci2*Ci2)> 0 %Check for
hitting a reflector
    A=Ai2;
    B=Bi2;
    C=Ci2;
    Delta=TubeRadius*TubeRadius*(A*A+B*B)-C*C;
    X1=(-A*C+B*sqrt(Delta))/(A*A+B*B);
    Y1=(-B*C-A*sqrt(Delta))/(A*A+B*B);
    X2=(-A*C-B*sqrt(Delta))/(A*A+B*B);
    Y2=(-B*C+A*sqrt(Delta))/(A*A+B*B);

    if Y1 > Y2
        FirstY = b2;
        FirstX = a2;
        SecondY = Y2;
        SecondX = X2;
        line([FirstX SecondX],[FirstY
SecondY],'color','y','linestyle','-')
        %NumFrame1 = NumFrame1+1;
        %Frames1(NumFrame1) = getframe;
        a1 = X1;
        b1 = Y1;
        a2 = X2;
        b2 = Y2;

    elseif Y2 > Y1
        FirstY = b2;
        FirstX = a2;
        SecondY = Y1;
        SecondX = X1;
        line([FirstX SecondX],[FirstY
SecondY],'color','y','linestyle','-')
        %NumFrame1 = NumFrame1+1;
        %Frames1(NumFrame1) = getframe;
        a1 = X2;
        b1 = Y2;
        a2 = X1;
        b2 = Y1;

    end
    ynumber = ynumber+1;
    YPlotValue(:,ynumber) = b1;
```

```
    ynumber = ynumber+1;
    YPlotValue(:,ynumber) = b2;
    DHit = 0;
    AbHit = 0;
    ReHit = 1;
    ReflexRay()

end
```

D.2.6 Subprogram (*ReflexRay.m*)

The subprogram is activated by the subprogram *Exposure*() when the ray hits the reflector. The *ReflexRay*() will determine whether the ray hits the heat transport tube, absorber fin, reflector, or is reflected out. First, *Reflection* variable will count number of reflections as a number of times of the *ReflexRay*() activated. The reflection direction is calculated by using a line reference perpendicular to the reflector at the reflected point. The reflect angle will be found by simply projecting a mirror image of an impact line from the line reference. The new line function is then assigned. Next, the ray will be tested for it hitting surface. A brown line will be drawn if the ray hit the absorber fin. Then, *SideRayEnter*() is activated and *AbsorberHit* variable is recorded. If the ray hits the reflector a yellow line is then plotted. And the subprogram *ReflexRay*() will be activated again. Last, if the ray does not hit the absorber or reflector the ray will reflect out. Then the green color will be assigned to the ray. The Matlab code for this process is shown below.

```
%Assign number of reflections
Reflection = Reflection + 1;


%Find reflex rays
Oa = a1;
Ob = b1;
Ra1 = a2;
Rb1 = b2;

%Assign perpendicular line Ax + By + C = 0
B = 1;
A = -Rb1 / Ra1;
C = 0;

%Find a reflex angle (Ra2,Rb2)
Ra2 = Oa - 2*A*(A*Oa + B*Ob + C)/(A*A + B*B);
Rb2 = Ob - 2*B*(A*Oa + B*Ob + C)/(A*A + B*B);

%Assign new line AAx + BBy + CC = 0
AA = -(Rb1-Rb2)/(Ra1-Ra2);
BB = 1;
CC = ((Rb1-Rb2)*Ra2/(Ra1-Ra2))-Rb2;

ynumber = ynumber+1;

%Check for the next hitting

if -CC/BB >= -Length && -CC/BB <0 %Check for hitting an absorber plate

    ExposureRay = ExposureRay + 1;

    FirstY = Rb1;
    FirstX = Ra1;
    SecondY = -CC/BB;
    SecondX = 0;
    %AbsorberHit = AbsorberHit + 1;
    line([FirstX SecondX],[FirstY
SecondY],'color',[0.5,0.5,0])%[ReflexFactor*0.9,ReflexFactor*0.5,0]
    %NumFrame1 = NumFrame1+1;
    %Frames1(NumFrame1) = getframe;
    YPlotValue(:,ynumber) = SecondY;
    DHit = 0;
    AbHit = 1;
    ReHit = 0;
    SideRayEnter()
    AbsorberHit = AbsorberHit + 0.95 *
(RFactor*Transmittance*ShadingEff) * (1-EndLossPercent);
    RFactor = 1;
elseif Rb2 < 0 %Check for hitting a reflector
    line([Ra1 Ra2],[Rb1 Rb2],'color','y','linestyle','-')
    %NumFrame1 = NumFrame1+1;
    %Frames1(NumFrame1) = getframe;
    a1 = Ra1;
    b1 = Rb1;
```

```
    a2 = Ra2;
    b2 = Rb2;
    YPlotValue(:,ynumber) = Rb2;
    DHit = 0;
    AbHit = 0;
    ReHit = 1;
    ReflexRay()

elseif Rb2 > 0 %Check for the loss ray
    line([Ra1 (-((BB*100)+ CC)/AA)],[Rb1 100],'color','g','linestyle','-
')
    GapLossRay=GapLossRay+1;
    %NumFrame1 = NumFrame1+1;
    %Frames1(NumFrame1) = getframe;
    ExposureRay = ExposureRay + 1;
    %YPlot(:,ynumber) = b2;
    DHit = 0;
    AbHit = 0;
    ReHit = 0;
    SideRayEnter()
end
```

D.2.7 Sub program (*SideRayEnter.m*)

The subprogram *SideRayEnter*() will analyze the ray at a longitudinal view. The tube length (*TubeLength*) is assigned as 2708 millimeters. Then, the reflectance index for each section of the ICPC tube is assigned, so each section will has it own reflectance index which is from the observation at the site. The tube will be divided into ten sections as the reflectance index is running from *RF1* to *RF10*. Then, the ray is project to the longitudinal view. The angle of incidence at the longitudinal view (*SideAngle*) is found by projecting the ray using basic geometric algebra into the longitudinal plane. Then, we also use two dimension x-y coordinate as the main coordinate system at the longitudinal plane. There are three cases to find the angle of incidence at the longitudinal view (*SideAngle*). Equation D.30 will show all three cases.

$$\theta_{Longitudinal} = \tan^{-1}\left(\frac{\cos\theta}{\sin\theta \times \cos(-\gamma_{Transverse})}\right) \qquad \gamma_{Transverse} < 0$$

$$\theta_{Longitudinal} = \tan^{-1}\left(\frac{\cos\theta}{\sin\theta \times \cos(\gamma_{Transverse})}\right) \qquad 0 \le \gamma_{Transverse} \le 90 \qquad \text{(D.30)}$$

$$\theta_{Longitudinal} = 90 + \tan^{-1}\left(\frac{\cos\theta}{\sin\theta \times \cos(\gamma_{Transverse} - 90)}\right) \qquad \gamma_{Transverse} > 90$$

Then, the line slope is assigned as *sAi*. The ICPC tube in longitudinal view is then plotted as the subprogram *DrawSideview*() is activated. The Matlab code is shown below.

```
%Assign initial -By=Ax+C

TubeLength = 2708;
SideAngle = 0;
SideTotalRay = 0;
SideLossRay = 0;
SideAbsorbRay = 0;
RF = 1;

%Assign reflectance index for each tube section
RF1 = 0.9348;
RF2 = 0.9348;
RF3 = 0.9348;
RF4 = 0.9348;
RF5 = 0.9348;
RF6 = 0.9348;
RF7 = 0.9348;
RF8 = 0.9348;
RF9 = 0.9348;
RF10 = 0.9348;


AbsFactor = 1;
colormap('jet')

hold off

if PlaneAz<0
    SideAngle=atand(cosd(AngleIncident)/(sind(AngleIncident)*cosd(-
PlaneAz)));
elseif PlaneAz>90

SideAngle=90+atand(cosd(AngleIncident)/(sind(AngleIncident)*cosd(PlaneAz
-90)));
elseif PlaneAz>0

SideAngle=atand(cosd(AngleIncident)/(sind(AngleIncident)*cosd(PlaneAz)))
;
```

```
else
    SideAngle=90;
end
if SideAngle == 90
    SideAngle = 89.9999;
end
sAi = -tand(SideAngle);
sBi = 1;

sAi1 = sAi;
sBi1 = sBi;
subplot(2,1,2);
hold off
DrawSideview()
```

Next, the subprogram *SideRayEnter*() will simulate an array of rays at the same angle (longitudinal view). The ray will be generated from the first ray that touches the ICPC to the last as the *C* value (*sCi*) is assigned. Each ray will be monitor as it is reflected by reflector or hits the absorber fin. First, the ray will be assigned to begin from the y value of 100, so the entry point will be $\left(\frac{-(100B+C)}{A},100\right)$. Then the ray will stop at the entry point as the ray enters the ICPC tube. The y-value of the entry point is prerecorded to the first value of *YPlotValue* array from *Exposure*(). So, the entry point on longitudinal view is $\left(\frac{-(BY_{entry}+C)}{A},Y_{entry}\right)$. Then, the pink color is assigned to the ray traveling to the entry point. There are three cases on how the ray hits the target tube. First, the ray is considered missing the absorber or reflected out. If the variable *DHit*, *AbHit*, and *ReHit* equal 0, the subprogram *SideRayEnter*() will be skipped. Second case is when there is a direct hit to the absorber fin. This is the case when the *ynumber* variable equals 2. The ray will be checked whether it loss or miss the absorber by checking the x-intersection. If the intersection is lees than 100 or more than 2538.5 then the ray will loss. The dark blue color will then be applied to the ray. If the ray is not loss, the red color will

be assigned to the line and the ray will stop at absorbed point

or $\left(\frac{-(BY_{absorb}+C)}{A}, Y_{eabsorb}\right)$. The Matlab code is shown below.

```
step = TubeLenght/200;
for sXi1 = 0:step:TubeLenght%from the first touching ray to the last
touching ray
    RF = 1;
    sCi=-sBi1*OutTubeRadius-sAi1*sXi1;
    sAi1=sAi;
    sBi1=sBi;
    sCi1=sCi;
    sYi1=OutTubeRadius;

    b1 = 100;
    a1 = -((sBi*100)+ sCi)/sAi;
    a2 = -((sBi*YPlotValue(:,1))+ sCi)/sAi;
    b2 = YPlotValue(:,1);
    line([a1 a2],[b1 b2],'color',[1,0,1])
    if DHit+AbHit+ReHit == 0
        Dump=0;
    elseif ynumber == 2

        a1 = a2;
        b1 = b2;
        b2 = YPlotValue(:,2);
        a2 = -((sBi*YPlotValue(:,2))+ sCi)/sAi;
        if a2 < 100 || a2 > 2538.5%Check for the loss ray
            line([a1 a2],[b1 b2],'color',[0,0.4,0.6])
            SideLossRay=SideLossRay+1;
            RF = 0;
        else
            line([a1 a2],[b1 b2],'color','r','linestyle','-')
        end
```

The last case is when the ray hits the reflector. When the *ynumber* is more than 2 , it indicate that there is at least one time the ray hits the reflector. A "for" loop is used to trace the ray until it hits the target or is reflected out. *YInt* variable is used to indicate times of reflector hit. The first YInt value is 2 as the ray first hits the reflector. The first reflected point is $\left(\frac{-(BY_{reflected}+C)}{A}, Y_{reflected}\right)$. Due to a cylindrical symmetry, the

distance along the longitudinal view Δx between any two nearest points of reflection is fixed. So, the range on x axis between the entry point and the reflected point is recorded. Then, the ray is checked whether it miss the reflector or not. The dark blue color will be assigned to the loss ray. If the ray hit the reflector, the ray will be determined which section of the reflector is hit and the reflection factor will be calculated responding to the location. The ten sections are from 100 to 350, 350 to 600, 600 to 850, 850 to 1100, 1100 to 1350, 1350 to 1600, 1600 to 1850, 1850 to 2100, 2100 to 2350, and 2350 to 2538.5. Each section will correspond to the reflection index assigned to the section. The reflection factor (*RF*) will be updated as the ray reflected each time. The yellow color will be applied to the reflected ray. The Matlab code for the process explaining before is shown below.

```
elseif ynumber > 2
        for YInt = 2:1:ynumber
            if YInt == 2
                a1 = a2;
                b1 = b2;
                b2 = YPlotValue(:,YInt);
                a2 = -((sBi*YPlotValue(:,YInt))+ sCi)/sAi;
                RangeX = a2-a1;

                if a2 < 100 || a2 > 2538.5%Check for the loss ray
                    line([a1 a2],[b1 b2],'color',[0,0.4,0.6]);
                    SideLossRay=SideLossRay+1;
                    RF = 0;
                    break
                else
                    if a2 < 350
                        RF = RF*RF1;

                    elseif a2 < 600
                        RF = RF*RF2;

                    elseif a2 < 850
                        RF = RF*RF3;

                    elseif a2 < 1100
                        RF = RF*RF4;
```

```
        elseif a2 < 1350
            RF = RF*RF5;

        elseif a2 < 1600
            RF = RF*RF6;

        elseif a2 < 1850
            RF = RF*RF7;

        elseif a2 < 2100
            RF = RF*RF8;

        elseif a2 < 2350
            RF = RF*RF9;

        elseif a2 < 2538.5
            RF = RF*RF10;

        end
        line([a1 a2],[b1 b2],'color','y','linestyle','-');
    end
```

After the first reflection, the *SideRayEnter*() will determined where the ray hits next. First, the next hit position will be assigned at ($x_n + \Delta x$, $y_{reflected,n}$). Then, the program checks for the ray that reflected out by checking that the ray misses the absorber fin or the x-intersection falls outside the interval of 300 to 2538.5. The green color is also assigned to the ray. Next, if the ray is not loss, the ray will be reflected of the reflector. The reflected location of the ray will be determined as the reflection index is different between each section of the ten sections. Then, the reflected factor (*RF*) is recalculated. The ray intensity will be reduced each time the ray reflected (equation D.31).

$$Ray\ intensity = \prod_{n}^{m} r_{n,m} \tag{D.31}$$

where $r_{n,m}$ is the reflection index at time n and m sections

The yellow color will be applied to the reflected ray. As the increasing *YInt* number the reflection calculation will be repeated until the *YInt* equals to *ynumber*. Last, the ray will

hit the absorber fin or reflected out. The position of the ray hitting absorber will be calculated as the y-value is will be on the line from reflected point to the exit point (imaginary point since the ray will hit absorber first). The ray will be drawn from the reflected point to the absorber hitting point

$$\left(\left(\frac{\Delta x}{Y_{cover}-Y_{reflector}}\times\left(Y_{absorber}-Y_{reflector}\right)\right)+x_{reflector},Y_{absorber}\right).$$ The brown color will

be applied to the ray as the ray hits absorber fin. The *EndLossPercent* variable is a variable that tracks the reduce ray intensity and the loss through the tube ends on the longitudinal view. The *EndLossPercent* is calculated by equation D.32.

$$EndLossPercent = 1-\left(\frac{\sum \text{reduced intensity rays (longitudinal view)}}{\text{total rays (longitudinal view)}}\right) \qquad \text{(D.32)}$$

Or, we can say that the average ray intensity on the longitudinal view at the same entry plane is 1 – *EndLossPercent.* The Matlab code explaining this processes is shown next.

```
            else
                a1 = a2;
                b1 = b2;
                b2 = YPlotValue(:,YInt);
                if YInt < ynumber
                    a2 = a1 + RangeX;
                    if a2 < 100 || a2 > 2538.5%Check for the loss ray
                        line([a1 a2],[b1 b2],'color','g','linestyle','-
');

                        SideLossRay=SideLossRay+1;
                        RF = 0;
                        break
                    else
                        if a2 < 350
                            RF = RF*RF1;

                        elseif a2 < 600
                            RF = RF*RF2;

                        elseif a2 < 850
                            RF = RF*RF3;
```

```
                        elseif a2 < 1100
                            RF = RF*RF4;

                        elseif a2 < 1350
                            RF = RF*RF5;

                        elseif a2 < 1600
                            RF = RF*RF6;

                        elseif a2 < 1850
                            RF = RF*RF7;

                        elseif a2 < 2100
                            RF = RF*RF8;

                        elseif a2 < 2350
                            RF = RF*RF9;

                        elseif a2 < 2538.5
                            RF = RF*RF10;

                        end

                        line([a1 a2],[b1 b2],'color','y','linestyle','-
');
                    end
                else
                    sy = Rb2;
                    sx = a1 + RangeX;
                    a2 = (((sx-a1)/(sy-b1))*(b2-b1))+a1;
                end
                if a2 < 100 || a2 > 2538.5%Check for the loss ray
                    line([a1 a2],[b1 b2],'color','g','linestyle','-');
                    SideLossRay=SideLossRay+1;
                    RF = 0;
                else
                    line([a1 a2],[b1 b2],'color',[0.5,0.5,0]);
                end
            end
        end
    end
    SideTotalRay = SideTotalRay + 1;
    SideAbsorbRay = SideAbsorbRay + RF;


end
EndLossPercent=1-(SideAbsorbRay/SideTotalRay);
```

D.2.8 Subprogram (*DrawSideView.m*)

The subprogram *DrawSideView*() is activated by the subprogram *SideRayEnter*(). The main purpose for this subprogram is to draw the ICPC tube in longitudinal view. Two straight lines are drawn from 0 to 2708 at y = 65 and -65 to form the outer glass surface, and two lines at y = 63 and -63 are drawn to form the inner glass surface. Another two red lines are plotted at y = 6 and -6 (*InRadius*) for a heat transport tube. Then, the two caps are drawn at tube's ends.

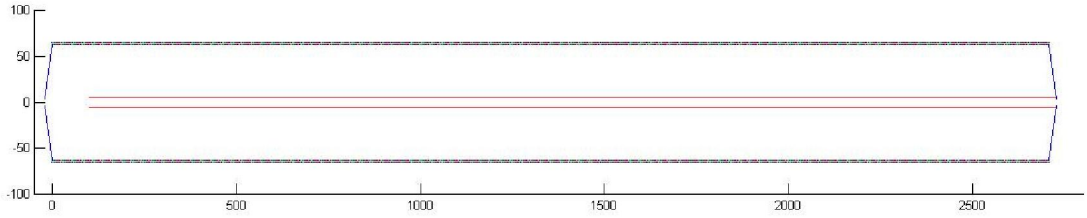

Figure D.2: ICPC longitudinal view

Figure D.2 shows the ICPC on the longitudinal view. Matlab code for the subprogram *DrawSideview*() is shown next.

```
TubeLength = 2708;
TubeRadius = 63;
OutTubeRadius = 65;

set(gca,'DataAspectRatio',[2 0.8 1],...
        'PlotBoxAspectRatio',[2 0.8 1])
axis([-50 2800 -100 100]);


%Draw inner glass tube
X = 0:1:TubeLength;
Y = -TubeRadius;
hold on
plot(X,Y)
Y = TubeRadius;
```

```
plot(X,Y)


%Draw outer glass tube
X = -2:1:TubeLength+2;
Y = -OutTubeRadius;
hold on
plot(X,Y)
Y = OutTubeRadius;
plot(X,Y)


%Draw copper tube
X = 100:1:TubeLength+20;
Y = -InRadius;

hold on
plot(X,Y,'-r')

Y = InRadius;
plot(X,Y,'-r')


%Draw tube cap left
X1 = 0;
Y1 = TubeRadius;
X2 = -20;
Y2 = 4;
line([X1 X2],[Y1 Y2])
hold on
X1 = 0;
Y1 = -TubeRadius;
X2 = -20;
Y2 = -4;
line([X1 X2],[Y1 Y2])
hold on


%Draw tube cap right
X1 = TubeLength;
Y1 = TubeRadius;
X2 = TubeLength+20;
Y2 = 4;
line([X1 X2],[Y1 Y2])
hold on
X1 = TubeLength;
Y1 = -TubeRadius;
X2 = TubeLength+20;
Y2 = -4;
line([X1 X2],[Y1 Y2])
```